The Dynamics of Excited Hydrogen Atoms in Strong Electric and Magnetic Fields

Thesis

The Dynamics of Excited Hydrogen Atoms in Strong Electric and Magnetic Fields

Orsola Rath

Thesis submitted for the Degree of Ph.D in the Faculty of Mathematics of the Open University

February 1990

Date of submission: 6 April 1990
Date of award: 8 November 1990

Abstract

This thesis concerns the study of dynamical systems whose classical dynamics exhibit chaotic motion. Two systems in which classical chaos plays an important role are investigated in this work. Both involve highly excited hydrogen atoms in strong external fields, in one case a periodic electric field and in the other a uniform magnetic field. These examples are chosen for their particular relevance to the study of the relationship between classical and quantum dynamics when the motion is irregular.

A three-dimensional classical simulation of the hydrogen atom in a microwave field is developed. This is then used for a study of the mechanism of ionisation and for an extensive comparison with experimental results. For this purpose a regularising transformation is developed, together with an asymptotic approximation for the case when the electron moves far from the atom. This reveals many interesting new features of the dynamics. Some explanations of the ionisation mechanism in different frequency ranges are given.

The hydrogen atom in a magnetic field is studied by using the adiabatic method, which is shown to be reliable for very accurate calculations of the energy levels even when the external field is very strong and most of the orbits are irregular. This system has both librational and rotational motion. Although the zero-frequency motion on the separatrix contradicts the assumption of adiabatic invariance, it is shown that in practice the adiabatic method may still be applied. A similar problem occurs because one of the fundamental frequencies is initially zero, but this is overcome by choosing the initial conditions appropriately.

An extensive review of the literature is given for both of these problems.

Acknowledgements

I would like to thank my supervisor, Dr. Derek Richards, whose help and guidance have been invaluable throughout, and the Open University for their financial support.

Declaration

No part of this thesis has previously been submitted for a degree or other qualification to this or any other university or institution. Certain parts of Chapters 3 and 4 have now been published, as indicated therein.

Contents

Introduction

In recent years much work has been devoted to the study of dynamical systems whose classical motion exhibits strong instability with respect to initial conditions, that is chaotic motion. The regular motion of physical systems is well understood, but the understanding of chaotic motion is one of the major open problems of contemporary physics. A better understanding of chaotic motion is of great importance in many areas of physics and chemistry. In chemistry, for example, it is relevant to the study of intramolecular energy transfer (Jortner 1980, Schwentner *et al.* 1984); in atomic physics it provides fundamental clues to the interpretation of photoabsorption spectra of highly excited atoms in magnetic fields (Rau 1980); in plasma physics it is relevant to the study of confinement of charged particles in electromagnetic fields, such as particles in an accelerator (Rechester and Rosenbluth 1978, Month and Herrera 1979, Jowett *et al* 1985); in astrophysics it is part of the basis upon which our understanding of the great quantity of observed data on white dwarfs (Angel 1977) and the study of the stability of our solar system are built (Wisdom 1987).

Some of the phenomena mentioned above are essentially of a quantal nature, and there is therefore a need to understand the manifestations of classical chaos in quantum mechanics. Establishing a correspondence between classical and quantum mechanics is a fundamental problem dating back to the early days of quantum mechanics. Solutions to particular problems such as the quantisation of some simple systems exist, but many questions are still unanswered, even for the case of regular motion, and clear manifestations of classical chaotic motion in a quantal system have not been

found. Clearly a much deeper understanding of classical chaos and more comparisons with experimental data are needed before this problem can be addressed properly.

Two examples in which classical chaos plays a significant role involve highly excited hydrogen atoms in strong fields, in one case a periodic electric field and in the other a uniform magnetic field. These systems allow both experimental and theoretical analyses and can thus give insight into the relationship between classical and quantal dynamics when the motion is irregular.

In this thesis both of these systems are studied by developing and applying techniques which enable a systematic study of the classical dynamics. In the first system the process being observed is ionisation by a periodic electric field. In classical dynamics this proceeds only via the unstable or chaotic orbits, for which the quantal analogue is not fully understood. Comparison with experimental results has provided us with an invaluable means of investigating discrepancies between classical and quantum dynamics. Many new and interesting features of the dynamics have come to light , not all related to the manifestations of classical chaos. Among these the most striking is the behaviour at resonances and at very low and very high scaled frequencies $n^3\omega$, typically less than 0.2 and greater than 1.2. Also, it has become apparent that the mechanism of ionisation is much more complicated than previously thought and needs to be understood better.

The second system, the hydrogen atom in a magnetic field, is investigated by using a semiclassical method based on the principle of adiabatic invariance, which states that some quantities are almost constant, for very long times, when the system varies slowly with time. This is the first application of the adiabatic method to a physical system which allows comparison with other theoretical and experimental data. The method is found to be very stable and provides results for a wide range of magnetic field strengths, even up to very high fields where the motion becomes irregular and perturbative approximations previously used to study this system fail. Furthermore, it provides intrinsic checks and simple tests to estimate the onset of irregular

motion. It is the only method at present that can provide semiclassical energy levels by using irregular trajectories. The hydrogen atom in a strong magnetic field is a very good candidate for the study of the transition from regular to chaotic motion and has proved a useful example of the application of the adiabatic method. Some important properties of the adiabatic method which have emerged enable the study of periodic trajectories and their role in the irregular region. This is particularly interesting in view of the link between periodic trajectories and quasi-Landau resonances, which are a feature of observed experimental spectra in the irregular regime (Holle *et al.* 1986).

The thesis is organised as follows. Chapter 1 is mainly introductory, and is divided into two parts. The first gives a very brief summary of the main properties of the hydrogen atom, with and without external fields, and reviews some recent works on the Stark effect. In the second part we develop a regularising transformation, used to avoid the problems caused by the Coulomb singularity. The equations for the direct and inverse transformation are given, as well as the equations of motion for the hydrogen atom in the new coordinates. Chapter 2 explains the adiabatic method and reviews the existing literature.

Chapter 3 is devoted to the study of the hydrogen atom in a magnetic field. The rotational and vibrational motions are analysed and appropriate initial conditions are derived for the quantisation of this system, which is carried out by applying the adiabatic method. Results are obtained for a wide range of the parameters involved and comparisons with existing theoretical and experimental results are given and discussed. We show that the adiabatic method can be used to calculate very accurately the energy levels of the hydrogen atom in a magnetic field even when the perturbation is much stronger than the Coulomb interaction and most of the orbits are irregular.

In Chapter 4 the problem of microwave ionisation of highly excited hydrogen atoms is studied extensively. An asymptotic approximation which makes the numerical simulation more efficient when the electron is far from

the origin is developed. The system is quantised and numerical integration is carried out for a microcanonical ensemble of initial orbits at several different values of the applied field strength and frequency. The convergence of the ionisation curve and the effect of switching the field on adiabatically are studied. The ionisation thresholds obtained with 1- and 3-dimensional models are compared and discrepancies between them are discussed, as well as selected examples from an extensive comparison with experiment. Very good agreement with experiment is achieved for scaled frequencies $0.2 < n^3\omega < 1$. Agreement deteriorates with increasing frequency; this tends to support theoretical predictions of quantal suppression of classical chaos (Casati *et al.* 1987). Particular attention is also devoted to the behaviour at resonances, and in this context some numerical and experimental results obtained with two microwave fields of different frequencies are presented.

In Chapter 5 we study a 2-dimensional area-preserving map which is constructed specifically to simulate the dynamics of the hydrogen atom in a microwave field. This serves to illustrate the effects of the adiabatic method and further justify and explain the results obtained in the preceeding chapters.

Chapter 6 briefly reviews some of the most important results. Their significance is discussed in the context of future work.

Chapter 1

The hydrogen atom

1.1 Introduction

The hydrogen atom is the simplest of all atomic systems. It consists of an electron of negative charge $-e$ and mass m_e which is electrically bound to a nucleus of positive charge e and mass m_p and moving in the Coulomb potential

$$V(\mathbf{r}) = -\frac{e^2}{|\,\mathbf{r}\,|}\,. \tag{1.1}$$

The Hamiltonian for this system is then

$$H(\mathbf{r},\mathbf{p}) = \frac{1}{2\mu}p^2 - \frac{e^2}{r}\,, \tag{1.2}$$

referred hereafter as the Coulomb Hamiltonian, where $\mathbf{r} = \mathbf{r}_e - \mathbf{r}_p$ is the relative coordinate and $\mu = \frac{m_e m_p}{m_e+m_p}$ is the reduced mass. Since $m_e \ll m_p$, $\mu \sim m_e(1 - m_e/m_p)$ and we can assume the nucleus to be infinitely heavy and stationary, so that $\mu = m_e$ and $\mathbf{r} = \mathbf{r}_e$; this amounts to neglecting the correction term $m_e/m_p \sim 1/1800$. The analysis of the motion of a particle in a central field is given by many books (see for example Born 1927 and Landau and Lifshitz 1965). Here the main properties relevant to the subsequent chapters are briefly described.

Since the potential is central the angular momentum, $\mathbf{L} = \mathbf{r} \times \mathbf{p}$, is conserved and the motion is confined to a plane. When the energy, E, is negative the motion is bounded and, because the potential varies inversely with r,

the orbit is an ellipse. The system is thus completely degenerate. The additional constant of motion is the Runge-Lenz vector, which points along the direction of the perihelion, (see Figure 1.1), and can be conveniently defined by:

$$\mathbf{A} = \left(\mathbf{p} \times \mathbf{L} - \mu e^2 \frac{\mathbf{r}}{r}\right) (\sqrt{2 \mid E \mid})^{-1} \ . \tag{1.3}$$

With this definition the magnitude of A is related to the eccentricity ε of the ellipse by $A = \mu e^2 \varepsilon$.

The constants of motion L and A define the symmetry group SO(4), whose Lie algebra is given by the relationships:

$$\begin{aligned} \{L_i, L_j\} &= \varepsilon_{ijk} L_k \\ \{A_i, L_j\} &= \varepsilon_{ijk} A_k \\ \{A_i, A_j\} &= \varepsilon_{ijk} L_k \ , \end{aligned} \tag{1.4}$$

where $\{\ ,\ \}$ denotes the Poisson brackets.

Let (ξ, η, ζ) be cartesian coordinates with ζ perpendicular to the plane of motion, i.e. along the angular momentum, and ξ along the major axis. The motion is then described by Kepler's equation

$$\omega t + \delta = u - \varepsilon \sin u = \theta_n \tag{1.5}$$

and

$$\begin{aligned} \xi &= a(\cos u - \varepsilon) \quad , \quad \eta = a\sqrt{1-\varepsilon^2} \sin u \\ \dot{\xi} &= -\frac{a\omega \sin u}{1 - \varepsilon \cos u} \quad , \quad \dot{\eta} = \frac{a\omega\sqrt{1-\varepsilon^2} \cos u}{1 - \varepsilon \cos u} \\ r &= a(1 - \varepsilon \cos u) \end{aligned} \tag{1.6}$$

where

ω = angular frequency of the classical motion = $e(\mu a^3)^{-1/2}$

δ = phase of the classical motion

t = time measured from a fixed origin

u = eccentric anomaly

a = semi-major axis of the ellipse

θ_n = mean anomaly.

The orientation of the elliptic orbit with respect to a fixed frame (x, y, z) can be described by the Euler angles $(\theta_m, \beta, \theta_l)$ which give the orientation of (ξ, η, ζ) with respect to (x, y, z). The notation θ_m and θ_l is used for the Euler angles instead of α and γ because these angles are the conjugate variables of the action variables I_m and I_l defined below. We have (Goldstein 1980):

$$\begin{aligned} x &= \xi(-\cos\beta \sin\theta_m \sin\theta_l + \cos\theta_m \cos\theta_l) - \eta(\cos\beta \sin\theta_m \cos\theta_l \\ &+ \cos\theta_m \sin\theta_l) + \zeta \sin\beta \sin\theta_m \\ y &= \xi(\cos\beta \cos\theta_m \sin\theta_l + \sin\theta_m \cos\theta_l) + \eta(\cos\beta \cos\theta_m \cos\theta_l \\ &- \sin\theta_m \sin\theta_l) - \zeta \sin\beta \cos\theta_m \\ z &= \xi \sin\beta \sin\theta_l + \eta \sin\beta \cos\theta_l + \zeta \cos\beta \ . \end{aligned} \tag{1.7}$$

The intercept of the (x, y) and (ξ, η) planes is called the *line of nodes*. As shown in Figure 1.1, θ_m is the angle between the line of nodes and the x-axis, β is the angle between the angular momentum and the z-axis, θ_l is the angle between A and the line of nodes.

The Coulomb Hamiltonian is completely separable in many coordinate systems; here spherical polar coordinates will be used. It is convenient to use a representation in which the system is separable, as this simplifies quantisation. We shall give here the well known EBK quantisation prescriptions (Einstein 1917, Brillouin 1926, Keller 1958) in which the objects of quantisation are the invariant tori in phase space, defined by the action variables. Using spherical polar coordinates the action variables are defined by:

$$I_k = \frac{1}{2\pi} \oint p_k \, dq_k \quad , \quad k = r, \theta, \phi \, . \tag{1.8}$$

The angle variables then vary between 0 and 2π. If, following Born (1927), we define a new set of action variables

$$\begin{aligned} I_n &= I_r + I_\theta + I_\phi \\ I_l &= I_\theta + I_\phi \\ I_m &= I_\phi \ , \end{aligned} \tag{1.9}$$

then these new action variables are the classical analogues of the quantum numbers n, l, m and their conjugate angle variables are the variables

$\theta_n, \theta_l, \theta_m$ described above. In terms of these variables the energy is given by:

$$E_n = -\frac{\mu e^4}{2I_n^2} , \tag{1.10}$$

showing that the system is completely degenerate, as noted before, and the angular frequency is given by

$$\omega_{at}(I_n) = \mu e^4 I_n^{-3} . \tag{1.11}$$

Bohr's correspondence principle relates the angular frequency of the classical motion ω_{at} to the frequency ω_n for transitions between quantum states of neighbouring principal quantum number n:

$$\Delta E_n = E_{n+1} - E_n \simeq \hbar\omega_{at} . \tag{1.12}$$

The action variables are related to the parameters determining the shape and orientation of the Kepler ellipse by:

$$a = \frac{I_n^2}{\mu e^2} , \quad \varepsilon^2 = 1 - \frac{I_l^2}{I_n^2} , \quad \cos\beta = \frac{I_m}{I_l} , \tag{1.13}$$

The EBK quantisation conditions are

$$I_k = 2\pi(n_k + \frac{\alpha_k}{4})\hbar. \tag{1.14}$$

where n_k are integers and α_k are the appropriate Maslov indices. In general for librations $\alpha_k = 2$, while for rotations $\alpha_k = 0$ (see for example the review by Percival 1977).

1.2 The hydrogen atom in an external field

When an external field is applied to the hydrogen atom the picture described above changes drastically. We shall summarise here the main consequences of applying either an electric or a magnetic field. The quadratic Zeeman effect and the problem of a hydrogen atom in a microwave field are treated extensively in chapters 3 and 4 respectively. Let us first consider the effect of

a static electric field F. Under a static electric field in the direction of the z-axis, only the projections of the total angular momentum and of the Runge-Lenz vector in the direction of the field are conserved and the degeneracy of the unperturbed system is lifted. This perturbed system is separable in parabolic coordinates. The quantal description of the Stark effect can be found for example in Landau and Lifshitz (1977) for the limit of low fields. In this limit classical (Born 1927) and quantal (Alliluev and Malkin 1974) perturbative methods have been applied for finding energy levels and shifts. Percival and Richards (1979) use the theory of the Stark effect to solve the rate equation for hydrogen in collision with charged particles and give an illuminating geometrical description of the motion, originally due to Bohr. The application of a weak static field produces a periodic time dependence in the eccentricity and the plane of the orbit. The plane of the orbit changes periodically with angular frequency ω_s, the Stark frequency:

$$\omega_s = \frac{3a}{2I_n} eF \ , \tag{1.15}$$

and the eccentricity changes periodically with frequency $2\omega_s$. For weak fields ω_s is much smaller than the fundamental angular frequency of the electron ω_n, in other words the characteristic time over which the plane of the orbit changes is very long compared with the period of the electron around the orbit, so that this motion can be considered separately. The correspondence principle relates the Stark frequency to the splitting between quantum levels:

$$\Delta E_s = \mid E_{n_e+2} - E_{n_e} \mid \simeq \hbar\omega_s \ , \tag{1.16}$$

where n_e is the electric quantum number related to the classical electric action $I_e = \mathbf{A} \cdot \mathbf{F}$.

Banks and Leopold (1978a, 1978b) used an exact classical treatment based on the assumption of adiabatic invariance of the actions to find explicit expressions for the critical ionisation energy E_c and critical field F_c and to calculate Stark shifts for all values of the electric field up to F_c. In their treatment of this problem they separate the Hamiltonian

$$H = \frac{1}{2\mu} p^2 - \frac{Ze^2}{r} + eFz \tag{1.17}$$

by using parabolic coordinates ξ, η, ϕ defined by

$$\xi = \frac{1}{2}(r+z) \ , \ \eta = \frac{1}{2}(r-z) \ , \ \phi = \tan^{-1}(\frac{y}{x}) \ .$$

Equation 1.17 then separates giving

$$\begin{aligned} \frac{1}{2\mu}p_\xi^2 + V_\xi(\xi) &= \frac{1}{2}p_\xi^2 + \frac{I_\phi^2}{8\mu\xi^2} - \frac{Z_1 e^2}{\xi} + eF\xi = E \qquad (1.18) \\ \frac{1}{2\mu}p_\eta^2 + V_\eta(\eta) &= \frac{1}{2}p_\eta^2 + \frac{I_\phi^2}{8\mu\eta^2} - \frac{Z_2 e^2}{\eta} + eF\eta = E \ , \end{aligned}$$

and I_ϕ = constant ≥ 0, with $Z_1 + Z_2 = Z$ and $0 \leq Z_1 \leq Z$. For a bounded physical solution the total energy E must lie in the range $\max(V_{\xi_{min}}, V_{\eta_{min}}) \leq E \leq V_{\eta_{max}} \leq 0$. For any value of the energy $E = V_\xi = V_\eta$ in this region, the equations $E = V_\xi$ and $E = V_\eta$ have each three real roots ξ_1, ξ_2, ξ_3, and η_1, η_2, η_3 respectively. The critical ionisation energy is defined by $E_c = V_{\eta_{max}}$, which implies $\eta_2 = \eta_3$.The energy E and the separation constants Z_1 and Z_2 are related implicitly to the actions I_ξ, I_η, I_ϕ and to the electric field F. By imposing the condition $\eta_2 = \eta_3$ in exact calculations relating I_ξ and I_η to E, Z, F, I_ϕ and the six real roots, Banks and Leopold obtain expressions for the critical field F_c and the critical energy E_c in terms of the functions $\Phi(u,v)$ and $\varepsilon(u,v)$, which are the scale-invariant forms of the electric field and the energy respectively. These functions are dimensionless and independent of $I = I_\xi + I_\eta + I_\phi$, but dependent on the dimensionless ratios u and v, which are chosen here as I_η/I and I_ϕ/I respectively. The critical field and the critical energy are written in the form

$$F_c = \frac{\mu^2 Z^2 e^5}{I^4}\Phi_c(u,v) \ ; \ E_c = -\frac{\mu^2 Z^2 e^4}{2I^2}\varepsilon_c(u,v) \ . \qquad (1.19)$$

The authors are then able to obtain values of F_c and E_c and of Stark shifts by using a polynomial fit to the functions $\Phi(u,v)$ and $\varepsilon(u,v)$, Their results are in very good agreement with quantal calculations of Stark shifts for strong fields obtained with a quantal asymptotic method by Damburg and Kolosov (1976a, b). Herrick (1976) uses a 2-parameter quantum variational method to estimate the critical electric field and energy for Rydberg atoms.

The problem of a hydrogen atom in a microwave field is of much current interest. The periodic nature of a microwave perturbation and its

range of frequencies are of particular importance. The splitting between energy levels n and $n+1$ in an excited hydrogen atom is approximately $\Delta E_n \approx 6.6 \times 10^6 n^{-3}$ GHz, which is in the microwave region for $n \sim 50-100$, thus microwaves cause resonant transitions between many adjacent levels. Furthermore, the energy splitting $\Delta E_n/\hbar$ is approximately the classical electron period (equation 1.12), so the system can be represented as a periodically forced non-linear oscillator, which is non-integrable and has irregular motion. This is one of the two atomic systems accessible to current experiments where the classical analogue is non-integrable in the region probed by experiment. Bayfield and Koch (1974) first reported the observation of microwave ionisation of highly excited hydrogen atoms and several other experimental works followed (Bayfield *et al* 1977, Koch 1982, Bayfield and Pinnaduwage 1985, Bayfield 1987, Koch *et al* 1987, Koch 1988). The quantum theoretical analysis of this problem is very difficult, because of the strong interaction that couples very many bound states and the problem of including the continuum. The classical analysis is easier and Hamilton's equations can be solved very accurately, but the validity of a classical approximation has to be proved. Classical mechanics has been shown to give fairly accurate results in a limited parameter range (Leopold and Percival 1978, 1979). The range of parameters for which classical mechanics is applicable is discussed in Chapter 4. The importance of this problem lies in the fact that classical ionisation occurs via unstable orbits, for which a quantal analogue is not yet understood. A deeper understanding of this problem can thus provide some insight into the relationship between classical and quantum dynamics in the chaotic regime. The hydrogen atom in a microwave field is treated extensively in chapter 4, where a three-dimensional semiclassical numerical model is used to study the dynamics and to obtain comprehensive statistics of ionisation for a wide range of frequencies. Comparisons with experiments and other one-dimensional numerical results are also given.

Another problem in which chaos appears to play an important role and which is thus of great interest for the same reasons is the hydrogen atom in a strong magnetic field. The Hamiltonian for an electron of charge e, mass μ,

moving in a Coulomb potential centered at the origin and a static magnetic field $\mathbf{B}$, along the z-axis is

$$H = \frac{p^2}{2\mu} - \frac{e^2}{r} + \frac{1}{2}\alpha \mathbf{L}\cdot\mathbf{B} + \frac{1}{8}\mu(\alpha B)^2(x^2+y^2) \qquad (1.20)$$

where $\alpha = e/\mu c$, c being the speed of light, and where $\mathbf{L}$ is the orbital angular momentum. The linear or paramagnetic term, $\frac{1}{2}\alpha\mathbf{L}\cdot\mathbf{B}$, breaks the symmetry of the Coulomb problem; it thus lifts the degeneracy of the unperturbed system and causes the linear Zeeman shift $\Delta E = \mu_B B L_z$, where $\mu_B = e\hbar/(2\mu c)$ is the Bohr magneton. The diamagnetic term, $\frac{1}{8}\mu(\alpha B)^2(x^2+y^2)$, makes H nonseparable. It has been shown (Herrick 1982) that in the limit of very low fields there exists an approximate spherical symmetry, and in the Landau limit there exists an approximate cylindrical symmetry. These regions have thus been analysed extensively in several works, but little is known about the intermediate region, which is the most interesting. In chapter 3 the adiabatic method is used to study the dynamics of the hydrogen atom in a magnetic field over a wide range of field strengths from the low field regime well into the intermediate region.

1.3 Regularisation

Throughout the work we shall use dimensionless variables, defined by the Kepler orbit of the initial state, so that the unit of length is the semi-major axis of the ellipse and the unit of time is the period of the orbit:

$$\mathbf{r}' = a^{-1}\mathbf{r} \;\;,\;\; \mathbf{p}' = a^{1/2}e^{-1}\mu^{-1/2}\mathbf{p} \;\;,\;\; t' = a^{-3/2}e\mu^{-1/2}t \;. \qquad (1.21)$$

With these variables the Hamiltonian 1.2 becomes, upon dropping the prime,

$$H = \frac{1}{2}p^2 - \frac{1}{r} \;. \qquad (1.22)$$

The Coulomb singularity causes numerical inefficiencies which can most elegantly be removed by moving into extended phase space and performing a canonical transformation. The Hamiltonian in extended phase space is (see, for example, Szebehely 1967)

$$\bar{\Gamma} = W + H \equiv 0 \qquad (1.23)$$

and the conjugate variables time, t, and energy, W, are treated equivalently to $\mathbf{r}$ and $\mathbf{p}$ by adding the two extra equations of motion

$$\frac{dt}{d\tau} = \frac{\partial \overline{\Gamma}}{\partial W} \quad , \quad \frac{dW}{d\tau} = -\frac{\partial \overline{\Gamma}}{\partial t} \; , \tag{1.24}$$

where τ is a variable labelling points along a phase curve, in this case trivially $\tau = t +$ constant and $W = -H$. In ordinary phase space canonical transformations to new time variables are not possible (Szebehely 1967), but in extended phase space, as the time is treated as an ordinary coordinate, it is possible to transform to a new time. A natural way of doing this and of removing the Coulomb singularity is to multiply $\overline{\Gamma}$ by $4r$ to obtain an equivalent new Hamiltonian Γ:

$$\Gamma = 4r\overline{\Gamma} = 4rW + 2rp^2 - 4 \equiv 0 \; . \tag{1.25}$$

Now transform to the new coordinates x_i, $i = 1, \ldots, 4$, defined by Cornish (1984).

$$\begin{aligned} x_1 &= r^{1/2} \cos\frac{\theta}{2} \cos\frac{\sigma+\phi}{2} \; , \\ x_2 &= r^{1/2} \cos\frac{\theta}{2} \sin\frac{\sigma+\phi}{2} \; , \\ x_3 &= r^{1/2} \sin\frac{\theta}{2} \cos\frac{\sigma-\phi}{2} \; , \\ x_4 &= r^{1/2} \sin\frac{\theta}{2} \sin\frac{\sigma-\phi}{2} \; . \end{aligned} \tag{1.26}$$

Note that $\sum_{i=1}^{4} x_i^2 = r$ and r, θ, ϕ are the usual spherical coordinates. Here σ is defined by introducing two complex variables ξ_A and ξ_B such that:

$$x + iy = 2\xi_A \overline{\xi}_B \quad , \quad z = \xi_A \overline{\xi}_A - \xi_B \overline{\xi}_B \; , \tag{1.27}$$

where $\overline{\xi}$ denotes the complex conjugate. Then σ is defined by:

$$\sigma = \arg \xi_A \xi_B \; . \tag{1.28}$$

From 1.26 it follows that, given x_i, $i = 1, \ldots, 4$, (x, y, z) are determined uniquely, but given (x, y, z) then (r, θ, ϕ) are determined but σ is arbitrary (Cornish 1984).

Conjugate momenta can be determined from the F_2-generating function,

$$\begin{aligned} F_2(\mathbf{P},\mathbf{q}) &= p_1 r^{1/2}\cos\frac{\theta}{2}\cos\frac{\sigma+\phi}{2} + p_2 r^{1/2}\cos\frac{\theta}{2}\sin\frac{\sigma+\phi}{2} \\ &+ p_3 r^{1/2}\sin\frac{\theta}{2}\cos\frac{\sigma-\phi}{2} + p_4 r^{1/2}\sin\frac{\theta}{2}\sin\frac{\sigma-\phi}{2}\ , \end{aligned} \tag{1.29}$$

where $\mathbf{P} = (p_1, p_2, p_3, p_4)$ and $\mathbf{q} = (r, \theta, \phi, \sigma)$, and are given by:

$$\begin{aligned} p_1 &= 2\left(r^{1/2}p_r\cos\frac{\theta}{2} - r^{-1/2}p_\theta\sin\frac{\theta}{2}\right)\cos\frac{\sigma+\phi}{2} - r^{-1/2}\frac{p_\phi+p_\sigma}{\cos\frac{\theta}{2}}\sin\frac{\sigma+\phi}{2} \\ p_2 &= 2\left(r^{1/2}p_r\cos\frac{\theta}{2} - r^{-1/2}p_\theta\sin\frac{\theta}{2}\right)\sin\frac{\sigma+\phi}{2} + r^{-1/2}\frac{p_\phi+p_\sigma}{\cos\frac{\theta}{2}}\cos\frac{\sigma+\phi}{2} \\ p_3 &= 2\left(r^{1/2}p_r\sin\frac{\theta}{2} + r^{-1/2}p_\theta\cos\frac{\theta}{2}\right)\cos\frac{\sigma-\phi}{2} + r^{-1/2}\frac{p_\phi-p_\sigma}{\sin\frac{\theta}{2}}\sin\frac{\sigma-\phi}{2} \\ p_4 &= 2\left(r^{1/2}p_r\sin\frac{\theta}{2} + r^{-1/2}p_\theta\cos\frac{\theta}{2}\right)\sin\frac{\sigma-\phi}{2} - r^{-1/2}\frac{p_\phi-p_\sigma}{\sin\frac{\theta}{2}}\cos\frac{\sigma-\phi}{2} \end{aligned} \tag{1.30}$$

where p_r, p_θ, p_ϕ and p_σ are the conjugate momenta. From the definition it follows that

$$p_1^2+p_2^2+p_3^2+p_4^2 = 4r\left(p_r^2 + \frac{p_\theta^2}{r^2} + \frac{p_\phi^2+p_\sigma^2}{r^2\sin^2\theta} - 2\frac{p_\phi p_\sigma}{r^2\sin^2\theta}\cos\theta\right). \tag{1.31}$$

Because σ is arbitrary we choose initially $\sigma = p_\sigma = 0$. Then as the Hamiltonian 1.25 is independent of σ, $p_\sigma = 0$ at all times and $\sum_{i=1}^4 p_i^2 = 4r\mathbf{p}^2$.

By applying the above transformation we can write Γ , equation 1.25, in the form of a pair of coupled 2-dimensional oscillators:

$$\begin{aligned} \Gamma &= \frac{1}{2}\mathbf{P}^2 + 4W\boldsymbol{x}^2 \equiv 4\ , \\ \boldsymbol{x}^2 &= x_1^2 + x_2^2 + x_3^2 + x_4^2\ . \end{aligned} \tag{1.32}$$

The equivalent reduction of Schrödinger's equation to two coupled oscillators may be achieved using group theoretical methods, see Delande and Gay (1984), but these methods appear to be less readily applicable in classical dynamics. Note that the value of Γ is constant. The equations of motion are now the 10 coupled equations

$$\frac{\mathrm{d}x_k}{\mathrm{d}\tau} = \frac{\partial\Gamma}{\partial p_k}\ ,\quad \frac{\mathrm{d}p_k}{\mathrm{d}\tau} = -\frac{\partial\Gamma}{\partial x_k}\ ,\quad k = 1,\ldots,4 \tag{1.33}$$

$$\frac{\mathrm{d}t}{\mathrm{d}\tau} = \frac{\partial\Gamma}{\partial W} = 4\boldsymbol{x}^2\ ,\quad \frac{\mathrm{d}W}{\mathrm{d}\tau} = -\frac{\partial\Gamma}{\partial t}\ , \tag{1.34}$$

where, because of the canonical transformation induced by the change from $\overline{\Gamma}$ to Γ, τ is not the same variable as in equation 1.24. In the absence of a field τ is the eccentric anomaly of the Kepler motion, equation 1.5

1.3.1 Inverse transformation: from regularised to cartesian coordinates

In chapters 3 and 4 we apply the above regularising transformation in order to study the dynamics of the hydrogen atom in a magnetic and in a microwave field respectively. The calculations performed also involve transforming back from regularised to cartesian coordinates. Here we outline the steps needed to obtain the inverse transformation and give the equations relating the two systems of coordinates.

Given the regularised coordinates $(x_i, p_i, i = 1, \ldots, 4)$, the cartesian position and momenta are given by:

$$\begin{aligned} x &= 2(x_1x_3 + x_2x_4) \\ y &= 2(x_2x_3 - x_1x_4) \\ z &= (x_1^2 + x_2^2) - (x_3^2 + x_4^2) \end{aligned} \tag{1.35}$$

and

$$\begin{aligned} p_x &= \frac{x}{2r^2}A + \frac{z}{2r^3}(x_1x_3 + x_2x_4)B - \frac{y}{2r^2\sin^2\theta}C \\ p_y &= \frac{y}{2r^2}A + \frac{z}{2r^3}(x_2x_3 - x_1x_4)B + \frac{x}{2r^2\sin^2\theta}C \\ p_z &= \frac{z}{2r^2}A + \frac{1}{2r^2}\left[(x_3^2 + x_4^2)(x_1p_1 + x_2p_2) - (x_1^2 + x_2^2)(x_3p_3 + x_4p_4)\right] , \end{aligned} \tag{1.36}$$

where

$$\begin{aligned} A &= x_1p_1 + x_2p_2 + x_3p_3 + x_4p_4 \\ B &= \frac{x_3p_3 + x_4p_4}{1 - \cos\theta} - \frac{x_1p_1 + x_2p_2}{1 + \cos\theta} \\ C &= x_1p_2 - x_2p_1 + x_4p_3 - x_3p_4 \\ \cos\theta &= z/r \ . \end{aligned}$$

When $\cos\theta = \pm 1$ the transformation 1.36 is singular and takes the following form:

$\cos\theta = +1$	$\cos\theta = -1$
$p_x = \frac{1}{2\sqrt{r}} p_3$	$p_x = \frac{1}{2\sqrt{r}} p_1$
$p_y = 0$	$p_y = 0$
$p_z = \frac{1}{2\sqrt{r}} p_1$	$p_z = -\frac{1}{2\sqrt{r}} p_3$

Equations 1.35 can be easily derived given the definition of regularised coordinates 1.26 and the relationship between cartesian and spherical coordinates

$$\begin{aligned} x &= r\sin\theta\cos\phi \\ y &= r\sin\theta\sin\phi \\ z &= r\cos\theta\ . \end{aligned} \tag{1.37}$$

Equations 1.36 are derived in the same way, given the relationships

$$\begin{aligned} p_r &= \frac{r^{-\frac{1}{2}}}{2}\left(p_1\cos\frac{\theta}{2}\cos\frac{\sigma+\phi}{2} + p_2\cos\frac{\theta}{2}\sin\frac{\sigma+\phi}{2} + p_3\sin\frac{\theta}{2}\cos\frac{\sigma-\phi}{2} + \right. \\ &+ \left. p_4\sin\frac{\theta}{2}\sin\frac{\sigma-\phi}{2}\right) \\ p_\theta &= \frac{r^{-\frac{1}{2}}}{2}\left(-p_1\sin\frac{\theta}{2}\cos\frac{\sigma+\phi}{2} - p_2\sin\frac{\theta}{2}\sin\frac{\sigma+\phi}{2} + p_3\cos\frac{\theta}{2}\cos\frac{\sigma-\phi}{2} + \right. \\ &+ \left. p_4\cos\frac{\theta}{2}\sin\frac{\sigma-\phi}{2}\right) \\ p_\phi &= \frac{r^{-\frac{1}{2}}}{2}\left(-p_1\cos\frac{\theta}{2}\sin\frac{\sigma+\phi}{2} + p_2\cos\frac{\theta}{2}\cos\frac{\sigma+\phi}{2} + p_3\sin\frac{\theta}{2}\sin\frac{\sigma-\phi}{2} + \right. \\ &- \left. p_4\sin\frac{\theta}{2}\cos\frac{\sigma-\phi}{2}\right) \end{aligned} \tag{1.38}$$

and

$$\begin{aligned} p_x &= p_r\sin\theta\cos\phi + \frac{p_\theta}{r}\cos\theta\cos\phi - \frac{p_\phi}{r\sin\theta}\sin\phi \\ p_y &= p_r\sin\theta\sin\phi + \frac{p_\theta}{r}\cos\theta\sin\phi + \frac{p_\phi}{r\sin\theta}\cos\phi \\ p_z &= p_r\cos\theta - \frac{p_\theta}{r}\sin\theta \end{aligned} \tag{1.39}$$

and equations 1.26 and 1.37. For example, by multiplying the first equation in 1.38 by $\sin\theta\cos\phi$ it is easy to verify that

$$\frac{x}{2r^2}A = p_r\sin\theta\cos\phi$$

and similarly

$$\frac{y}{2r^2}A = p_r \sin\theta \sin\phi \quad , \quad \frac{z}{2r^2}A = p_r \cos\theta \ ,$$

$$\frac{z}{2r^2}(x_1x_3 + x_2x_4)B = p_\theta \cos\theta \cos\phi \quad , \quad \frac{z}{2r^2}(x_2x_3 + x_1x_4)B = p_\theta \cos\theta \sin\phi \ ,$$

$$\frac{y}{2r\sin\theta}C = p_\phi \sin\phi \quad , \quad \frac{x}{2r\sin\theta}C = p_\phi \cos\phi \ ,$$

$$\frac{1}{2r}\left[(x_3^2 + x_4^2)(x_1p_1 + x_2p_2) - (x_1^2 + x_2^2)(x_3p_3 + x_4p_4)\right] = -p_\theta \sin\phi \ .$$

Apart from the first term, which is quite straightforward, all the others require some rather long and tedious applications of simple trigonometric formulae.

is an invariant torus. The *action variables* I_k $(k = 1, \ldots, N)$ are defined by:

$$I_k = \oint_{C_k} \mathbf{p} \cdot d\mathbf{q} \ , \tag{2.1}$$

where $\mathbf{p}$ and $\mathbf{q}$ are conjugate position and momentum coordinates and the C_k are N topologically independent closed curves on the torus that cannot be deformed to one point. In general the curves C_k are not classical trajectories. The motion on the torus is parametrised by the *angle variables* θ_k canonically conjugated to the actions I_k. The equations of motion for these variables are I_k = constant and $\theta_k = \omega_k t + \delta$, where $\omega_k = \partial H / \partial I_k$ is the angular frequency. If the ω_k are not rationally related, then a trajectory on the torus passes arbitrarily close to each point, i.e. the motion is ergodic on the torus, and the trajectories are not closed. If on the other hand there exist integers s_k such that

$$\sum_k s_k \omega_k = 0 \quad (s \neq o)$$

then there is a resonance and the trajectories are closed, i.e. the motion is confined to invariant tori of dimension lower than N. Resonances are of crucial importance when an integrable system is perturbed.

Let us consider a system H obtained by perturbing an integrable system H_0:

$$H(I, \theta) = H_0(I) + \varepsilon H_1(I, \theta) \quad 0 < \varepsilon \ll 1 \ . \tag{2.2}$$

The variables I are no longer constants of the motion for H. If invariant tori exist for this system, then there must be new action and angle variables (J, ϕ) such that $H(I, \theta) = H(J)$, where the new variables are given by a canonical transformation with generating function $S(J, \theta)$. The problem of finding invariant tori for 2.2 is then reduced to finding this generating function. In the non-degenerate case if $\varepsilon \ll 1$ a perturbative approximation gives:

$$S(J, \theta) = \theta \cdot J + i\varepsilon \sum_{\mathrm{m} \neq 0} \frac{H_{1\mathrm{m}}(\mathrm{J})}{m \cdot \omega_o(J)} e^{im \cdot \theta} + \mathcal{O}(\varepsilon^2) \ , \tag{2.3}$$

where $\omega_o(I)$ is the angular frequency on the unperturbed torus and $H_{1\mathrm{m}}(\mathrm{I})$

are Fourier coefficients in the expansion

$$H_1(I,\theta) = \sum_{\mathrm{m}} H_{1\mathrm{m}}(\mathrm{I}) e^{i\boldsymbol{m}\cdot\boldsymbol{\theta}} \ .$$

The convergence of 2.3 is then crucial to the existence of new invariant tori. If $\boldsymbol{m}\cdot\boldsymbol{\omega}_0 = 0$ for some m, the series diverges and the corresponding resonant torus is destroyed. Even for non-resonant frequencies, though, it is always possible to find some m for which $\boldsymbol{m}\cdot\boldsymbol{\omega}_0$ is arbitrary small. In many physical problems the motion of interest lies on tori that are not close to low order resonances, i.e. $\boldsymbol{m}\cdot\boldsymbol{\omega}_0$ is only small for very large $\boldsymbol{m}$, and for these large $\boldsymbol{m}$ the Fourier coefficients $H_{1\mathrm{m}}$ are very small, so that the series 2.3, truncated to a few terms in ε, was successfully used to predict long-time motion. Nevertheless these results do not prove anything about the existence of invariant tori, which concerns the motion for infinite times. The Kolmogorov-Arnold-Moser (KAM) theorem (see Arnold 1978) established a condition for the existence of perturbed invariant tori for the Hamiltonian 2.2 in the limit of small perturbations, by proving the convergence of an accelerated iteration-perturbation process for the torus generator S, for all initial tori whose frequency ratios are 'sufficiently' irrational. The condition for the convergence of this process is:

$$| \boldsymbol{m}\cdot\boldsymbol{\omega}_0 | \geq \gamma \, | \boldsymbol{m} |^{-\nu} \qquad \forall \boldsymbol{m} \tag{2.4}$$

where ν is a constant dependent on the number of degrees of freedom and on the smoothness of H_1, and γ increases with ε and $| H_1 |$ and also depends on the nonlinearity of the unperturbed Hamiltonian H_0. The theorem was proved by Arnold (1961, 1962) for analytic H_1, following a conjecture by Kolmogorov (1954), and by Moser (1962) for H_1 possessing a sufficient number of continuous derivatives. Thus for sufficiently small perturbations ($\varepsilon \ll 1$) those invariant tori which are sufficiently far from a resonance are preserved, albeit slightly distorted. The invariant tori of the perturbed system are continuous deformations of the unperturbed tori. We can see from the KAM condition that the gaps around resonances where invariant tori might not exist are bigger for lower order resonances. The KAM theorem

does not tell us anything about these gaps. We shall see later by using the formalism of canonical maps how resonant tori are destroyed and give rise to a rich and complicated dynamics.

2.2 Adiabatic invariance

By applying the adiabatic method EBK quantisation can still be carried out when the invariant tori start being destroyed. The principle of adiabatic invariance has a long history and was of crucial importance in the development of the old quantum theory (Ehrenfest 1916). Its application to the study of Hamiltonian systems was proposed by Solove'v (1978), who later used it to determine energy levels of a hydrogen atom in crossed electric and magnetic fields (Grozdanov and Solove'v 1982). The adiabatic method has subsequently been applied to a number of Hamiltonian systems and tested by a variety of workers (Johnson 1985, Skodjie *et al.* 1985, Grozdanov et al. 1986, Taylor and Grozdanov 1987). Dana and Reinhardt (1987) have applied it to the Standard Map. All these applications of the adiabatic method are for non-degenerate systems, while here the method is applied to a degenerate system.

Adiabatic invariants occur when the Hamiltonian is a slowly varying function of time, or when one component of the motion is oscillating much more rapidly than others. Here we only deal with the former case. Expressing the slow time variation in the form

$$H = H(\mathbf{q}, \mathbf{p} : \lambda), \quad \lambda = \varepsilon t, \ | \varepsilon | \ll 1 \ , \tag{2.5}$$

where H is the Hamiltonian explicitly dependent upon the parameter λ, the quantity $\mathbf{F}(t) = \mathbf{F}(\mathbf{q}, \mathbf{p} : \lambda)$ is an adiabatic invariant if

$$| \mathbf{F}(0) - \mathbf{F}(t) | < \kappa\varepsilon, \quad 0 < t < 1/\varepsilon \ , \tag{2.6}$$

for some constant, κ, independent of ε: for a more rigorous definition see Arnold (1978, page 298). Note that adiabatic invariants are not constant but usually oscillate about a slowly varying mean value with amplitude $O(\varepsilon)$

with a period approximately that of the unperturbed (λ = constant) motion; see for example Arnold (1978) and Percival and Richards (1982). Ehrenfest (1916) assumed, but did not prove, that when they exist the action variables are adiabatic invariants.

A rigorous proof of this theorem exists only for one-freedom systems (Arnold 1962, see also Percival and Richards 1982) since for many-freedom systems small divisors destroy a crucial assumption of the theory, as explained below. However, numerical evidence suggests that for many systems and for reasonable values of ε the initial and final values of the action are, on average, numerically similar even in the 'weakly' irregular region.

In general the Hamiltonian can be written in the form

$$H(\mathbf{q},\mathbf{p}:\lambda) = H_0(\mathbf{q},\mathbf{p}) + \lambda H_1(\mathbf{q},\mathbf{p}) , \quad 0 \le \lambda \le 1 , \tag{2.7}$$

where $H_0(\mathbf{q},\mathbf{p})$ is an integrable Hamiltonian with angle-action variables $(\boldsymbol{\theta},\mathbf{I})$. In order to exploit the principle of adiabatic invariance we assume that in the relevant region of phase space H has angle-action variables $(\boldsymbol{\phi},\mathbf{J})$, parametrically dependent upon λ, which reduce to $(\boldsymbol{\theta},\mathbf{I})$ when $\lambda = 0$; that is, the tori of H are topologically similar to those of $H(\lambda)$. In practice small divisors destroy this similarity so making rigorous proofs difficult, but when most of the tori of $H(\lambda)$ are similar to those of H the numerical approximation works well.

We replace $H(\mathbf{q},\mathbf{p}:\lambda)$ by a related time-dependent Hamiltonian:

$$K(\mathbf{q},\mathbf{p},t) = H_0(\mathbf{q},\mathbf{p}) + f(s)H_1(\mathbf{q},\mathbf{p}), \quad s = t/T \tag{2.8}$$

where $f(s)$ is some smooth function with $f(s) = 0$ for $s \le 0, f(s) = 1$ for $s \ge 1$, $f'(0) = f'(1) = 0$ and $f'(s) > 0$ for $0 < s < 1$. The precise choice of $f(s)$ is irrelevant if the principle of adiabatic invariance is valid and if T is sufficiently large by comparison with the fundamental periods of $H(\lambda)$. Numerical studies (Johnson 1985) confirm this.

In principle we want to evolve an initial torus, $\tau(0)$, labelled by the initial actions,

$$\mathbf{I} = (\mathbf{n} + \boldsymbol{\gamma})\hbar , \quad t = 0 \tag{2.9}$$

to a time $t = T$: according to the adiabatic principle $\tau(0)$ should evolve to a torus $\tau(1)$ of $H(1)$ with actions $\mathbf{J} = (\mathbf{n} + \gamma)\hbar$, through all intermediate tori $\tau(\lambda), 0 \leq \lambda \leq 1$. However, each intermediate Hamiltonian, $H(\lambda)$, will generally have resonant islands and the passage of τ through these will produce in places a complicated convoluted surface. Usually these convolutions are not too serious as the very numerous higher-order resonances, which have long periods, are, for analytic Hamiltonians, very narrow and so for not too large values of T the torus $\tau(\lambda)$ passes through each resonance relatively rapidly, so these do not distort τ seriously. The lower-order resonances cause more serious convolutions, but there are fewer of these and usually they can be avoided, see Skodje et al. (1985), Taylor and Grozdanov (1987) and below. When the resonances become very dense, problems arise, but this is when the classical motion becomes chaotic and the tori no longer exist. The method has intrinsic checks for this occurrence.

In practice we cannot easily evolve whole tori, but only orbits on it. An individual orbit initially on $\tau(0)$ will at time $t = T$ lie close to $\tau(1)$ so at this time its energy is an approximation to

$$E(\mathbf{n}) = H(\mathbf{J}; \lambda) , \quad \lambda = 1 . \tag{2.10}$$

If the chosen orbit managed to avoid all resonances this would be a good approximation to $E(\mathbf{n})$ and the errors would be $O(1/T)$ or smaller. But, as it is not known how much an individual orbit is affected by resonances, it is necessary to integrate an ensemble of N orbits with initial conditions distributed uniformly over $\tau(0)$. Then the variation, σ, of the final energies provides an estimate of the effects of the resonances and the means are estimates of $E(\mathbf{n})$:

$$E(\mathbf{n}) = \frac{1}{N} \sum_{k=1}^{N} E_k , \tag{2.11}$$

$$\sigma^2 = \frac{1}{N} \sum_{k=1}^{N} (E_k - E(\mathbf{n}))^2 , \tag{2.12}$$

E_k being the final energy of the kth orbit and N being the total number of orbits. It should be pointed out here that equation 2.11 gives the same

result as first order perturbation theory. To see this, let us consider again the time-dependent Hamiltonian $K(\mathbf{q},\mathbf{p},t)$, equation 2.8. The time independent terms $H_0(\mathbf{q},\mathbf{p})$ and $H_1(\mathbf{q},\mathbf{p})$ can be expressed as functions of action and angle variables by:

$$H_0 = H_0(\mathrm{I}) \tag{2.13}$$

$$H_1 = H_1(I,\theta) = \sum_{k} V_{\mathrm{k}} e^{ik\cdot\theta} , \tag{2.14}$$

and the variation of K over the time interval $(0,T)$ is:

$$K(\mathbf{q},\mathbf{p},T) - K(\mathbf{q},\mathbf{p},0) = \int_0^T \frac{\partial K}{\partial t} dt = \int_0^T f' H_1 \tag{2.15}$$

$$= \sum_{k} \int_0^T V_{\mathrm{k}}(\mathrm{I}) e^{ik\cdot\theta} f' dt . \tag{2.16}$$

Let us now use perturbation theory. By assuming $K(T)-K(0)$ small, both I and θ can be replaced by unperturbed values so, given $\theta = \omega t+\delta = \omega t+\theta_0$, the variation of K is

$$K(\mathbf{q},\mathbf{p},t) - K(\mathbf{q},\mathbf{p},0) = \sum_{k} V_{\mathrm{k}}(\mathrm{I}) e^{ik\cdot\theta_0} \int_0^T f' e^{ik\cdot\omega t} dt . \tag{2.17}$$

The integral in 2.17 can be evaluated as follows. Consider integrals of the form

$$J = \int_0^{1/\varepsilon} e^{i\Omega t} \frac{df}{dt} dt .$$

Assuming $\Omega \neq 0$ and implementing the change of variable $x = \varepsilon t$ gives:

$$J = \int_0^1 e^{i\Omega x/\varepsilon} \frac{df}{dx} dx =$$

$$= \frac{\varepsilon}{i\Omega} \left[e^{i\Omega x/\varepsilon} f^{(1)} \right]_0^1 - \frac{\varepsilon}{i\Omega} \int_0^1 e^{i\Omega x/\varepsilon} f^{(2)} dx .$$

As $f^{(1)}(0) = f^{(1)}(1) = 0$, $J = O(\varepsilon^2)$. Similarly if $f^{(2)}(0) = f^{(2)}(1) = 0$, $J = O(\varepsilon^3)$ and if $f^{(p)}(0) = f^{(p)}(1) = 0$ then $JO(\varepsilon^{p+1})$. If $\Omega = 0$ this analysis is invalid. In this case $J = f(1) - f(0) = 1$. Now, assuming $| k\cdot\omega | > \varepsilon$, $k \neq 0$ and applying the result obtained above to 2.17, we get

$$K(T) - K(0) = V_0(\mathrm{I}) = < K_1 > , \tag{2.18}$$

which is the result of first order perturbation theory.

In chapter 3 the adiabatic method is used successfully to calculate the energy levels for the hydrogen atom in a magnetic field. In chapter 5 it is applied to a canonical map specifically constructed to simulate the dynamics of the hydrogen atom in a microwave field.

Previous applications of the adiabatic method have concentrated on model systems. A number of authors have studied slightly different forms of the 2-dimensional system consisting of two non-linearly coupled harmonic oscillators (Johnson 1985, Skodjie et al. 1985, Grozdanov et al. 1986). All authors find semiclassical energy levels in good agreement with other semiclassical and quantal calculations in the regions where the systems are still fairly regular and mainly for low-lying energy levels. Skodjie et al. (1985) point out that the adiabatic method imposes no limitation on the number of degrees of freedom and apply it to two 4- and 5-dimensional analogues of the Hénon-Heiles system. The applicability of the adiabatic method to systems with any degree of freedom is of great importance, as this is the only semiclassical method that can be easily used for systems of two or more degrees of freedom. Skodjie and Borondo (1986) study 1- and 2-dimensional Morse oscillators up to the chaotic regime. They compare semiclassical and quantal wavefunctions and show that semiclassical wavefunctions exhibit regular nodal patterns, in agreement with the quantum wavefunctions, even when the corresponding classical trajectories are chaotic. A systematic study to determine the best form of the switching function is carried out by Johnson (1985), who compares 5 different functions by testing them on the 1-dimensional forced harmonic oscillator

$$H = \frac{1}{2}(p^2 + \omega^2 q^2) + f(t)\lambda q \ , \tag{2.19}$$

where $f(t)$ is a switching function which changes monotonically over the time interval $0 \leq t \leq T$ and has the values $f(0) = 0$ and $f(T) = 1$, and the parameter λ determines the strength of the perturbation. He defines a non-adiabaticity parameter $U(T)$, by

$$U(T) = \int_0^T f'(t) e^{-i\omega t} dt \ , \tag{2.20}$$

where $f'(t)$ is the first derivative of the switching function. The parameter $U(T)$ is proportional to the energy uncertainty σ, equation 2.12. An approximate upper bound to $U(T)$ is calculated for each switching function. As expected the linear function gives the worst results, while other functions continuous through the second or third derivatives produce smaller departures from adiabaticity (between two and three orders of magnitude smaller than the linear function for an adiabatic switch lasting up to 70 periods) and converge much faster to the adiabatic limit as T increases. The value of the non-adiabaticity parameter is similar for all these functions. The intrinsic non-adiabaticity caused by the passage through resonances is investigated by Dana and Reinhardt (1987) in the adiabatically switched standard map:

$$\begin{aligned} I_{n+1} &= I_n + K f(n/2N) \sin\theta_n \\ \theta_{n+1} &= \theta_n + I_{n+1} \ , \end{aligned} \tag{2.21}$$

where K is the stochasticity parameter, N is a large integer and $f(n/N)$ is a discrete switching function. The authors define the nonadiabaticity $\Delta J(N)$ as

$$\Delta J(N) = \left(\frac{1}{2\pi} \int_0^{2\pi} \left(F(\theta; J, 2N) - J \right)^2 \, d\theta \right)^{1/2} \ , \tag{2.22}$$

where J is the action of the initial unperturbed torus and F is defined by the adiabatic curve $C_n = (I_n, \theta_n)$ obtained after n iterations ($n \leq 2N$):

$$\begin{aligned} I_n &= F(\theta; J, n) \\ \theta_n &= G(\theta; J, n) \ . \end{aligned} \tag{2.23}$$

Adiabatic invariance is satisfied if $\Delta J(N) \to 0$ as $N \to \infty$. During the switching process 2.21 the instantaneous frequency or winding number changes, in the sense that tori of action J at different values of K are generally associated with different winding numbers. Thus the curve 2.23 necessarily crosses regions of island chains, associated with rational winding numbers p_i/q_i. Numerical calculations by Dana and Reinhardt (1987) indicate that the nonadiabaticity 2.22 tends to a non-vanishing value (the "intrinsic nonadiabaticity") as $N \to \infty$ if the duration of the crossing is of the same order

of a time scale $T_i \sim q_i K_i^{-q_i/2}$, where K_i is the value of K at the crossing. The value of this intrinsic adiabaticity is found to be nearly proportional to the width of the main island chain crossed, provided the other island chains crossed have much smaller widths. The island chains crossed are determined by the authors from the Farey tree in an interval containing the range of variation of the winding numbers.

Recently Brown et al. (1987) have obtained rigorous results for the error in the adiabatic approximation in the case of ergodic Hamiltonian systems, i.e. systems whose motion ergodically covers the energy surface. Given a slowly time-dependent, $N-$dimensional ergodic system with Hamiltonian $H(\mathbf{q}, \mathbf{p}, t)$, they consider the volume inside the surface $H =$ constant

$$\mu(E,t) = \int\int U[E - H(\mathbf{q}, \mathbf{p}, t)] d^N q d^N p \,, \tag{2.24}$$

where U is the unit step function and E is the energy. The volume μ is an adiabatic invariant. Given an initial condition and the corresponding energy $E = E_0$ at $t = 0$, an approximation to the energy at all subsequent times is obtained via $\mu(E,t) = \mu(E_0, 0)$. The error in this approximation at time T is measured by the averaged distance of the energy surfaces at $t = 0$ and $t = T$. This is found to depend on the behaviour of a certain correlation function $C(t)$ involving the orbits of the time-dependent Hamiltonian. Their theory predicts that:

1. if $\int_0^\infty C(t)dt < \infty$, then the error scales like T^{-1},
2. if $C(t) \to t^{-1}$ for $t \to \infty$, then the error scales like $T^{-1} \ln T$,
3. if $C(t) \to t^{-\xi} (0 < \xi < 1)$ for $t \to \infty$, then the error scales like $T^{-\xi}$.

In the case of non-ergodic Hamiltonian systems, i.e. when there exist invariant tori, no rigorous result is obtained, although numerical calculations for a particular example of non-ergodic Hamiltonian

$$H = p_x^2 + p_y^2 + f(t)x^2 + y^2 + x^2 y^2$$

give an approximate fit to a power law for the error.

Chapter 3

The hydrogen atom in a magnetic field

3.1 Introduction

The hydrogen atom in a magnetic field is one of the simplest problems in atomic physics which appears to be non-integrable, yet it is still a long way from being completely understood. Although the paramagnetic interaction has been understood for a long time, the effects of the diamagnetic interaction, which causes the Hamiltonian to be non-separable, require further investigation and are the subject of much current work. A complete understanding of this problem is of great importance in astrophysics, where the observed magnetic fields are very high (see for example Angel 1977), and in the interpretation of photoabsorption spectra of Rydberg atoms.

Extensive work, both theoretical and experimental, has been done in the weak field regime, where the ratio of the mean magnetic force and the mean Coulomb force is small. In this regime there exists an approximate spherical symmetry, which is related to the existence of an adiabatic invariant (Solov'ev 1981)

$$\Lambda = 4A^2 - 5A_z \ , \tag{3.1}$$

where $\mathbf{A} = (A_x, A_y, A_z)$ is the Runge-Lenz vector defined earlier (equation 1.3). The quantum mechanical operator corresponding to Solov'ev's invariant was obtained independently by Herrick (1982) using group theory. Wintgen and Friedrich (1986) show that, as a consequence of this result, it is possible to find a representation in which the Hamiltonian for this problem

is approximately separable. Investigations have shown that at low fields the classical trajectories are quasi-periodic. This regime has been investigated using a variety of classical, semiclassical and quantal methods (see for example Clark and Taylor 1982, Delos *et al.* 1983). For very high fields, where the mean magnetic force is much bigger than the mean Coulomb force, the dynamics of the motion approaches that of a free charged particle in a magnetic field and there exists an approximate cylindrical symmetry. Classically an electron moving in a uniform magnetic field B describes a helical orbit whose axis is along the field direction with constant radius $r = p_t/(eB)$, where p_t is the projection of the linear momentum onto the plane perpendicular to the field. If z is the direction of the field, the projection p_z is also a constant of the motion, as can be seen by transforming into cylindrical polar coordinates where the coordinate z does not appear explicitly in the Hamiltonian. The energy of the electron is $E = (k + 1/2)\hbar\omega_c + p_z^2/2m_e$, where ω_c is the cyclotron frequency. The separation of Landau energy levels is $\hbar\omega_c$. In the intermediate regime, where the magnetic and Coulomb forces are of comparable strength, no dynamical symmetries exist and no perturbative approach can be valid. Very little is known about this regime. The very different symmetries of the forces responsible for the non-separability of the problem suggest that the motion might be completely featureless, but experiments in this regime (Garton and Tomkins 1969) have demonstrated the existence of regular features in the spectrum, later called quasi-Landau resonances. The separation between these observed peaks is roughly $1.5\hbar\omega_c$. These peaks have been widely interpreted (Castro *et al.* 1980, Holle *et al.* 1986) as resonant photoabsorption into quantum states correlated to classical periodic orbits in the plane perpendicular to the magnetic field. One-dimensional semiclassical calculations of the spectrum of such states (Edmonds 1970, Gallas *et al.* 1980) have obtained a $1.5\hbar\omega_c$ spacing for levels near the zero-field threshold, but these theories have been much less successful in estimating absolute values of the energy levels.

Most available experimental results deal with alkali atoms (see for example Castro *et al.* 1980, Delande and Gay 1981, Welch *et al.* 1989) and

only recently have experiments been performed on hydrogen atoms (Holle *et al.* 1986 and 1988, Wiebusch *et al.* 1989). These experiments are mainly restricted to the strong field regime, apart from the recent work by Holle *et al.* (1988) which explore the spectrum of the hydrogen atom from the regular into the chaotic regime. Numerical diagonalisation of the Hamiltonian has been performed using a basis of spherical functions (Zimmerman *et al.* 1980, Castro *et al.* 1980) or, following Edmonds (1973), of Sturmian functions (Clark and Taylor 1982, Delande and Gay 1986a,b). These methods are based on expanding the solution of the Schrödinger equation in eigenstates of angular momentum:

$$\psi_{nm}(\mathbf{r}) = \frac{1}{r} \sum_{l \geq |m|}^{\infty} \Phi_l^{nm}(r) \Theta(lm) \Phi(m) \tag{3.2}$$

The radial functions $\Phi_l^{nm}(r)$ are then represented either in terms of the spherical functions $R_{nl}(r)$ associated with the bound states of the unperturbed hydrogen atom, or in terms of some other set of functions. This representation therefore is not complete, since it does not include the continuum. It is nevertheless useful in the low field regime. The continuum can be included by using a basis of Sturmian functions (Rotenberg 1962, 1970)

$$S_{sl}(r) = \left(\frac{(s-l-1)!}{2(s+l)!} \right)^{1/2} \exp(-r)(2r)^{l+1} L_{s-l-1}^{2l+1}(2r) \,, \tag{3.3}$$

where $s = l+1, l+2, \ldots$, and $L_{s-l-1}^{2l+1}(2r)$ are generalised Laguerre polynomials (see for example Abramowitz and Stegun 1965). Typically 1000 or more basis states are required to obtain good convergence. These calculations are expensive computationally, so a more efficient method has been developed by Delande and Gay (1986a), which exploits the dynamical symmetries of the Hamiltonian to define a more convenient basis set. By using a set of symmetrised Sturmian functions Delande and Gay (1986a) obtain accurate values of the energy levels with a basis of less than a 100 states. Their method has been shown to be accurate in the strong field regime, but as the field increases the convergence of the eigenvalues in the Sturmian basis is destroyed. Earlier works investigated this regime by using a model in which

the electron is confined to the plane perpendicular to the magnetic field (Edmonds 1970, Starace 1973). This, however, is unsatisfactory in view of recent evidence (Holle *et al.* 1986) that periodic trajectories outside the z=0 plane play a major role in the interpretation of quasi-Landau resonances in observed spectra.

As an apparently non-integrable system the hydrogen atom in a magnetic field is expected to show a classical transition from regular to chaotic motion. Understanding its dynamics in the strong field regime can therefore provide great insight into the quantal manifestations of classical chaos. Evidence of the classical transition has been shown in various works using surface of section plots (Edmonds and Pullen 1980a, b and c, Robnik 1981, Harada and Hasegawa 1983, Delande and Gay 1986b) and very recently the stability of some classical periodic orbits has been studied by calculating the Liapunov exponents (Wintgen 1987b). The analysis of the statistical properties of quantal level spectra has been proposed (Mc Donald and Kaufmann 1979, Bohigas *et al.* 1984) as a means of identifying a quantal analogue of the classical transition. The distribution of energy level spacings has been shown to change from Poisson to Wigner type over the range of parameters for which the classical transition occurs (Delande and Gay 1986b, Wintgen and Friedrich 1986), as was suggested by Berry (1985). Statistical distributions of energy levels based on random matrix theory compare very well with available experiments, however a recent work (Wintgen 1987a) has pointed out the existence of long-range correlations which are directly connected to classical periodic orbits and cannot be described by random matrices. Thus a better understanding of the classical dynamics and of the stability of orbits can provide a powerful tool for direct comparison between classical and quantal dynamics.

Here we apply a method based on the principle of adiabatic invariance to obtain the energy levels of the hydrogen atom over a wide range of magnetic field strength, from the weak into the strong field regime.

The application of this method to the quadratic Zeeman effect is particularly interesting as a test of the method for several reasons. First, the

unperturbed Hamiltonian is degenerate so care has to be taken with the initial conditions, moreover one of the fundamental frequencies is initially zero and this seems to contradict the assumptions of adiabatic invariance. We show that in practice this causes no problems if the initial conditions are chosen correctly. Second, the unperturbed Hamiltonian has both librational and rotational motion; the zero-frequency motion on the separatrix again would suggest a break-down of this method. In practice this seems to cause no problems, although quantisation in the region of the separatrix is less accurate. Finally, for high fields this system is dominated by chaotic trajectories. In this region no semiclassical quantisation method has yet been found. We show that for this problem the adiabatic method provides a reliable method for fields up to the region where chaotic motion dominates.

The method is described in section 2. In section 3 we give the results of our numerical calculations and comparisons are made with results obtained by other authors.

3.2 Theory

We find approximate semiclassical energy levels by constructing approximate quantised invariant tori using the principle of adiabatic invariance. The method is described in chapter 3. For the problem considered here we can use the time-dependent Hamiltonian

$$K(\mathbf{q},\mathbf{p},t) = H_0(\mathbf{q},\mathbf{p}) + f(s)H_1(\mathbf{q},\mathbf{p}) \ , \tag{3.4}$$

where $s = t/T$, T being the length of the adiabatic switch, H_0 is the Coulomb Hamiltonian, equation 1.2, and

$$H_1 = \frac{1}{2}\alpha \mathbf{L}\cdot\mathbf{B} + \frac{1}{8}(\alpha B)^2(x^2+y^2) \ ,$$

with $\alpha = e/\mu c$, c being the speed of light. We use the adiabatic switch function

$$f(s) = \begin{cases} 0 & s \leq 0 \\ s^2(2-s^2) & 0 \leq s \leq 1 \\ 1 & 1 \leq s \end{cases} ,$$

We follow the method described in chapter 2 and integrate from $t = 0$ to $t = T$ an ensemble of N orbits with initial conditions uniformly distributed over an initial invariant torus $\tau(0)$ labelled by the initial actions

$$\mathrm{I} = (\mathrm{n} + \gamma)\hbar \ , \quad t = 0 \ . \tag{3.5}$$

An estimate of the energy at time $t = T$ is then given by the mean of the final energies of the orbits:

$$E(\mathrm{n}) = \frac{1}{N} \sum_{k=1}^{N} E_k \ , \tag{3.6}$$

and a measure of the nonadiabaticity caused by the resonances is given by the variation, σ, of the final energies:

$$\sigma^2 = \frac{1}{N} \sum_{k=1}^{N} (E_k - E(\mathrm{n}))^2 \ . \tag{3.7}$$

In order to apply this method to the QZE there are two subsidiary problems which need prior attention. First, we need an initial torus, $\tau(0)$, labelled by the action variables of the unperturbed system; but this is the Coulomb Hamiltonian, equation 11 below, and is degenerate so has infinitely many sets of angle-action variables: so it is necessary is to chose the correct variables. As in classical degenerate perturbation theory, see Born (1960), this choice is made by finding the angle-action variables of the averaged Hamiltonian, that is the Hamiltonian in the 'slow' variables, obtained by averaging over the 'fast' variables - in this case the electron motion around the unperturbed Kepler ellipse. This is directly equivalent to the diagonalisation of the quantal secular equation, see Landau and Lifshitz (1965, page 133). The second problem is the numerical integration of Hamilton's equations: the Coulomb singularity causes serious inefficiencies and we have found, in other problems (Leopold and Richards 1985, Rath and Richards 1990) that removal of this singularity by regularisation improves numerical efficiency considerably. This method was first used for the quadratic Zeeman effect by Edmonds (1970) but for $m = 0$; for $m \neq 0$ a different transformation is necessary, which is given in chapter 1.

3.2.1 Initial Conditions

The Hamiltonian for an electron of charge e, mass μ, moving in a Coulomb potential centred at the origin and a static magnetic field B, along the z-axis is given by equation 1.20 above. It is convenient to remove the term linear in B by observing the system in a reference frame rotating in a positive sense about the z-axis at the Larmor frequency, $\omega_L = \alpha B/2$, so the Hamiltonian becomes

$$H = H_0 + \frac{1}{8}\mu(\alpha B)^2(x^2 + y^2) , \tag{3.8}$$

$$H_0 = \frac{1}{2\mu}p^2 - \frac{e^2}{r} . \tag{3.9}$$

Since only this Hamiltonian will be used the same symbols have been kept to denote the coordinates in the rotating frame. A uniform magnetic field will cause the orbits to be compressed in the direction perpendicular to the field and will have little effect in the field direction. The Kepler ellipse will precess in space. If the period of precession is long compared to the electron period, the action I_n is an adiabatic invariant and we can approximate the motion by averaging over the 'fast' variables (I_n, θ_n). The averaged Hamiltonian, obtained by taking the mean of the perturbation over one unperturbed orbit, can be conveniently written as:

$$H = H_0 + \frac{1}{8}\mu(a\alpha B)^2\overline{H}(\theta_l, I_l) , \tag{3.10}$$

where $\overline{H}(\theta_l, I_l) = < x^2 + y^2 >_{\theta_n} a^{-2}$. The energy levels in this approximation are then given by:

$$H = -\frac{1}{2I_n^2} + \frac{1}{8}\mu(a\alpha B)^2\overline{H}(J_k) , \tag{3.11}$$

J being the action variable of $\overline{H}$.

It is shown by Richards (1983) that, apart from a constant, the averaged Hamiltonian can be written in the form,

$$\overline{H} = \frac{5\gamma^2 \sin^2\theta}{2p^2} + \frac{5\cos^2\theta}{2} - \frac{p^2(3 + 5\cos 2\theta)}{4} - \frac{\gamma^2(3 - 5\cos 2\theta)}{4} , \tag{3.12}$$

where $p = I_l/I_n, \gamma = I_m/I_n = m/n, \theta = \theta_l$. The Hamiltonian $\overline{H}$ describes the mean motion of the magnitude of the angular momentum and the direction of the perihelion. It is the same as the adiabatic invariant Λ introduced by Solov'ev (1981), equation 3.1 but expressed in different variables. For $\gamma < 1/\sqrt{5}$ there are two types of motion depending upon the mean energy $\overline{E}$: for $\gamma\sqrt{5} - 2\gamma^2 < \overline{E} < E_s = (1+\gamma^2)/2$ the motion is libratory about the centres $\theta = \pi/2, 3\pi/2, p^2 = \gamma\sqrt{5}$ and the amplitude of the motion in the θ-direction is relatively small, see below. For $E_s < E < (5-3\gamma^2)/2$ the motion is rotational. The separatrix, that is the contour of $\overline{H}$ with energy E_s separating rotational from librational motion, has equation

$$p(\theta) = \frac{\gamma\sqrt{5}\sin\theta}{(1-5\cos^2\theta)^{1/2}}\ , \quad \theta_s \le \theta \le \pi - \theta_s\ , \tag{3.13}$$

where

$$\sin\theta_s = 2[5(1-\gamma^2)]^{-1/2}\ , \quad 0 \le \theta_s \le 2/\pi\ , \tag{3.14}$$

with a similar equation for the separatrix surrounding $\theta = 3\pi/2$.

The librational motion corresponds to oscillations about the minimum energy, $E = \gamma\sqrt{5} - 2\gamma^2$. On these orbits the angular momentum oscillates about $I_l \sim 5^{1/4}(I_n I_m)^{1/2}$ so the eccentricity is always close to unity, $\varepsilon \simeq 1 - 5^{1/2} I_m/I_n$, and as $\theta_l \sim \pi/2$ or $3\pi/2$ the angle between the Runge-Lenz vector and the z-axis is small, approximately $(I_m/I_n)^{1/2}5^{-1/4}$; the Kepler ellipse is elongated and aligned along the z-axis. At the other extreme, on the rotational motion close to the maximum energy, $E = (5-3\gamma^2)/2$, θ_l lingers about 0 and π (see figure 3 or 4 of Richards 1983), $I_l \sim I_n$, so the orbits are nearly circular and the electron spends most of the time close to the $0xy$-plane, in contradistinction to the librational motion for which $x^2 + y^2$ is always very small. This illustrates why the librational states are affected very little by the field and are therefore the states of lowest energy. The rotational states on the other hand are affected most. For $\gamma > 1/\sqrt{5}$ there is only the rotational motion.

For the present work we need a set of N points uniformly distributed on the quantised tori of $\overline{H}$; so we need the angle-action variables (ϕ, J) in each region. The action variable is relatively easy to determine: in the rotational

region we need to solve the implicit equation,

$$\int_0^{2\pi} d\theta\ p(\theta, \overline{E}_k) = 2\pi(n-k)/n \ \ , \ k = 2K_{max}+1, \ldots, n-m \qquad (3.15)$$

where K_{max} is an integer proportional to the area $\mathcal{A}$ enclosed by the separatrix,

$$\mathcal{A} = \frac{n}{2\pi}\left[\pi - 2\sin^{-1}\frac{2}{5\sqrt{1-\gamma^2}} - 2\gamma\sin^{-1}\sqrt{\frac{1-5\gamma^2}{1-\gamma^2}}\right] , \qquad (3.16)$$

and where $J_k = k\hbar/n$ and the integer label k is chosen to be largest for the highest energy level. In the librational region

$$\oint d\theta\ p(\theta, \overline{E}_k) = 2\pi(k+\frac{1}{2})/n \ \ , \quad k = 1, \ldots, K_{max} \ , \qquad (3.17)$$

and the energy levels are doubly degenerate, corresponding to motion about the centres $\theta = \pi/2$ and $\theta = 3\pi/2$ respectively.

In both cases $p(\theta, \overline{E})$ is an appropriate root of $\overline{H}(\theta, p) = \overline{E}$. The angle variable, ϕ, is most conveniently defined in the rotational region by

$$\phi(\theta) = -\Omega\int_0^{\theta} d\theta\ \frac{\partial p(\theta, \overline{E})}{\partial E} \ \ , \quad \Omega = \frac{\partial \overline{E}}{\partial J} \ , \qquad (3.18)$$

so that $\phi(\theta) = \theta + f(\theta)$, $f(\theta)$ being a periodic function of θ with zero mean value. Then the N equally spaced values of ϕ in the range $(0, 2\pi)$ give N values of θ, $\theta_r, r = 1, \ldots, N$, satisfying

$$\int_{\theta_r}^{\theta_{r+1}} d\theta\ \frac{\partial p(\theta, E)}{\partial E} = -\frac{\pi}{2N\Omega} \ \ , \quad E = E_k \ , \qquad (3.19)$$

for each k. Arbitrarily we chose $\phi_1 = \theta_1 = 0$. The angle variable in the librational region is defined by

$$\phi(\theta) = -\Omega\int_{\theta_{min}}^{\theta} d\theta\ \frac{\partial p(\theta, E)}{\partial E} \ , \qquad (3.20)$$

where θ_{min} is the minimum of the function

$$\theta(p, E_k) = \sin^{-1}\left(\frac{4p^4 - p^2(\gamma^2+5-2E)}{5(p^4 - p^2(\gamma^2+1)+\gamma^2}\right)^{1/2} . \qquad (3.21)$$

The N values of θ corresponding to a uniform distribution in ϕ are then obtained from equation 3.20 with the choice $\phi_1 = 0, \theta_1 = \theta_{min}$. In this case $p(\theta, E)$ is double-valued, so the numerical search for the zeroes of equation 3.20 is carried out on both branches.

The set of variables $\theta_r, p_r(\theta_r, E_k)$ $r = 1, \ldots, N$, together with M equally spaced values of θ_n and the actions I_n and I_m provide our initial conditions which uniformly sample the initial torus of each energy level.

The action variables of the unperturbed motion are related to the parameters determining the shape and orientation of the Kepler ellipse by:

$$a = \frac{I_n^2}{\mu e^2} \ , \quad \varepsilon^2 = 1 - \frac{I_l^2}{I_n^2} \ , \quad \cos\beta = \frac{I_m}{I_l} \ , \tag{3.22}$$

where a is the semi-major axis and ε the eccentricity of the ellipse on which the electron moves, and β is the angle between the angular momentum vector and the z-axis. The conjugate angle variables are:

$$\theta_n = \omega t + \text{constant} = u - \varepsilon \sin u \tag{3.23}$$

$$\theta_l = \text{angle between the perihelion and the line of nodes} \tag{3.24}$$

$$\theta_m = \text{angle between the } x-\text{axis and the line of nodes} \tag{3.25}$$

3.2.2 Regularisation

By using the dimensionless variables defined in chapter 1, equation 1.20, the Hamiltonian 1.1 becomes, upon dropping the prime,

$$K = \frac{1}{2}p^2 - \frac{1}{r} + \frac{1}{2}f(s)\left(\frac{B}{B_0}\right)^2 (x^2 + y^2) \tag{3.26}$$

where B_0 is the magnetic field

$$B_0 = \frac{2c\mu^2 e^3}{I_n^3} \simeq 4.691 \times 10^5 n^{-3} \text{ Tesla} = 4.691 \times 10^9 n^{-3} \text{ Gauss} \ . \tag{3.27}$$

Following the method described in chapter 1 we move into extended phase space and remove the Coulomb singularity by multiplying $\overline{\Gamma}$ by $4r$ to obtain an equivalent new Hamiltonian Γ:

$$\Gamma = 4r\bar{\Gamma} = 4rW + 2rp^2 - 4 + 2rf(s)\left(\frac{B}{B_0}\right)^2 (x^2 + y^2) \equiv 0 \ . \tag{3.28}$$

By applying the transformation defined by Cornish (1984) (see Chapter 1) we can write Γ , equation 1.23, in the form of a pair of coupled two-dimensional oscillators:

$$\Gamma = \frac{1}{2}\mathbf{p}^2 + 4Wx^2 + 8f(s)\left(\frac{B}{B_0}\right)^2 x^2(x_1^2+x_2^2)(x_3^2+x_4^2) \equiv 4 \qquad (3.29)$$

where

$$x^2 = x_1^2 + x_2^2 + x_3^2 + x_4^2 \, .$$

Note that the value of Γ is constant. The equations of motion are now

$$\begin{aligned}
\frac{\mathrm{d}x_k}{\mathrm{d}\tau} &= \frac{\partial\Gamma}{\partial p_k} = p_k \quad , \quad k = 1,\ldots,4 \qquad (3.30)\\
\frac{\mathrm{d}p_k}{\mathrm{d}\tau} &= -\frac{\partial\Gamma}{\partial x_k} = 8Wx_k + 16f(s)\left(\frac{B}{B_0}\right)^2 (x_3^2+x_4^2)(x_k+x^2), k = 1,2\\
\frac{\mathrm{d}p_k}{\mathrm{d}\tau} &= -\frac{\partial\Gamma}{\partial x_k} = 8Wx_k + 16f(s)\left(\frac{B}{B_0}\right)^2 (x_1^2+x_2^2)(x_k+x^2), k = 3,4\\
\frac{\mathrm{d}t}{\mathrm{d}\tau} &= \frac{\partial\Gamma}{\partial W} = 4x^2\\
\frac{\mathrm{d}W}{\mathrm{d}\tau} &= -\frac{\partial\Gamma}{\partial t} = -8\frac{\partial f(s)}{\partial t}\left(\frac{B}{B_0}\right)^2 x^2(x_1^2+x_2^2)(x_3^2+x_4^2) \, ,
\end{aligned}$$

where, because of the canonical transformation induced by the change from $\overline{\Gamma}$ to Γ, τ is not the same variable as in equation 1.23. In the absence of a field τ is the eccentric anomaly of the Kepler motion, equation 1.5.

3.3 Results and Conclusions

In this section we present results of the adiabatic theory for a few values of the quantum numbers n and m and a variety of field strengths. For the numerical integration of the equations of motion we found the 8th order Runge-Kutta-Fehlberg an efficient method. For the solution of equation 3.19 we use NAG routine D02CHF, for the solution of equations 3.15 and 3.17 NAG routine C05AJF and for the inversion of the Kepler's equation 1.5 we use Halley's method (Ledermann 1981), which is necessary for $\varepsilon \simeq 1$ where second derivatives must be taken into account. In all cases we adjusted the various tolerances to ensure convergence, so that errors quoted are due to the method and not our numerical procedures.

In Figure 3.1 we show the variation of the final energies, E_k, equation 3.7, with initial angle variable θ_n, for the field strengths $B = 1, 4$ and 11 Tesla and for the rotational state $n = 30, m = 1, k = 28$. Other quantum numbers, not shown here, have similar curves. In this example we show the relative variation $(E_k - < E_k >)/\sigma$ as a function of θ_n with $\theta_l = \pi/2$; other values of θ_l , and the variation of θ_l for fixed θ_n give similar graphs. Thus for these moderate fields the energy is a smoothly varying function of θ. For stronger fields a different picture emerges which we shall discuss later.

In Figure 3.2 we consider the variation of the standard deviation, σ, with the switch-on time, T, for $n = 30, m = 1$ and for various k and three different field strengths, for these quantum numbers $K_{max} = 4$, equation 3.17. In Figure 3.2a, $B = 1$ Tesla, $\sigma(T)$ decreases initially and reaches an asymptotic value at about $T = 700$, or about 100 unperturbed electron periods (2π), but this asymptotic value is strongly dependent upon k and, as we shall see, B. In distinction to the example quoted by Skodje *et al.* (1985, figure 2) σ does not decrease significantly for $T > 700$. In Figure 3.2b and 3.2c, $B = 4$ and 9 Tesla respectively, a similar pattern is shown but the asymptotic values of σ are larger. The general picture which emerges from these graphs is that a switch-on time of about 100 unperturbed periods is sufficient for $\sigma(T)$ to reach its asymptotic value. In most cases dealt with below we used $T = 700$.

In Figure 3.3 we plot σ(B) for $T = 700, n = 30, m = 1$ and various k. The main trend shown in this graph is that $\sigma(B)$ increases monotonically with B; also it appears that the levels $k = 1, 28$, farthest from the separatrix, have smaller σ, however, as shown in Figure 3.4, this is only partially true. It would appear from Figure 3.3 that σ continues to rise as the field strength increases. However, calculations at $B = 10, 11, ..., 15$ give $\sigma \sim 10^{-2}$ for all k. In this region, as will be shown below, the system is predominantly irregular.

In Figure 3.4 we show the variation in σ as a function of k for $B = 4, 9, 12$ Tesla. Here the vibrational states $k = 2, 3$ and the rotational states $k = 9, 10$ are closest to the separatrix. In the weak field case, 4 Tesla, the variation is smooth, either side of the separatrix. For the higher fields the variation

in $\sigma(k)$ becomes more erratic, but the range over which σ varies becomes smaller; for examples at $B = 4$ Tesla $\Delta \log \sigma = 2.65$ and at $B = 12$ Tesla $\Delta \log \sigma = 0.85$. It is apparent from these results that, although there are clear patterns in the behaviour of σ as the magnetic field increases, none of these point to a sudden break-down of the adiabatic approximation, which would suggests a sharp transition from regular to irregular motion.

Other quantities show dramatic changes in their behaviour for high fields. The relative variation of the energy levels $(E_k - < E_k >)/\sigma$ as a function of θ_n changes from a smooth (Figure 3.1) to an irregular rapidly oscillating function. Calculations for a few different values of k show that the number of oscillations changes from two (low fields) to many as the magnetic field increases. The value of the field at which the number of oscillation increases depends upon k. We also investigated the stability of orbits by computing the final distance of orbits started on the same torus with slightly different initial angle coordinates. Given the initial coordinates $x(0)$ and $x'(0)$, with $| x(0) - x'(0) | \sim 10^{-6}$, and the final coordinates $x(t)$ and $x'(t)$, the relative distance $d_{rel} = (| x(t) - x'(t) |)/(| x(0) - x'(0) |)$ was calculated and averaged over 20 orbits (some calculations with 40 orbits did not show any significant difference) for various k at values of the magnetic field ranging from 1 to 13 Tesla. For low fields $< d_{rel} >$ is of the order of 1, but for higher fields it increases suddenly by several orders of magnitude, and the values of B at which the change occurs is different for different values of k. A summary of these results is given in Figure 3.5a, which shows the values of B at which the motion becomes irregular, as measured by the changes in $< d_{rel} >$ and in the number of oscillations of $(E_k - < E_k >)/\sigma$ as a function of θ_n. There is good agreement between these crude estimates. Figure 3.5b is similar, but for the case $m = 14$. Here the values of B at which the motion becomes irregular are higher than for $m = 1$ and the variation with k is much less pronounced. Computations of $\sigma(B)$ for $n = 30, m = 14$ also show that the results for different values of k are all similar as opposed to the case $m = 1$ (Figure 3.3). Since for $m = 14$ all the levels are rotational, it is possible that these differences are due to the absence of the separatrix; also, since L_z is

bigger, the Coulomb singularity may be playing a smaller role.

As mentioned before, the standard deviation σ increases with the magnetic field. When σ becomes comparable with the energy splitting between adjacent energy levels the adiabatic approximation breaks down. Calculations carried out for the pairs $k = 0, 1, k = 18, 19, k = 26, 27$ show that this starts to happen between 9 Tesla and 13 Tesla, which is in agreement with the onset of irregular motion described above. The behaviour of the ratio between σ and the energy splitting is shown in Figure 3.6.

We now turn to a comparison of the energy levels given by this method with those of other calculations. For these comparison we write the energy levels in the form

$$n^2 E_{n,k} = -\frac{1}{2} + n^2 \Delta E_{n,k} \quad \text{atomic units} \tag{3.31}$$

and give the energy shifts $n^2 \Delta E$ in atomic units.

Our first comparison is with some of the results quoted by Delos *et al.* (1983) (see Table 3.1) for $n = 30, m = 1$ and $B = 1$, which is a fairly low field as the field at which adjacent n-manifolds overlap is $B_c/\text{Tesla} \simeq 4.2 \times 10^5 n^{-7/2} = 2.8$ (see Richards 1983, equation 4.3). In this example there are about 4 states in each well, equation 3.16; all are given by quantal first order perturbation theory with errors around 0.3-0.4%. The two lowest levels are also given with the same order of accuracy by the semiclassical theory, but the upper two have large errors due to the barrier, which affects similarly the lowest rotational state $k = 9$. The higher rotational states are all given by the adiabatic method with errors smaller than 0.3%.

The next low field comparison is with the results of Clark and Taylor (1982) (see Table 3.2) for the smaller principal quantum number $n = 23, m = 1$ for which there are about 3 states in each well, and the critical field B_c is 7.2 Tesla. This comparison shows similar accuracy as in the previous comparison and, as there, the errors are largest near the separatrix, $k = 2, 8$.

For higher fields we compare our results with those of Delande and Gay (1986a) (see Table 3.3) for $n = 33, m = 3$ and the highest rotational state $k = 30$. In this case the critical field B_c is 2.03 Tesla and the highest field

for which comparisons are made is nearly four times this. In all cases the error in $n^2\Delta E_n$ is less than 0.3%.

Many authors have shown numerically that the Hamiltonian 3.8 is not integrable, and produces irregular trajectories. Delande and Gay (1983) suggest that for fields $B > B_{IR}$, where B_{IR} is the value of the field at which the diamagnetic and Coulomb forces are of comparable strength,

$$B_{IR} = 2.35 \times 10^5 n^{-3} \text{Tesla} \tag{3.32}$$

the classical system is irregular, that is most of the trajectories become chaotic or irregular. Our tests show that the value of the field at which the system becomes irregular depends on the quantum numbers m and k; for example for $n = 30$, where $B_{IR} \simeq 8.7$ Tesla, we find values between 7.5 and 12.5 Tesla (see Figures 3.5 and 3.6). In the region where $B = B_{IR}$ the symmetries associates with the Coulomb and the Landau regimes interfere with each other and no approximate symmetry is expected to be conserved. It is remarkable that our calculations give accurate results even for $B > B_{IR}$. Various reasons can be suggested to explain this. The work of Dana and Reinhardt (1987)(see also Reinhardt and Dana (1987)) on the Standard Map suggests that even in the chaotic region the adiabatic method works if the switch-on times are not too long, where the critical time is associated with the time required to cross the main island chain. Also, the value of B_{IR}, equation 3.35, is only a rough estimate of the onset of chaos. Our calculations show that the value of B at which most orbits become irregular varies with the quantum number k, in particular it is higher than B_{IR} for $k \simeq n - m$ (highest rotational states). The comparisons made for $B > B_{IR}$ are all for the highest rotational state of the manifold $n = 33, m = 3$. In this case our estimate, using the methods described above, of the value of magnetic field strength at which the motion becomes irregular is about 8.5 Tesla, while $B_{IR} \simeq 6.54$ Tesla. More quantal results are needed to check the adiabatic method at these very high fields.

We have shown that the adiabatic method can be used to find the energy levels of a strongly perturbed hydrogen atom as long as the initial tori are chosen correctly; the zero-frequency motion of the unperturbed system does

not cause any problems. We have also shown that the method can be used either side of a separatrix of the unperturbed motion and that, because most quantum states do not coincide with the separatrix energy, the levels provided by this method are as accurate as primitive EBK-quantisation. Finally we have shown that the method provides accurate energy levels for all field strengths up to the point at which most orbits are chaotic.

Table 3.1

Energy levels for $n = 30, m = 1, B = 1$ Tesla; in this case there are 4 states inside the separatrix. (a) Present classical adiabatic theory, (b) Semi-classical results of Delos et al (1983), (c) Quantal results of Hulet, quoted by Delos et al (1983), (d) First order quantal perturbation theory by Hulet, quoted by Delos et al (1983). Here $B_c \simeq 2.8$ Tesla and $B_{IR} \simeq 8.7$ Tesla. The energy is given in atomic units, see equation 3.31.

k	(a) Classical adiabatic theory	(b) Classical perturbation theory	(c) Exact quantum	(d) Quantum perturbation theory
0	2.34(−4)	2.35(−4)	2.36(−4)	2.36(−4)
			2.36(−4)	2.36(−4)
1	4.45(−4)	4.46(−4)	4.45(−4)	4.45(−4)
			4.49(−4)	4.49(−4)
2	6.30(−4)	6.30(−4)	6.30(−4)	6.26(−4)
			6.30(−4)	6.30(−4)
3	7.81(−4)	7.80(−4)	7.77(−4)	7.73(−4)
			7.81(−4)	7.81(−4)
9	8.60(−4)	8.59(−4)	8.68(−4)	8.68(−4)
10	9.27(−4)	9.26(−4)	9.25(−4)	9.25(−4)
11	1.01(−3)	1.01(−3)	1.01(−3)	1.00(−3)
12	1.10(−3)	1.10(−3)	1.10(−3)	1.10(−3)
16	1.56(−3)	1.56(−3)	1.56(−3)	1.55(−3)
20	2.16(−3)	2.16(−3)	2.16(−3)	2.15(−3)
24	2.89(−3)	2.89(−3)	2.89(−3)	2.88(−3)
28	3.75(−3)	3.76(−3)	3.76(−3)	3.70(−3)

Table 3.2

Energy levels for $n = 23, m = 1, B = 4.7$ Tesla; in this case there are 2 states inside the separatrix. (a) Present classical adiabatic theory, (b) Quantum calculations with a basis of Sturmian functions by Clark and Taylor (1982). Here $B_c \simeq 7.2$ Tesla and $B_{IR} \simeq 19.3$ Tesla. The energy is given in atomic units, see equation 3.31.

k	(a) Classical	(b) Quantum
0	1.33(−3)	1.33(−3)
		1.33(−3)
1	2.49(−3)	2.48(−3)
		2.48(−3)
7	3.90(−3)	3.94(−3)
8	4.31(−3)	4.29(−3)
9	4.81(−3)	4.81(−3)
10	6.03(−3)	6.03(−3)
11	6.38(−3)	6.37(−3)
12	6.74(−3)	6.73(−3)
13	7.52(−3)	7.51(−3)
14	8.36(−3)	8.35(−3)
15	9.27(−3)	9.26(−3)
16	.102(−1)	.102(−1)
17	.113(−1)	.113(−1)
18	.124(−1)	.124(−1)
19	.135(−1)	.135(−1)
20	.148(−1)	.147(−1)
21	.161(−1)	.160(−1)
22	.174(−1)	.174(−1)

Table 3.3

Energy of the $n = 33, m = 3, k = 30$ state, the highest rotational state, for various magnetic fields . (a) Present classical adiabatic theory, (b) Quantal calculation with Sturmian basis. Here $B_c \simeq 2.03$ Tesla and $B_{IR} \simeq 6.54$ Tesla, but see text. The energy is given in atomic units, see equation 3.31.

B/Tesla	(a) Classical	(b) Quantum
0.654	3.02(−3)	3.02(−3)
3.270	6.935(−2)	6.912(−2)
6.998	2.634(−1)	2.627(−1)
7.847	3.168(−1)	3.161(−1)

Chapter 4

The hydrogen atom in a microwave field

4.1 Introduction

Bayfield and Koch (1974) first reported the observation of microwave ionisation of highly excited hydrogen atoms. Their experiment was performed on a beam of hydrogen atoms prepared with principal quantum number n in the range $63 \leq n \leq 69$ which was then passed through a microwave cavity, where the beam was exposed to $\sim$ 300 cycles of a 9.9 GHz microwave field polarised along the direction of the beam. Fringe fields at the entrance and exit of the cavity affected the beam in a way equivalent to gradually switching the field on and off. The ionisation was measured as a function of the field amplitude. Later more experiments followed (Bayfield *et al.* 1977, Koch 1982, Bayfield and Pinnaduwage 1985, Bayfield 1987, Koch *et al.* 1987, Koch 1988).

4.1.1 Koch experiment: three-dimensional atom

In the more recent experiments by Koch (1982) a fast beam of hydrogen atoms, weighted in n approximately as n^{-3}, was produced by electron-transfer collisions of a $\sim$ 14 keV proton beam in a Xe gas cell. A double resonance method employing two CO_2 lasers was used to excite atoms in the $(n, n_1, \mid m \mid) = (7, 0, 0)$ extremal Stark state to a selected $(n, 0, 0)$ state, via the $(10, 0, 0)$ state. Both laser beams crossed the atomic beam at shallow angles and did not enter the microwave cavity. The substate distribution

produced by the laser excitation was altered, before the atoms entered the cavity, by a small perturbation to the field caused by the mechanical features of the endcaps of the cavity. Field ionisation in a set of static electric field plates located before the cavity was used to diagnose the distribution entering it and a comparison with Monte Carlo calculations based on a result by Damburg and Kolosov (1979) showed that it could be characterised by equally populated substates of a given level. This corresponds to a micro-canonical distribution of classical electron trajectories in three dimensions. Inside the cavity each atom experienced about 300 oscillations of the field with constant amplitude F_0, between a slow rise and fall of the field over about 40-80 oscillations near the entrance and exit of the cavity. Ionisation was measured using two different methods. In the first method a static voltage applied to the cavity enabled 'energy-labelled' detection of protons produced inside the cavity. However the static electric field produced by this voltage outside the cavity can ionise atoms with $n \gtrsim 75$. For quantum numbers $n \geq 74$ a different method was used for which the static voltage was set to zero. The excited hydrogen atoms were then ionised and detected after the cavity by a longitudinal static electric field. In this experiment both ionised and highly excited atoms are detected without distinction. A discussion of what is intended by ionisation is given in section 4.2. Measurements of how the signal was quenched by the microwave field gave an indirect measure of the ionisation. Experiments were performed over the range $n = 32 - 90$. Their results are discussed in Section 4.3, where they are compared to results obtained with a new three-dimensional classical model.

4.1.2 Bayfield experiment: one-dimensional atom

In the experiment by Bayfield and Pinnaduwage (1985) a 1keV beam of excited hydrogen atoms was produced by electron-exchange collisions in an argon gas cell. The beam was first passed through a strong static field region ($\sim$ 23530 V/cm) where a collinear CO_2 laser selectively excited $(n, n_e, m) = (7, -6, 0)$ atoms to the $(10, -9, 0)$ state, and then passed through a weak static field region ($F_s \sim 5.5$ V/cm) where the same laser in-

duced a transition to the $(60, -59, 0)$ extremal Stark state. These Stark states are essentially one-dimensional. In this region the atoms passed through a long waveguide, where the microwave field is parallel to F_s. The laser-excited atoms were detected further on during passage through a microwave cavity and measurement of the ion current. Ionisation curves were obtained by observing the reduction in laser-excited atom content in the hydrogen beam caused by the presence of the waveguide microwaves. Some results are given for $n = 60$ and $n = 63$. One drawback of this experiment is that it is not known what effect the laser field, collinear to the beam throughout the experiment, has on the dynamics of the atoms in the waveguide. Consequently it is not clear how to simulate these experiments numerically. In this experiment the atom is initially prepared in the Stark level of lowest energy within a given high n manifold, and is therefore initially essentially one-dimensional (Kleppner *et al.* 1983). It has been suggested (Bardsley and Sundaram 1985) that, because the matrix elements coupling Stark states decrease strongly with increasing changes in Δn_e, all transitions to states other than the extremal Stark states can be ignored. In agreement with this Bayfield and Pinnaduwage find $\Delta n_e < 3$, even at ionising microwave strengths. The above argument and the experimental results then suggest that the atoms remain one-dimensional during the interaction with the microwave field.

Leopold and Richards (1987) examine the behaviour of extremal Stark states of excited hydrogen atoms under the influence of parallel static and microwave fields and find the conditions under which the assumption that the atoms remain one-dimensional is valid. A classical hydrogen atom in extremal Stark state is represented by a distribution of ellipses with eccentricity ε close to unity:

$$1 - \frac{1}{n} \leq \varepsilon \leq 1$$

and with the angle between the Runge-Lenz vector $\mathbf{A}$, equation 1.3, and the field direction $\hat{\mathbf{F}}$ close to π

$$| \hat{\mathbf{A}} \cdot \hat{\mathbf{F}} + 1 | \leq \sqrt{2/n} \, ,$$

so that the electron is always close to the field axis. In the presence of a microwave field of amplitude F_m, but no static field, it was shown by Leopold and Richards (1986) that this configuration is unstable and that the ellipse precesses with a period proportional to $1/F_m$. The introduction of a static field F_s always slows this precession, because the static field produces the opposite effect: as is well known, the linear configuration is stable in the static field limit ($F_m = 0, F_s \neq 0$). For resonant fields, i.e. when the frequency of the microwave field is close to the unperturbed frequency of the atom, the authors are able to show analytically that there exists a critical value F_s^c of the static field, dependent on the microwave field and frequency, at which the linear configuration becomes stable. This is done by applying standard Floquet theory to the equations of motion of the averaged Hamiltonian, so F_s^c is the value of the field at which the fixed point of the averaged Hamiltonian becomes stable. For the resonant case $\omega = 1$ it is found that the linear configuration is stable for $F_s \geq 0.217 F_m$. The above analysis cannot be applied to non-resonant frequencies. In this case numerical evidence is given for the existence of a critical field needed to keep the system one-dimensional.

4.1.3 Scaling laws

The problem analysed here satisfies simple scaling laws, introduced for this problem by Leopold and Percival (1979), which reduce the number of parameters upon which the system is dependent. This is a particular case of a general result of classical mechanics. Given a system of N particles interacting through Coulomb forces, if trajectories $\mathbf{r}_i(t)$ $(i = 1, \ldots N)$ satisfy the equations of motion and λ is a positive scale factor, then new trajectories $\mathbf{r}'_i(t)$ also satisfy the equations of motion provided

$$\mathbf{r}'_i(t') = \lambda \mathbf{r}_i(t) \tag{4.1}$$

$$t' = \lambda^{3/2} t \,. \tag{4.2}$$

Velocities, energies and actions are scaled according to:

$$v' = \lambda^{-1/2} v \tag{4.3}$$

$$E' = \lambda^{-1} E \tag{4.4}$$

$$I' = \lambda^{1/2} I \,, \tag{4.5}$$

and any quantity with dimensions

$$M^a L^{3b} T^{-2b} \quad , \quad (a, b \text{ real}) \,, \tag{4.6}$$

is classically scale invariant. This includes as a particular case ($a = b = 0$) any dimensionless quantity.

Because of these laws the dynamics of our system and in particular the ionisation probability will only depend on the dimensionless ratios $\omega/\omega_{at} = \Omega_0$ and $F/F_{at} = F_0$, where

$$\omega_{at} = \frac{\text{a.u.}}{n_0^3} = \text{frequency of the unperturbed electron motion} \tag{4.7}$$

$$F_{at} = \frac{\text{a.u.}}{n_0^4} = \text{mean Coulomb force} \,, \tag{4.8}$$

and n_0 denotes the initial level. In fact it follows from the scaling laws that if I and I' are two principal actions corresponding to quantum numbers n and n', then the orbits with parameters (I, F, ω) and $(I', F(I/I')^4, \omega(I/I')^3)$ are identical. In our calculations we use scaled variables Ω_0 and F_0 with $I' = 1$, and, since the size of the unperturbed orbit is proportional to $a_0 n_0^2$, this is chosen as our unit of length.

4.1.4 Theory

The experiments described above have inspired a number of theoretical papers attempting to understand the dynamics of microwave ionisation. In all these experiments the Coulomb and microwave fields are typically of comparable strengths, the atom is subjected to many field oscillations, and the principal quantum number is usually large ($n \geq 30$). The dynamics of the system is thus very complicated and quantal solutions are prohibitively expensive because of the large quantum numbers and the need of including the continuum. Consequently all theoretical papers so far involve one or more of the following approximations:

1. use of classical dynamics,

2. restriction to 1 or 2 dimensions,

3. ignoring the continuum, in classical dynamics by using angle-action variables, or in quantum mechanics by using a bound-state basis,

4. approximation of the microwave field by a series of impulses,

5. no adiabatic switch.

The most general Hamiltonian is given by[1]

$$H(\boldsymbol{r},\boldsymbol{p}) = \frac{1}{2}p^2 - \frac{1}{r} + z(F_s + A(t)F_m\cos(\omega t + \alpha)) \ , \qquad (4.9)$$

where $\boldsymbol{r}$ and $\boldsymbol{p}$ are the position and momentum of the electron, F_s is the amplitude of the static field, F_m and ω are the maximum amplitude and frequency of the microwave field, and $A(t)$ is an envelope function representing the fringe fields outside the cavity, which must be taken into account in accurate simulations of experiments. The phase α is also important if the envelope function $A(t)$ changes significantly over a time comparable to a few unperturbed electron periods. If the change is much slower, however, our numerical checks have shown that the classical ionisation probability is independent of α. The length of the switch needed to ensure this is longer for one-dimensional simulations than it is for three-dimensional. Details are given in section 4.3.

As we have seen above, there are currently two types of experiments. In those of Koch and co-workers the static field is zero, so $F_s = 0$ in equation 4.9, and the envelope function $A(t)$ grows from 0 to 1 over $\sim$ 40 to 80 field cycles, remains at unity for several hundred field cycles, and then returns gradually to 0 in a symmetric fashion. The atoms are prepared in an initial state of known principal quantum number n and equally populated substates

[1]The correct form of this Hamiltonian is actually slightly different (Richards 1990):

$$H(r,p) = \frac{1}{2}p^2 - \frac{1}{r} + z[F_s + \frac{F_m}{\omega}\frac{d}{dt}(A(t)\cos(\omega t + \alpha))] \ ,$$

but this reduces to 4.9 if the field envelope changes little during one field period, and this condition is satisfied in the experiments described here.

(l, m). This experiment can therefore be described by the three-dimensional Hamiltonian

$$H(\boldsymbol{r},\boldsymbol{p}) = \frac{1}{2}p^2 - \frac{1}{r} + zA(t)F_m \cos(\omega t + \alpha) \; . \tag{4.10}$$

In the experiment of Bayfield and co-workers the static field is non-zero, $F_s \neq 0$, and the envelope function $A(t)$ has no constant section. The atoms are prepared in an extremal Stark state and for very large n the electron is constrained to lie close to the z-axis. A good approximation of this experiment is therefore given by the one-dimensional Hamiltonian

$$H(z,p) = \frac{1}{2}p^2 - \frac{1}{z} - z(F_s + A(t)F_m \sin(\omega t + \alpha)) \; , \quad z \geq 0 \; . \tag{4.11}$$

Almost all quantal and many classical calculations are nevertheless performed using the simpler one-dimensional Hamiltonian

$$H(z,p) = \frac{1}{2}p^2 - \frac{1}{z} - zF_m \sin \omega t \; , \quad z \geq 0 \; . \tag{4.12}$$

The first theoretical work which gave reasonable agreement with the experiments of Bayfield and Koch (1974) used a classical Monte-Carlo trajectory method (Leopold and Percival 1979). In this work the model is described by the Hamiltonian

$$H(\boldsymbol{r},\boldsymbol{p}) = \frac{1}{2}p^2 - \frac{1}{r} + zA(t)F_m \cos \omega t \; , \tag{4.13}$$

where $\boldsymbol{r}$ and $\boldsymbol{p}$ are the position and momentum of the electron, F_m and ω are the maximum amplitude and frequency of the field, and the envelope function $A(t)$ is defined by:

$$A(t) = \begin{cases} \exp[\lambda(t - t_i)] & 0 \leq t \leq t_i \\ 1 & t_i \leq t \leq t_f \\ \exp[-\lambda(t - t_i)] & t_f \leq t \leq T \; . \end{cases} \tag{4.14}$$

This envelope function simulates the effects of perturbations to the field at the entrance and exit of the microwave cavity in the experiment. The initial conditions at $t = 0$ were chosen by standard Monte-Carlo methods from a microcanonical distribution, which corresponds to the actual initial

distribution of states in the experiment, as noted before. Using this method Leopold and Percival (1979) performed computer simulations of the experiments by Bayfield and Koch (1974) and Bayfield *et al.* (1977) with samples of 45 and 200 trajectories respectively, for the case $n = 66, \omega/\omega_{at} = 0.43$. Agreement with the experiment is good. An important result of this work is the observation that the ionisation occurs classically only via unstable trajectories, which do not lie on invariant tori; orbits on invariant tori do not ionise. In particular it is found that the ionisation probability $P_{ion}(t)$ obeys approximately the law

$$P_{ion}(t) = (1 - Q_T)[1 - \exp(-\beta(t)t)] \,, \tag{4.15}$$

where Q_T is the probability that an orbit lies on an invariant torus (Arnol'd and Avez 1968) of the Hamiltonian 4.9 during the period when $A(t)$ is constant. Also, this work demonstrated the ability of classical mechanics to describe an excited atom in a microwave field, for a scaled $\omega/\omega_{at} = 0.43$.

Further classical simulations (Jones *et al.* 1980) investigate the dependence of the ionisation probability on the frequency ω and amplitude F of the microwave field. These simulations were performed with ω/ω_{at} in the range 0.01 to 10.0 and F/F_{at} in the range 0.06 to 0.2, where ω_{at} is the characteristic angular frequency of the electron in the unperturbed atom and F_{at} is the characteristic force exerted on the electron by the proton. They found considerable structure in the curves giving the ionisation probability as a function of the frequency ω/ω_{at} and classified three different regions:

1. $\omega/\omega_{at} \gg 1$. In this region they found that, for the range of field amplitudes and lengths of integration times considered, the ionisation always tends to zero.

2. $\omega/\omega_{at} \ll 1$. This is the static limit. In this region they found no ionisation for $F/F_{at} < 0.129$.

3. $\omega/\omega_{at} \sim 1$. In this region they found the greatest amount of ionisation.

In the light of new results presented here (section 4.3) this classification does not hold. The reason for this is explained in section 4.2. By subsequently

restricting the motion to two dimensions in the $x-y$ plane the authors were also able to examine in more detail individual trajectories. A plot of an orbit which ionises after passing through a highly excited state shows very clearly how the orbit changes as the electron approaches the perihelion.

Leopold and Richards (1986) study the effect of a resonant microwave field on a classical 2-dimensional hydrogen atom with Hamiltonian

$$H = \frac{1}{2}(p_x^2 + p_y^2) - \frac{1}{r} + F_m x \cos\omega t \ , \quad r^2 = x^2 + y^2 \ , \qquad (4.16)$$

where F_m and ω are the amplitude and the frequency of the field respectively. Following Meerson *et al.* (1982) they use an averaging approximation which, for weak resonant applied fields, allows the problem to be decomposed into two almost non-interacting systems of one degree of freedom. The motion predicted by this approximation is then compared with that given by the exact equations of motion. They find that, even for quite large field strengths of about 50% of that required to ionise some orbits, the decoupling holds in some regions of the phase space, but the detailed behaviour of the orbits suggested by the approximation does not agree with the actual motion at these relatively high field strengths. This discrepancy is explained by noting that the higher harmonics, ignored by the averaging approximation, change the motion in the neighbourhood of rational invariant tori. The decoupling provided by the averaging approximation allows the authors to apply a variant of the resonance-overlap criterion (Chirikov 1979) to estimate the critical field F_0^c at which ionisation occurs. They find

$$F_0^c \Omega_0^{1/3} = 0.025 \ .$$

Here the field strength and frequency are expressed in scaled units $F_0^c = F/F_{at}$ and $\Omega_0 = \omega/\omega_{at}$ (see section 4.1.3). This value of the critical field is lower than that calculated with the same method for the one-dimensional case (Jensen 1984, Leopold and Richards 1985; see also below, eq. 4.18), because the resonant regions in two dimensions are slightly wider.

A three-dimensional model which simulates the experiments by Koch (1982) is described in Section 4.2 and results and comparisons are given in

Section 4.3. Preliminary results have been published (van Leeuwen *et al.* 1985, Koch *et al.* 1987) and show very good agreement.

Much of the existing literature on the problem of a hydrogen atom in a microwave field deals with one-dimensional models. There are several reason for this. First of all the restriction to one dimension is up to now the only way to apply quantum dynamics to this problem. Secondly, even when classical dynamics is used, the one-dimensional model is much simpler and less costly in terms of computational resources and allows a straightforward application of Chirikov's resonance overlap criterion to estimate the onset of chaos. Also, there seem to be actual experimental situations that can be realistically described by a one-dimensional model. One is the so-called surface-state electron, that is an electron weakly bound to the surface of liquid helium (Jensen 1982, 1984 and references therein), the other is a microwave experiment of the type performed by Bayfield and Pinnaduwage (1985) where the atom is prepared in an extremal Stark state and a static electric field of sufficient strength is added (see Leopold and Richards 1987). However a one-dimensional model is not a good approximation of those experiments in which the atom is prepared in a state with equally populated substates (van Leeuwen *et al.* 1985). In view of the fact that the application of quantum mechanics is at present only feasible in one dimension, it is important to have classical results for this model and to understand the differences between one- and three-dimensional dynamics, as this will help understanding the relationship between classical and quantal dynamics.

Jensen (1982) first proposed the surface-state electron (SSE) as an appropriate model for studying the quantum dynamics of a time-dependent system which exhibits classical stochasticity. He was motivated partly by the greater simplicity of this problem, partly by the fact that the available experiments on microwave ionisation (Bayfield and Koch 1974, Bayfield *et al.* 1977) were only able to probe the semiclassical regime (high principal quantum number n). Spectroscopic studies of the unperturbed SSE found that the energy levels are given by the hydrogenic formula

$$E_n = -Z^2\mathcal{R}/n^2 \ , \ n = 1, 2, 3, \ldots, \tag{4.17}$$

where $\mathcal{R} = 13.6\text{eV}$ and Z is the effective charge, in this case $Z \sim 7.1 \times 10^{-3}$. This correspond to a one-dimensional description of the SSE which assumes an attractive potential due to the image charge and a repulsive barrier at the surface due to Pauli exclusion (Grimes *et al.* 1976). A system consisting of an SSE in the presence of an oscillating microwave field with polarization normal to the helium surface is easier to study, both classically and quantally, than a three-dimensional hydrogen atom. Furthermore, since the binding energies and characteristic frequencies of the SSE are four orders of magnitude smaller than those for real hydrogen atoms, this system was regarded as a good candidate for experimental investigation also for low principal quantum numbers, although as far as we know no experiments of this sort have ever been carried out. An estimate of the classical thresholds for ionisation is obtained by applying Chirikov's resonance overlap criterion, which gives

$$F_0^c \sim 0.05\Omega_0^{-1/3} , \tag{4.18}$$

where F_0^c and Ω_0 are the scaled field and the scaled frequency respectively, as described previously, (see section 4.1.3).

Leopold and Richards (1985) use a regularising transformation based upon the use of extended phase space to remove the singularity of the one-dimensional Hamiltonian and integrate the equations of motion for samples of orbits in the range $0.4 \leq \Omega_0 \leq 1.1$ and $0.02 \leq F_0 \leq 0.26$. Most calculations were performed using a sudden switch-on of the microwave field, but an adiabatic switch-on was also considered, where the amplitude F of the field is modulated by a switch-on function $A(t)$: $F(t) = A(t)F$, with

$$A(t) = \begin{cases} 0 & t < 0 \\ \frac{1}{2}\left(1 + \tanh \frac{2x-1}{4x(1-x)}\right) & 0 \leq t < t_1 \\ 1 & t_1 \leq t , \end{cases} \tag{4.19}$$

where $x = t/t_1$ and t_1 is the length of the adiabatic switch. Graphs of the ionisation probability as a function of time and as a function of the field strength are given for both cases, which show a dramatic difference between calculations with an adiabatic and a sudden switch-on. Second

order perturbation theory is applied to the regularised Hamiltonian to obtain an estimate of the critical field using the resonance-overlap criterion. It shows that this estimate is in close agreement with numerical calculations and is an improvement on previous estimates (Jensen 1984) obtained by taking into account only first order resonances.

The study of the quantal dynamics of a one-dimensional hydrogen atom in a microwave field of amplitude F and frequency ω requires solving the Schrödinger equation

$$i\frac{\partial\psi}{\partial t} = -\frac{1}{2}\frac{\partial^2\psi}{\partial x^2} - \frac{1}{x}\psi + xF\cos\omega t\psi \ . \tag{4.20}$$

Here and in the following equations atomic units $e = m_e = \hbar = 1$ are used. The usual approach to the solution of this equation is to expand the wave function $\psi(x,t)$ in terms of an appropriate set of basis functions in order to reduce the problem to the solution of a set of ordinary differential equations. Formally, if $\psi(x,t)$ is expressed in terms of the bound and continuum eigenfunctions of the unperturbed Hamiltonian,

$$\psi(x,t) = \sum_{n=1}^{\infty} a_n(t)\phi_n(x) + \int a_k(t)\phi_k(x)\ dk \ , \tag{4.21}$$

then equation 4.20 reduces to a set of ordinary differential equations for the amplitudes a_n

$$i\frac{da_n}{dt} = E_n a_n + F\cos\omega t \sum_{m=1}^{\infty} < n|x|m > a_m + F\cos\omega t \int < n|x|k > a_k\ dk \tag{4.22}$$

$$i\frac{da_k}{dt} = E_k a_k + F\cos\omega t \sum_{m=1}^{\infty} < k|x|m > a_m + F\cos\omega t \int < k|x|k' > a_{k'}\ dk' \ . \tag{4.23}$$

However, no analytical solution has been found and equations 4.22 and 4.23 are usually solved by truncating the infinite sums and integrals and using some approximation to take into account the coupling to the continuum.

Casati *et al.* (1984) considered an approximation with a truncated basis of hydrogenic states which excluded the continuum completely. Equation 4.20 was reduced to:

$$i\frac{da_n}{dt} = E_n a_n + F\cos\omega t \sum_{m=m_{min}}^{m_{max}} < n|x|m > a_m \ . \tag{4.24}$$

Here m_{min} was approximately 20-40 levels lower than the initial excited state n_0, which is the usual range taken because deexcitation to levels $n \ll n_0$ is difficult. The total number of states used was about 200. Their results indicate that, for scaled frequencies $\Omega_0 > 1$, the quantal excitation probability is significantly less than the corresponding classical one for weak fields (see equation 4.28 below). This is supported by further calculations (Casati *et al.* 1986a) where a Sturmian basis of up to 600 states was used in order to partially incorporate the effect of the coupling to the continuum. The comparison was carried out by studying the classical distribution function $f(n,t)$, which gives the number of particles with given n at time t, and the quantum probability distribution over the unperturbed levels. In previous works (Delone *et al.* 1983, Jensen 1984) it was found that in the limit of high frequencies ($\Omega_0 > 1$) and for field strengths $F > F_c$, where F_c is the critical field calculated using Chirikov's resonance overlap criterion, the classical process of excitation is diffusive and the classical distribution function obeys a Fokker-Planck type equation:

$$\frac{\partial f}{\partial w} = \frac{1}{2}\frac{\partial}{\partial n}(D\frac{\partial f}{\partial n}) \tag{4.25}$$

where w is dimensionless time, measured in units of the field period $w = \omega t/2\pi$, and $D = D(n)$. A quasi-linear approximation gives

$$D(n) \approx 2F_0^2 n^3/(\Omega_0^{7/3} n_0) \ , \tag{4.26}$$

where n_0 is the initial principal quantum number, and the amplitude and frequency of the applied field are expressed in scaled units (see Section 4.1.3). As Jensen (1984) pointed out, the quasi-linear treatment of the evolution of the distribution of the trajectories in action which leads to a Fokker-Planck type equation is only valid as long as the perturbation is not too large. For $\Omega_0 \gg 1$ the time averaged quantum probability distribution $\overline{f_n} = \overline{\mid a_n \mid^2}$ is conjectured (Casati *et al.* 1987) to have the form

$$\overline{f}_n \propto \exp(-2 \mid n - n_0 \mid /l) \ , \tag{4.27}$$

where l is the localization length. If the n-dependence of D is disregarded, that is in the approximation D = const., Casati *et al.* (1987) find $l \approx$

$D(n_0) = 2F_0^2 n_0^2 \Omega_0^{-7/3}$. In the limit of high scaled frequencies and under the more general assumption of a non-constant D ($D = D(n)$), the same authors state that the localization length is finite only for

$$F_0 < F_0^q = \Omega_0^{7/6}/\sqrt{6n} \; . \tag{4.28}$$

This result was arrived at by assuming that a mechanism of quantum limitation of diffusion previously shown to exist in the kicked rotator model (Casati *et al.* 1979) also applies to the hydrogen atom in a microwave field.

Thus F_0^q defines the quantum localization threshold. Of course, for delocalization to occur the condition $F_0 > F_0^c$ must also be satisfied. An extension of these calculations to two dimensions (Casati *et al.* 1987) gives a lower quantum localization threshold. This is consistent with recent results obtained by comparing experiment and classical three-dimensional calculations at frequencies $\Omega_0 \geq 1$ (Galvez *et al.* 1988). It was found here that, although quantal ionisation thresholds tend to rise above those for the onset of classical chaos as Ω_0 rises above 1, there is still some agreement in the range $1 \leq \Omega_0 \leq 2$, but the experimental threshold rises systematically above the classical one for $\Omega_0 > 2$.

Very recently new results (Leopold and Richards 1988a) have shed some light on the problem of this discrepancy between quantal and classical calculations at high scaled frequencies. It is shown that significant differences are due to a violation of the stationary-phase approximation, namely when this violation occurs the quantal transition probabilities are much lower than the equivalent classical probabilities. A condition for the violation of the stationary-phase approximation is given, which depends upon the scaled frequency, the scaled field strength and the initial quantum number. This is shown to be equivalent to a violation of the uncertainty principle. When

$$\Omega_0^{5/3} > 1.13 n_0 F_0 \quad \text{and} \quad \Omega_0 \gg 1 \; , \tag{4.29}$$

then the stationary-phase approximation is invalid and $P^{cl} > P^q$. This condition is different from that given by Casati *et al.* (1984, 1986b) and was obtained using different physical principles. It seems likely, therefore, that

both conditions need to be satisfied for the classical and quantal probabilities to agree. A further cause of disagreement between classical and quantal probabilities derives from the fact that at these frequencies the quantal dynamics can be represented by few 'quasi-resonant' states, i.e. states whose energy separation is close to an integer multiple of that of the field frequency, causing the classical approximation to break down. It is important to note that, as Leopold and Richards (1988a) pointed out, the violation of the uncertainty principle is closely related to the singularity of the Hamiltonian for the hydrogen atom. As the effect of the Coulomb singularity is particularly marked in one-dimensional models, it is reasonable to assume that these models overestimate the differences between classical and quantal probabilities. This assumption is further supported by the result by Casati *et al.* (1987) that the quantum localization threshold in two dimensions is much lower than that obtained for a one-dimensional model, although it is not yet possible to check it directly because the extension of quantal calculations to two and three dimensions is beyond the reach of modern computers.

In addition to the discrepancies reported between classical and quantal numerical calculations for high frequencies, remarkable differences have been found in the ionisation curves obtained experimentally and with classical numerical calculations when the scaled frequency is very small, $\Omega_0 \lesssim 0.2$. These differences are mainly due to quantal effects. It has in fact been shown (Richards 1987, see below) that in the limit of small frequencies the quantum dynamics is satisfactorily described by a very small basis, typically 3 or 4 states, so there is complex resonant behaviour not seen in classical dynamics. Typically the experimental ionisation curves show structure, rather than being monotonically increasing, and peaks occur below the classical critical field for the onset of chaos (subthreshold ionisation)(see Figure 4.29). By using a quantum one-dimensional model Blümel and Smilansky (1987) are able to reproduce these features and explain them in terms of avoided crossings between many Floquet eigenvalues. Their model is based on projection operators so that the equations of motion are written as a set of two coupled equations, one for the bound and one for the continuum states respectively.

By formally integrating the equation for the continuum the Schrödinger equation is then reduced to an integro-differential equation in which the kernel describing the bound-continuum transitions is subsequently approximated by a combination of decaying exponentials. Continuum-continuum transitions are neglected. Briefly, given the Hamiltonian

$$H(z,t) = H_0(z) + V(z,t) \tag{4.30}$$

$$H_0(z) = \frac{p^2}{2} - \frac{1}{z} \; ; \quad V(z,t) = Fz\sin\omega t \; , \tag{4.31}$$

the energy spectrum of H_0 is defined by:

$$H_0 \mid n> = E_n \mid n> \; , \quad E_n = -\frac{1}{2n^2} \; , \quad n = 1,2,\ldots \tag{4.32}$$

$$H_0 \mid k> = E_k \mid k> \; , \quad E_k = \frac{1}{2}k^2 \; , \quad k \geq 0 \; , \tag{4.33}$$

and the projection operators $B = \sum_n \mid n >< n \mid$ and $C = \int dk \mid k >< k \mid$ project onto the bound and continuum spaces respectively. Multiplying the Schrödinger equation

$$i \mid \dot{\psi} >= H(z,t) \mid \psi > \tag{4.34}$$

from the left by B or C gives the following equations for the projected wavefunction:

$$i \mid \dot{\psi}_B >= H_{BB} \mid \psi_B > + H_{BC} \mid \psi_C > \tag{4.35}$$

$$i \mid \dot{\psi}_C >= H_{CB} \mid \psi_B > + H_{CC} \mid \psi_C > \tag{4.36}$$

Formal integration of 4.36 gives

$$\mid \psi_C(t) >= \frac{1}{i}\int_0^t K(t,t')H_{CB}(t') \mid \psi_B(t') > dt' \; , \tag{4.37}$$

where $K(t,t')$ is the C-space Greens function, and by inserting this result the Schrödinger equation gives:

$$i \mid \dot{\psi}_B(t) >= H_{BB} \mid \psi_B(t) > + \frac{1}{i}\int_0^t H_{BC}(t)K(t,t')H_{CB}(t') \mid \psi_B(t') > dt' \; , \tag{4.38}$$

which can be written in terms of the bound space amplitudes $b_n(t) = < n \mid \psi_B(t) >$ as

$$\begin{aligned} i\dot{b}_n &= -\frac{1}{2n^2} b_n(t) + F \sin\omega t \sum_m < n \mid z \mid m > b_m(t) \\ &- iF \sin\omega t \sum_m \int_0^t K_{nm}(t,t') F \sin\omega t' b_m(t') dt' \ . \end{aligned} \tag{4.39}$$

In order to solve this equation continuum-continuum transitions are negleted by writing the elements $K_{nm}(t,t')$ as

$$K_{nm}(t,t') = \int_0^\infty < n \mid z \mid k > \exp[-\frac{1}{2}k^2(t-t')] < k \mid z \mid m > \ dk \ .$$

These expressions are then further approximated by a finite series of decaying exponentials.

A new method that may make quantal three-dimensional calculations possible at low frequencies has been developed by Richards (1987). Using an approximation valid for small scaled frequencies, a set of coupled equations is derived which can be solved using a relatively small basis. The starting point is the static limit of the one-dimensional system consisting of an electron in a Coulomb and a microwave field:

$$H = \frac{p^2}{2\mu} - \frac{e^2}{x} - xf(\Omega_0 t) \ , \quad x \geq 0 \ . \tag{4.40}$$

When f is a constant, if $f < 0$ the spectrum of H is discrete. If $f > 0$ the spectrum of H is continuous (see Figure 4.1), but for large quantum numbers ($n \geq 30$) and for energies below the classical saddle,

$$E < E_s(f) = -2e\sqrt{f} \qquad (f > 0) \tag{4.41}$$

the lifetimes of the resonant states are so long that this part of the spectrum may be considered discrete. Richards (1987) uses these adiabatic states as a basis for an expansion of the time-dependent wave function $|t>$ in the limit when the field frequency Ω_0 is small with respect to the unperturbed energy splitting, i.e. when the scaled frequency $\Omega_0 \ll 1$. The use of these adiabatic states introduces a significant part of the time dependence of the wavefunction into the basis, thus reducing the number of basis states required. When

$f < 0$ then

$$| t >= \sum_k | k, f > a_k(t) \exp\left[-\frac{i}{\hbar}\int^t dt E_k(f(t))\right] \quad (f < 0)\ , \qquad (4.42)$$

where

$$H(f) | k, f >= E_k(f) | k, f > \ . \qquad (4.43)$$

When a continuum is needed in the case $f > 0$ an expansion of the same type as equation 4.42 is used, but a complex energy term is included to take into account the continuum and the effects of tunnelling. Inserting these expansions in the time-dependent Schrödinger equation gives

$$\begin{aligned} \frac{da_n}{dt} &= -\frac{\mathcal{E}_n(f)}{\hbar} a_n \qquad (4.44) \\ &- \dot{f} \sum_p \frac{< n, f \mid \partial H/\partial f \mid p, f >}{E_n(f) - E_p(f)} a_p \exp\left[\frac{i}{\hbar}\int_{t_0}^t dt (E_n(f) - E_p(f))\right] \ , \end{aligned}$$

here $\mathcal{E}_n(f) = 0$ when $f < 0$. After obtaining approximations for the lifetimes, the energy levels and the matrix elements, equation 4.44 was integrated with initial quantum numbers $n_0 = 30, 60$ and various field strengths. The author was thus able to obtain the relative variation of the ionisation probability with the system parameters. The main result of these calculations is to show that the ionisation probability has a resonant structure clearly associated with the $n_0 \rightarrow n_0 + 1$ transition, which is of course absent in the classical approximation.

A different approach to the problem of a hydrogen atom in a microwave field, involving the approximation of the field by a series of discrete impulses, must also be mentioned for completeness. This approximation was first introduced by Dhar *et al* (1983). Since it greatly simplifies the computation of the quantum dynamics, it was hoped to provide a good model for the study of the behaviour of quantum systems whose classical analogue exhibit irregular motion. The Hamiltonian for the hydrogen atom in a microwave field is approximated by replacing the sinusoidal external field with a superposition of periodic delta functions:

$$H(t) = -\frac{1}{2}\nabla^2 - \frac{1}{r} + Fz \sum_{N=1}^{s} \delta(t - NT)\ , \qquad (4.45)$$

where F is the strength of the field directed along the z axis and T is the period between two consecutive impulses. Here the system is three-dimensional and atomic units ($e = \hbar = m_e = 1$) have been used. If $\Phi(\mathbf{r}, NT_-)$ is the solution of the time-dependent Schrödinger equation for 4.45 immediately before the N^{th} impulse, then the state immediately after is

$$\Phi(\mathbf{r}, NT_+) = \exp(-iFz)\Phi(\mathbf{r}, NT_-) \; . \tag{4.46}$$

It is apparent that the solution of this problem is numerically much simpler than the solution for the sinusoidal field, as it reduces to the solution for the free motion between impulses plus equation 4.46 at each impulse. If both wavefunctions in equation 4.46 are expanded in a basis of M discrete hydrogenic states, then the total probability for ionisation after the Nth impulse is given by:

$$P_{ion}^N = 1 - \sum_{k=0}^{M} \mid c_k^N \mid^2 \; , \tag{4.47}$$

where $\mid c_k^N \mid^2$ is the probability that the atom will be in the kth unperturbed level after the Nth impulse. The continuum states are not explicitly included. Numerical calculations were performed with the hydrogen atom initially in a Rydberg state with quantum numbers $n = 9$ and $m = 0$ and allowed to evolve for 300 impulses. They observed very long-lived two-state resonances, which occurred whenever the frequency of the external field was close to the transition frequency. No evidence of chaotic behaviour was found: for a weak field the solutions were quasi-periodic and the system showed quantum recurrence.

Blümel and Smilansky (1984) also considered the effect of equal periodic impulses on a one-dimensional system and compared classical and quantal calculations. They used the Hamiltonian

$$H = p^2 - \frac{2}{z} - \beta z \sum_k \delta(t - kT) \; , \tag{4.48}$$

where z and p are dimensionless variables. Here again the time evolution is reduced to the free motion between impulses plus the appropriate interaction

at each impulse. The latter is given classically by:

$$\begin{aligned} p_k^{(+)} &= p_k^{(-)} + \beta \ , \ z_k^{(+)} = z_k^{(-)} \\ E_k^{(+)} &= p_k^{(+)2} - 2/z_k^{(+)} = E_k^{(-)} + 2p_k^{(-)}\beta + \beta^2 \ , \end{aligned} \tag{4.49}$$

where $-$ and $+$ denote the solutions just before and just after the impulse, while the free motion is more conveniently described in terms of angle-action variables:

$$I_{k+1} = I_k^{(+)} \ , \ \theta_{k+1} = [\theta_k^{(+)} + \omega(I_k^{(+)})T] \bmod 2\pi \ . \tag{4.50}$$

These equations of motion require the canonical transformation $(I_k, \theta_k) \rightarrow (p_k, z_k)$ or $(p_k, z_k) \rightarrow (I_k, \theta_k)$ at each step, thus excluding the unbounded motion, since this transformation is not defined for $p^2 - 2/z > 0$. By calculating the trace of the one-step classical stability matrix and the Lyapunov exponents, the nature of the classical dynamics was shown to be chaotic in large regions of the phase space, whose size depends on the parameters β and I. Consequently the authors assumed that the energy is gained through a diffusive process and obtained an estimate for the ionisation probability

$$P_I \simeq K\beta^2 / < E >= K\beta^2 / < I^{-2} > \ , \tag{4.51}$$

where K is a parameter dependent on the form of the energy distribution. The authors also point out that, due to the Coulomb singularity, any orbit with $z < 8I^2(\beta I)^2$, or equivalently $\theta < 32/3(\beta I)^3$, will ionise. If θ is assumed uniformly distributed in $[0, 2\pi]$, this gives the ionisation probability per step

$$P_I \simeq \frac{16}{3\pi}(\beta I)^3 \ . \tag{4.52}$$

The estimates for the ionisation probability given by diffusive (4.51) and direct (4.52) ionisation are different. Note that the latter assumes independent ionising events, and is therefore valid only for very short times. Numerical calculations performed by Blümel and Smilansky (1984) support the assumption that ionisation is due to a diffusive energy gain. Quantal calculations were carried out with an Hamiltonian obtained by straightforward quantisation of 4.48. The bound states are completely specified by the

principal quantum number n, which is the quantum analogue of the classical action, and the time evolution for the bounded motion is given by:

$$\mid \Psi_{k+1} >= e^{-iTH_0} e^{-iPVP} \mid \Psi_k > , \tag{4.53}$$

where $P = \sum_{n=1}^{\infty} \mid n >< n \mid$ is the projection operator.

Calculations were performed using a truncated basis of approximately 100 states, mostly with initial quantum number $n_0 = 10$ and various values of the parameters β and T. Localisation of the wavefunction was checked by calculating the spread of the initial state over the quasienergy states. They concluded that quantum localisation suppresses the stochastic features that characterise the classical dynamics. Some calculations which included the continuum gave the same results for the bound motion, to within a few percent.

Carnegie (1984) carried out extensive classical calculations on a hydrogen atom perturbed by periodic impulses using one- and three-dimensional models and both equal and alternate impulses. He was able to compare his results with those for the quantal model (Dhar *et al.* 1983) as well as those for a classical model with a sinusoidal field (Leopold and Percival 1979). For the first comparison he used an ensemble of orbits initially in the Stark state $n = 9, m = 0$, with an external field described by equal periodic impulses. A comparison of the ionisation rates for various fields does not show very good agreement, although the agreement gets better for higher fields (higher ionisation rates). It looks as if there is no agreement at threshold. For the second comparison an initial microcanonical ensemble was chosen, and the external field was described by the potential

$$V = zFA(t) \sum_{n=1}^{M} (-1)^n \delta(n\pi/\omega - t) , \tag{4.54}$$

where F is the strength of the field, π/ω is the time between impulses, and $A(t)$ is an envelope function corresponding to that used by Leopold and Percival (1979) in their simulation (see equation 4.14):

$$A(t) = \begin{cases} \frac{\exp[\lambda(t-t_i)][1+\exp(\lambda\pi/\omega)]}{2(1+\lambda^2/\omega^2)} & 0 \le t \le t_i \\ 1 & t_i \le t \le T . \end{cases} \tag{4.55}$$

Here t_i is the length of the adiabatic switch and T is the total time over which the field is applied: $T = M\pi/\omega$.

He found values of the percentage ionisation much higher than those obtained by Leopold and Percival (1979) with a sinusoidal field. Furthermore, a graph of the ionisation rate versus the scaled field frequency did not show any structure at all, while in the microwave case clear peaks are observed at resonances.

Recently Leopold and Richards (1988b) carried out a thorough analysis of the dynamics of the one-dimensional model of the hydrogen atom when the applied microwave field is represented by a smooth sinusoidal function and when it is represented by a series of impulses. They concluded that the dynamics of the two models is fundamentally different and therefore the impulsive model should not be used either as an approximation to experiment or to compare the classical and quantal dynamics of the ionisation process. The sinusoidal field $F\cos\Omega t$ is replaced by a series of alternating impulses, giving an Hamiltonian with the general form

$$H = \frac{p^2}{2} - \frac{1}{z} + z \sum_{k=1}^{k=2N} f_k \delta(t - kT - t_0) \,, \tag{4.56}$$

where t_0 is an initial phase, $T = \pi/N\Omega$ is the interval between impulses, and the size of each impulse is given by:

$$f_k = \frac{2F}{\Omega} \sin(\frac{\pi}{2N}) \cos(\frac{k\pi}{N}) \qquad N \text{ odd} \tag{4.57}$$

$$= \frac{2F}{\Omega} \sin(\frac{\pi}{2N}) \cos(\frac{(k+1/2)\pi}{N}) \quad N \text{ even} \,. \tag{4.58}$$

Explicit results are given mainly for $N = 2$, but other cases are also discussed. The behaviour and the number of periodic orbits is studied and shown to be quite different for the two models. Graphs showing the singular regions and the loci of stable and unstable fixed points show that the the bifurcation sequence of the stable periodic orbits is completely different from that obtained with a sinusoidal field (Leopold and Richards 1985). The fundamental reason for these differences is the Coulomb singularity. Furthermore, the region of the phase space in which the unperturbed orbits

have a frequency greater than the applied field comprises mostly regular orbits for sinusoidal fields, and mostly chaotic orbits for impulsive fields. It would therefore be interesting to perform the same type of analysis in two and three dimensions, where the effect of the singularity is less pronounced. Although this is not available, since it is very difficult to find periodic orbits for systems of more than one degree of freedom, the results by Carnegie (1984) reported above suggest that even in higher dimension the Coulomb singularity and the impulses combine to give different effects. Other results for a microwave field in two and three dimension show that the ionising orbits are almost one-dimensional and that the threshold for ionisation in one, two and three dimension are close, which suggests that even a three-dimensional impulsive model would be a poor approximation to the microwave field. Another difference between the impulses and the sinusoidal field is the fact that the replacement of $\cos \Omega t$ by a series of impulses adds more harmonics to the applied field. This could explain the lack of resonant structure in the frequency dependency of the ionisation probability due to impulses.

4.2 Description of the dynamics and method

The dynamics of an electron in a combined Coulomb field and strong microwave field is described by a Hamiltonian which is neither integrable nor near-integrable (4.9). The motion of such a system is qualitatively different from that of integrable systems, it is very complicated and still not completely understood. Another problem is caused by the singularity at the origin in the Hamiltonian 4.9. This causes inefficiencies in the numerical simulation of the motion. Section 1.3 shows how the singularity can be removed by using a regularising transformation and this has been applied in chapter 3 to a similar Hamiltonian for the quadratic Zeeman effect. Following the analogous procedure described there we first write the Hamiltonian in extended phase space and remove the singularity, then a further canonical

transformation is applied to give:

$$\begin{aligned}\Gamma &= \frac{1}{2}(p_1^2+p_2^2+p_3^2+p_4^2)+4W(x_1^2+x_2^2+x_3^2+x_4^2)\\ &+ 4A(t)F((x_1^2+x_2^2)^2-(x_3^2+x_4^2)^2)\cos\omega t-4\ ,\end{aligned} \tag{4.59}$$

where the new coordinates x_i and p_i $(i=1,\ldots,4)$ are given by equations 1.26 and 1.30, and t and W are conjugate coordinates. The equations of motion are then:

$$\begin{aligned}\dot{x}_i &= p_i\ , \quad i=1,\ldots,4\\ \dot{t} &= \frac{\partial\Gamma}{\partial W}=4r\\ \dot{p}_i &= -8Wx_i-16A(t)Fx_iX_{12}\cos\omega t\ , i=1,2\\ \dot{p}_i &= -8Wx_i+16A(t)Fx_iX_{34}\cos\omega t\ , i=3,4\\ \dot{W} &= -\frac{\partial\Gamma}{\partial t}=4F(X_{12}^2-X_{34}^2)\left(A(t)\omega\sin\omega t-\frac{\partial A(t)}{\partial t}\cos\omega t\right)\ ,\end{aligned} \tag{4.60}$$

where $X_{ij}=x_i^2+x_j^2$. In the numerical simulations the following switch-on functions have been used:

$$A(s)=\begin{cases}0 & s\le 0\\ \frac{1}{2}(1+\tanh\frac{1}{4}(\frac{1}{1-s}-\frac{1}{s})) & 0<s<1\\ 1 & 1\le s\end{cases}\ , \tag{4.61}$$

and

$$A(s)=\begin{cases}0 & s\le 0\\ s^2(2-s^2) & 0<s<1\\ 1 & 1\le s\end{cases}\ , \tag{4.62}$$

where $s=t/t_1$ and t_1 is the length of the adiabatic switch.

Some qualitative observations can be made about the trajectories in this system. In the absence of a microwavefield the electron moves in an elliptical orbit with characteristic binding energy and frequency. In the absence of the Coulomb field the electron moves uniformly with a superimposed sinusoidal oscillation and has characteristic mean kinetic energy and frequency. The velocity of the electron in this case is

$$\mathbf{v}=\mathbf{v}_0-\frac{F}{m\omega}\mathbf{z}\sin\omega t\quad(\mathbf{v}_0=\text{const})\ . \tag{4.63}$$

In neither case does the electron lose or gain energy on average, but when both Coulomb and microwavefield are present the electron can gain or, more rarely, lose energy. Different types of phenomena can occur, depending on the ratio of the unperturbed frequency to the field frequency and on the ratio of the Coulomb field to the microwave field. The range of values of the scaled frequency Ω_0 for which ionisation occurs increases as the field strength F increases. The ionisation probability is a complicated function of the frequency, it is non-monotonic and has sharp minima at certain values of the frequency. These features will be discussed in the next section.

Early numerical computations (Leopold and Percival 1979) led to a classification of the trajectories into four classes:

C1 Trajectories on tori, which never ionise;

C2 Trajectories that ionise rapidly;

C3 Trajectories passing through one or more extremely highly excited states (EHE) with relatively sudden transitions between them before ionising;

C4 Trajectories which pass through a sequence of EHE states but do not ionise during the time of computation. These would probably ionise eventually.

More recent results (see next section) show that this actually reduces to two different classes:

(1) Regular (stable) trajectories, which are confined to invariant tori and never ionise. (Class C1)

(2) Irregular (unstable) trajectories, which we believe do eventually all ionise. This comprises classes C2 to C4. The ionisation time and the time spent in EHE depends on the parameters of the system (mainly the scaled frequency), as will be explained below, and is not related to the initial conditions in the phase-space.

For trajectories of the first type there is no effective energy transfer and the distance of the electron from the proton remains similar to the size of the original unperturbed orbit: we expect the invariant tori on which these

orbits lie to be relatively close to the unperturbed tori, so that on a stable orbit $\max(r(t))$ is bounded from above. We also expect most stable orbits to be numerically stable, so that the constants of motion, that is I_m and Γ, are conserved by our numerical procedures as accurately as required. In practice we find that there is an almost complete correlation between those orbits for which $\max(r(t)) < 3$ (where the unit of length is given by the size of the unperturbed orbit $a_0 n_0^2$, see Section 4.1.3) for long times, that is of the order of thousands of unperturbed electron periods, and orbits for which the relative accuracy of I_m and Γ can be controlled. We deem these orbits to be stable. With this definition stable orbits do not ionise.

For trajectories of the second type, tests for scaled frequencies $0.4 \lesssim \Omega_0 \lesssim 1.5$ have shown that if the electron does not rapidly gain enough energy to ionise, it moves away from the proton into a highly eccentric elliptical orbit whose perihelion is at similar distance from the proton as the unperturbed initial major axis but whose aphelion is several times further away. These orbits are very stable far from the proton (where the binding is weaker), but change suddenly every time the electron approaches the perihelion and can either ionise, or be excited to a higher state, or, more rarely, to a less excited state. We find that for these orbits it is impossible to control the accuracy of I_m and Γ in our numerical calculations: the relative errors are typically $O(10^{-4})$, and in most cases $\max(r(t))$ is an increasing function of time. All orbits that ionise are unstable. We do not know whether all unstable orbits eventually ionise, but our calculations suggest that unstable orbits which do not ionise are statistically insignificant.

This analysis suggests that, given a sample of N orbits, if $n(r_m > 3)$ is the number of orbits for which $\max(r(t)) > 3$ after an integration time T, then the ionisation probability for times $t \gg T$ is

$$P_I = n(r_m > 3)/N \ . \tag{4.64}$$

Whether or not this estimate can be used to determine the ionisation probability at $t = T$ depends on how rapidly an electron passes through the region $r > 3$.

We found that the dominant parameter affecting the dynamics of this system is the scaled frequency. At low frequencies ($\Omega_0 < 1$) the orbits either ionise very quickly or not at all. As $\Omega_0 \rightarrow 0$ the field variation becomes adiabatic with respect to the electron motion and affects the atom as if it were a static field. In this regime it has been shown (Richards 1987) that in the one-dimensional case the dynamics can be described by an adiabatic Hamiltonian and the mechanism of ionisation is more easily understood. The potential consists of a well with a barrier moving between the two extreme configurations shown in Figure 4.1 and an orbit is assumed ionised when it goes over the barrier. This qualitative description can be extended to three dimensions, although it is more difficult to prove its validity. This depends on the assumption that an electron never comes back after having gone beyond the barrier. Our analysis of the three-dimensional motion shows that this is only true for scaled frequencies $\Omega_0 \lesssim 0.2$, as can be seen from Figures 4.3b, 4.6b to 4.9b. Here we plot the probability $P_3 = P(3 < \max(r(t)) < 9)$ that the maximum distance of the orbit from the origin is between 3 and 9 as a function of time and for various scaled frequencies. In all cases the final ionisation probability is chosen to be approximately 50 %, so that the scaled force is different for each curve. For the lowest frequency chosen, $\Omega_0 = 0.0828$, (Figure 4.3b) we see that $P_3 \simeq 0$, showing that the electron crosses the region $3 < r < 9$ very quickly, and the assumption that the electron will not come back once it has gone beyond the barrier must therefore hold. As the frequency increases P_3 becomes bigger, thus invalidating the assumption on which the qualitative description of the ionisation given above depends. At the highest frequency, $\Omega_0 = 2.599$, $P_3 \simeq 0.6$ and it is clear that the electrons which will eventually ionise do so by slow migration to orbits of increasingly large principal action I_n: the larger the frequency the slower this diffusion. This is illustrated over the whole frequency range in Figures 4.10 to 4.16, where the distribution of final action is given for various fields. We can see that for low and medium frequencies ($\Omega_0 = 0.0828$, Fig. 4.10, and $\Omega_0 = 0.497$ and 0.587, Fig. 4.11 and 4.12) the final actions of invariant orbits remain close to their initial value for all values of the applied field:

$0.95 \lesssim I_f \lesssim 1.0$ for $\Omega_0 = 0.0828$, and $0.95 \lesssim I_f \lesssim 1.1$, for $\Omega_0 = 0.497$ and 0.587. As the frequency increases the final actions start getting bigger, at first ($\Omega_0 = 0.832$, Fig. 4.13) over a small range ($0.95 \lesssim I_f \lesssim 1.30$) and for only $\sim 40\%$ to $\sim 60\%$ of invariant orbits, depending on the field, and eventually ($\Omega_0 > 1$, Fig. 4.15 and 4.16) for more and more orbits and up to $I_f \sim 1.60$. At $\Omega_0 = 0.994$ (Fig. 4.14) this trend is interrupted, as the final actions of most invariant orbits are again clustered in the range $0.95 \lesssim I_f \lesssim 1.1$, for most values of the applied field. This is due to the large island corresponding to the lowest resonance $\Omega_0 = 1$. The ionisation criterion given by equation 4.64 is therefore always valid for scaled frequencies $\Omega_0 < 0.2$, but for higher frequencies can only be interpreted as the long-time limit. A second criterion is obtained by using the compensated energy (Leopold and Percival 1979), defined by

$$E_c = \frac{-1}{r} + \frac{1}{2}[p_x^2 + p_y^2 + (p_z - \frac{F}{\omega}\sin\omega t)^2] \,, \tag{4.65}$$

which is approximately constant for large r: if $r \gg 1$ and the field is switched off adiabatically, then E_c tends to the energy. Thus if $r \gg 1$ and $E_c > 0$ we assume the orbit ionised. At low scaled frequency, $\Omega_0 < 0.2$, the $1/\omega$ factor in equation 4.65 dominates, E_c is no longer constant and this criterion is of little value. Therefore, for scaled frequencies $\Omega_0 < 0.2$ we assume that an orbit is ionised if $\max(r(t)) > 3$, and for larger scaled frequencies if $r \geq R_m \gg 1$ and $E_c > 0$; in practice we choose $R_m = 9$.

The calculations carried out here are designed for comparison with the experiments of Koch and co-workers. When comparing experiment and simulation it is necessary to be very careful that the theoretical and experimental definitions of ionisation are identical and that the modelling of the microwave field is as close as possible to the experiment. In most experiments 'ionisation' means the sum of ionisation and excitation to states with $n > n_c = (1.3 - 1.5)n_0$ in the interaction region. The cut-off value n_c was determined by static field ionisation in detection and deflection electric fields. The actual microwave field distribution inside and near the cavity was calculated numerically for each cavity and frequency and the absolute

magnitude of the field strength was determined to an estimated accuracy of 5%. This makes it possible to reproduce correctly in simulations the envelope function $A(t)$ that turned on, maintained and turned off the microwave field.

For the Koch experiments tests have shown that the initial extremal Stark states produced by laser excitation were altered by a small perturbation to the field before entering the cavity, and produced a distribution characterised by equally populated substates and unchanged principal quantum number n. This is the quantal microcanonical distribution, in which the energy is fixed, the square of the eccentricity is uniformly distributed in $(0,1)$ and all the n^2 corresponding (l,m) states have equal probability. The initial conditions for the classical numerical simulation will have to be chosen accordingly. Classically the position and velocity of the electron can be defined uniquely by the 6 quantities

$$\cos\beta,\ \ \varepsilon,\ \ \theta_l,\ \ \theta_n,\ \ \theta_m,\ \ E\ .$$

These classical quantities correspond to the three quantum numbers and three conjugate variables. It is shown by Abrines and Percival (1966) that for the microcanonical distribution all the above variables, apart from the energy, are statistically independent and uniformly distributed over the following intervals:

$$\varepsilon\ \epsilon(0,1)\ ,\ \cos\beta\ \epsilon(-1,1)\ ,\ \theta_l\ \epsilon(0,2\pi)\ ,\ \theta_n\ \epsilon(0,2\pi)\ ,\ \theta_m\ \epsilon(0,2\pi)\ .$$

In the case treated here a rotation around the field axis z does not affect the dynamics, so θ_m is initially set to zero. A uniform distribution is given for all the other variables, the initial values being chosen by using a sequence of pseudo-random numbers.

In our calculations scaled variables F_0, Ω_0 (see Section 4.1.3) are used throughout with $I' \equiv 1$. The equations of motion are solved numerically using an 8^{th} order Runge-Kutta-Fehlberg method. Near the origin numerical integration with these coordinates is about 4 times more efficient than numerical integration with Cartesian coordinates. A long way from the origin

$(r \gg 1)$ the motion is very slow and it is more efficient to use Cartesian coordinates together with an approximation to the equations of motion obtained by expanding in powers of $1/r$. This is given below.

4.2.1 Asymptotic approximation for $r \gg 1$

The Hamiltonian in Cartesian coordinates is given by equation 4.9. Here we derive an approximation for large r in the general case where the field is allowed to have any direction. For simplicity we neglect the switching function $A(t)$, so

$$H(\mathrm{r},\mathrm{p}) = \frac{1}{2}p^2 - \frac{1}{r} + \mathbf{F}\cdot\mathrm{r}\cos\omega t\ , \tag{4.66}$$

where $\mathbf{F} = (F_x, F_y, F_z)$. This simplification is only used to make the notation less cumbersome, it does not affect the result and it is trivial to introduce $A(t)$ again in the equations. Let us now assume that the electron is a long way from the origin at a time t_0:

$$\mathrm{r}(t_0) = (X,Y,Z) = \mathbf{R}\ ,\ |\ \mathbf{R}\ | \gg 1\ . \tag{4.67}$$

If $\mathbf{r}(t) = \mathbf{R} + \mathbf{q}(t)$, where $\mathbf{q} = (q_x, q_y, q_z)$, $\mathbf{q}(t_0) = 0$, $|\ \mathbf{q}(t)\ | \ll |\ \mathbf{R}\ |$ and $|\ \mathbf{r}(t)\ | \geq |\ \mathbf{R}\ |$, then we can write

$$\begin{aligned}\frac{1}{r} &= \frac{1}{(R^2 + 2\mathbf{R}\cdot\mathbf{q} + \mathbf{q}^2)^{1/2}} = \\ &= \frac{1}{R} - \frac{\mathbf{R}\cdot\mathbf{q}}{\mathbf{R}^3} - \frac{\mathbf{q}^2}{2R^3} + \frac{3}{2}\frac{(\mathbf{R}\cdot\mathbf{q})^2}{R^5} + \mathcal{O}(\frac{1}{R^4})\ .\end{aligned} \tag{4.68}$$

By neglecting all terms $\mathcal{O}(R^{-4})$ the Hamiltonian can then be approximated by

$$H = \frac{1}{2}\mathbf{p}^2 + \frac{\mathbf{R}\cdot\mathbf{q}}{\mathbf{R}^3} + \frac{\mathbf{q}^2}{2R^3} - \frac{3}{2}\frac{(\mathbf{R}\cdot\mathbf{q})^2}{R^5} + \mathbf{F}\cdot\mathbf{q}\cos\omega t\ , \tag{4.69}$$

and the equations of motion become

$$\begin{aligned}\dot{\mathbf{p}} = -\frac{\partial H}{\partial \mathbf{q}} &= \frac{1}{R^3}\mathbf{R} + \frac{1}{R^5}B\mathbf{q} + \mathbf{F}\cos\omega t \\ \dot{\mathbf{q}} = \frac{\partial H}{\partial \mathbf{p}} &= \mathbf{p}\ ,\end{aligned} \tag{4.70}$$

where B denotes the matrix

$$\begin{pmatrix} R^2-3X^2 & -3XY & -3XZ \\ -3XY & R^2-3Y^2 & -3YZ \\ -3XZ & -3YZ & R^2-3Z^2 \end{pmatrix}$$

From equation 4.70 it follows

$$\ddot{\mathbf{q}} + \frac{1}{R^5}B\mathbf{q} = -\frac{1}{R^3} - \mathbf{F}\cos\omega t \ . \tag{4.71}$$

In order to uncouple these equations and solve them, we need to diagonalise B, i.e. we must find a matrix A such that

$$A^{-1}BA = D = \begin{pmatrix} \lambda_1 & 0 & 0 \\ 0 & \lambda_2 & 0 \\ 0 & 0 & \lambda_3 \end{pmatrix} \tag{4.72}$$

where $\lambda_1, \lambda_2, \lambda_3$ are the eigenvalues of B. B is a symmetric real matrix, hence it can be diagonalised. From matrix theory we know that A is the matrix whose columns are the eigenvectors of B. It is straightforward to find the eigenvalues of B, they are:

$$\lambda_1 = -2R^2, \quad \lambda_2 = \lambda_3 = R^2 \ . \tag{4.73}$$

From the equations $(B - \lambda_i)u_i = 0,\ i = 1,2,3$, it turns out that the corresponding eigenvectors must have the form:

$$\begin{aligned} u_1 &= (a, a\frac{Y}{X}, a\frac{Z}{X}) \\ u_2 &= (-\frac{b_1Y + c_1Z}{X}, b_1, c_1) \\ u_3 &= (-\frac{b_2Y + c_2Z}{X}, b_2, c_2) \ , \end{aligned} \tag{4.74}$$

where a, b_i and c_i, $i = 1,2$, are any real functions of the coordinates X, Y, Z. The choice of a, b_i and c_i is not unique, but it is restricted in our case by the need to be dimensionally consistent, i.e. the three eigenvectors should all have the same dimension. We therefore impose the condition that the

eigenvectors have dimension of a length and, additionally, that they should be mutually orthogonal:

$$\dim(u_i) = L,\ i = 1,2,3 \tag{4.75}$$

$$< u_i, u_j > = 0,\ i,j = 1,2,3 \quad i \neq j\ . \tag{4.76}$$

With these conditions the eigenvalues are given by

$$\begin{aligned} u_1 &= (X,Y,Z) \\ u_2 &= (-\frac{XY}{X+Z}, \frac{X^2+Z^2}{X+Z}, -\frac{YZ}{X+Z}) \\ u_3 &= (-Z,0,X)\,, \end{aligned} \tag{4.77}$$

so the matrices in equation 4.72 are:

$$A = \begin{pmatrix} X & -\frac{XY}{X+Z} & -Z \\ Y & \frac{X^2+Z^2}{X+Z} & 0 \\ Z & -\frac{YZ}{X+Z} & X \end{pmatrix} \tag{4.78}$$

and

$$A^{-1} = \frac{1}{R^2(X^2+Z^2)} \begin{pmatrix} X(X^2+Z^2) & Y(X^2+Z^2) & Z(X^2+Z^2) \\ -XY(X+Z) & (X^2+Z^2)(X+Z) & -YZ(X+Z) \\ -R^2Z & 0 & R^2X \end{pmatrix} \tag{4.79}$$

A becomes singular, and therefore cannot be used, when $X + Z = 0$. By imposing different restrictions on the eigenvectors it is always possible to find another matrix $\bar{A}$ such that $\bar{A}^{-1}B\bar{A} = D$, non-singular when $X + Z = 0$. In general $\bar{A}$ will be singular on a different subspace (e.g. $Y = 0$) and its elements will be defined in different units, not of length, since the subspace where the singularity occurs is determined by the choice of dimension and the fact that all eigenvector should have the same dimension. In our calculations, if the r-large approximation happens to start at a point $\mathrm{r}(t_0)$ where $X + Z = 0$, instead of using a different transformation we start the approximation at a slightly different point $\mathrm{r}(t_0 - t)$ such that $x(t_0 - t) + z(t_0 - t) \neq 0$, where $\mid \mathrm{r}(t_0 - t) \mid \sim \mid \mathrm{R} \mid$ and $t \ll t_0$. This expedient is the simplest way of getting round the problem, it is consistent with the assumptions

on which the approximation is based and does not affect the subsequent calculation, since the singularity only affects the initial transformation but not the approximate equations of motion. Having obtained a diagonalising transformation, equation 4.71 now becomes

$$\ddot{\mathbf{w}} + \frac{1}{R^5} D\mathbf{w} = -\frac{1}{R^3} - A^{-1}\mathbf{F}\cos\omega t \ , \tag{4.80}$$

where $\mathbf{w} = A^{-1}\mathbf{q}$ and $\ddot{\mathbf{w}} = A^{-1}\ddot{\mathbf{q}}$. This can now be uncoupled to give

$$\begin{aligned}
\ddot{w}_x - \frac{2}{R^3} w_x &= -\frac{1}{R^3} - \frac{1}{R^2}(xF_x + yF_y + zF_z)\cos\omega t \\
\ddot{w}_y + \frac{1}{R^3} w_y &= -\frac{x+z}{R^2(x^2+z^2)}(x(xF_y - yF_x) + z(zF_y - yF_z))\cos\omega t \\
\ddot{w}_z + \frac{1}{R^3} w_z &= -\frac{1}{x^2+z^2}(xF_z - zF_x)\cos\omega t \ .
\end{aligned} \tag{4.81}$$

By introducing the notation

$$\begin{aligned}
k_2^1 = \frac{2}{R^3} \ , \ G_1 &= \frac{1}{R^2}(xF_x + yF_y + zF_z) \\
k_2^2 = \frac{2}{R^3} \ , \ G_2 &= \frac{x+z}{R^2(x^2+z^2)}(x(xF_y - yF_x) + z(zF_y - yF_z)) \\
G_3 &= \frac{1}{x^2+z^2}(xF_z - zF_x) \ ,
\end{aligned}$$

equations 4.81 can be written more neatly as

$$\begin{aligned}
\ddot{w}_x - k_1^2 w_x &= -\frac{k_1^2}{2} - G_1\cos\omega t \\
\ddot{w}_y + k_2^2 w_y &= -G_2\cos\omega t \\
\ddot{w}_z + k_2^2 w_z &= -G_3\cos\omega t \ ,
\end{aligned} \tag{4.82}$$

which can be solved analytically to give:

$$\begin{aligned}
w_x(t) &= \frac{1}{2}(1 - \cosh k_1\tau) + \frac{1}{k_1} p_{w_x}(t_0)\sinh k_1\tau \\
&\quad - \frac{G_1}{\omega^2 + k_1^2}(\cos\omega t - \cos\omega t_0 \cosh k_1\tau + \frac{\omega}{k_1}\sin\omega t_0 \sinh k_1\tau) \\
w_y(t) &= \frac{p_{w_y}(t_0)}{k_2}\sin k_2\tau \\
&\quad + \frac{G_2}{k_2^2 - \omega^2}(\cos\omega t + \frac{\omega}{k_2}\sin\omega t_0 \sin k_2\tau - \cos\omega t_0 \cos k_2\tau)
\end{aligned}$$

$$
\begin{aligned}
w_z(t) &= \frac{p_{w_z}(t_0)}{k_2}\sin k_2\tau \\
&\quad + \frac{G_3}{k_2^2-\omega^2}(\cos\omega t + \frac{\omega}{k_2}\sin\omega t_0 \sin k_2\tau - \cos\omega t_0 \cos k_2\tau)
\end{aligned}
$$

and

$$
\begin{aligned}
p_{w_x}(t) &= \frac{1}{2}\sinh k_1\tau + p_{w_x}(t_0)\cosh k_1\tau \\
&\quad + \frac{G_1}{\omega^2+k_1^2}(\omega(\sin\omega t - \sin\omega t_0 \cosh k_1\tau) + k_1 \cos\omega t_0 \sinh k_1\tau) \\
p_{w_y}(t) &= p_{w_y}(t_0)\cos k_2\tau \\
&\quad - \frac{G_2}{k_2^2-\omega^2}(\omega(\sin\omega t - \sin\omega t_0 \cos k_2\tau) + k_2 \cos\omega t_0 \sin k_2\tau) \\
p_{w_z}(t) &= p_{w_z}(t_0)\cos k_2\tau \\
&\quad - \frac{G_3}{k_2^2-\omega^2}(\omega(\sin\omega t - \sin\omega t_0 \cos k_2\tau) + k_2 \cos\omega t_0 \sin k_2\tau)\ ,
\end{aligned}
$$

where $\tau = t - t_0$ and $\mathrm{p}_w(t) = (p_{w_x}(t), p_{w_y}(t), p_{w_z}(t)) = A^{-1}\mathrm{p}(t) = A^{-1}(p_x(t), p_y(t), p_z(t))$. In our calculations, where scaled variables are used with $n_0 = 1$ (section 4.1.3), these analytical solutions are used whenever $r(t) > R = 9$. The system is then evolved in time in steps of 2π and a check on the magnitude of r is made at the end of each step. If r becomes again smaller than 9 a conversion is made back to regularised coordinates and the time evolution is carried on as before by numerical integration of the exact equations of motion.

As observed previously, any orbit for which $r(t) > 9$ is unstable, so this asymptotic approximation is used only for unstable orbits which cannot be integrated exactly and therefore it does not introduce serious errors and at the same time it provides an efficient way of estimating the time-dependence of the excited states population. In some cases it is not needed, as 'ionisation' can be defined to have occurred when $r(t) > 9$.

4.3 Results

The equations of motion 4.60 were integrated for a microcanonical ensemble of initial conditions at several values of the field strength and at frequencies ranging from $\Omega_0 = 0.05$ to $\Omega_0 = 2.5$. The number of trajectories used was about 200-300 in each case. This was enough to provide good statistics,with the standard deviation for the ionisation ratio P_I varying from about 10% to 1% for values of P_I ranging from 0.1 to 0.9 respectively. Most calculations were performed with an adiabatic switch-on and -off T_a lasting 30 periods of the applied field and the system was allowed to evolve under the maximum value of the field for a time $T_m = 300$ periods. In a few representative cases T_a and T_m were varied to check the effect of the adiabatic switch and the 'convergence' of our results.

If scaled variables are used, the main parameters of the system are the scaled microwave field $F_0 = n_0^4 F$ and the scaled microwave frequency $\Omega_0 = n_0^3 \omega$ (see section 4.1.3). Let us first consider the ionisation curves, i.e. graphs of the ionisation ratio P_I versus the field strength F_0. For almost all frequencies the ionisation curves are monotonic and featureless, rising from 0 to 1. Although this general description applies to all frequencies, there are big differences in the ionisation curve from one frequency to the next. The only other universal observation that can be made is that there is a general tendency of the curves to rise faster at lower frequencies. For example at $\Omega_0 = 0.2$ the ionisation ratio rises from 10% to 90% over the scaled field range $F_0 = 0.1 - 0.125$, while at $\Omega_0 = 1.72$ the same rise is achieved over the much wider range $F_0 = 0.025 - 0.11$. Some typical values are given in Table 4.1.

Ω_0	0.2	0.5	0.7	1.0	1.18	1.72	2.7
$F_0(10\%)$	0.100	0.062	0.033	0.045	0.030	0.025	0.035
$F_0(90\%)$	0.125	0.100	0.060	0.120	0.087	0.110	0.220

Table 4.1 Approximate values of the scaled fields needed for 10% and 90% ionisation for various scaled frequencies.

If we consider the variation of the ionisation threshold with the scaled microwave frequency Ω_0, a different picture emerges. For example a graph of the field which produces 10% ionisation, $F(10\%)$ versus Ω_0 shows a definite series of peaks, which coincide with rational values of the scaled frequency $\Omega_0 = 1, 1/2, 1/3, 2/3...$, and a similar pattern is reproduced at all thresholds. This is illustrated in Figure 4.2 for the 10% and 90 % thresholds; here the corresponding experimental curves are also shown by the dots. We can see that there is generally very good agreement between experimental results and classical simulation, apart from some differences near the resonant frequencies mentioned above. At these frequencies there are island structures in the phase space that affect the dynamics; the nature of the dynamics near resonances will be discussed below. In addition to the special case of resonant frequencies, it turns out that there are five subregions of the frequency in which the behaviour of this system shows characteristic differences. These are:

R1 $0 \leq \Omega_0 n_0 < 1$: In this adiabatic region there are no transitions between the adiabatic states and for $F_0 < 0.1298$ ionisation occurs only through tunnelling. The quantal threshold is lower than the classical one, which tends to 0.1298 as the frequency tends to zero.

R2 $1 \leq \Omega_0 n_0 < 10$: Here the quantum dynamics is dominated by relatively few adiabatic states (Richards 1987), so there is the possibility of quantal resonances. Because only few states are needed classical dynamics fails. The resonances between these states provide an explanation for the structure seen in experimental ionisation curves and the seemingly erratic changes with quantum number.

R3 $0.2 \leq \Omega_0 < 1.1$: In this region many quantal states are coupled together and the classical and quantal descriptions agree, except at a few resonant frequencies. The agreement between our 3-dimensional calculations and the experimental results is very good, but it is important to stress that these results were limited to comparisons of the ionisation probability, defined in the experiment as excitation above

$n = 92$, and for times of about 300 field oscillations. It is not obvious what would happen if these conditions are changed. These points will be discussed further in Chapter 6.

R4 $1.1 \leq \Omega_0 < 2.0$: This is a border region in which the classical dynamics is beginning to break down, and the experimental and quantal ionisation thresholds gradually rise above the classical ones. Nevertheless in this region the quantal ionisation probabilities show evidence of the classical phase-space structures. This was observed by Jensen *et al.* (1989), who show that the inhibition of quantum transport is due to the selective excitation of wave functions that are highly localised near unstable periodic orbits in the classical phase space.

R5 $2.0 \leq \Omega_0$: In this region the classical approximation breaks down, as the quantal motion is dominated by relatively few quasi-resonant states (Richards *et al.* 1989a). The effective density of states is thus drastically reduced: instead of an infinite number of relevant states between the initial level n_0 and the continuum there are only $n_0/2\Omega_0$.

In order to present a picture as clear and complete as possible, three main areas of investigation are considered separately. Firstly, a systematic study of the convergence of the ionisation curves is presented. Secondly, results obtained with converged parameters over the whole range of field strengths and frequencies are analysed. Particular attention is given to the behaviour of the ionisation curves at resonant and non-resonant frequencies and at low and high frequencies; the ionisation thresholds obtained with one- and three-dimensional models are compared and discrepancies between these two models are discussed. Other interesting results are also discussed, such as the distribution of final actions and energies and the dependence of the ionisation on the initial distribution of the eccentricity. Finally, selected examples are given from an extensive comparison with the experimental results of Koch and co-workers (Koch 1982, 1988). In addition some numerical and experimental results obtained with two microwave fields of different frequencies are presented. This slightly different system is discussed for its

relevance to the understanding of the behaviour near resonances.

4.3.1 Convergence of the ionisation curve

Here we examine the effects of varying the type and length of the adiabatic switch and the length of the total integration time. For many frequencies over the whole range we compared results obtained with two different adiabatic switch functions $f_1(t)$ and $f_2(t)$:

$$f_1(t) = \begin{cases} x^2(2-x^2) & 0 & \leq t \leq & T_a \\ 1.0 & T_a & < t \leq & T - T_a \\ y^2(2-y^2) & T - T_a & < t \leq & T \end{cases} \tag{4.83}$$

$$f_2(t) = \begin{cases} \frac{1}{2}[1 + \tanh(\frac{1}{4}(\frac{1}{1-x} - \frac{1}{x}))] & 0 & \leq t \leq & T_a \\ 1.0 & T_a & < t \leq & T - T_a \\ \frac{1}{2}[1 + \tanh(\frac{1}{4}(\frac{1}{1-y} - \frac{1}{y}))] & T - T_a & < t \leq & T \end{cases} \tag{4.84}$$

where $x = t/T_a$, $y = (T-t)/T_a$ and T is the total integration time: $T = T_m + 2T_a$. We found that, given a fixed total integration time, the ionisation probabilities obtained using either function agree within the statistical errors when T_a lasts about 30 periods. This is in slight contrast with similar tests performed with the one-dimensional model: in that case in order to get agreement between results obtained with different adiabatic functions the length of the adiabatic switch has to be much longer, typically between 60 and 100 periods.

The dependence of the ionisation on the integration time T_m was tested by comparing results obtained with $T_m = 300$ and $T_m = 600$ periods of the applied field. Also, plots of $P_{inv} = 1 - P_I$ versus t were obtained for many different frequencies at values of the applied field such that the final ionisation ratio was $\sim 10\%, 30\%, 50\%, 80\%$. These are given in Figures 4.3a to 4.9a. Since different orbits ionise at different times, these curves are expected to fall initially with a finite slope and then approach an asymptotic value. The behaviour we actually see differs from this ideal picture and depends on the frequency and on the strength of the field. For frequencies $\Omega_0 \leq 1$ the curves P_{inv} versus t do indeed appear to stabilise around the

final value of ionisation before the field starts being switched off, if the final ionisation is bigger than 30%. For very weak fields, giving less than 30% ionisation, the ionisation curves for frequencies in the upper part of this region reached an asymptotic value only if the integration time was increased still further. In general in the asymptotic region a small decrease can still be seen, but is probably due to numerical errors. The main observation to be made is that, although all ionisation curves for this range of frequency reach an asymptotic value provided the integration time is long enough, they do so extremely quickly for very low frequencies ($\Omega_0 < 0.2$). This behaviour is consistent with the validity of the adiabatic approximation for low frequencies, discussed in the previous section.

For frequencies $\Omega_0 > 1$ the time needed for stabilisation increases rapidly with the frequency and for $\Omega_0 > 2$ this increase becomes more marked; for example, in the case $\Omega_0 = 5$ an asymptotic value was reached only after many thousand field periods. A simple explanation of this observation is that the relevant time-scale is not the period of the applied field, but that of the orbits. Although this is certainly true, it is not sufficient to account for the behaviour observed, which is due to the different mechanism of ionisation characteristic of this frequency range. For high frequencies the amount of direct ionisation occurring is negligible: the irregular orbits diffuse slowly in action and therefore take a very long time to ionise. The diffusion rate D depends on the frequency as: $D =< \Delta I^2(\omega) > /(2\pi\omega(I))$.

The different stabilisation times for the ionisation curves at low fields (such that $P_I \leq 30\%$) and higher fields arise from the fact that at low fields many unstable orbits take a long time to ionise, whilst at higher fields the ionisation process is typically quicker. It is very important to know the length of time needed for stabilisation of a particular ionisation curve when comparing with experiments where the atoms are in the microwave field for only about 300 periods. If this time is not long enough for the curve to reach an asymptotic value this will add to the difficulty in performing a meaningful comparison. The main problem here lies in defining 'ionisation', as discussed at the end of section 4.2.

As the length of the adiabatic switch-on is increased, keeping T_m fixed, two conflicting effects will come into play:

1. If T_m is shorter than the time needed to reach an asymptotic value, the ionisation ratio will tend to increase because the total integration time becomes longer. We expect this effect to be relatively small, particularly at low fields, because the additional integration time is restricted to the adiabatic switch, when the field is mostly much smaller than its maximum value.

2. The ionisation ratio will tend to decrease because the longer adiabatic switch-on will tend to bring onto or nearer to invariant tori more orbits that would have otherwise been unstable at the maximum field. This effect should be negligible if the different values of T_a are all much longer than any characteristic period of the system. In practice of course this is never achieved. These dynamical changes induced by an adiabatic switch-on have been discussed in some generality in Chapter 2. In Chapter 5 they are illustrated explicitly for a map constructed to simulate the one-dimensional hydrogen atom in a microwave field.

We can therefore conclude that, since effect 1 is always negligible for long enough T_m and effect 2 is always present due to the impossibility of making T_a longer than any characteristic period of the system, the ionisation rate P_i always decreases as the adiabatic switch T_a increases. In practice we do not actually see this: the magnitude of effect 2 depends significantly only on the main periods of the system and therefore produces an appreciable change only if these are very long; otherwise any change is completely undetectable, being of the same order as the numerical and statistical errors incurred in the simulation.

The results of calculations performed with different values of T_a and a fixed value of T_m, long enough to achieve stabilisation, are given in Table 4.2. We find that the variation of the ionisation with T_a is strongly dependent on the frequency. For all non-resonant frequencies the change in P_I remains within the statistical errors.

$\Omega_0 = 0.4165$

	T_a		
F_0	30	60	100
.060	.05 ± .01	.05 ± .01	.04 ± .01
.070	.53 ± .03	.55 ± .03	.57 ± .03
.080	.81 ± .03	.79 ± .03	.80 ± .03

$\Omega_0 = 0.5$

	T_a		
F_0	30	60	100
.062	.09 ± .02	.04 ± .01	.02 ± .01
.080	.41 ± .03	.35 ± .03	.30 ± .03
.093	.71 ± .03	.66 ± .03	.63 ± .03

$\Omega_0 = 1.0$

	T_a		
F_0	30	60	100
.045	.11 ± .02	.10 ± .02	.06 ± .02
.070	.40 ± .03	.34 ± .03	.30 ± .03
.090	.70 ± .03	.61 ± .03	.61 ± .03

$\Omega_0 = 1.2586$

	T_a		
F_0	30	60	100
.030	.04 ± .01	.04 ± .01	.04 ± .01
.060	.57 ± .03	.61 ± .03	.59 ± .03
.110	.93 ± .02	.95 ± .02	.95 ± .02

$\Omega_0 = 1.5$

	T_a		
F_0	30	60	100
.040	.07 ± .01	.08 ± .01	.06 ± .01
.060	.39 ± .03	.46 ± .03	.40 ± .03
.100	.82 ± .02	.85 ± .02	.88 ± .02

Table 4.2 Variation of P_I with T_a for three resonant and two non-resonant frequencies at various fields. The integration time at the maximum value of the field was $T_m = 300$.

		T_a		
	F_0	30	60	100
$\Omega_0 = 0.4165$	.060	.06 ± .01	.07 ± .01	.06 ± .01
	.070	.53 ± .03	.54 ± .03	.55 ± .03
	.080	.81 ± .03	.81 ± .03	.80 ± .03

		T_a		
	F_0	30	60	100
$\Omega_0 = 0.5$	.062	.10 ± .02	.04 ± .01	.03 ± .01
	.080	.41 ± .03	.35 ± .03	.30 ± .03
	.093	.71 ± .03	.66 ± .03	.63 ± .03

		T_a		
	F_0	30	60	100
$\Omega_0 = 1.0$	.045	.14 ± .02	.13 ± .02	.12 ± .02
	.070	.43 ± .03	.37 ± .03	.30 ± .03
	.090	.70 ± .03	.63 ± .03	.62 ± .03

		T_a		
	F_0	30	60	100
$\Omega_0 = 1.2586$	.030	.09 ± .01	.10 ± .01	.09 ± .01
	.060	.69 ± .03	.68 ± .03	.71 ± .03
	.110	.98 ± .02	.99 ± .02	.98 ± .02

		T_a		
	F_0	30	60	100
$\Omega_0 = 1.5$	.040	.16 ± .01	.11 ± .01	.10 ± .01
	.060	.61 ± .03	.62 ± .03	.55 ± .03
	.100	.91 ± .02	.91 ± .02	.91 ± .02

Table 4.3 Variation of $P_I(r > 3)$ with T_a for three resonant and two non-resonant frequencies at various fields. The integration time at the maximum value of the field was $T_m = 300$.

In the case of resonant frequencies, on the other hand, P_I is very sensitive to variations in T_a. At low and medium fields P_I decreases as T_a increases, and vice versa at high fields. These variations are also reproduced when the length of the integration time at the maximum value of the field is doubled ($T_m = 600$). Furthermore, they are not dependent on the ionisation criterion. As we found that orbits with radius bigger than 3 do eventually ionise, we calculated $P_I(r > 3)$ in all the cases given in Table 4.2 and the same variation with T_a was reproduced, even though in some cases these two ionisation criteria give very different ionisation ratios. The results for $P_I(r > 3)$ are given in table 4.3. It is interesting to note that the differences between $P_I(r > 3)$ and P_I are always within the statistical errors for $\Omega_0 < 1$, but for higher frequencies $P_I(r > 3)$ becomes increasingly bigger than P_I. It seems that the mechanism of ionisation is different for high frequencies: while for $\Omega_0 < 1$ orbits ionise very quickly once they get far from the nucleus ($r > 3$), for $\Omega_0 > 1$ the orbits tend to remain much longer in highly excited states before eventually ionising. This is consistent with the interpretation of excitation in the case of high frequency as a diffusive process.

4.3.2 Analysis of results with converged parameters and comparison with one-dimensional simulations

Having determined appropriate values for the parameters and their effect on the calculations, we were then able to perform meaningful simulations. Results were obtained throughout the frequency range $\Omega_0 = 0.0828 - 2.599$ with $T_a = 30$ and $T_m = 300$ periods, appropriate for the Koch experiment.

We have seen above and in section 4.2 that there exist at least three approximately defined ranges of frequency in which the mechanism of ionisation is different. Obviously this is due to the dynamics of the system being different in these ranges, and this can be seen from the behaviour of other observables. Figures 4.10 to 4.16 show the distribution of final actions for invariant orbits at various field strengths and for representative frequencies throughout the range. We can see that for the lowest frequency ($\Omega_0 = 0.0828$, Figure 4.10) the final actions of invariant orbits are almost

unchanged. This is the case for frequencies $\Omega_0 \lesssim 0.2$ and it applies also to other parameters of the orbit, for example the eccentricity, as described below. For these very low frequencies the orbits either ionise or remain very close to their initial configuration. For higher frequencies in the intermediate range the distribution of final actions is similar, although it starts creeping up to higher values (up to 1.10), particularly when the applied field is strong (see Figures 4.11 and 4.12). The number of orbits with final actions bigger than 1 is still nevertheless a very small percentage of the invariant orbits. The different dynamics of the system in this frequency range is not reflected by these final distributions. When the frequency becomes higher still ($\Omega_0 = 0.832$, Figure 4.13) we start to see a completely different picture. At fairly low values of the applied field (giving $\sim$ 20% ionisation) $\sim$ 60% of invariant orbits have final actions I_f in the range 0.95-1.05 and all the others have I_f distributed with increasingly smaller percentages between 1.10 and 1.30. As the field increases the final actions of invariant orbits become more uniformely distributed between 0.95 and 1.30, pointing to the beginning of a diffusion mechanism. For the higher frequency $\Omega_0 = 0.994$ (Figure 4.14) the picture almost reverts to what we saw for lower frequencies: similar values of I_f as above are reached, but only a very small percentage of invariant orbits has high final actions, while most are again clustered around 0.95-1.05, even when the applied field is strong enough to give 70% ionisation. This behaviour is associated with the very large island at $\Omega_0 = 1$. For the much higher frequencies $\Omega_0 = 1.647$ and $\Omega_0 = 2.599$ (Figures 4.15 and 4.16) the final actions of invariant orbits span the whole range between 0.95 and 1.60 even for fairly weak applied fields, and the distribution becomes more uniform as the field increases. This is a clear illustration of the dynamics becoming diffusive.

Figures 4.17 to 4.23 are scatter plots of the final against initial eccentricity squared (ϵ_f^2 versus ϵ_i^2). Here we can again roughly classify the behaviour according to the same frequency ranges. For $\Omega_0 = 0.0828$ (Figure 4.17) the initial eccentricities of almost all invariant orbits remain very close to their initial values. For $\Omega_0 = 0.497$ (Figure 4.18) the picture is similar, al-

though there are more cases where $\varepsilon_f^2 \gg \varepsilon_i^2$. The scatter plot looks mainly like a band of small width along the diagonal, widening for $\varepsilon_i^2 \gtrsim 0.8$. For $\Omega_0 = 0.587$ (Figure 4.19) the distribution of final eccentricities displays the same features as described for the previous case, but the deviations from the diagonal become more pronounced. For $\Omega_0 = 0.832$ (Figure 4.20) the distribution is similar, although with even larger deviations from the diagonal, when the applied field is low (giving $\sim 20\%$ ionisation); but for higher values of the field the distribution departs significantly from what was observed for smaller frequencies and tends to fill the triangle above the diagonal, i.e. most invariant orbits become elongated. At $\Omega_0 = 0.994$ (Figure 4.21) the same behaviour is repeated and becomes noticeable also when the applied field is weak. The scatter plots of final against initial eccentricity for $\Omega_0 = 1.647$ (Figure 4.22) appear very similar, but a closer look reveals a new feature: it seems that for orbits with very small initial eccentricity ($\varepsilon_i^2 \lesssim 0.1$) the eccentricity remains almost unchanged. For $\Omega_0 = 2.599$ (Figure 4.23) we can see a definite, quite remarkable invariance for $\varepsilon_i^2 \lesssim 0.2$. For $\varepsilon_i^2 \gtrsim 0.2$ the distribution tends to be above the diagonal.

We recall that the curves giving the ionisation thresholds as a function of the frequency Ω_0 have peaks coinciding with resonances. The special behaviour that these graphs suggest is associated with resonances is borne out by other results. A systematic study is carried out over 5 resonant and 4 non-resonant frequencies spanning the whole range. These are: $\Omega_0 = 1/3$, 0.4165, 1/2, 0.7414, 1, 1.2586, 3/2, 1.7414, 2.

A striking difference between resonant and non-resonant cases is shown by the distribution of the angle of ejection of ionised orbits: in the case of resonant frequencies this distribution is virtually uniform, whereas in the non-resonant case there is a strong tendency for the ionised atom to be ejected along the axis. This is illustrated in Figure 4.24 for four resonant and four non-resonant frequencies. In all cases the ionisation was 100% and the initial orbits were all circular and in a plane perpendicular to the field. A similar picture, but with less pronounced differences is obtained with an initially microcanonical distribution.

Circular orbits in a plane perpendicular to the field turn out to be the most stable; this is analogous to the effect seen when a static field is applied, described in section 1.2. The ionisation threshold for these orbits is several times higher than that for a microcanonical distribution, as shown in Table 4.4 below.

Ω_0	$F(10\%)$	$F(10\%)_{\perp,O}$
0.3333	0.085 ± 0.002	0.155 ± 0.005
0.4165	0.061 ± 0.002	0.105 ± 0.005
0.5	0.062 ± 0.002	0.150 ± 0.005
0.7414	0.028 ± 0.002	0.100 ± 0.005
1.0	0.044 ± 0.002	0.200 ± 0.005
1.2586	0.033 ± 0.002	0.355 ± 0.005
1.5	0.042 ± 0.002	0.355 ± 0.005
1.7414	0.061 ± 0.002	0.600 ± 0.005

Table 4.4 Threshold fields for 10% ionisation. The first column gives the results for orbits with an initial microcanonical distribution, the second one gives the results for orbits initially circular and in a plane perpendicular to the field axis.

The stability of circular and nearly circular orbits, independently of their orientation, is apparent if we look at the distribution of the initial eccentricity of the orbits which ionise. This is shown in Figure 4.25 for four resonant and four non-resonant frequencies. We can see that in all cases out of all the ionised orbits less than 5% started with $\varepsilon^2 < 0.2$. Orbits which started with $\varepsilon^2 \sim 1$ and uniform orientation with respect to the direction of the field do not appear to be particularly unstable; in fact, for the two lowest non-resonant frequencies shown, $\Omega_0 = 0.4165$ and $\Omega_0 = 0.7414$, orbits with $0.8 < \varepsilon^2 < 1$ are as unlikely to ionise as those with $\varepsilon^2 < 0.2$. However 'straight line' orbits ($\varepsilon = 1$) which start along the direction of the field are more unstable. These orbits ionise much quicker than any others, as is shown by their ionisation curves. Two examples and the comparison with the corresponding ionisation curves for a uniform initial distribution are given in Figure 4.26. .

The greater instability of straight line orbits which start along the direction of the field provides a partial explanation for some of the discrepancies

found between the results for one- and three-dimensional models, in particular the fact that all one-dimensional ionisation curves are much steeper. This instability also explains the agreement found at threshold. As Ω_0 increases the differences between one- and three-dimensional models become more pronounced. We have seen previously (section 4.2) that for high frequencies the effect of the field is only appreciable when the electron is close to the nucleus, where it moves fast because of the Coulomb singularity. This phenomenon inevitably leads to a greater ionisation rate in one dimension, since in that case every orbit passes through the singularity. The qualitative behaviour of the ionisation probability as a function of the frequency is nevertheless similar in the two models, as shown for example in Figure 4.27. Some examples showing the different rates at which one- and three-dimensional ionisation curves rise are given in Figures 4.28, 4.29 and 4.30 for $\Omega_0 = 0.0647$, 0.0828 and 0.1669 respectively. In these figures the one- and three-dimensional results are denoted by the full and empty circles respectively. We can see that, although the two curves have very different slopes, the thresholds are similar. Agreement at threshold is found for most frequencies $\Omega_0 \leq 2.0$. At higher scaled frequencies the disagreement between the two models increases greatly and extends to the threshold values; for example at $\Omega_0 = 5.6$ the value of the field needed for 10% ionisation is $F_0(10\%) \simeq 0.026$ in one dimension, and $F_0(10\%) \simeq 0.052$ in three dimensions (Richards 1989). Another difference we found was that the one-dimensional simulation required a longer adiabatic switch, at least for frequencies $\Omega_0 > 0.2$. For example in the range of intermediate frequencies for $T_a = 30$ periods of the field the one-dimensional results are still sensitive to the particular form of the switch function and to the initial phase of the field. Only for $T_a = 60 - 100$ does the dynamics become independent of the initial phase as it should be.

4.3.3 Comparison with experimental results

Some representative examples are presented here from an extensive comparison of our three-dimensional numerical simulation with experimental results. The experimental arangement is described in section 4.1.1. In all

the experiments the cavity frequency ω was fixed and the initial principal quantum number n_0 was known precisely. By varying n_0 for a fixed ω it was possible to obtain a stepwise variation in the scaled frequency Ω_0. The scaled frequency is related to the cavity frequency and to n_0 by

$$\Omega_0 = \frac{\omega}{\omega_{at}(n_0)} = \frac{\omega}{GHz}(kn_0)^3 \,, \tag{4.85}$$

where $k = 0.00533757$. Most experimental results were obtained with a cavity frequency $\omega = 9.9233$ GHz, with the value of the principal quantum number n_0 in the range $n = 32-90$. This gives the range of scaled frequencies $\Omega_0 = 0.05 - 1.1$.

Each atom experienced approximately 300 microwave oscillations in the cavity, with constant field amplitude determined to $\pm$ 5%. The experimental error in the field amplitude is important because the ionisation is very sensitive to small variations in the field. As mentioned previously, due to fringe fields the atom also experienced about 40-80 microwave oscillations at the entrance and exit of the cavity with slowly increasing and decreasing amplitude respectively.

The highly-excited atoms were detected either by microwave ionisation in the microwave cavity, or by static electric field ionisation in a longitudinal field ioniser located downstream of the cavity. The first method is referred to as 'ionisation', the second one as 'quenching'. Note that with the ionisation method atoms with $n_0 \geq 75$ can be ionised by the additional longitudinal static field produced. This of course must be taken into account when comparing with simulations.

In general there is remarkable agreement between the experimental and our numerical results, as can be seen for example in Figure 4.31. However there are some notable exceptions. These occur at very low frequencies (see for example Figure 4.29), resonances (Figure 4.32), and very high frequencies. As we shall see, in each case this is due to quantal effects, and therefore a classical model is not a very good approximation at these frequencies.

At low scaled frequencies $\Omega_0 = 0.0494 - 0.1375$, corresponding to $n_0 = 32 - 45$, the experimental ionisation curves have plateaux and local maxima

which are not reproduced by the simulation , and the experimental ionisation threshold is usually lower (Richards *et al* 1989b). In fact for $\Omega_0 < 0.1$ the quantal dynamics of the system can be described with only very few basis states (Richards 1987) and much of the structure seen in the experimental ionisation curves can be explained in terms of resonances in a two-state system (see discussion in section 4.1.4). An exception to the usual monotonically increasing behaviour of the classical ionisation curves is found in the case $n_0 = 35, \Omega_0 = 0.0647$ (Figure 4.28). Here the classical ionisation probability has a local minimum at $F \approx 0.145$, which is not due to statistical errors: this has been checked (Richards *et al.* 1989b) by increasing the number of orbits in each simulation to about 600. The experimental curve has a low plateau in the range $0.115 < F < 0.1225$, whereas the classical ionisation probability only becomes becomes different from zero at $F = 0.120$. Apart from this discrepancy at the threshold, and the classical local minimum, the three-dimensional classical curve agrees very well with the experiment. The local maximum around threshold in the experiment is probably due to a combination of several resonances from many m-states. At $n_0 = 38, \Omega_0 = 0.0828$ (Figure 4.29) similar behaviour is observed, but here the local maximum in the experimental curve is much higher and agreement between experiment and three-dimensional simulation is only achieved for high fields ($F > 0.145$). At $n_0 = 48, \Omega = 0.1669$ (Figure 4.30) there is much better agreement, except at threshold, where the classical curve rises faster.

In the intermediate frequency range, $0.1 < \Omega_0 < 1.0$, the agreement between the experiment and classical dynamics is extremely good, except at resonances. Figure 4.31 shows the comparison for $\Omega = 0.587$ and we can see that the agreement is almost perfect. In the resonant case $\Omega = 0.496$, though, there are significant differences (Figure 4.32). In general both classical and quantal dynamics are more stable near a resonance, but there are differences depending on the width of the resonance. Classical and quantal dynamics are similar only if the width of the islands is large enough for many quantum states to be trapped inside. If the area enclosed by the

separatrix is $O(\hbar)$ then, although the classical motion inside the separatrix remains trapped, the wave function centered on the island centre is spread significantly outside the separatrix. Thus the effect of the islands is much less pronounced in the experiment than it is in the classical simulation.

Although we do not yet have available enough high-frequency experimental results for detailed comparison, we know that certain discrepancies must arise because the classical and quantal dynamics are different in this range. As we have seen (Section 4.1.4), the quantal dynamics is expected to be more stable at these frequencies (Casati *et al* 1984, 1986, Leopold and Richards 1988a). Existing experimental results (Galvez *et al* 1988, Bayfield *et al.* 1989) confirm that for $\Omega_0 > 2.0$ the experimental thresholds for ionisation are higher than those predicted by classical mechanics.

4.3.4 Ionisation in the presence of two microwave fields

As we have seen previously, curves giving the ionisation threshold as a function of the frequency show considerable structure, with local maxima occurring at resonances. Therefore the system is most stable at the resonances. This is explained classically by the trapping of orbits inside the resonance islands in phase space. Thus, the lower the order of the resonance, the wider the region of stability, as can be seen in Figure 4.2. If this is the main reason for stability, then the addition of a second frequency, which destroys the resonance, would make the system less stable. We know that the classical resonance islands do play a role, because maxima occur both experimentally and in simulation. However experimental and numerical ionisation curves show marked discrepancies at resonances, whilst agreeing very well everywhere else in the intermediate frequency range, and this suggests that quantal effects are playing an important part. A partial explanation is given above, but a more complete understanding is needed. The study of the hydrogen atom in the presence of two microwave fields of different frequencies may provide some clues to the explanation of these quantal effects, particularly since experimental two-frequency results are now becoming available (Moorman *et al* 1988).

In these experiments the addition of a second frequency produced a very marked reduction of the ionisation threshold at resonance, supporting the classical explanation that the stability is reduced because one-frequency resonance islands in phase space are destroyed. However, in some experimental two-frequency curves non-monotonic structures appear. These structures are similar to those observed in some one-frequency experimental curves at low scaled frequency, known to be of quantal origin (see section 4.3.3), suggesting a related origin also in this case, and making a classical interpretation of these results more difficult. A similar, but less pronounced, reduction of the ionisation threshold was observed also at non-resonant frequencies.

Our simulations show similar behaviour, although the experimental non-monotonic structures are not reproduced. The calculations were carried out using the Hamiltonian

$$H = \frac{1}{2}p^2 - \frac{1}{r} + zA_1(t)F_1 \sin(\omega_1 t + \phi_1) + zA_2(t)F_2 \sin(\omega_2 t + \phi_2) \ , \quad (4.86)$$

where $A_1(t)$ and $A_2(t)$ are adiabatic functions as in equation 4.84, expressing the switch-on and switch-off of each respective field. The integration of the equations of motion for the above Hamiltonian required a straightforward modification of the one-frequency simulation. Results were obtained with two different frequencies of 7.5816 and 11.89 GHz, in order to compare with the experiment. Figure 4.33 shows the ionisation probability as a function of the frequency in the neighbourhood of the resonance 1/2 as the amplitude of the second microwave field is increased from 0 to 0.01 but keeping the total amplitude constant. We can see that as the second field becomes stronger the local minimum becomes shallower, i.e. the system becomes less stable.

Comparisons with experimental two-frequency results are currently under way and it is hoped that the dynamics of this more complicated system can be at least partially explained in the light of the one-frequency results presented in the previous sections, since a weak additional microwave field can be treated as a perturbation. There is at present no general theory which explains two-frequency ionisation, but some classical and quantal calculations at low scaled frequencies have been carried out recently (Blümel

et al. 1989) which show that theoretical quantal results agree well with experiment. Much more work remains to be done on this subject.

Chapter 5

A simple model of the hydrogen atom

In this chapter we study a 2-dimensional area-preserving map constructed specifically to simulate the dynamics of the hydrogen atom perturbed by a microwave field. This simple model provides a convenient framework in which to illustrate and understand the effects of the adiabatic method and thus justify and further explain the results obtained in the previous chapters.

An area-preserving map in M dimensions is a transformation f of the space onto itself such that the Jacobian of the transformation is 1. For any point $\mathbf{x}_0$ in the space, f gives rise to a sequence $\mathbf{x}_n$ defined by

$$\mathbf{x}_{n+1} = f(\mathbf{x}_n) \, .$$

Time-independent Hamiltonian systems can be conveniently described in terms of area-preserving maps by means of a Poincaré surface of section. For an N-dimensional system $H(\mathbf{q}, \mathbf{p})$ the trajectories lie on a $(2N-1)$-dimensional energy surface in phase space: $H(q_1, \ldots, q_N, p_1, \ldots, p_N) = H_0$. This equation determines any coordinate, say p_N, in terms of all the others. Thus without loss of information one can consider the projection of the motion onto the $(2N-1)$-dimensional subspace defined by $p_N = 0$. A surface of section is then a $(2N-2)$-dimensional surface defined by q_N =constant, with coordinates $q_1, \ldots, q_{N-1}, p_1, \ldots, p_{N-1}$. A trajectory in phase space will cross the surface of section at successive points which can be obtained from one another by a canonical transformation f generated by the equations of motion. Consequently the area enclosed by a curve on the surface of section

is conserved on successive crossings. Hamilton's equations thus generate an area-preserving map on a surface of section. The dynamics of hamiltonian systems is therefore closely related to the behaviour of area-preserving maps. For systems with two degrees of freedom a convenient choice of surface of section leads to the twist map

$$\begin{aligned} I_{n+1} &= I_n \\ \theta_{n+1} &= \theta_n + 2\pi\alpha(I_{n+1}) \ , \end{aligned} \tag{5.1}$$

where I and θ denote action and angle variables respectively, and α is the rotation number: $\alpha(I) = \omega_1(I)/\omega_2(I)$.

For integrable systems a trajectory will lie on an invariant torus, whose intersection with the Poincaré surface of section is an invariant curve. All iterates of an initial point generated by the map on a surface of section must then lie on such a curve. If an initial point (I_0, θ_0) is on a resonant torus, then the motion is periodic of some period n and (I_0, θ_0) is a fixed point of f^n. Resonant and nearly resonant tori are the first to be destroyed when an integrable system is perturbed. The study of maps provides some understanding of the dynamics of perturbed systems in the gaps where the resonant tori existed. Given a rational rotation number $\alpha(I) = r/s$, consider the fixed points of period s lying on the circle at the intersection of the torus with the surface of section. The Poincaré-Birkhoff theorem states that some fixed points remain under a perturbation and their number is always an even multiple of s, usually $2s$. This result follows from KAM theory and the fact that the map is area-preserving.

Here we want to approximate with a map a one-dimensional hydrogen atom in a microwavefield of amplitude F and frequency ω. The Hamiltonian for this system is

$$H = \frac{1}{2}p^2 - \frac{1}{z} + Fz\sin\omega t \ . \tag{5.2}$$

By using atomic units this can be written in action-angle variables (θ, I) as

$$H = -\frac{1}{2I^2} + F\left[\frac{3I^2}{2} - 2I^2\sum_{s=1}^{\infty}\frac{J'_s(s)}{s}\cos(s\theta)\right]\sin\Omega t \ , \tag{5.3}$$

where $J_s'(x)$ denotes the derivative of an ordinary Bessel function, the term in square brackets is the Fourier expansion of $z(\theta, I)$, and the following relationships have been used:

$$z(\theta, I) = 2I^2 \sin^2 \phi \ , \ p(\theta, I) = \frac{1}{I \tan \phi} \ , \ \theta = 2\phi - \sin 2\phi \ ,$$

The equations of motion are then:

$$\dot{\theta} = \frac{\partial H}{\partial I} = \frac{1}{I^3} - F \sin \Omega t \frac{\partial z(\theta, I)}{\partial I} \tag{5.4}$$

$$\dot{I} = -\frac{\partial H}{\partial \theta} = F \sin \Omega t \frac{\partial z(\theta, I)}{\partial \theta} \ . \tag{5.5}$$

By integrating these equations over one field period, i.e. from $t_0 = 0$ to $t = 2\pi/\Omega$ we can get the solution in the form of a discrete map. We note here that integrating over one field period introduces a fundamental difference between the resulting map and maps that have been derived by integrating over one unperturbed period of the orbit. In the latter case an iteration $I_n \rightarrow I_{n+1}$ corresponds to a transformation of the original variable $I(t) \rightarrow I(t + T(I(t)))$ through a time interval T(I), dependent upon the initial point I(t); this does not matter in classical dynamics, since it is possible to keep track of the time elapsed along any orbit, but the quantal evolution of the map corresponds to the iterate of a curve in phase space, so the correspondence between the original time and the number of iterations is lost. This is the case, for example, with the Quantum Kepler Map recently introduced by Casati *et al.* (1987, 1988) as an approximate evolution operator for the one-dimensional hydrogen atom in a periodic electric field.

If we integrate the equations 5.4 and 5.5 over one field period in the unperturbed case $F = 0$ the solution is:

$$\begin{aligned} I_{n+1} &= I_n \\ \theta_{n+1} &= \theta_n + \frac{2\pi}{I_{n+1}^3} \ , \end{aligned} \tag{5.6}$$

while for $F \neq 0$ the solution has the form:

$$\begin{aligned} I_{n+1} &= I_n + f(I_{n+1}, \theta_n, F) \\ \theta_{n+1} &= \theta_n + \frac{2\pi}{I_{n+1}^3} + g(I_{n+1}, \theta_n, F) \ . \end{aligned} \tag{5.7}$$

The functions f and g have no known analytical form. It is possible to find an approximate solution by truncating the Fourier series in 5.2, although this still requires some cumbersome analysis and gives quite complicated functions of I_{n+1} and θ_n for f and g. For our purposes we only need to reproduce the basic properties of the original equations of motion. It is therefore sufficient that the functions f and g are chosen such that: (a) the map has fixed points at $I = k^{1/3}$, for $k = 1, 2, ...$, (b)the motion becomes chaotic only above a critical value of I, depending on the strength of the perturbation, and (c) the map is area-preserving. In order for 5.7 to be area-preserving it has to be generated by a generating function (see Lichtenberg and Liebermann 1983)

$$F_2 = I_{n+1}\theta_n + 2\pi\mathcal{A}(I_{n+1}) + \mathcal{B}(I_{n+1}, \theta_n) \tag{5.8}$$

with

$$\begin{aligned} \frac{1}{I_{n+1}^3} &= \frac{d\mathcal{A}}{dI_{n+1}} \\ f &= -\frac{\partial \mathcal{B}}{\partial \theta_n} \\ g &= \frac{\partial \mathcal{B}}{\partial I_{n+1}} . \end{aligned}$$

We choose $\mathcal{B} = \varepsilon^{(1/I_{n+1})^2} \cos\theta_n$, where ε is the strength of the perturbation, chosen to represent the field strength F, giving the map

$$\begin{aligned} I_{n+1} &= I_n + \varepsilon^{(1/I_{n+1})^2} \sin\theta_n \\ \theta_{n+1} &= \theta_n + \frac{2\pi}{I_{n+1}^3} - 2\frac{\log\varepsilon}{I_{n+1}^3}\varepsilon^{(1/I_{n+1})^2} \cos\theta_n . \end{aligned} \tag{5.9}$$

The fixed points of this map are:

$$I \simeq k^{1/3}, \quad \theta = n\pi; \quad n,\ k \text{ integers} .$$

In 5.9 I_{n+1} is defined implicitly in terms of I_n, but can easily be obtained by Newton's method. Typical orbits of 5.9 are shown in Figure 5.1 for $\varepsilon = 0.001, 0.01, 0.015, 0.02$. From this figure we can see that the phase space is characterised by different types of orbits. There are K.A.M. curves, or

rotational tori, and resonance islands, whose centres are periodic orbits with various periods. The separatrix surrounding the resonance islands becomes smeared in a band of chaos as ε starts to increase. For low values of ε these bands are enclosed between invariant curves, which act as barriers to the motion, but as ε increases the invariant curves start to break up. We shall see how this picture is modified when the perturbation is switched on adiabatically.

Adiabatic switch-on of the perturbation is achieved by using the discrete switch-on function defined by:

$$A(n, N_a) = \begin{cases} 0 & s \leq 0 \\ s^2(2 - s^2) & 0 \leq s \leq 1 \\ 1 & 1 \leq s \end{cases},$$

where N_a is the length (in number of steps) of the adiabatic switch, and s is $\frac{n}{N_a}$. The function $A(n, N_a)$ is the discrete analogue of $f(s)$, used in Chapter 4.

Figure 5.2 shows the orbits in phase space obtained with the same initial conditions as Figure 5.1, for two values of ε, but here the perturbation is switched on adiabatically over 1000 iterations of the map. The difference is quite dramatic: most of the initial points that with a sudden switch-on gave rise to chaotic orbits now end up on either invariant curves or periodic orbits. For the initial values chosen, when the action is not too large the chaotic behaviour is completely removed. As ε increases, the range of initial values of I for which this takes place becomes smaller. A better way of illustrating the effect of the adiabatic switch is to show the time evolution, with and without adiabatic switch-on, of a set of points (I_0, θ_0) initially on a given unperturbed torus. Figure 5.3 shows the N^{th} iterates of two sets lying on the lines $I = 1.1$ and $I = 1.236068$, as N_a is increased from 10 to 4000 iterations. Figure 5.4 is analogous, but for a higher value of ε. We can see that for the low value of ε both initial sets end up on a smooth curve, even for values of N_a as low as 10. When ε is higher the following is seen. For all values of N_a the set of higher initial action never ends up on a smooth curve . At such high values of the perturbation, increasing the adiabatic

switch fails to reduce chaotic behaviour seen when $N_a = 0$ (Figure 5.4b), and adiabatic invariance breaks down (Figure 5.4a). The lower action set stays close to a rotational curve and appears mostly regular, apart from a rapid oscillatory behaviour at the hyperbolic points.

Adiabatic invariance is verified using the non-adiabaticity parameter $\Delta J(N)$ defined by Dana and Reinhardt (1987) (see equation 2.22). We find that the behaviour of $\Delta J(N)$ for this map is similar to that described by Dana and Reinhardt for the standard map. By calculating the dependence of $\Delta J(N)$ on the length of the adiabatic switch and the amplitude of the perturbation we are able to provide further evidence of the reliability of the adiabatic method for semiclassical quantisation and to give quantitative results.

Figure 5.5 shows the time-dependence of $\Delta J(N)$ for different values of ε, with initial action $I = 1, 1.236060$, and 1.1. We can see that for low values of the action (Figure 5.5a) and of the perturbation the non-adiabaticity parameter gets smaller as the adiabatic switch gets longer. However, for higher values of the action (Figure 5.5c) and of the perturbation, $\Delta J(N)$ increases, rather than decreasing, with the length of the adiabatic switch, and adiabatic invariance breaks down. This actually happens after a small initial decrease over a short time. It is this initial effect that in some cases enables semiclassical quantisation to be carried out even when adiabatic invariance breaks down, provided the length of the adiabatic switch is not too long.

We can also reproduce qualitatively and analyse some of the effects that an initial adiabatic switch has on the subsequent dynamics of a hydrogen atom in a microwave field. In particular it is possible to see that switching the field on adiabatically reduces the ionisation rate: given a fixed number of iterations after the perturbation has reached its peak, P_I is highest when $N_a = 0$ and then it decreases as N_a increases, and levels off for $N_a \geq 500$. Such a stabilising effect is greater at resonances. This behaviour is shown in Figure 5.6.

Chapter 6

Conclusions and further work

In this thesis we have studied two non-linear dynamical systems that exhibit a transition from regular to irregular or 'chaotic' behaviour. Both involve the hydrogen atom in external fields. Since these are not artificial models, but real systems, they allow both experimental and theoretical investigation, thus providing real testing grounds for what is known as the problem of 'quantum chaos', that is the correspondence between quantal systems and their classical counterparts when the latter exhibits a transition to chaos.

The first system is the time-independent problem of the hydrogen atom in a strong magnetic field. We have applied a method based on the principle of adiabatic invariance to obtain the energy levels of this system over a wide range of magnetic field strengths. By comparing our results with experimental data we have shown that, as long as the initial tori are chosen correctly, the adiabatic method can be used to find the energy levels of a strongly perturbed hydrogen atom, even with up to very high fields where the motion becomes irregular. Some properties of the adiabatic method have emerged which may facilitate the study of periodic orbits in the irregular regime. This is relevant to the problem of the relationship between periodic trajectories and quasi-Landau resonances (Holle *et al.* 1986) and to the connected theory of 'scars'. A scar in the eigenfunctions of a quantum system is a region of enhanced probability in the neighbourhood of a classical periodic orbit. Scars were first observed by Heller (1984) in the eigenfunctions of the stadium. Recently they have been identified in other classically chaotic systems

(Waterland *et al.* 1988, Jensen *et al.* 1989) and in particular also for excited hydrogen atoms in a strong magnetic field (Wintgen and Hönig 1989), where a correspondence has been established between scarred wavefunction and modulations in the photoabsorption spectra, with frequency equal to the classical orbital frequency. Our understanding of these phenomena is still mainly qualitative and more work needs to be done. Another open problem concerns the formulation of theory which describes the transition from a Poisson to a Wigner distribution for the energy spectra as the corresponding classical system exhibits a transition from regular to irregular motion. Existing theoretical formulae (Berry and Robnik 1984, Hasegawa *et al.* 1988) are not very satisfactory (see for example Wintgen and Friedrich 1987) and need improving.

The second problem studied here is the time-dependent system of an excited hydrogen atom in a microwave field. We have studied this theoretically and numerically and comparisons have been made with experimental results over a very wide range of the system parameters. This has yielded much information about the dynamics of this system and its dependence on the various parameters, providing the basis for a comprehensive theoretical model of the classical dynamics and advancing our understanding of the quantal behaviour.

Many parameters are needed to define a given experiment or simulation, but we have found, and it is generally agreed upon, that the main ones are the initial principal quantum number n_0, the strength of the applied field F_m, and its frequency ω. When scaled units are used (see section 4.1.3), in the classical limit these three parameters reduce to two, the scaled field amplitude F_0 and the scaled frequency Ω_0. One of the main results of this study concerns the dependence of this system upon the scaled frequency: as discussed earlier, comparison of classical calculations and experimental results (Koch 1982, 1988) suggest that there are at least five frequency ranges in which the dynamics has different characteristics and needs different theoretical models. These have been described in section 4.3 and are, briefly, as follows:

R1 $0 \leq \Omega_0 n_0 < 1$: This is an adiabatic region in which there are no transitions between the adiabatic states and for $F_0 < 0.1298$ ionisation occurs only through tunnelling.

R2 $1 \leq \Omega_0 n_0 < 10$: Here the quantum dynamics is dominated by relatively few adiabatic states (Richards 1987), and classical dynamics fails.

R3 $0.2 \leq \Omega_0 < 1.1$: In this region many quantal states are coupled together and the classical and quantal descriptions agree, except at a few resonant frequencies. The agreement between our 3-dimensional calculations and the experimental results is very good.

R4 $1.1 \leq \Omega_0 < 2.0$: This is a border region in which the classical dynamics is beginning to break down, and the experimental and quantal ionisation thresholds gradually rise above the classical ones.

R5 $2.0 \leq \Omega_0$: In this region the classical approximation breaks down, as the quantal motion is dominated by relatively few quasi-resonant states (Richards *et al.* 1989a).

The boundaries of these regions are not well-defined and the values we give are based on empirical observation. The analysis of results obtained from three-dimensional simulations leads us to propose different mechanisms of ionisation in these ranges. Theoretical models that justify and explain this classification, mainly based on the one-dimensional dynamics, have been formulated (Jensen 1982 and 1984, Richards 1987, Richards *et al.* 1989, Leopold and Richards 1989).

Care must be taken, however, when drawing conclusions from comparisons with experiments, since the results we have are not completely general. Firstly, we have compared only the ionisation probability; secondly and most important, the experiments are for a particular cut-off, as ionisation is defined as excitation above $n = 92$, and for a given number of field oscillations. It is not obvious what would happen in those regions where the classical three-dimensional simulation now agrees with the experiment, if the cut-off quantum number were higher or the number of field periods were increased.

It seems feasible that for the weak fields giving 10% ionisation the classical and quantal thresholds will start to disagree: if the cut-off is increased to the point where the local scaled frequency, $\omega(n/n_0)^3$, becomes larger than unity the local behaviour of the classical and quantal solutions becomes different; in particular the classical solutions will just diffuse to the continuum, while the quantal solutions will be dominated by the quasi-resonant states. It is therefore desirable that experiments are carried out where these parameters are varied. The effect of varying the total interaction time is particularly important, especially at high scaled frequencies as the theory suggests that classical dynamics ought to be more accurate the shorter the interaction time. It has been suggested (Casati *et al.* 1988) that the quantal dynamics follows the classical, diffusive behaviour until a characteristic time τ_B, the 'break time', after which the diffusion stops and the wavepacket remains localised.

A limited study of the effect of changing the total interaction time has been carried out here, and we have also compared results obtained by varying the form and length of the envelope $A(t)$, but more is needed both numerically and experimentally.

The dependence of the system upon the other main parameter, the amplitude of the applied field, has been systematically explored. Full ionisation curves have been obtained for many different values of the frequency over the whole range, and compared with one-dimensional and experimental results. One of the open problems in this context is the value of the field beyond which ionisation occurs (ionisation threshold) and the range over which classical and quantal calculations of the threshold should agree. Current theories conflict, as reported in section 4.1.4. The only experimental results available so far (up to $\Omega_0 \sim 2.7$) fit all these theories. Further experiments at higher frequencies are planned to try to resolve this controversy.

It is hoped that future experiments and numerical simulations will help in formulating a theory. The work so far shows that a single theory which covers all the frequency regions described above is not feasible, because of the different dynamics. There is a need for better theories to describe each

of these regions separately. In particular in region R2 there are at least three outstanding problems. Firstly, we do not have a rigorous theory which uses the adiabatic states as it is not known how to treat the quantum dynamics of the escape over a slow moving barrier, which is in fact a very difficult problem; secondly, we need more rigorous estimates of the resonance widths; thirdly, we need a three-dimensional quantal theory. Similar problems apply in region R3, and in addition we need a description of the motion in the vicinity of the resonance islands: a theory is needed to explain the role that the 'scars' of unstable classical periodic orbits play in determining the structure of the wavefunctions, and how this is related to the local stability found in quantal and experimental measurements of the threshold fields. For region R4, which is on the boundary between a classical and a quantal region, the dynamics is very complicated and a simple theory is a long way off. We know that classical dynamics still plays a role, as ionisation probabilities show evidence of the classical phase-space structures (Jensen *et al.* 1989), but classical and quantal results diverge steadily as the frequency increases. In region R5 it is clear that classical dynamics breaks down, at least for weak fields. An important open problem here is simply, under what circumstances is classical dynamics valid? How short must the interaction time be? How strong must the field be? Can the system be made to behave classically by adding a second high frequency or noise? This particular development would involve interesting theoretical problems, because quantal Floquet theory could not be applied to a system with added noise.

From the analysis of the results of the three-dimensional simulation developed in this work we have reached the important conclusion that classically almost all unstable orbits ionise, and the small percentage that does not is statistically insignificant. The fact that classical ionisation only occurs through unstable orbits is of particular relevance to the comparison between classical and quantal dynamics, since a quantal analogue of unstable orbits does not exist. In this context it would be also very interesting to relate the stability of classical orbits to their initial conditions, although this is extremely difficult because of the great number of parameters involved. Some

observations are reported here relating the stability of orbits to their initial eccentricity and orientation. More work is needed to provide theoretical explanations and to discover the role of other parameters.

The most important future development to aim for is the theoretical analysis and simulation of the quantal dynamics of this system. As described in section 4.1.4, some work has already been carried out and more is under way in one dimension (Casati *et al.* 1984, 1987, 1988, Blümel and Smilanski 1987, Richards 1987, Leopold and Richards 1988a, 1989). Quantal three-dimensional calculations have so far proved impossible. These will ultimately be necessary for a full understanding of the behaviour of this system, but the inherent difficulties that three-dimensional quantum mechanics entails suggest that for the foreseeable future both experiments and theory should concentrate on one-dimensional systems. We need therefore better experiments, where an appropriate static field, collinear with the microwave field is present in order to preserve the one-dimensional behaviour of the atoms, and where all the experimental details, including the form and length of the envelope function, are known accurately, so that a proper comparison with numerical simulation can be carried out. Since a static field must be present in the experiment, we also need theories which include this.

In the meantime, the use of classical dynamics and careful comparisons with experimental results has provided us with considerable insight into the quantal dynamics. The breakdown of agreement between classical simulations and experiment has led to the identification of quantal effects. Future work on quantal one-dimensional models may provide the means of quantifying these effects. It is not clear, however, to what extent these one-dimensional models provide a good description of the dynamics. Comparisons between one- and three-dimensional classical models such as those carried out here should provide important clues and help to define the limitations of one-dimensional quantal models.

Throughout this work we have found that the properties of the Coulomb potential make this system rather special. It would be interesting to study

the relationship between the hydrogen atom in a periodic field and other, non-singular potentials with periodic fields. This is particularly relevant for high frequencies, since the Coulomb singularity produces motion having all frequencies present, whereas a smoother potential produces motion dominated by lower frequencies, so that the averaging methods of Gavrila and Pont (Gavrila 1986, Pont and Gavrila 1987, Pont 1989) are valid.

References

Abramowitz M and Stegun I A 1965 "Handbook of Mathematical Functions" New York, Dover

Abrines R and Percival I C 1966 Proc Phys Soc **88** 861

Alliluev S P and Malkin I A 1974 Sov Phys JEPT **39** 627-32

Angel J R P 1977 Astrophys J **216** 1-17

Arnold V I 1961 Sov Math Dokl **2** 501

Arnold V I 1962 Sov Math Dokl **3** 136-40

Arnold V I 1978 "Mathematical Methods of Classical Mechanics" New York, Springer

Arnold V I and Avez A 1968 "Ergodic Problems of Classical Mechanics" New York, Benjamin

Banks D and Leopold J G 1978a J Phys B **11** L5-9

Banks D and Leopold J G 1978b J Phys B **11** 37-46

Bardsley J N and Sundaram B 1985 Phys Rev A **32** 689-91

Bayfield J E 1987 Comm At Mol Phys **20** 245

Bayfield J E, Casati G, Guarneri I and Sokol D W 1989 Phys Rev Lett **63** 364-7

Bayfield J E and Koch P M 1974 Phys Rev Lett **33** 258-61

Bayfield J E, Gardner L D and Koch P M 1977 Phys Rev Lett **39** 76-9

Bayfield J E and Pinnaduwage L A 1985 J Phys B **18** L49

Berry M V 1985 Proc Royal Soc London A **400** 229-51

Berry M V and Robnik M 1984 Phys Rev A **17** 2413

Blümel R, Jaeckel G and Smilansky U 1989 Phys Rev A **39** 450-3

Blümel R and Smilansky U 1984 Phys Rev A **30** 1040-51

Blümel R and Smilansky U 1987 Z Phys D **6** 83-105

Bohigas O, Giannoni M J and Schmit C 1984 Phys Rev Lett **52** 1-4

Born M 1927 "Atomic Physics", Ungar, New York

Brillouin L 1926 J Phys (Paris) **7** 353-68

Brown R, Ott E and Grebogi C 1987 Phys Rev Lett **59** 1173-6

Carnegie A 1984 J Phys B **17** 3435-48

Casati G, Chirikov B V, Ford J and Izrailev F M 1979 Lecture Notes in Physics **93** 334

Casati G, Chirikov B V and Shepelyansky D L 1984 Phys Rev Lett **53** 2525-8

Casati G, Chirikov B V, Guarnieri I and Shepelyansky D L 1986a Phys Rev Lett **56** 2437

Casati G, Chirikov B V, Guarnieri I and Shepelyansky D L 1986b Phys Rev Lett **57** 823

Casati G, Chirikov B V, Shepelyansky D L and Guarnieri I 1987 Phys Rep **154** 77-123

Casati G, Guarnieri I and Shepelyansky D L 1988 IEEE J of Quantum Electronics **24** 1420-44

Castro J C, Zimmermann M L, Hulet R G, Kleppner D and Freeman R R 1980 Phys Rev Lett **45** 1780-3

Chirikov B V 1979 Phys Rep **52** 263-379

Clark C W and Taylor K T 1982 J Phys B **15** 1175-93

Cornish F H J 1984 J Phys A **17** 323-7

Damburg R J and Kolosov V V 1976a J Phys B **9** 3149-57

Damburg R J and Kolosov V V 1976b Proc 5th International Conference on Atomic Physics, Berkeley, California, Abstracts pp. 202-3

Damburg R J and Kolosov V V 1979 J Phys B **12** 2637-43

Dana I and Reinhardt W P 1987 Physica D **28** 115-42

Delande D and Gay J C 1981 Phys Lett **82A** 399-403

Delande D and Gay J C 1986a J Phys B **19** L173-8

Delande D and Gay J C 1986b Phys Rev Lett **57** 2006-9

Delone N B, Krainov V P and Shepelyansky D L 1983 Sov Phys Usp **26** 551

Delos J B, Knudson S K and Noid D W 1983 Phys Rev A **28** 7-21

Dhar A K, Nagarajan M A, Izrailev F M and Whitehead R R 1983 J Phys B **16** L17-22

Edmonds A R 1970 J Physique **31** C4-71

Edmonds A R 1973 J Phys B **6** 1603-15

Edmonds A R and Pullen R A 1980a Imperial College Reprint /79-80/28

Edmonds A R and Pullen R A 1980b Imperial College Reprint /79-80/29

Edmonds A R and Pullen R A 1980c Imperial College Reprint /79-80/30

Ehrenfest P 1916 Versl Kön Akad Amsterdam **25** 412 , English translation in "Sources of Quantum Mechanics" ed. B L Van der Waerden, Dover NY 1967

Einstein A 1917 Verh Dtsch Phys Ges **19** 82-9

Galvez E J, Sauer B E, Moorman L, Koch P M and Richards D 1988 Phys Rev Lett **61** 2011-4

Garton W R S and Tomkins F S 1969 Astrophys J **158** 839

Gavrila M 1986 in "Fundamentals of Laser Atom Interactions", Lecture Notes in Physics **278** p. 3, Springer-Verlag

Gay J C and Delande D 1983 Comm At Mol Phys **13** 275-97

Goldstein H 1980 'Classical Mechanics', London, Addison

Grimes C C, Brown T R, Burns M L and Zipfel C L 1976 Phys Rev B **13** 140-7

Grozdanov T P and Solove'v E A 1982 J Phys B **15** 1195-204

Grozdanov T P, Saini S and Taylor H S 1986 Phys Rev A **33** 55-67

Harada A and Hasegawa H 1983 J Phys A **16** L259-63

Hasegawa H, Mikeska H J and Frahm H 1988 Phys Rev A **38** 395

Hedges R M, Skodje R T, Borondo F and Reinhardt W P 1984 in "ACS Symposium Series No 2663" ed D G Truher

Heller E J 1984 Phys Rev Lett **53** 1515-8

Herrick D R 1976 J Phys Chem **65** 3529-35

Herrick D R 1982 Phys Rev A **26** 323-9

Holle A, Wiebusch G, Main J, Hager B, Rottke H and Welge K H 1986 Phys Rev Lett **56** 2594-7

Holle A, Wiebusch G, Rottke H and Welge K H 1988 Phys Rev Lett **61** 161-4

Jensen R V 1982 Phys Rev Lett **49** 1365-8

Jensen R V 1984 Phys Rev A **30** 386-97

Jensen R V, Leopold J G and Richards D 1988 J Phys B **21** L527-31

Jensen R V, Sanders M M, Saraceno M and Sundaram B 1989 Phys Rev Lett **63** 2771-5

Johnson B R 1985 J Chem Phys **83** 1204-17

Jones D A, Leopold J G and Percival I C 1980 J Phys B **13** 31-40

Jortner J 1980 in "Radiationless Processes" ed Di Bartolo B, NATO ASI Series B **62** 103-56

Jowett J M, Month M and Turner S (eds) 1985 "Nonlinear dynamic aspects of particle accelerators" Lecture Notes in Physics **247** Springer Verlag

Keller J B 1958 Ann Phys 4 180-8

Kleppner D, Littman M G and Zimmerman M L 1983 in "Rydberg States of Atoms and Molecules" ed Stebbings R F and Dunning F B pp. 73-116 Cambridge University Press

Koch P M 1982 J Physique Colloq **43** 183-210

Koch P M 1988 'Microwave ionisation of highly excited hydrogen atoms' in "Electronic and Atomic Collisions" eds Gilbody H B, Newell W R, Reed F H and Smith A C H, Elsevier Science

Koch P M, van Leeuwen K A H, Rath O, Richards D and Jensen R V 1987 in "The Physics of Phase Space" Lecture Notes in Physics **278** 106-113 Springer-Verlag

Kolmogorov A N 1954 Dokl Akad Nauk SSSR **98** 527

Landau L D and Lifshitz E M 1965 "Mechanics" Oxford, Pergamon

Landau L D and Lifshitz E M 1977 "Quantum Mechanics" Oxford, Pergamon

Ledermann W (ed) 1981 "Handbook of Applicable Mathematics" vol 3, New York, Wiley

Leopold J G and Percival I C 1978 Phys Rev Lett **33** 258-61

Leopold J G and Percival I C 1979 J Phys B **12** 709-21

Leopold J G and Richards D 1985 J Phys B **18** 3369-94

Leopold J G and Richards D 1986 J Phys B **19** 1125-42

Leopold J G and Richards D 1987 J Phys B **20** 2369-82

Leopold J G and Richards D 1988a Phys Rev A **38** 2660-3

Leopold J G and Richards D 1988b J Phys B **21** 25-34

Leopold J G and Richards D 1989 J Phys B **22** 1931-61

Lichtenberg and Lieberman 1983 "Regular and Stochastic Motion" New York, Springer

Mc Donald S W and Kaufmann A N 1979 Phys Rev Lett **42** 1189-91

Meerson B I, Oks E A and Sarosov P V 1982 J Phys B **15** 3599-614

Month M and Herrera J C (eds) 1979 "Nonlinear dynamics and the beam-beam interaction" AIP Conf Proc **57**, New York

Moorman L, Galvez E J, Sauer B E, Mortazawi-M A, van Leeuwen K A H, van Oppen G and Koch P M 1988 Phys Rev Lett **61** 771-4

Moser J 1962 "On invariant curves of area-preserving mappings on an annulus", Nachr Akad Wiss Göttingen Math Phys K1 1

Percival I C 1977 Adv Chem Phys **36** 1-61

Percival I C and Richards D 1982 "Introduction to Dynamics" Cambridge, Cambridge University Press

Percival I C and Richards D 1979 J Phys B **12** 2051-65

Pont M 1989 Phys Rev A **40** 5659-72

Pont M and Gavrila M 1987 Phys Lett A **123** 469

Rath O and Richards D 1990 in preparation

Rau A R P 1980 Comm At Mol Phys **10** 19-30

Rechester A A and Rosenbluth M N 1978 Phys Rev Lett **40** 38-41

Reinhardt W P and Dana I 1987 Proc R Soc Lond A **413** 157-70

Richards D 1983 J Phys B **16** 749-65

Richards D 1987 J Phys B **20** 2171-92

Richards D 1989 'The Coulomb potential and microwave ionisation', Talk presented at the 1989 Conference on 'Aspects of Electron-Molecule Scattering and Photoionisation', Yale University, New Haven, Connecticut, USA

Richards D 1990 in preparation

Richards D, Leopold J G and Jensen R V 1989a J Phys B **22** 417-33

Richards D, Leopold J G, Koch P M, Galvez E J, van Leeuwen K A H, Moorman L, Sauer B E and Jensen R V 1989b J Phys B **22** 1307-33

Robnik M 1981 J Phys A **14** 3195-216

Rotenberg M 1962 Ann Phys **19** 262-78

Rotenberg M 1970 Adv Atom Mol Phys **6** 233-68

Skodje R T, Borondo F and Reinhardt W P 1985 J Chem Phys **82** 4611-32

Solove'v E A 1978 Sov Phys JEPT **48** 635-9

Solove'v E A 1981 JEPT Lett **34** 265-8

Starace A F 1973 J Phys B **6** 585-90

Szebehely V 1967 "Theory of Orbits" (Academic Press)

Taylor H S and Grozdanov T P 1987 in "Stochasticity and Intramolecular Redistribution of Energy" ed. Lefebvre R and Mukamel S, 81-94

van Leeuwen K A H, Oppen G V, Renwick S, Bowlin J B, Koch P M, Jensen R V, Rath O, Richards D and Leopold J G 1985 Phys Rev Lett **55** 2231-4

Waterland R L, Yuan J-M, Martens C C, Gillinan R E and Reinhardt W P 1988 Phys Rev Lett **61** 2733-6

Welch G R, Kash M M, Chun-ho Iu, Long Hsu and Kleppner D 1989 Phys Rev Lett **62** 893-6

Wiebusch G, Main J, Krüger K, Rottke H, Holle A and Welge K H 1989 Phys Rev Lett **62** 2821-4

Wintgen D 1987a Phys Rev Lett **58** 1589-92

Wintgen D 1987b J Phys B **20** L511-5

Wintgen D and Friedrich H 1986 Phys Rev Lett **57** 571-4

Wintgen D and Friedrich H 1987 Phys Rev A **35** 1464

Wintgen D and Hönig A 1989 Phys Rev Lett **63** 1467-70

Wisdom J 1987 Proc Roy Soc Lond A **413** 109-29

Zimmermann M L, Kash M M and Kleppner D 1980 Phys Rev Lett **45** 1092-4

TABLE OF FIGURES

$< \sigma >= (\sigma_k + \sigma_{k+1})/2$, for $n = 30$, $m = 1$. The curve (a) was calculated for the pair of energy levels $k = 0, 1$, (b) for $k = 18, 19$, and (c) for $k = 26, 27$.

Figure 4.1 Graphs showing the one-dimensional potential (4.32) when (a) $f < 0$ and the spectrum is purely discrete ; and (b) $f > 0$, when the spectrum has no discrete part.

Figure 4.2 Graph giving the 10% (higher curve) and 90% scaled threshold fields as a function of scaled frequency. The solid line gives the results of the classical simulation, and the dots represent the experimental results.

Figure 4.3 Graphs showing the time-dependence of the ionisation probabilities at various field strengths (a), and time-dependence of the various probabilities based on the magnitude of R_m (b), for $\Omega_0 = 0.0828$, $n_0 = 38$.

Figure 4.4 Graph showing the time-dependence of the ionisation probabilities at various field strengths, for $\Omega_0 = 0.496$, $n_0 = 69$.

Figure 4.5 As in Fig. 4.4, with $\Omega_0 = 0.587$, $n_0 = 73$.

Figure 4.6 Graphs showing the time-dependence of the ionisation probabilities at various field strengths (a), and time-dependence of the various probabilities based on the magnitude of R_m (b), for $\Omega_0 = 0.832$, $n_0 = 82$.

Figure 4.7 As in Fig. 4.6, with $\Omega_0 = 0.994$, $n_0 = 87$.

Figure 4.8 As in Fig. 4.6, with $\Omega_0 = 1.647$, $n_0 = 67$, and a cavity frequency of 36 GHz.

Figure 4.9 As in Fig. 4.8, with $\Omega_0 = 2.599$, $n_0 = 78$.

Figure 4.10 Graph showing the final distribution of the action for a field giving $\sim 50\%$ ionisation, in the case $\Omega_0 = 0.0828$, $n_0 = 38$.

Figure 4.11 Graphs showing the final distribution of the action for various fields, in the case $\Omega_0 = 0.496$, $n_0 = 69$.

Figure 4.12 As in Fig. 4.11, with $\Omega_0 = 0.587$, $n_0 = 73$.

Figure 4.13 Graphs showing the final distribution of the action for various fields (a-c), and the time-dependence of the probabilities of excitation to levels less than and greater than $1.2\, n_0$, together with the ionisation probability (d), in the case $\Omega_0 = 0.832$, $n_0 = 82$.

Figure 4.14 As in Fig. 4.13, with $\Omega_0 = 0.994$, $n_0 = 87$.

Figure 4.15 As in Fig. 4.13, with $\Omega_0 = 1.647$, $n_0 = 67$, and a cavity frequency of 36 GHz.

Figure 4.16 As in Fig. 4.15, with $\Omega_0 = 2.599$, $n_0 = 78$.

Figure 4.17 Graph showing the scatter plot of final against initial eccentricity squared for a field giving $\sim 50\%$, in the case $\Omega_0 = 0.0828$, $n_0 = 38$.

Figure 4.18 Graphs showing scatter plots of final against initial eccentricity squared for various field strengths, in the case $\Omega_0 = 0.496$, $n_0 = 69$.

Figure 4.19 As in Fig. 4.18, with $\Omega_0 = 0.587$, $n_0 = 73$.

Figure 4.20 As in Fig. 4.18, $\Omega_0 = 0.832$, $n_0 = 82$.

Figure 4.21 As in Fig. 4.18, with $\Omega_0 = 0.994$, $n_0 = 87$.

Figure 4.22 As in Fig. 4.18, with $\Omega_0 = 1.647$, $n_0 = 67$, and a cavity frequency of 36 GHz.

Figure 4.23 As in Fig. 4.22, with $\Omega_0 = 2.599$, $n_0 = 78$.

Figure 4.24 Distribution of angle of ejection of ionised orbits for (a) four non-resonant and (b) four resonant frequencies. The initial orbits were all circular and in a plane perpendicular to the field.

Figure 4.25 Distribution of initial eccentricity (ε^2) of ionised orbits for (a) four non-resonant and (b) four resonant frequencies.

Figure 4.26 Ionisation curves obtained with initial microcanonical distribution (o) and with straight line orbits (*) in the cases (a) $\Omega_0 = 0.5$ and (b) $\Omega_0 = 0.7414$.

Figure 4.27 Graph showing the variation of the classical ionisation probability with frequency for a fixed field. For the 1-dimensional curve, $F_0 = 0.111$, $T_a = 0$ and the total integration time was 150 periods. For the 3-dimensional curve $F_0 = 0.130$, $T_a = 20$ periods and total time = 180 periods. The dotted lines show the extent of the statistical errors.

Figure 4.28 Comparison of ionisation curves for $\Omega_0 = 0.0647$, $n_0 = 35$: the solid and empty circles are the 1-dimensional and 3-dimensional classical simulations respectively, and the solid line gives the experimental result.

Figure 4.29 As in Fig. 4.28, with $\Omega_0 = 0.0828$, $n_0 = 38$.

Figure 4.30 As in Fig. 4.28, with $\Omega_0 = 0.1669$, $n_0 = 48$.

Figure 4.31 Comparison of the experimental (—) and 3-dimensional classical (•) ionisation curves for $\Omega_0 = 0.587$, $n_0 = 73$.

Figure 4.32 As in Fig. 4.10, with $\Omega_0 = 0.496$, $n_0 = 69$.

Figure 4.33 Graph showing the ionisation probabilities near the 1/2 resonance when a second microwave field is added. The total field strength is constant: $F_1 + F_2 = 0.07$.

Figure 5.1 Typical orbits of the map 5.9 for four values of the perturbation. The points marked '+' are the initial values of the iteration.

Figure 5.2 As in Figure 5.1 but with only two values of the perturbation and with an initial adiabatic switch lasting 1000 iterations.

Figure 5.3 (a) Graphs showing the N^{th} iterates of two sets of 200 points with initial values $I = 1.1$ and $I = 1.236068$ respectively, uniformly distributed in θ, immediately after the adiabatic switch, for four different values N_a, with $\varepsilon = 0.001$; (b) the N^{th} iterates of two sets of 100 points with the same initial conditions as in (a), but without an adiabatic switch.

Figure 5.4 (a) and (b) as in Figure 5.3, with $\varepsilon = 0.01$.

Figure 5.5 Graphs showing the dependence of the non-adiabaticity parameter on the adiabatic switch at two different values of the perturbation, for initial values of the action (a) $I = 1.0$, (b)$I = 1.1$, and (c) $I = 1.236068$.

Figure 5.6 Ionisation curves obtained with different values of the adiabatic switch with initial values (a) $I = 1.0$ and (b) $I = 1.236068$. Here ionisation is defined by $I > 2.0$.

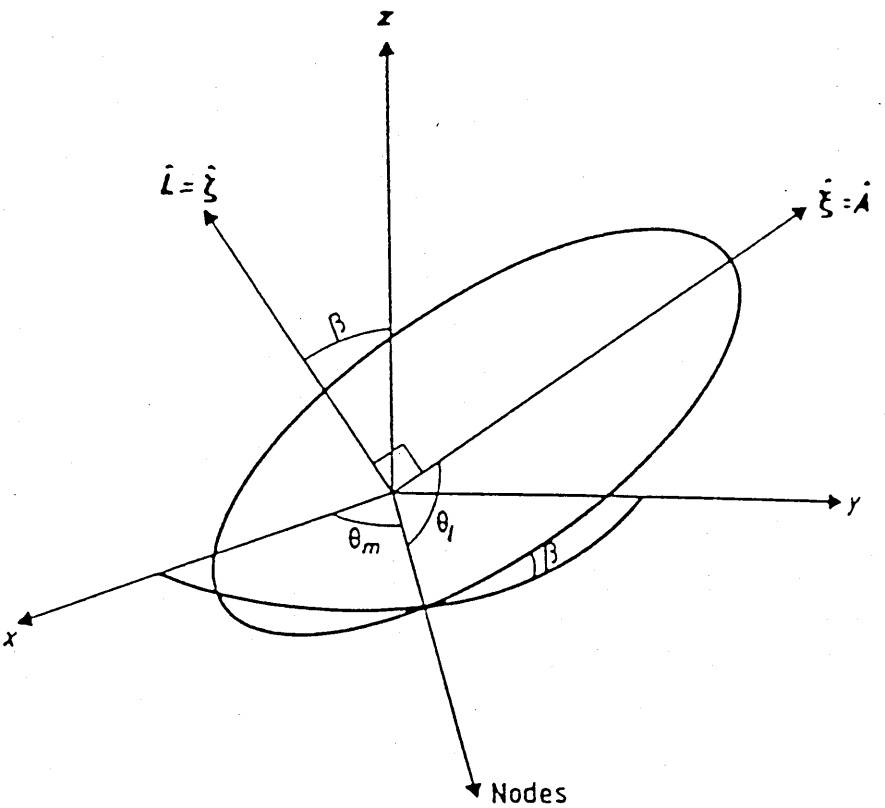

Figure 1.1

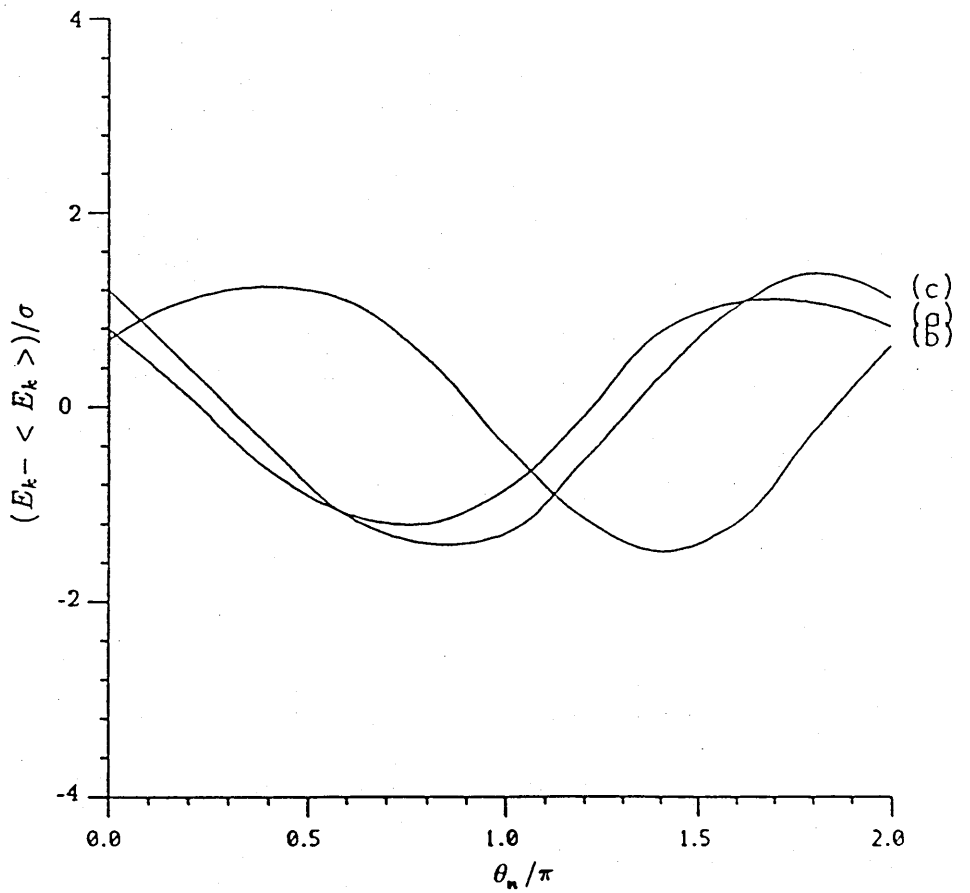

Figure 3.1

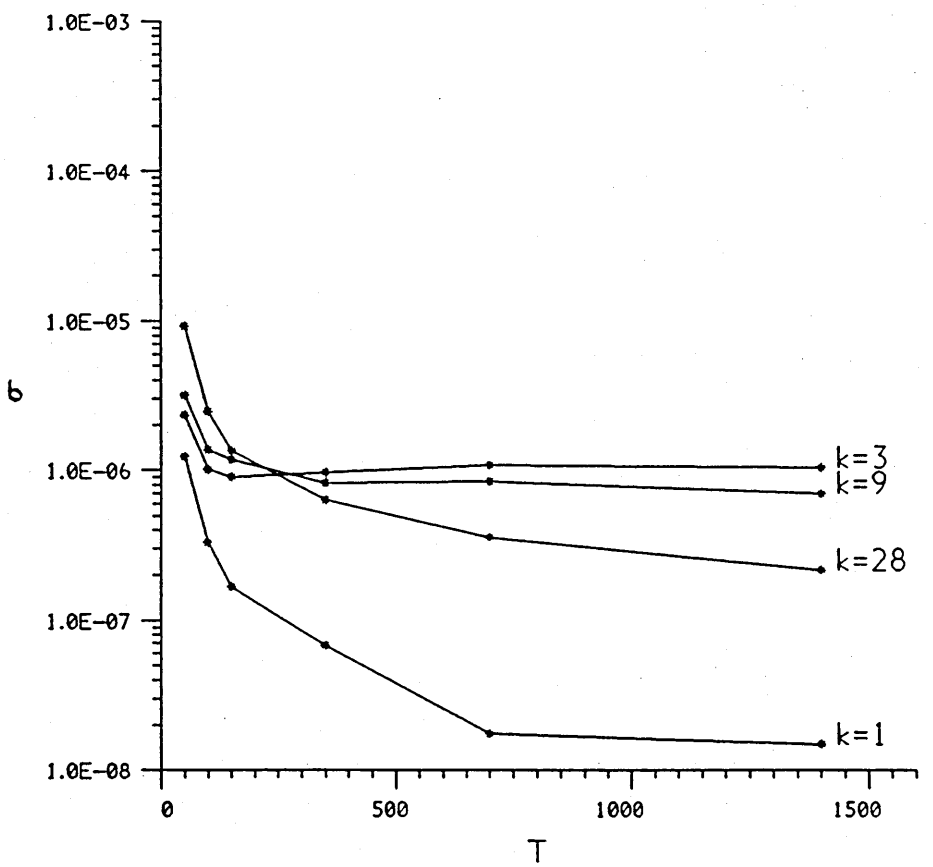
1.0E-03
1.0E-04
1.0E-05
1.0E-06
1.0E-07
1.0E-08
σ
0
500
1000
1500
T
k=3
k=9
k=28
k=1

Figure 3.2a

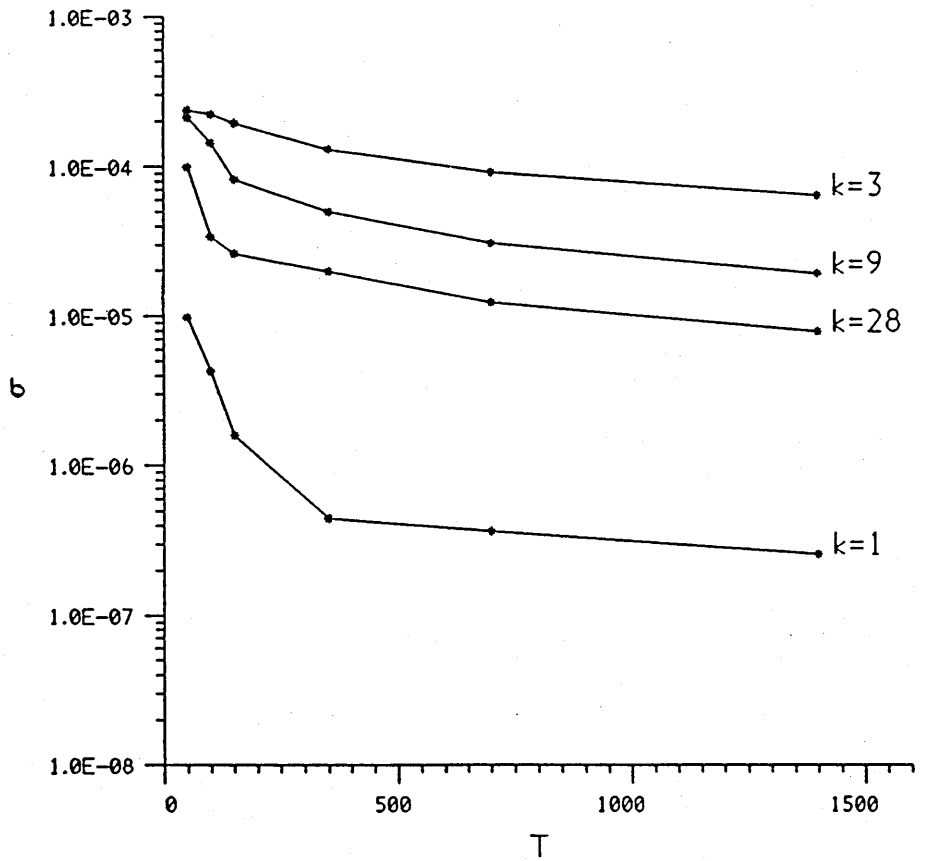
1.0E-03
1.0E-04
1.0E-05
1.0E-06
1.0E-07
1.0E-08
σ
0
500
1000
1500
T
k=3
k=9
k=28
k=1

Figure 3.2b

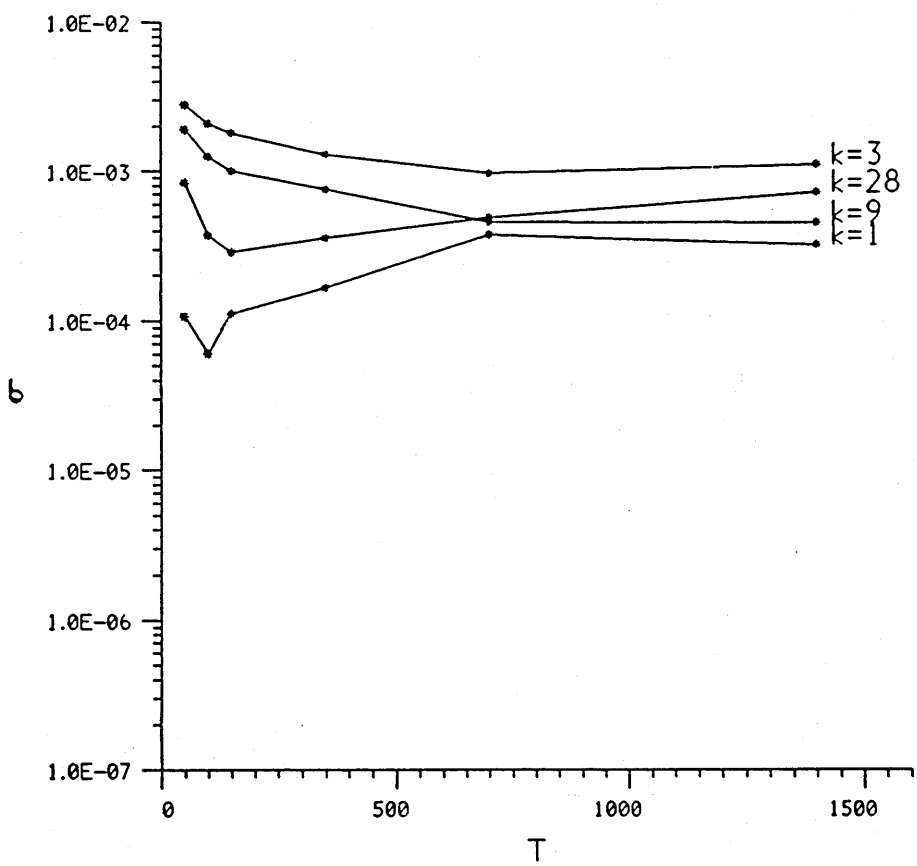
1.0E-02
1.0E-03
1.0E-04
1.0E-05
1.0E-06
1.0E-07
b
0
500
1000
1500
T
k=3
k=28
k=9
k=1

Figure 3.2c

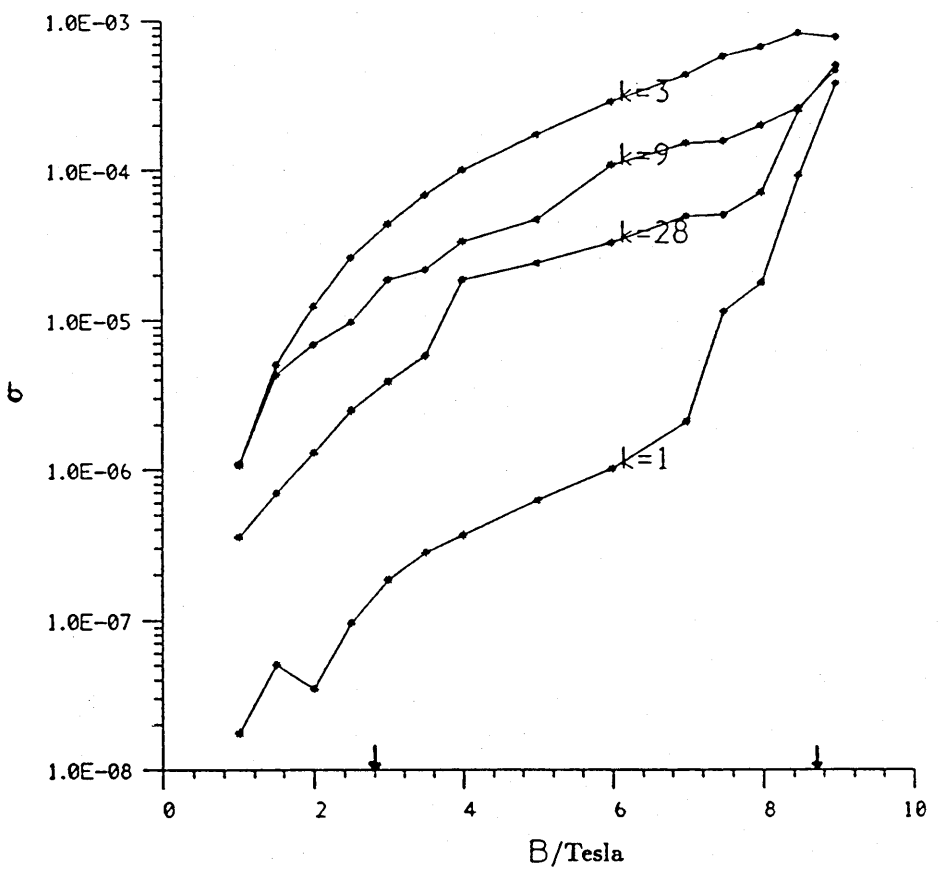
1.0E-03
1.0E-04
1.0E-05
1.0E-06
1.0E-07
1.0E-08
σ
k=3
k=9
k=28
k=1
0
2
4
6
8
10
B/Tesla

Figure 3.3

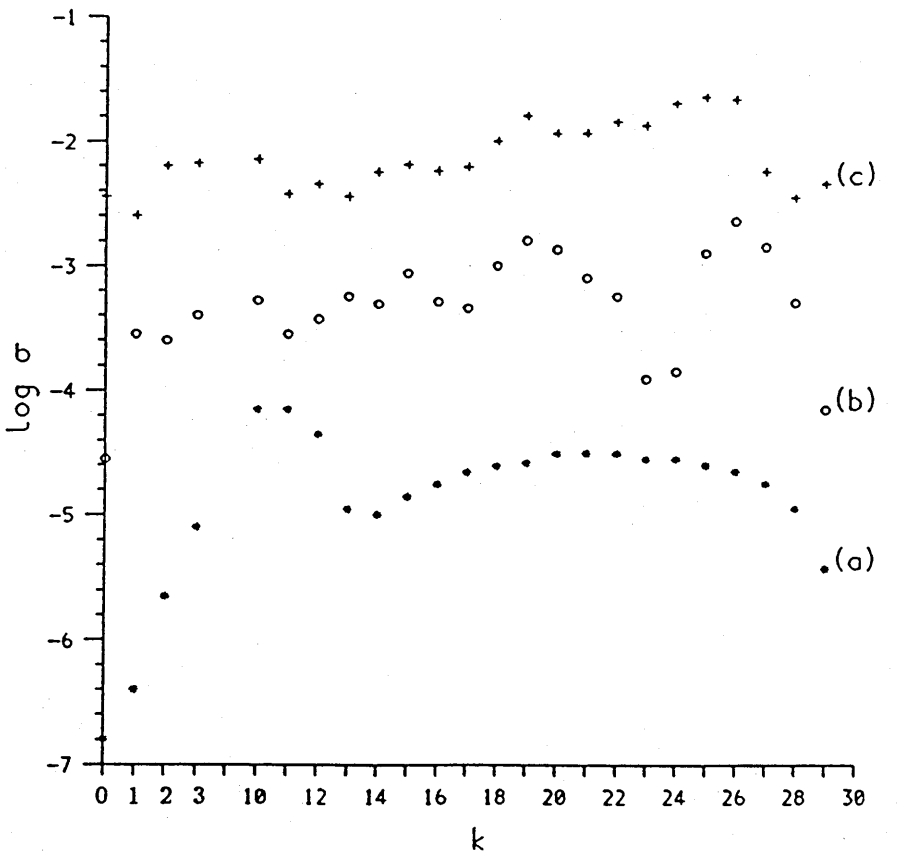

Figure 3.4

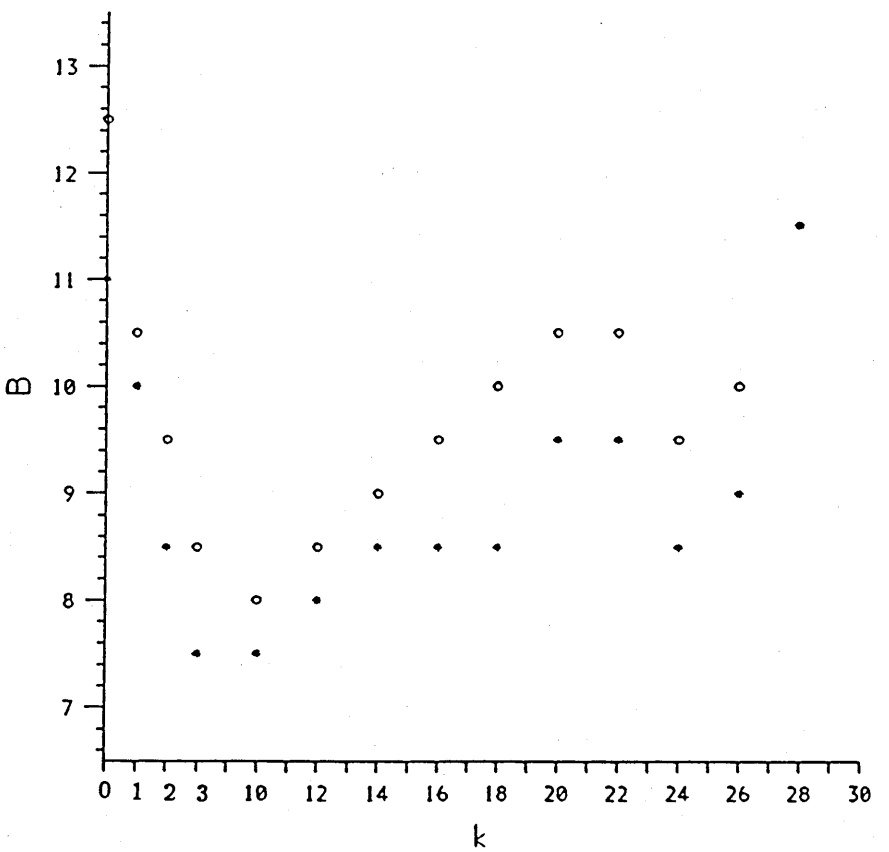

Figure 3.5a

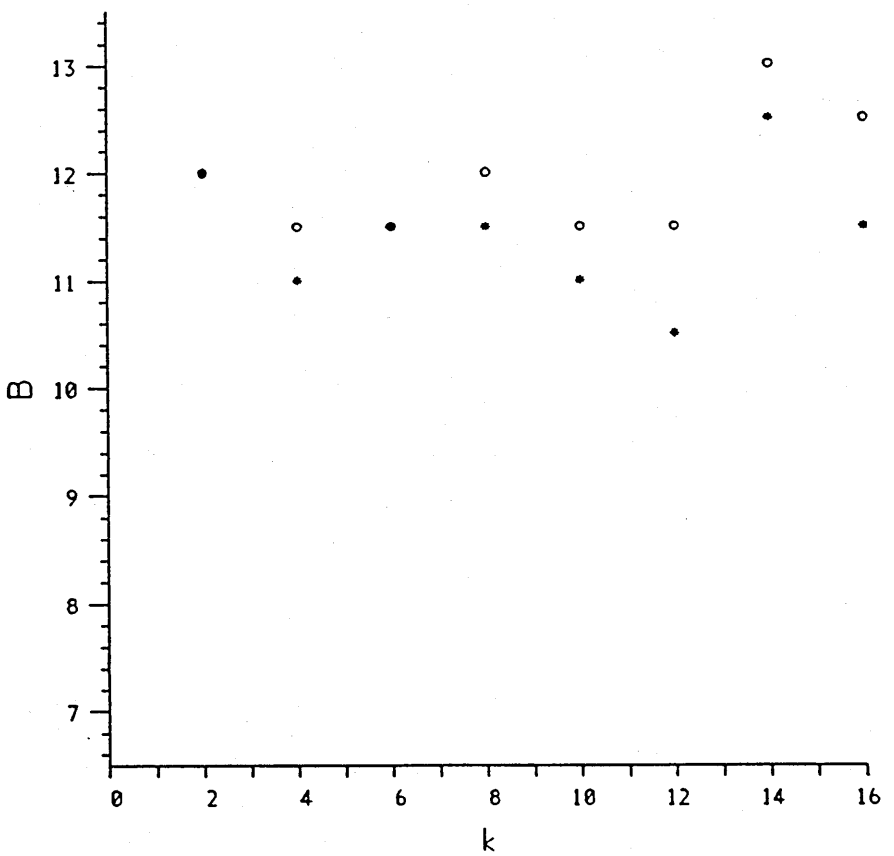

Figure 3.5b

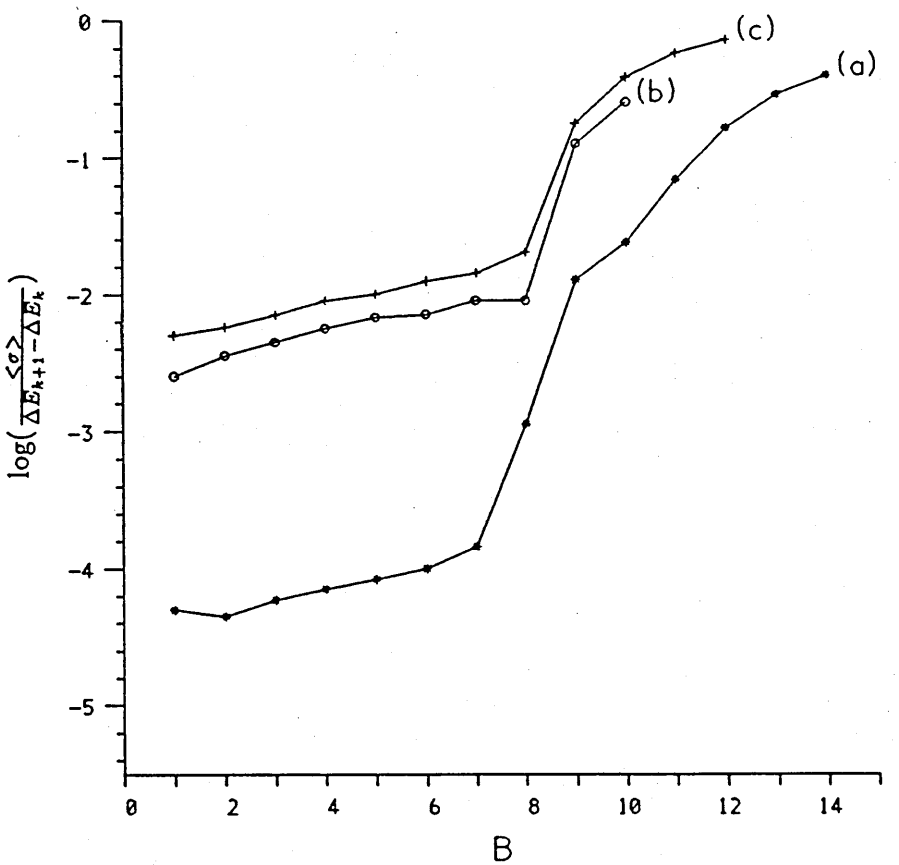

Figure 3.6

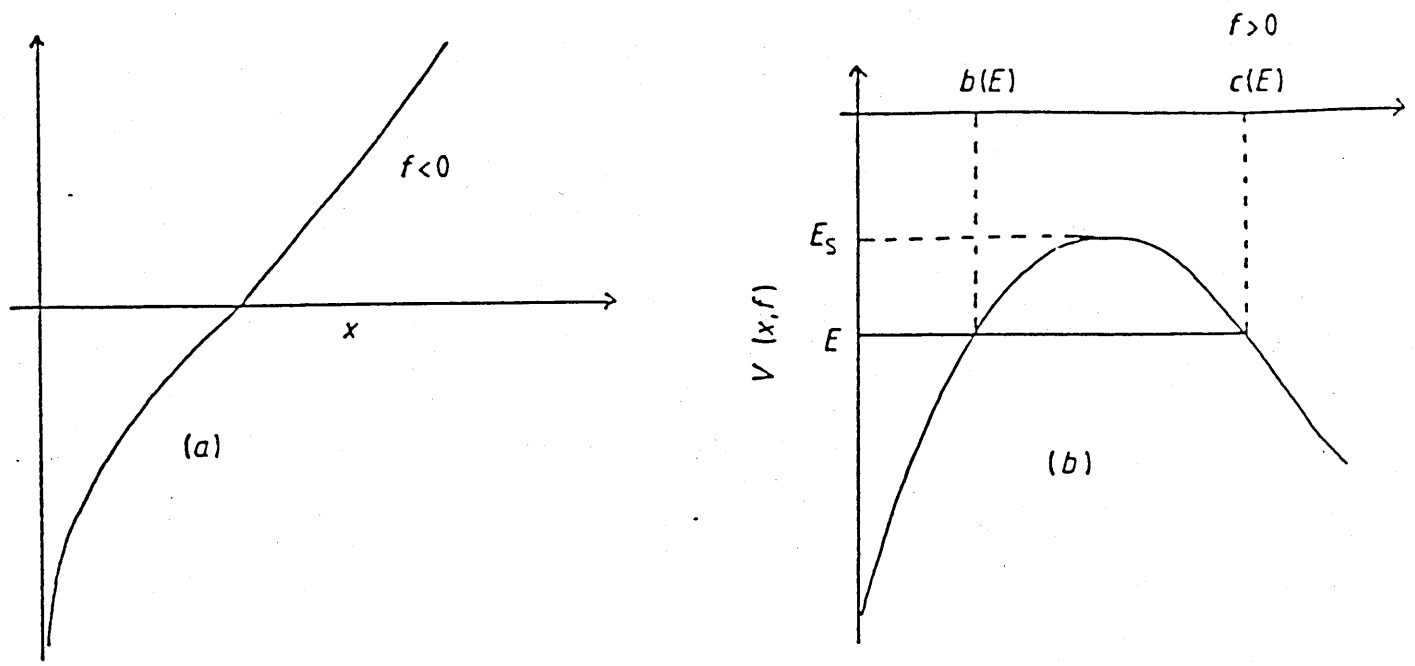

Figure 4.1

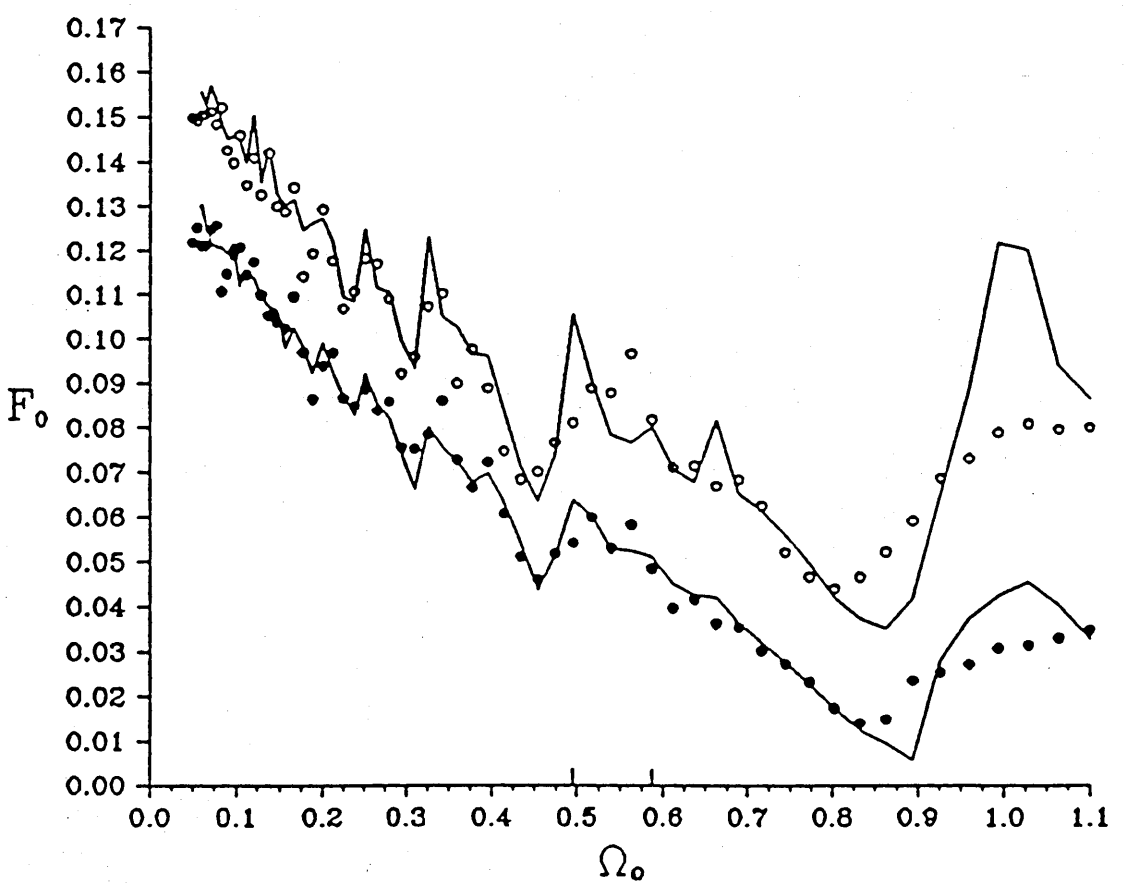
0.17
0.16
0.15
0.14
0.13
0.12
0.11
0.10
0.09
0.08
0.07
0.06
0.05
0.04
0.03
0.02
0.01
0.00
F_0
0.0
0.1
0.2
0.3
0.4
0.5
0.6
0.7
0.8
0.9
1.0
1.1
Ω_0

Figure 4.2

$$n_0 = 38,\ \Omega_0 = 0.0828$$

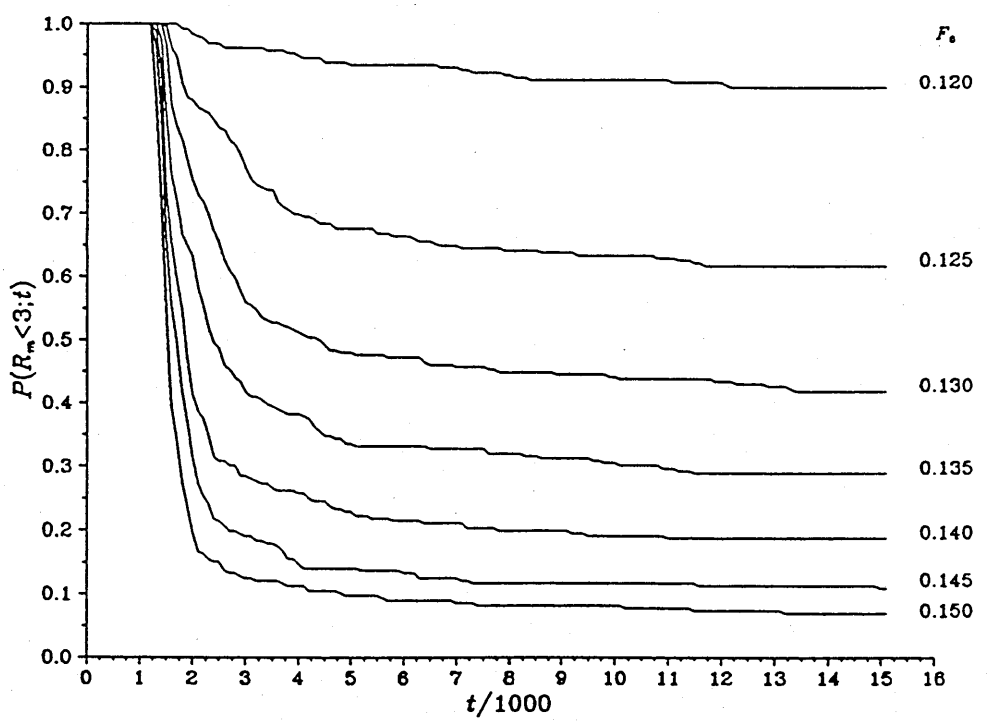

Figure 4.3a

$$F_0 = 0.130,\ n_0 = 38,\ \Omega_0 = 0.0828$$

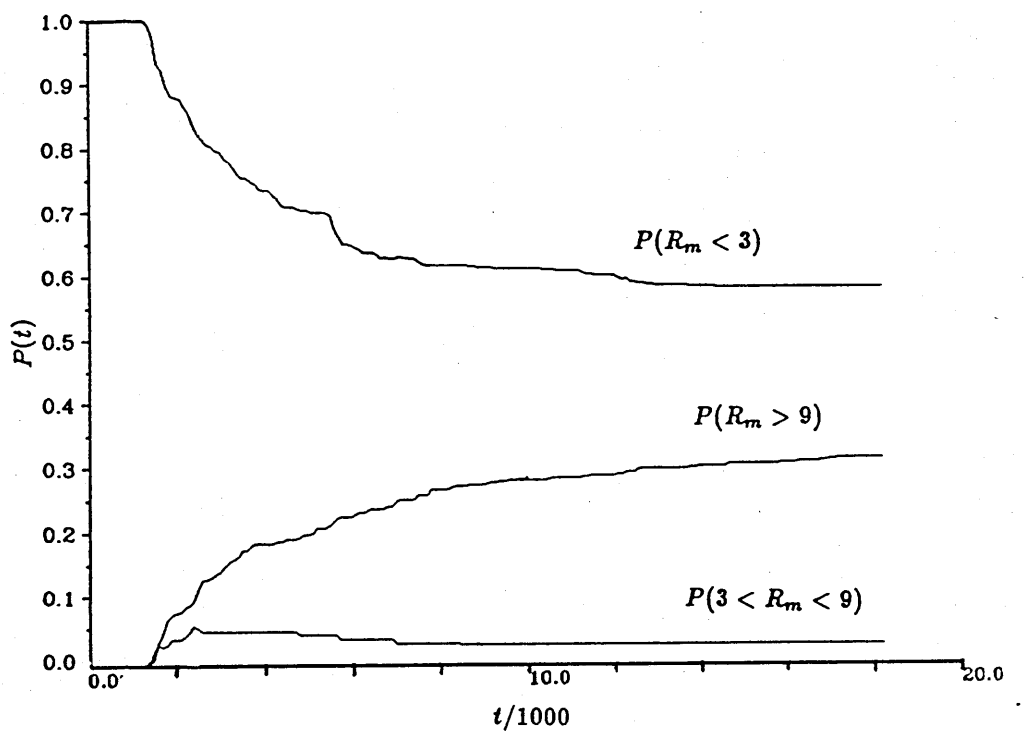

Figure 4.3b

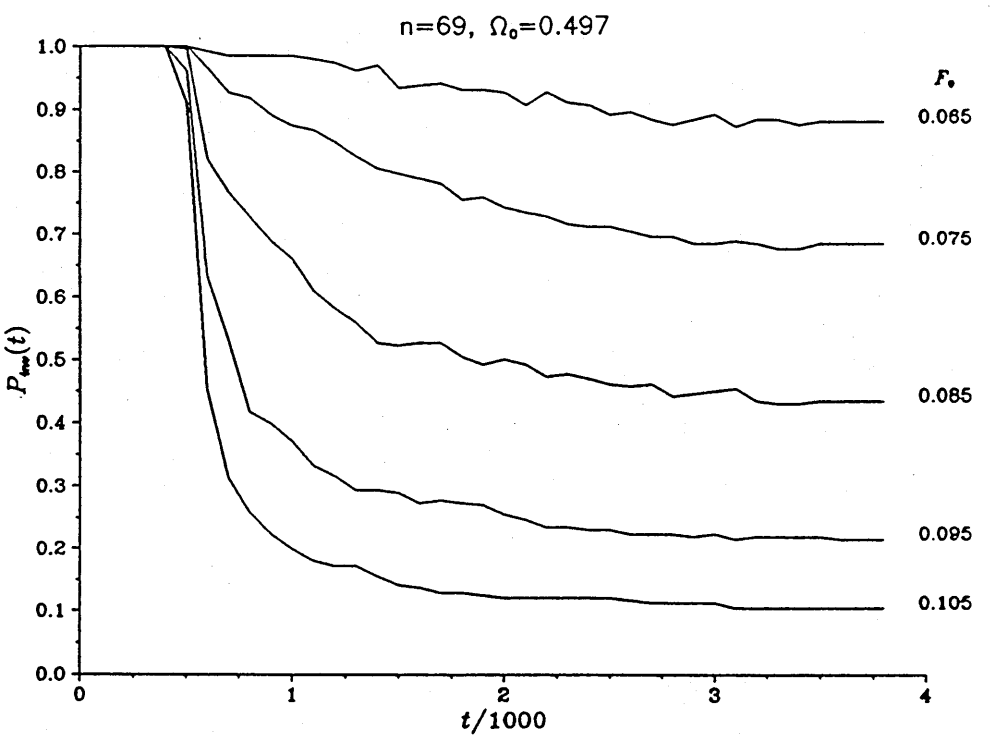
n=69, Ω_0=0.497
$P_{esc}(t)$
1.0
0.9
0.8
0.7
0.6
0.5
0.4
0.3
0.2
0.1
0.0
0
1
2
3
4
$t/1000$
F_e
0.065
0.075
0.085
0.095
0.105

Figure 4.4

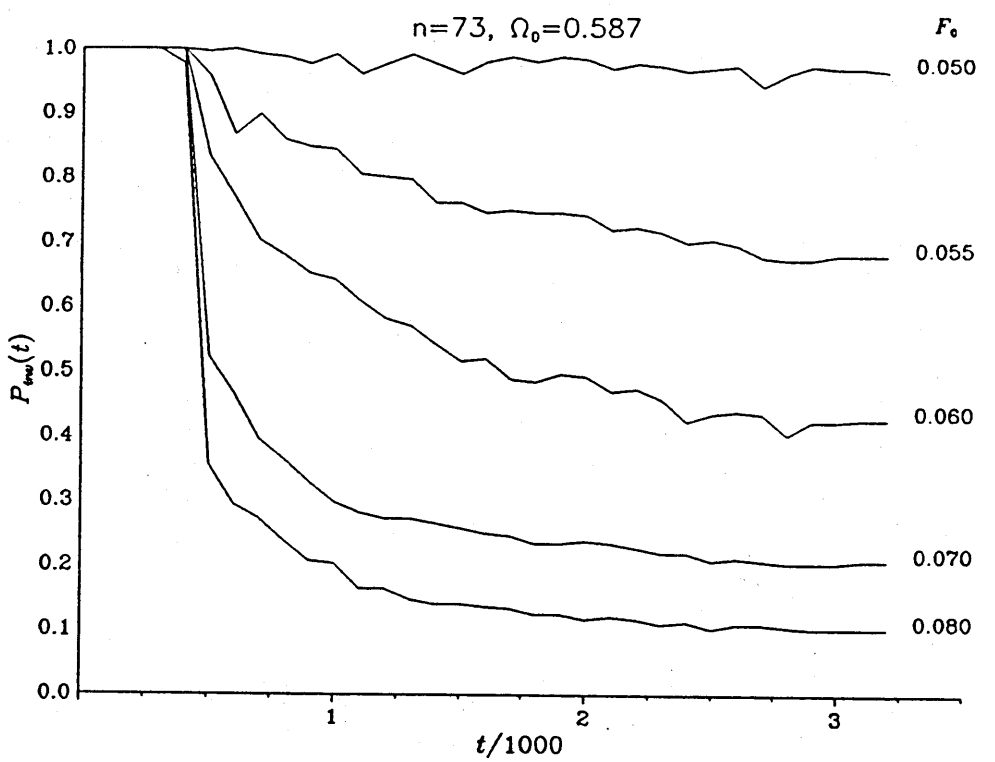
n=73, Ω_0=0.587
F_0
0.050
0.055
0.060
0.070
0.080
$P_{trap}(t)$
1.0
0.9
0.8
0.7
0.6
0.5
0.4
0.3
0.2
0.1
0.0
1
2
3
t/1000

Figure 4.5

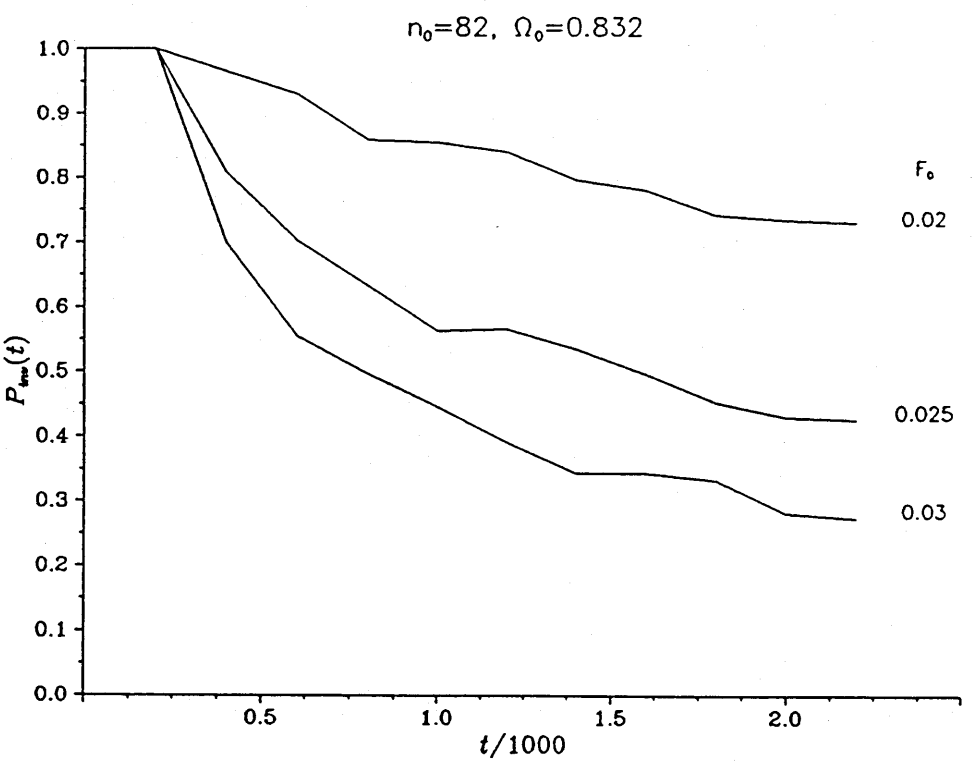
n_0=82, Ω_0=0.832
1.0
0.9
0.8
0.7
0.6
0.5
0.4
0.3
0.2
0.1
0.0
$P_{surv}(t)$
0.5
1.0
1.5
2.0
t/1000
F_0
0.02
0.025
0.03

Figure 4.6a

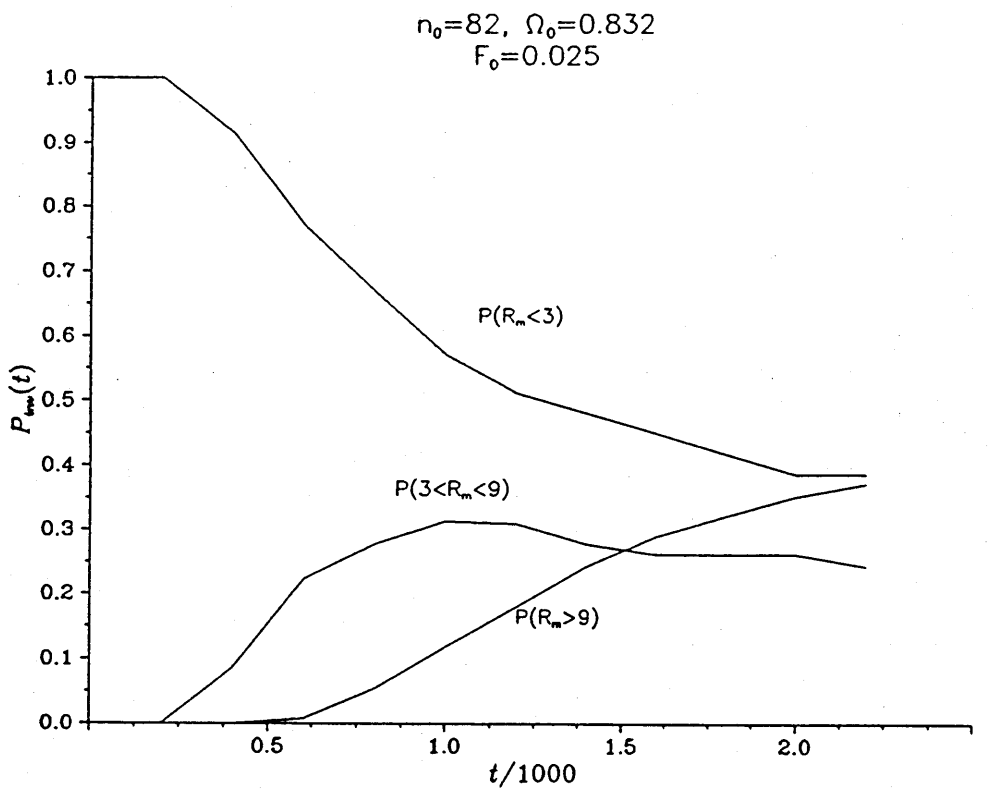
n_0=82, Ω_0=0.832
F_0=0.025
1.0
0.9
0.8
0.7
0.6
0.5
0.4
0.3
0.2
0.1
0.0
$P_{sw}(t)$
P(R$_m$<3)
P(3<R$_m$<9)
P(R$_m$>9)
0.5
1.0
1.5
2.0
t/1000

Figure 4.6b

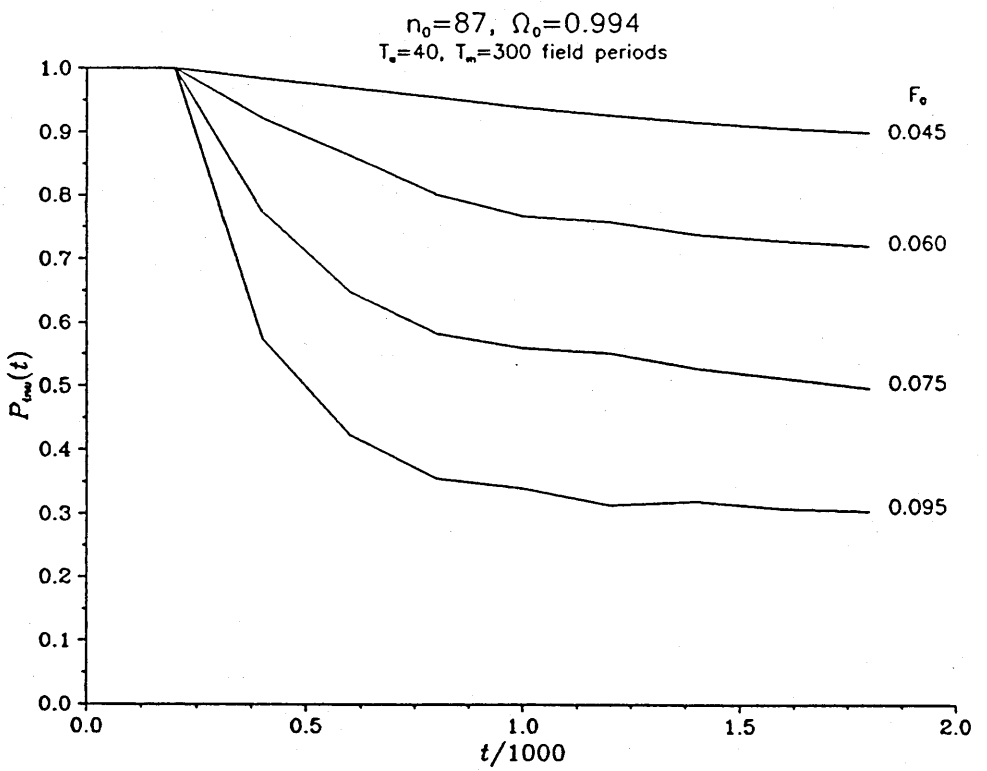
n_0=87, Ω_0=0.994
T_e=40, T_m=300 field periods
F_e
0.045
0.060
0.075
0.095
$P_{tot}(t)$
1.0
0.9
0.8
0.7
0.6
0.5
0.4
0.3
0.2
0.1
0.0
0.0
0.5
1.0
1.5
2.0
$t/1000$

Figure 4.7a

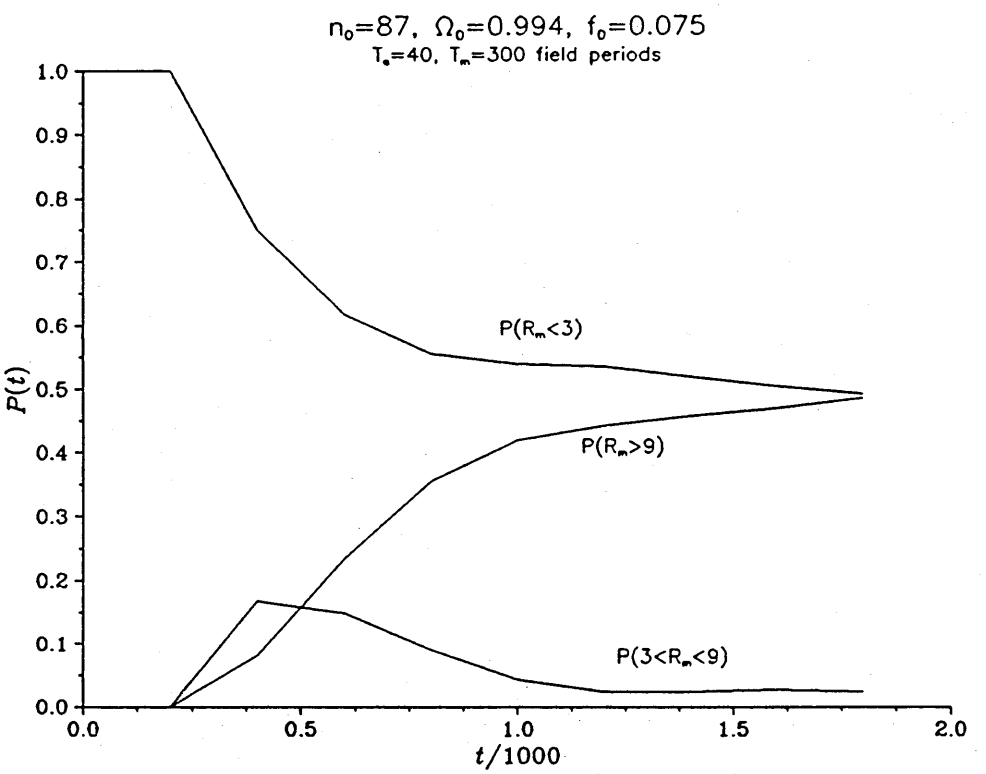
n_0=87, Ω_0=0.994, f_0=0.075
T_e=40, T_m=300 field periods
P(t)
t/1000
P(R$_m$<3)
P(R$_m$>9)
P(3<R$_m$<9)
1.0
0.9
0.8
0.7
0.6
0.5
0.4
0.3
0.2
0.1
0.0
0.0
0.5
1.0
1.5
2.0

Figure 4.7b

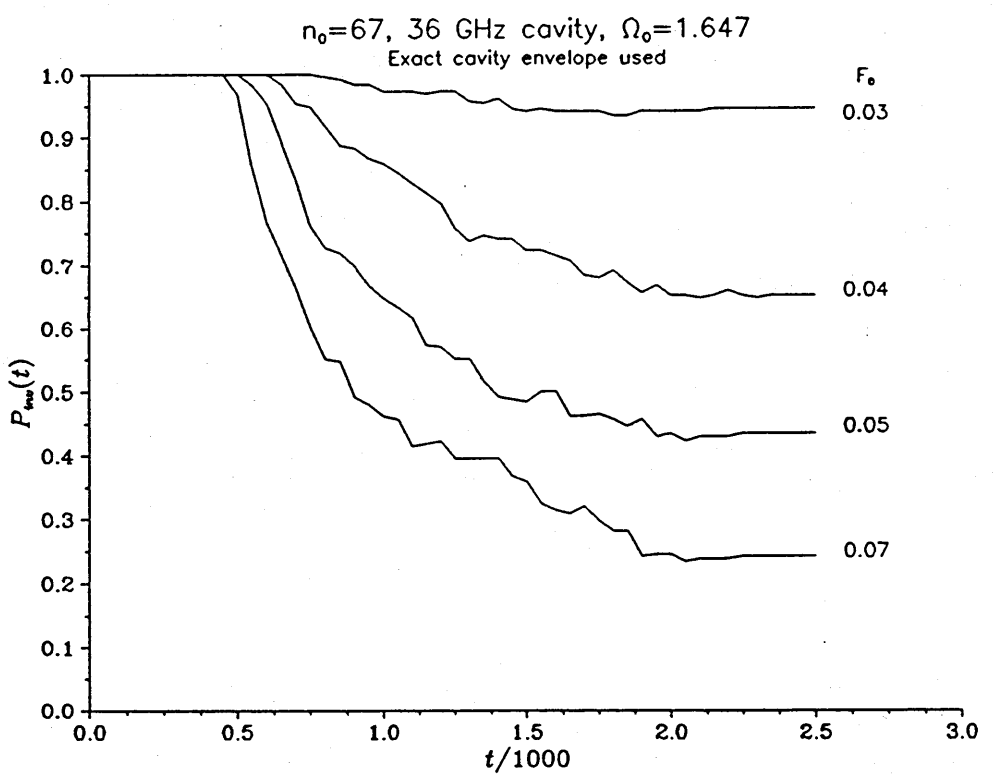
n_0=67, 36 GHz cavity, Ω_0=1.647
Exact cavity envelope used
F_0
0.03
0.04
0.05
0.07
$P_{sys}(t)$
1.0
0.9
0.8
0.7
0.6
0.5
0.4
0.3
0.2
0.1
0.0
0.0
0.5
1.0
1.5
2.0
2.5
3.0
t/1000

Figure 4.8a

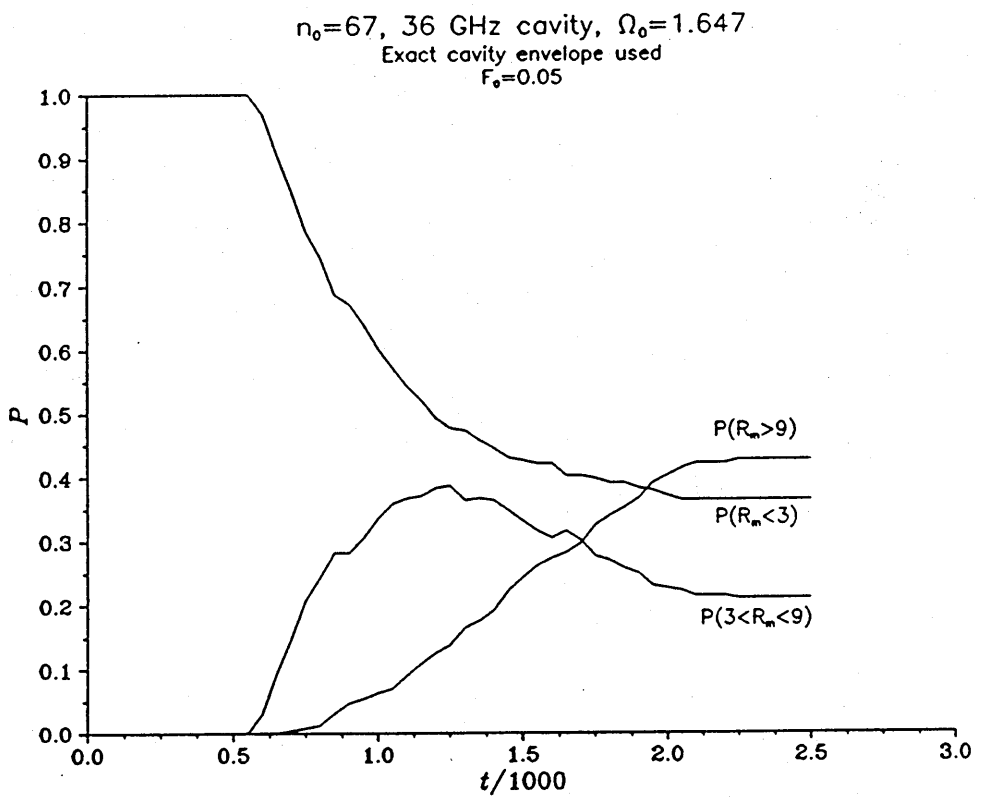
n_0=67, 36 GHz cavity, Ω_0=1.647
Exact cavity envelope used
F_0=0.05
P
1.0
0.9
0.8
0.7
0.6
0.5
0.4
0.3
0.2
0.1
0.0
0.0
0.5
1.0
1.5
2.0
2.5
3.0
t/1000
P(R$_m$>9)
P(R$_m$<3)
P(3<R$_m$<9)

Figure 4.8b

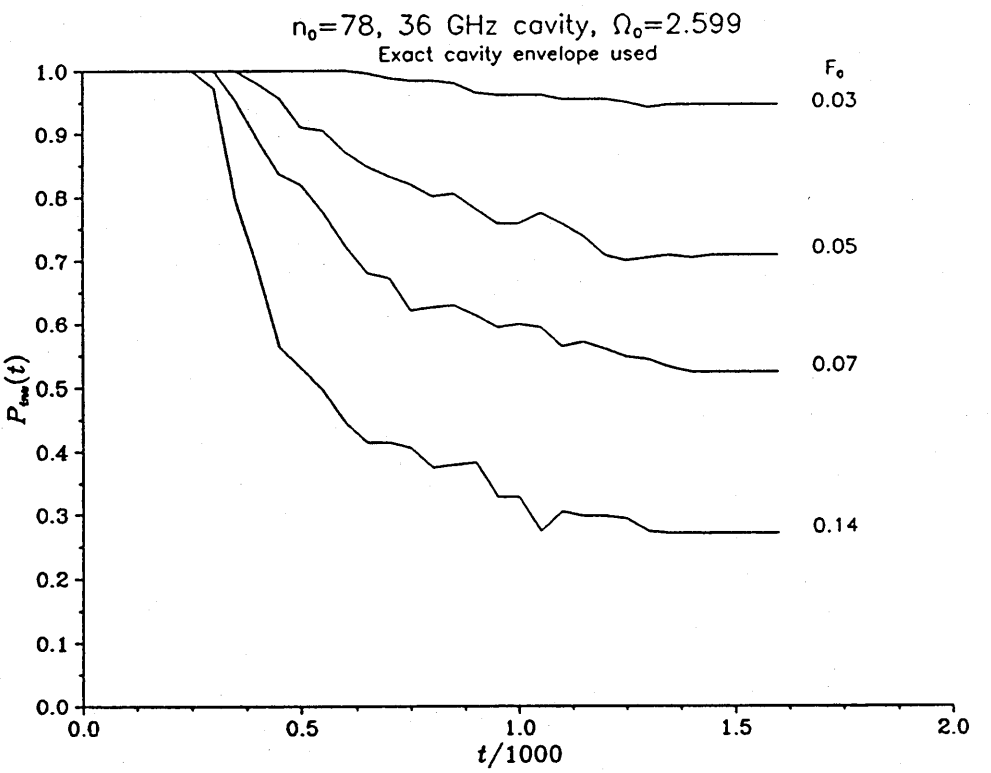
n_0=78, 36 GHz cavity, Ω_0=2.599
Exact cavity envelope used
F_0
0.03
0.05
0.07
0.14
$P_{trans}(t)$
1.0
0.9
0.8
0.7
0.6
0.5
0.4
0.3
0.2
0.1
0.0
0.0
0.5
1.0
1.5
2.0
$t/1000$

Figure 4.9a

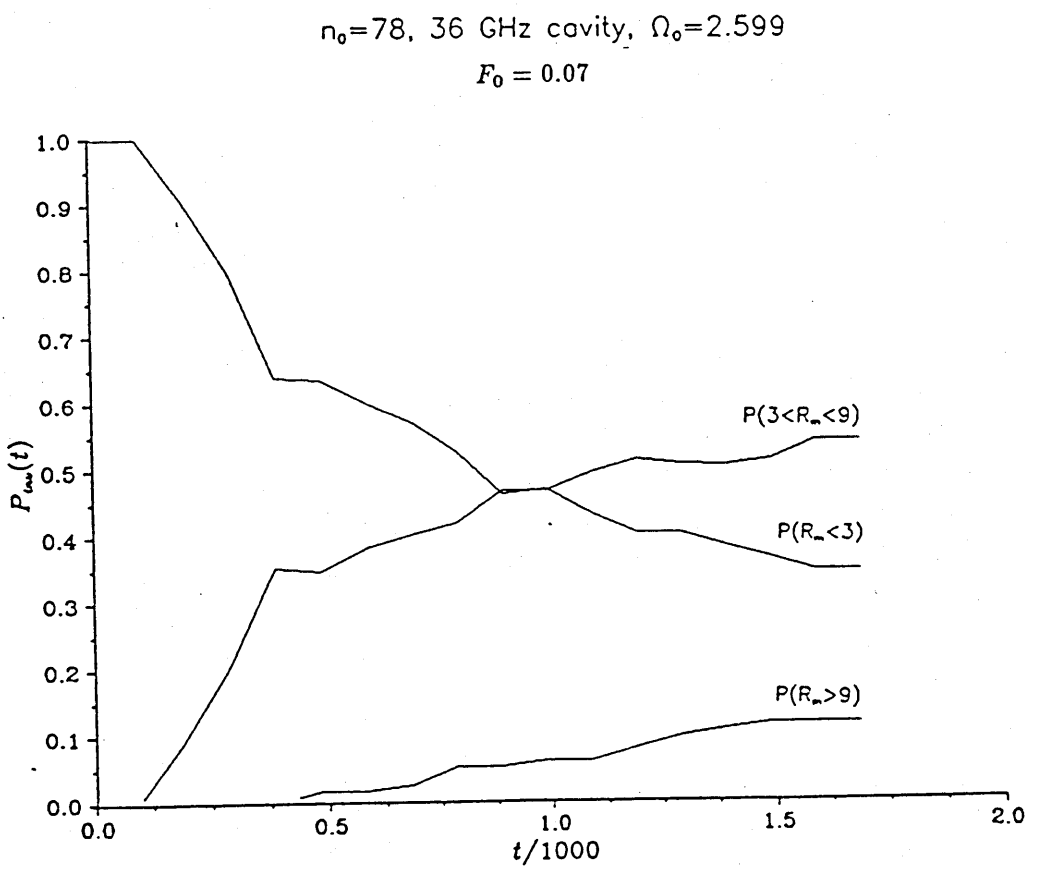
n_0=78, 36 GHz cavity, Ω_0=2.599
$F_0 = 0.07$
1.0
0.9
0.8
0.7
0.6
0.5
0.4
0.3
0.2
0.1
0.0
$P_{\omega_m}(t)$
P(3<R<9)
P(R<3)
P(R>9)
0.0
0.5
1.0
1.5
2.0
$t/1000$

Figure 4.9b

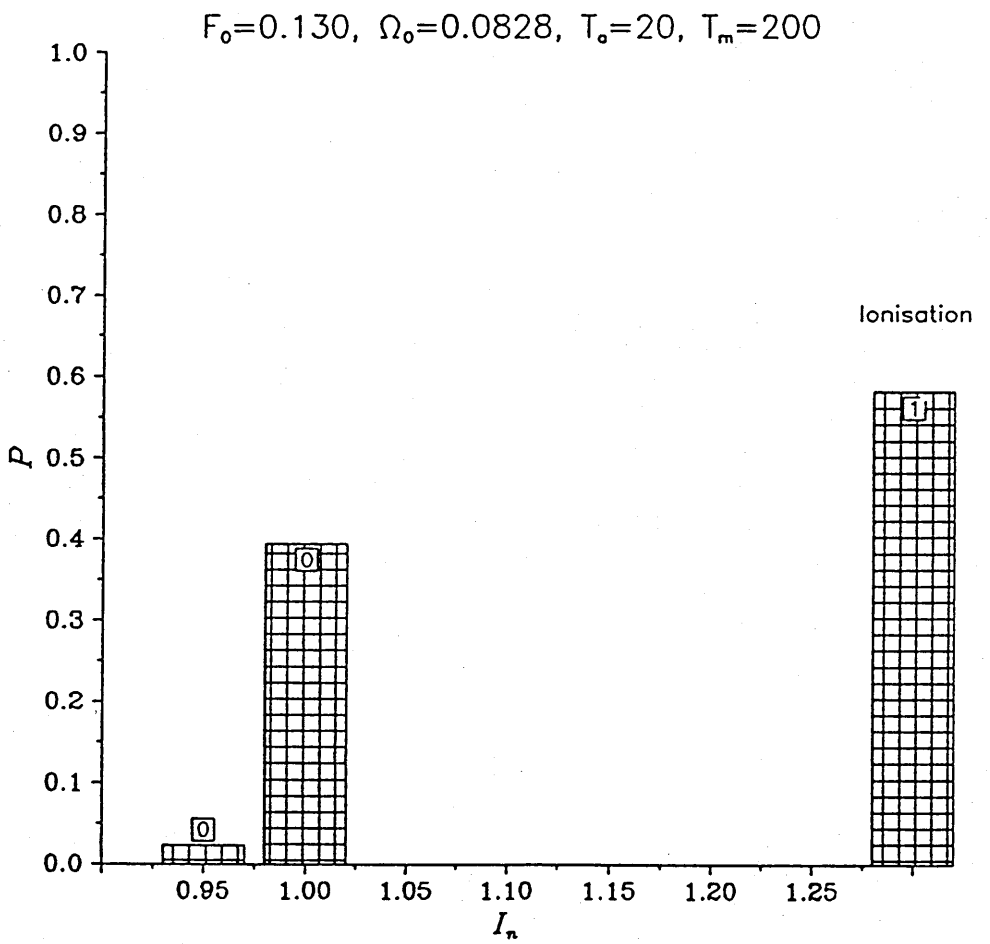
F₀=0.130, Ω₀=0.0828, Tₐ=20, Tₘ=200
1.0
0.9
0.8
0.7
0.6
0.5
0.4
0.3
0.2
0.1
0.0
P
Ionisation
0
0
1
0.95
1.00
1.05
1.10
1.15
1.20
1.25
Iₙ

Figure 4.10

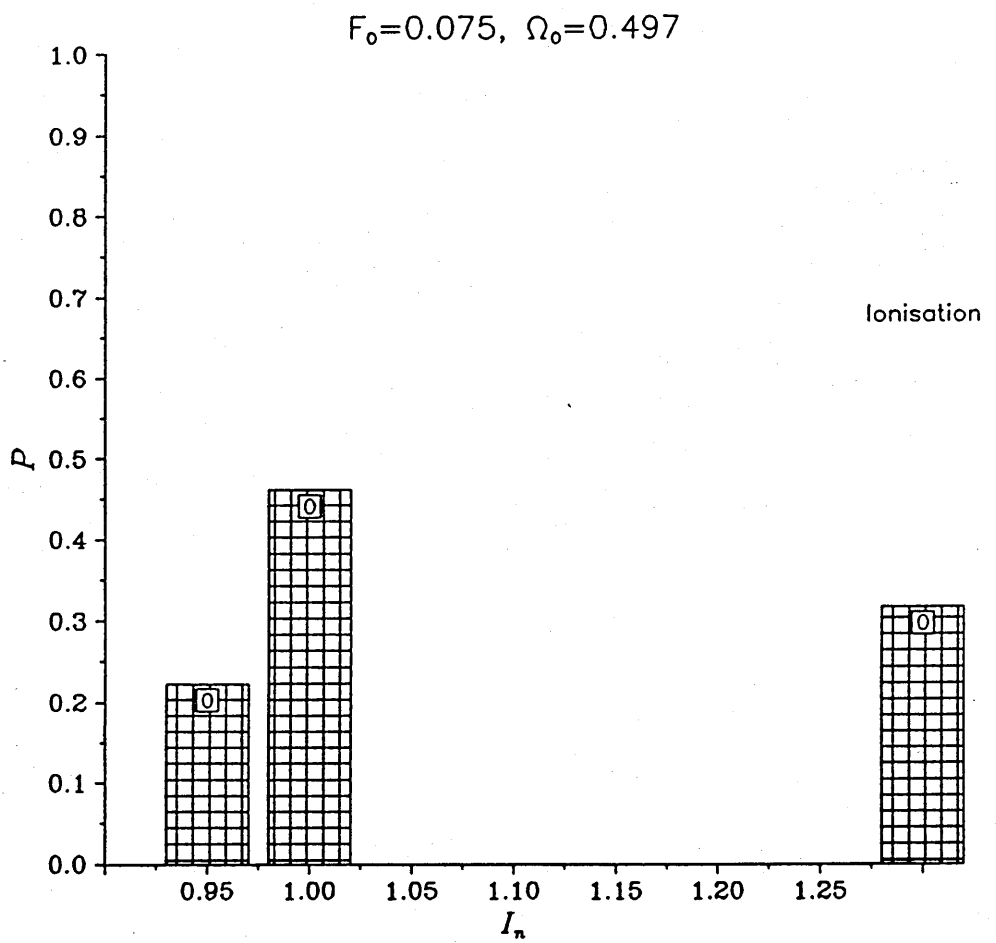
F₀=0.075, Ω₀=0.497
Ionisation
P
1.0
0.9
0.8
0.7
0.6
0.5
0.4
0.3
0.2
0.1
0.0
0
0
0
0.95
1.00
1.05
1.10
1.15
1.20
1.25
Iₙ

Figure 4.11a

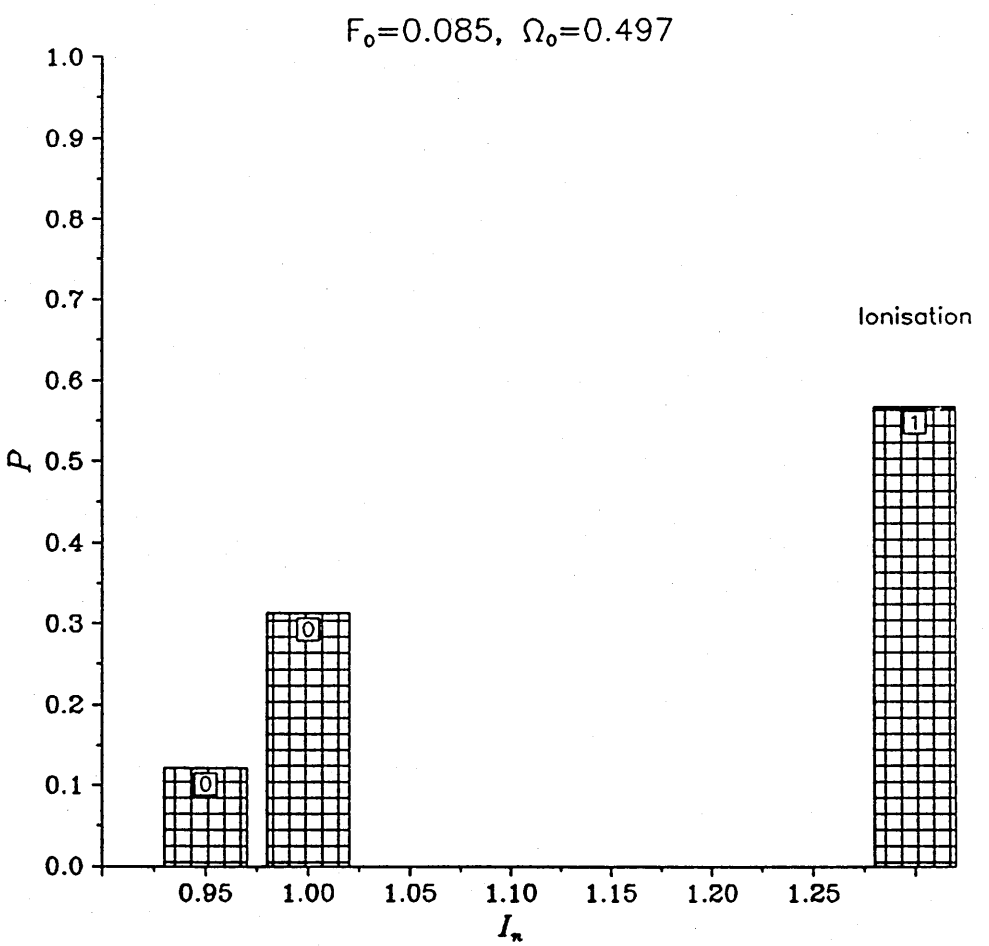
F_0=0.085, Ω_0=0.497
1.0
0.9
0.8
0.7
0.6
0.5
0.4
0.3
0.2
0.1
0.0
P
Ionisation
0
0
1
0.95
1.00
1.05
1.10
1.15
1.20
1.25
I_n

Figure 4.11b

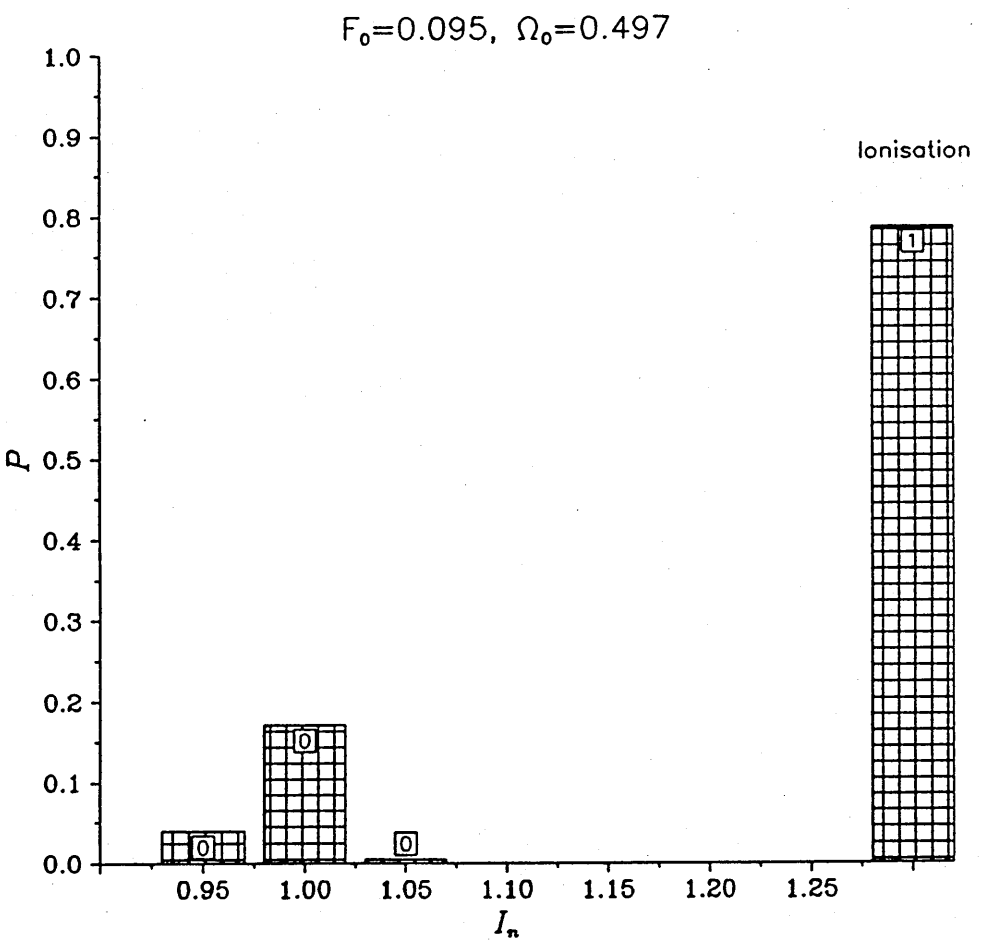
F_0=0.095, Ω_0=0.497
Ionisation
P
I_n
1.0
0.9
0.8
0.7
0.6
0.5
0.4
0.3
0.2
0.1
0.0
0.95
1.00
1.05
1.10
1.15
1.20
1.25
0
0
0
1

Figure 4.11c

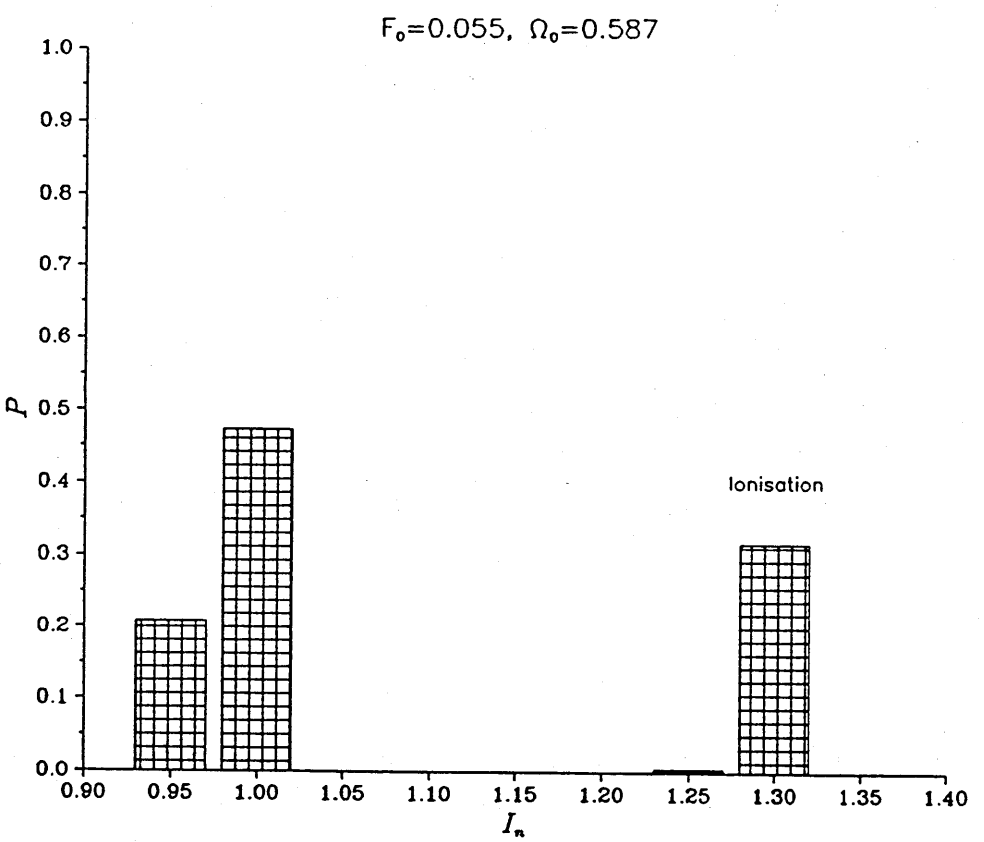
F₀=0.055, Ω₀=0.587
1.0
0.9
0.8
0.7
0.6
0.5
0.4
0.3
0.2
0.1
0.0
P
Ionisation
0.90
0.95
1.00
1.05
1.10
1.15
1.20
1.25
1.30
1.35
1.40
I_n

Figure 4.12a

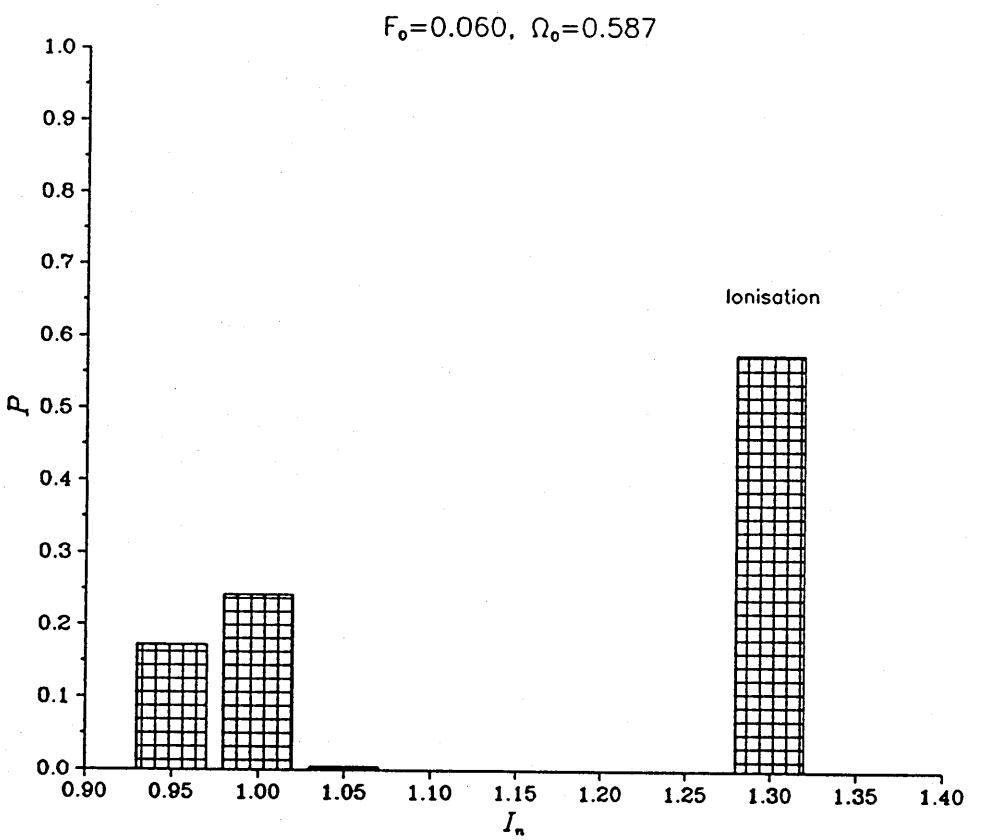
F_0=0.060, Ω_0=0.587
Ionisation
P_i
I_n
1.0
0.9
0.8
0.7
0.6
0.5
0.4
0.3
0.2
0.1
0.0
0.90
0.95
1.00
1.05
1.10
1.15
1.20
1.25
1.30
1.35
1.40

Figure 4.12b

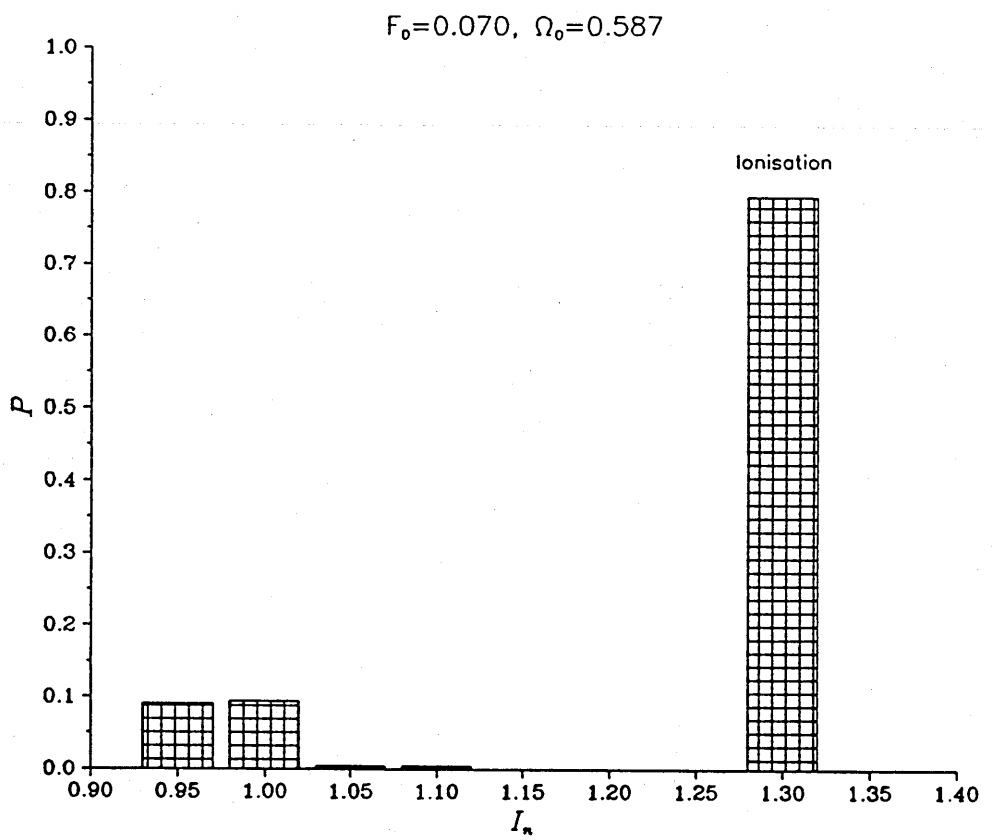
F_0=0.070, Ω_0=0.587
Ionisation
P
1.0
0.9
0.8
0.7
0.6
0.5
0.4
0.3
0.2
0.1
0.0
0.90
0.95
1.00
1.05
1.10
1.15
1.20
1.25
1.30
1.35
1.40
I_n

Figure 4.12c

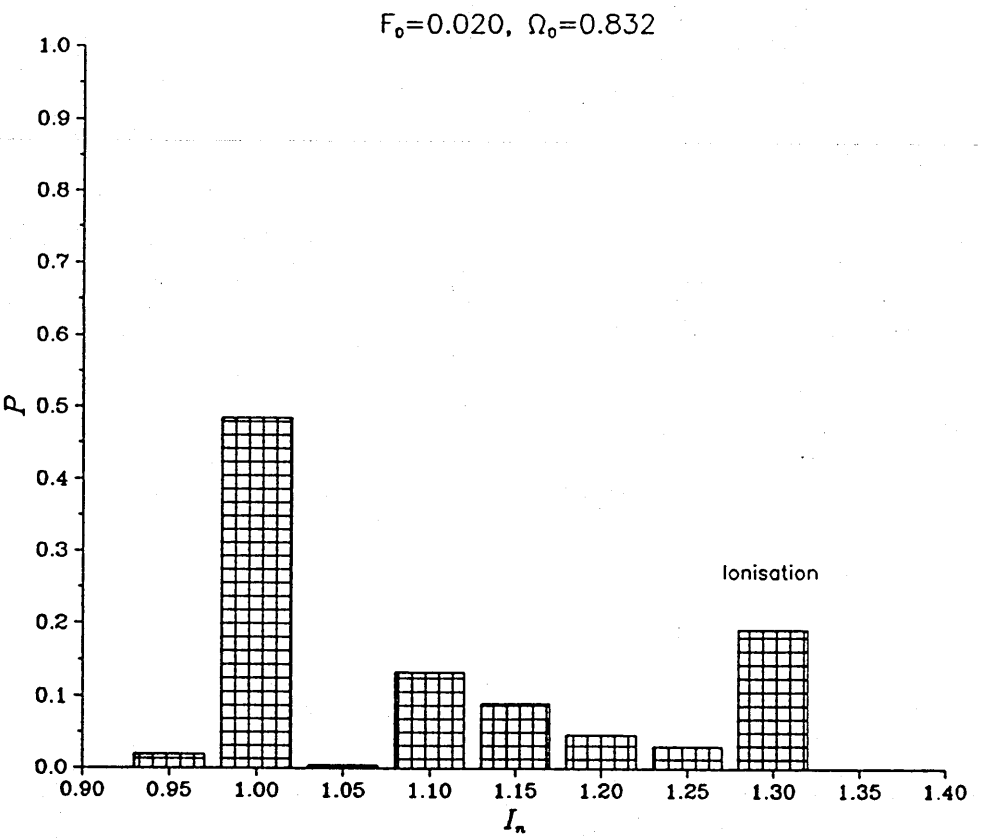
F_0=0.020, Ω_0=0.832
1.0
0.9
0.8
0.7
0.6
0.5
0.4
0.3
0.2
0.1
0.0
P
Ionisation
0.90
0.95
1.00
1.05
1.10
1.15
1.20
1.25
1.30
1.35
1.40
I_n

Figure 4.13a

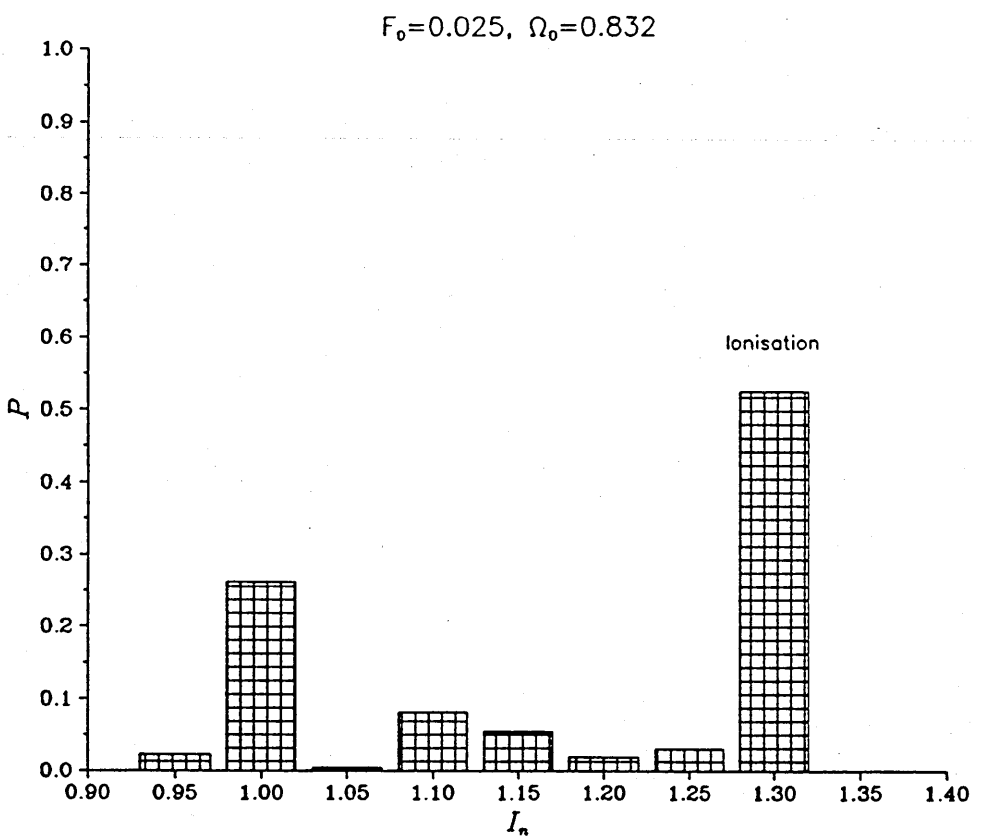
F_0=0.025, Ω_0=0.832
1.0
0.9
0.8
0.7
0.6
0.5
0.4
0.3
0.2
0.1
0.0
P_n
Ionisation
0.90
0.95
1.00
1.05
1.10
1.15
1.20
1.25
1.30
1.35
1.40
I_n

Figure 4.13b

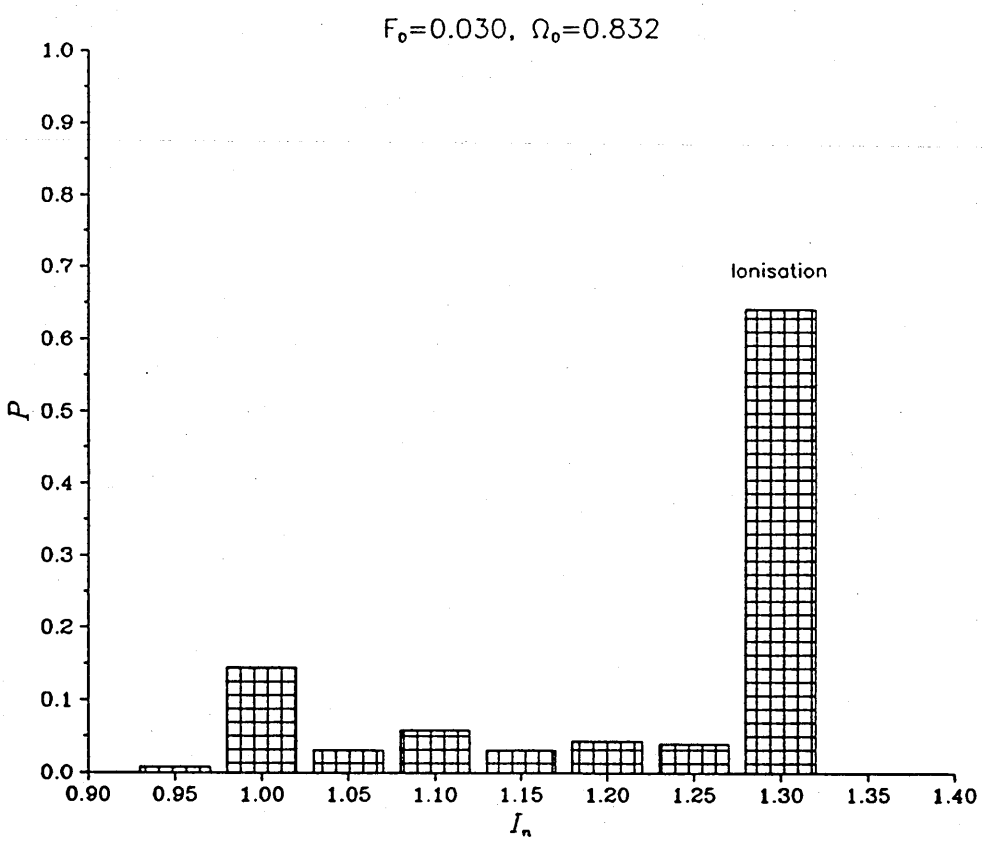
F₀=0.030, Ω₀=0.832
Ionisation
P
1.0
0.9
0.8
0.7
0.6
0.5
0.4
0.3
0.2
0.1
0.0
0.90
0.95
1.00
1.05
1.10
1.15
1.20
1.25
1.30
1.35
1.40
I_n

Figure 4.13c

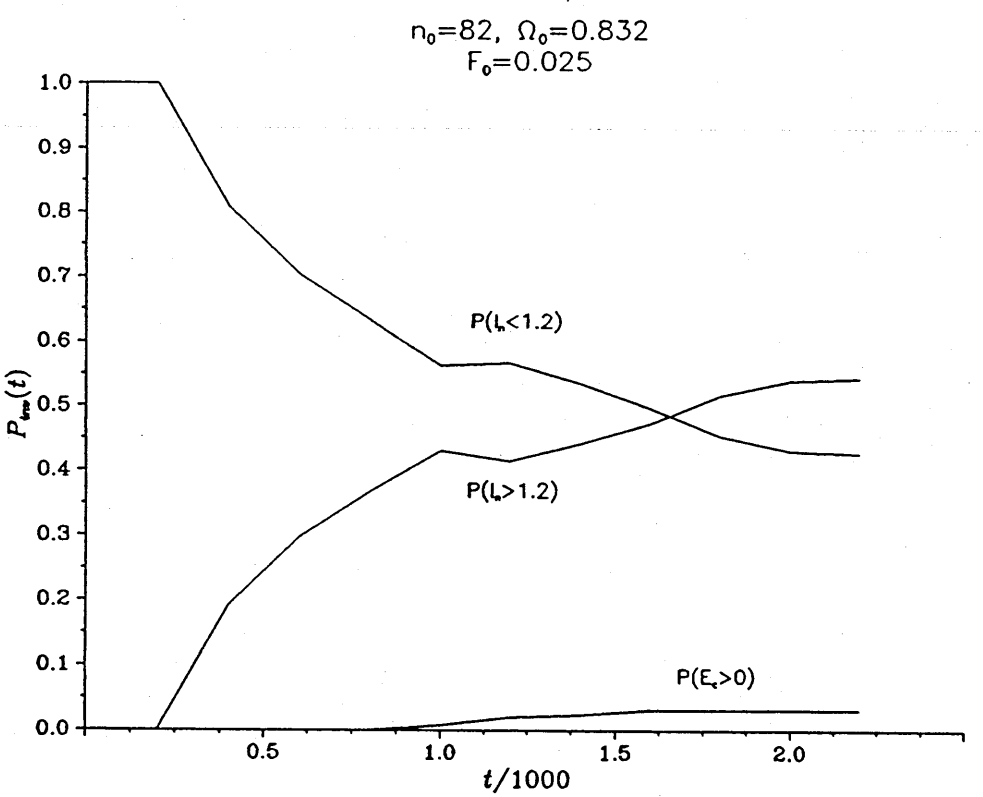
n_0=82, Ω_0=0.832
F_0=0.025
1.0
0.9
0.8
0.7
0.6
0.5
0.4
0.3
0.2
0.1
0.0
$P_{ens}(t)$
P(L<1.2)
P(L>1.2)
P(E>0)
0.5
1.0
1.5
2.0
t/1000

Figure 4.13d

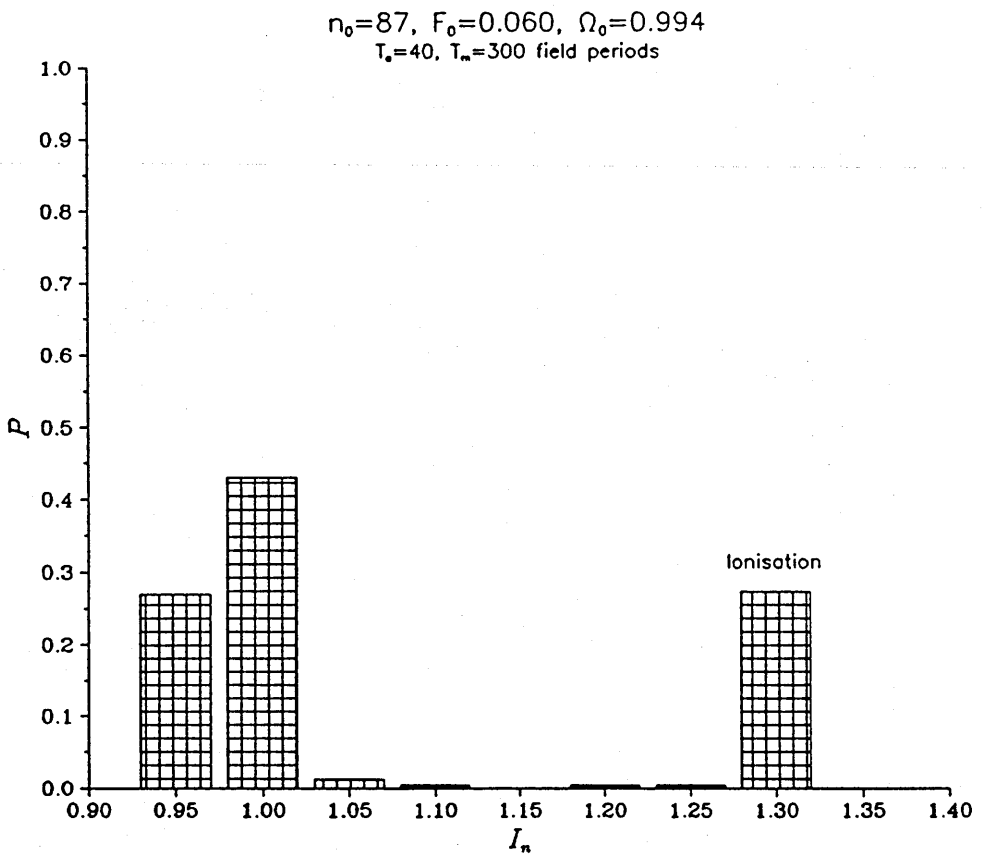
n_0=87, F_0=0.060, Ω_0=0.994
T_e=40, T_m=300 field periods
1.0
0.9
0.8
0.7
0.6
0.5
0.4
0.3
0.2
0.1
0.0
P_n
Ionisation
0.90
0.95
1.00
1.05
1.10
1.15
1.20
1.25
1.30
1.35
1.40
I_n

Figure 4.14a

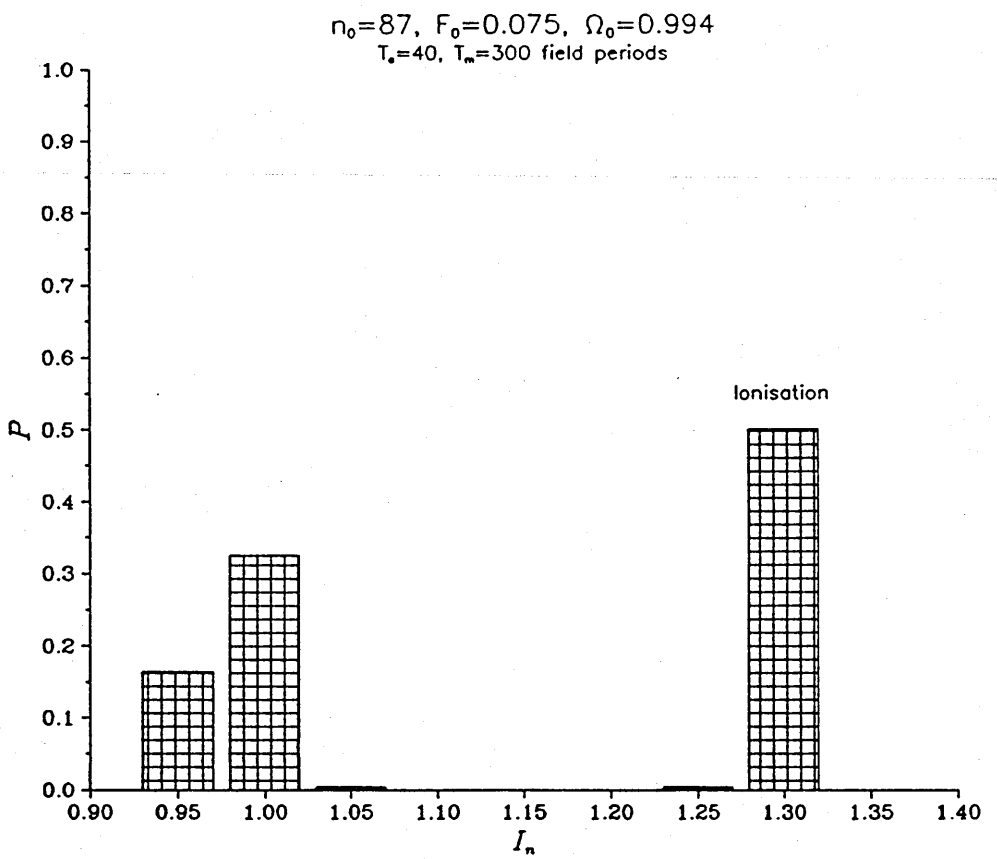
n_0=87, F_0=0.075, Ω_0=0.994
T_e=40, T_m=300 field periods
Ionisation
P_n
I_n
1.0
0.9
0.8
0.7
0.6
0.5
0.4
0.3
0.2
0.1
0.0
0.90
0.95
1.00
1.05
1.10
1.15
1.20
1.25
1.30
1.35
1.40

Figure 4.14b

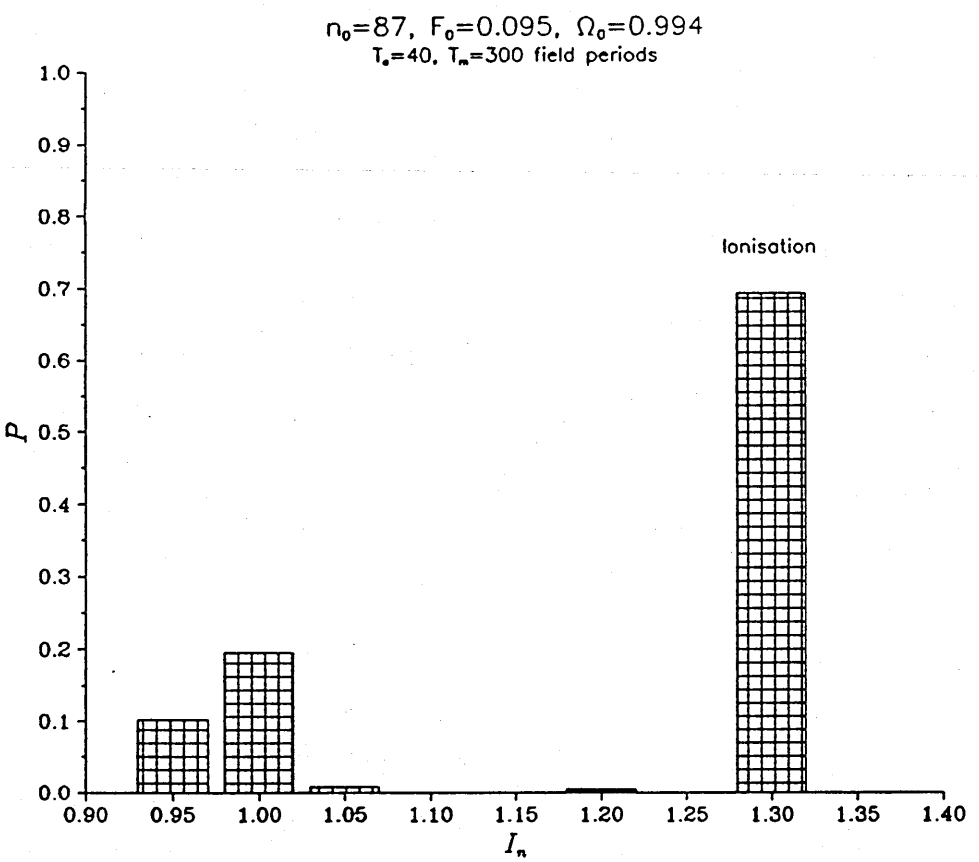
n_0=87, F_0=0.095, Ω_0=0.994
T_e=40, T_m=300 field periods
Ionisation
P_n
I_n
1.0
0.9
0.8
0.7
0.6
0.5
0.4
0.3
0.2
0.1
0.0
0.90
0.95
1.00
1.05
1.10
1.15
1.20
1.25
1.30
1.35
1.40

Figure 4.14c

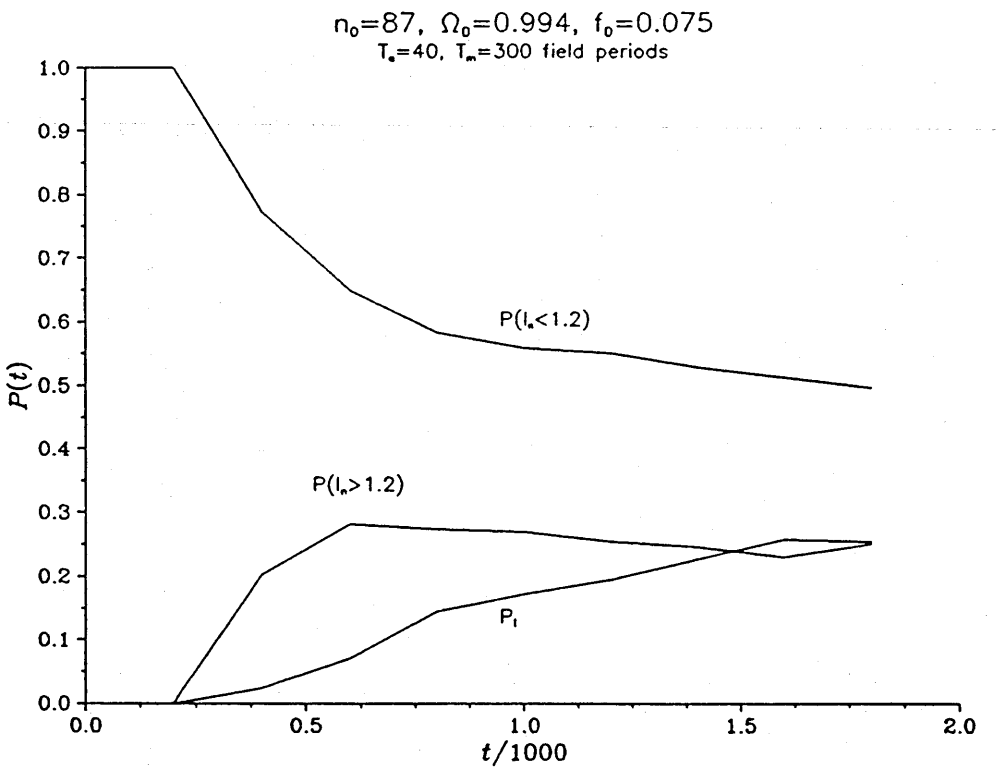
n_0=87, Ω_0=0.994, f_0=0.075
T_e=40, T_m=300 field periods
P(t)
P(l$_n$<1.2)
P(l$_n$>1.2)
P$_t$
t/1000
0.0
0.1
0.2
0.3
0.4
0.5
0.6
0.7
0.8
0.9
1.0
0.0
0.5
1.0
1.5
2.0

Figure 4.14d

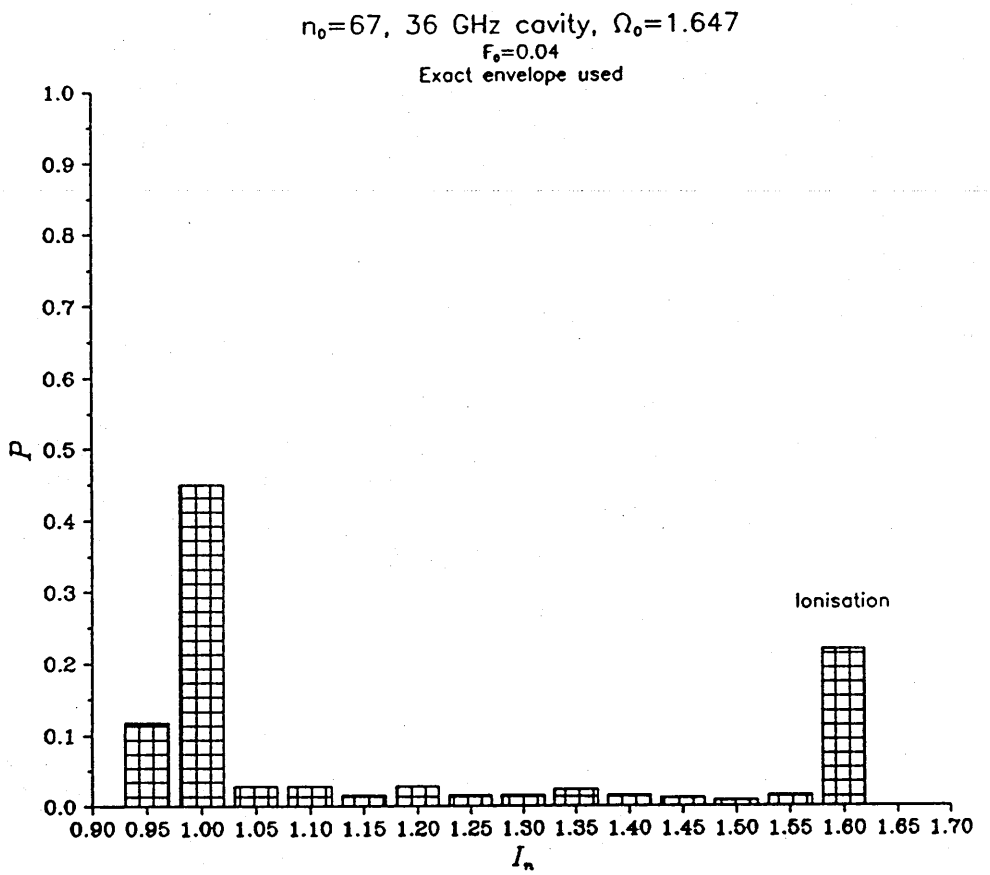
n_0=67, 36 GHz cavity, Ω_0=1.647
F_0=0.04
Exact envelope used
1.0
0.9
0.8
0.7
0.6
0.5
0.4
0.3
0.2
0.1
0.0
P_n
Ionisation
0.90 0.95 1.00 1.05 1.10 1.15 1.20 1.25 1.30 1.35 1.40 1.45 1.50 1.55 1.60 1.65 1.70
I_n

Figure 4.15a

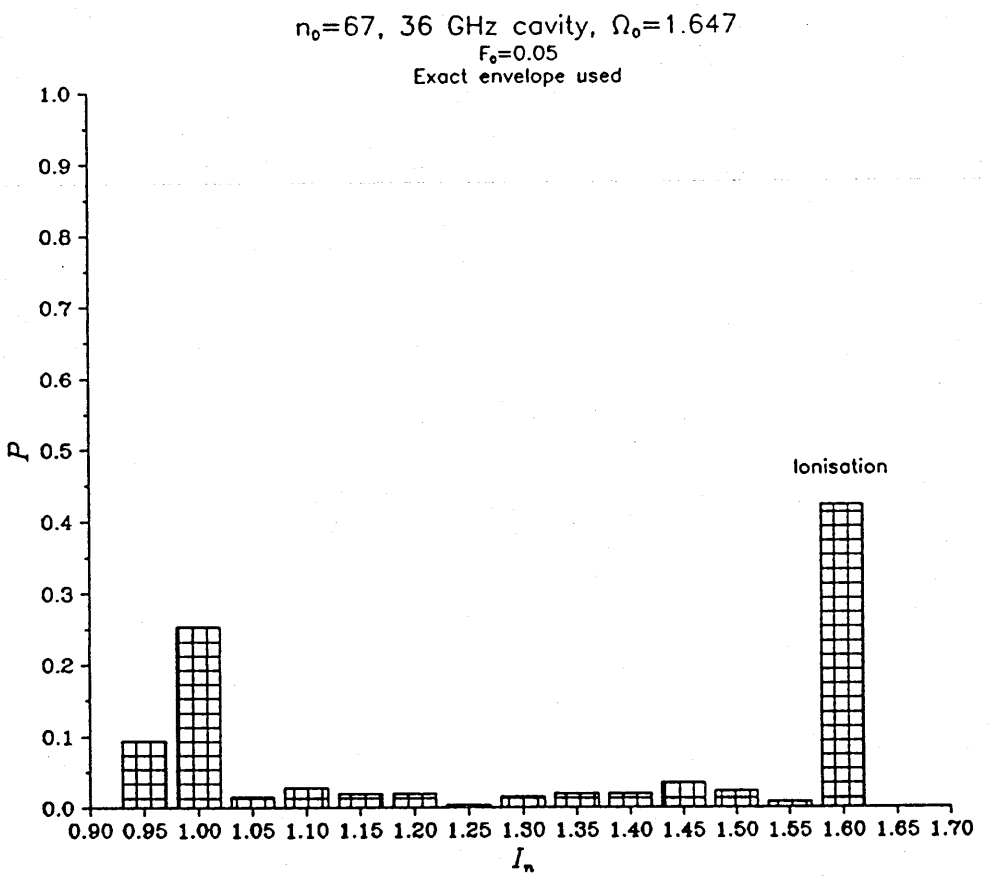
n_0=67, 36 GHz cavity, Ω_0=1.647
F_0=0.05
Exact envelope used
1.0
0.9
0.8
0.7
0.6
0.5
0.4
0.3
0.2
0.1
0.0
P_n
Ionisation
0.90 0.95 1.00 1.05 1.10 1.15 1.20 1.25 1.30 1.35 1.40 1.45 1.50 1.55 1.60 1.65 1.70
I_n

Figure 4.15b

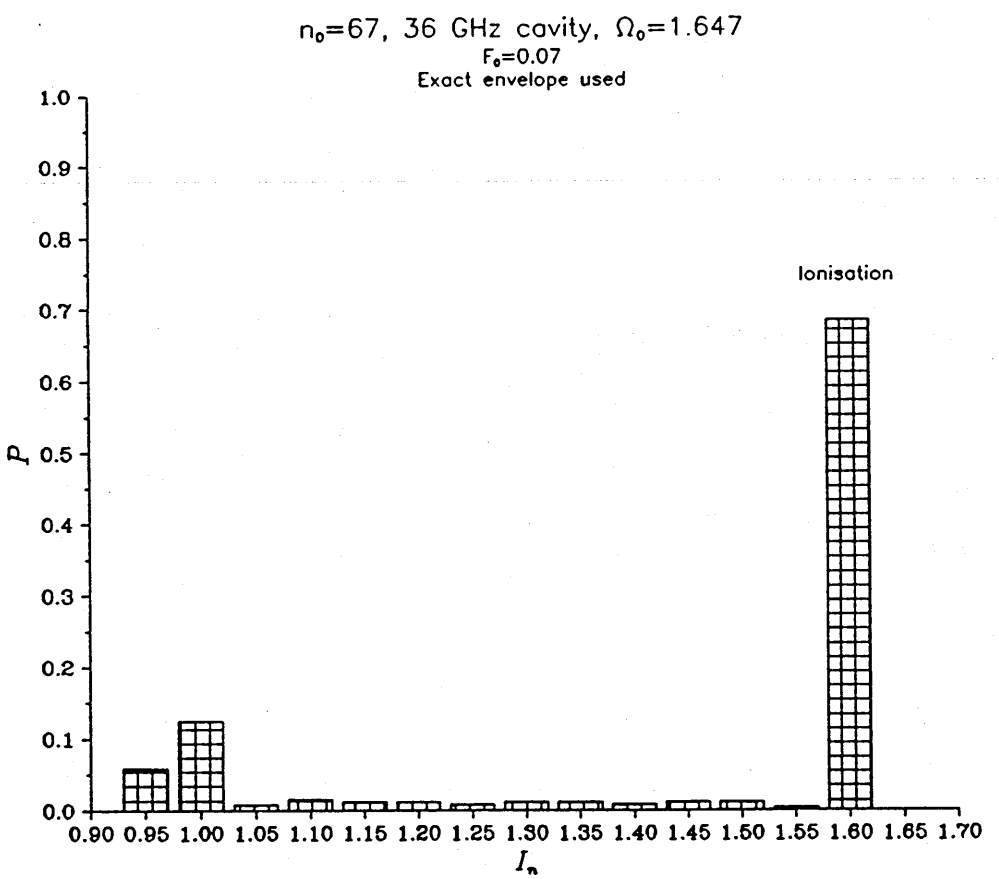
n_0=67, 36 GHz cavity, Ω_0=1.647
F_e=0.07
Exact envelope used
Ionisation
P_n
1.0
0.9
0.8
0.7
0.6
0.5
0.4
0.3
0.2
0.1
0.0
0.90 0.95 1.00 1.05 1.10 1.15 1.20 1.25 1.30 1.35 1.40 1.45 1.50 1.55 1.60 1.65 1.70
I_n

Figure 4.15c

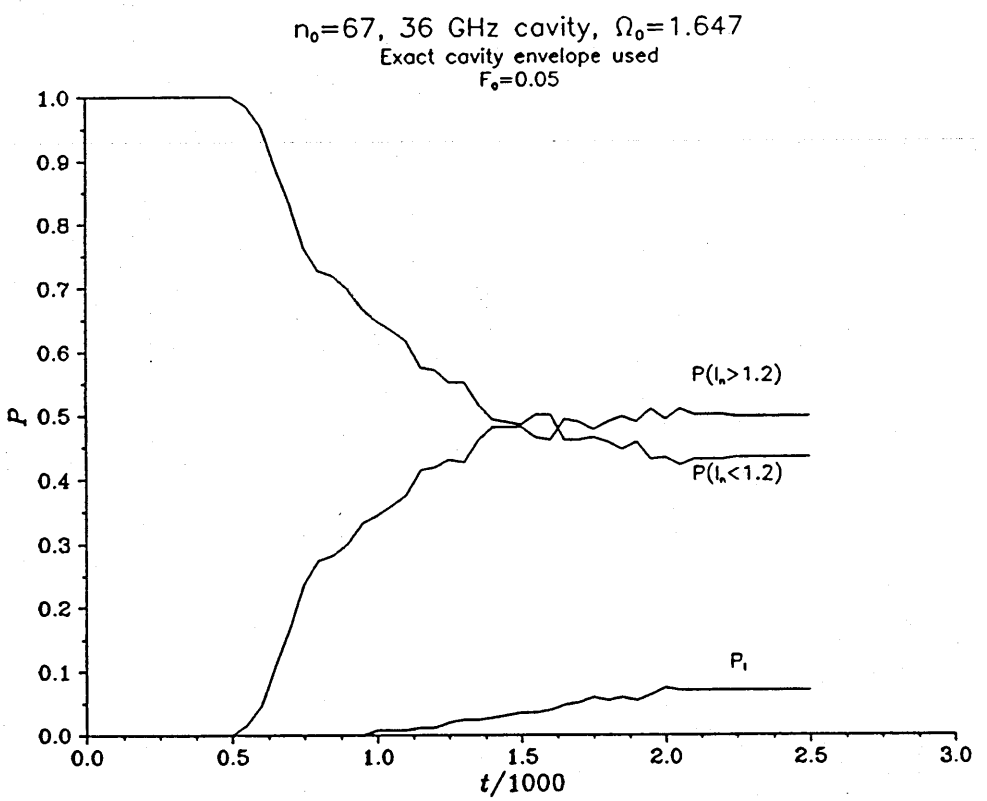
n_0=67, 36 GHz cavity, Ω_0=1.647
Exact cavity envelope used
F_0=0.05
1.0
0.9
0.8
0.7
0.6
0.5
0.4
0.3
0.2
0.1
0.0
P_i
P(I_n>1.2)
P(I_n<1.2)
P_t
0.0
0.5
1.0
1.5
2.0
2.5
3.0
t/1000

Figure 4.15d

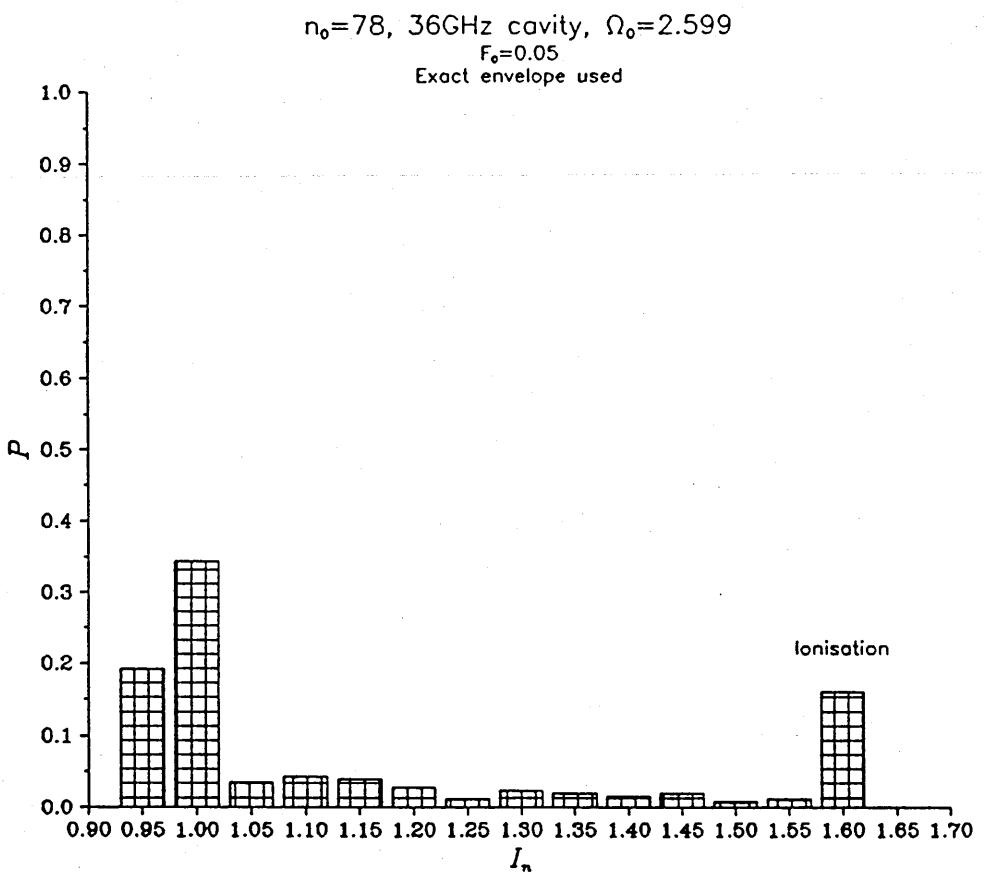
n_0=78, 36GHz cavity, Ω_0=2.599
F_0=0.05
Exact envelope used
1.0
0.9
0.8
0.7
0.6
0.5
0.4
0.3
0.2
0.1
0.0
P_n
Ionisation
0.90 0.95 1.00 1.05 1.10 1.15 1.20 1.25 1.30 1.35 1.40 1.45 1.50 1.55 1.60 1.65 1.70
I_n

Figure 4.16a

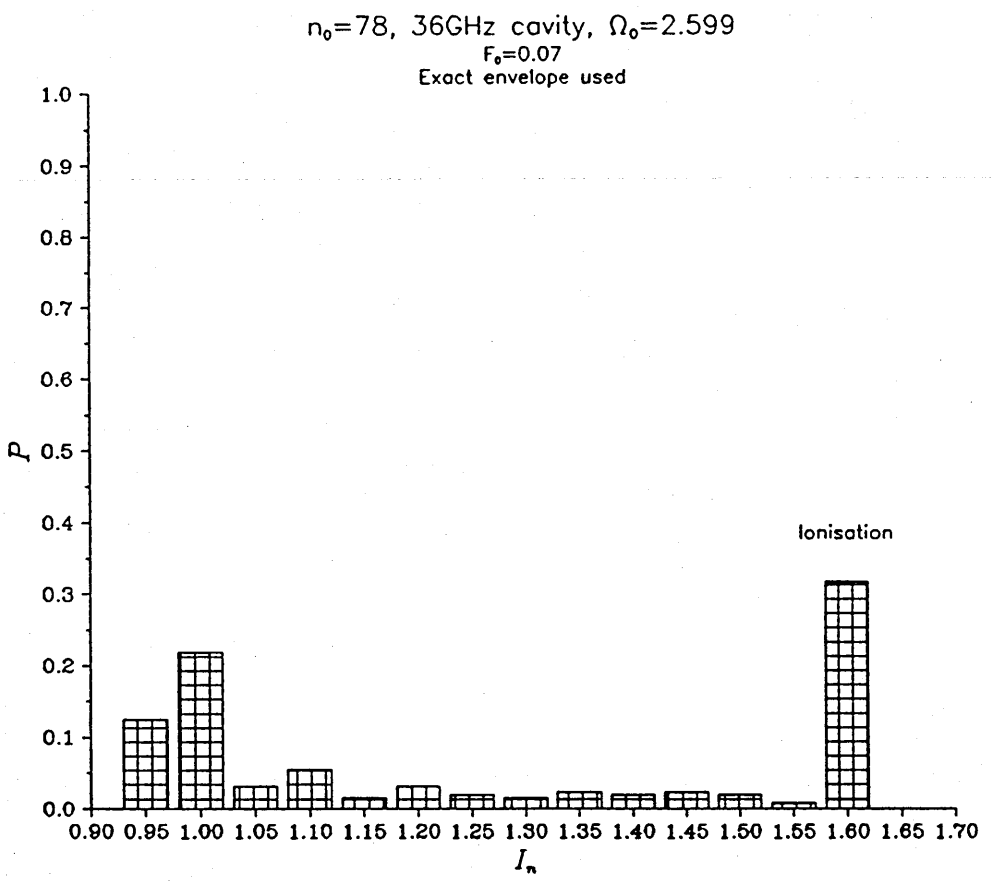
n_0=78, 36GHz cavity, Ω_0=2.599
F_0=0.07
Exact envelope used
1.0
0.9
0.8
0.7
0.6
0.5
0.4
0.3
0.2
0.1
0.0
P_n
Ionisation
0.90 0.95 1.00 1.05 1.10 1.15 1.20 1.25 1.30 1.35 1.40 1.45 1.50 1.55 1.60 1.65 1.70
I_n

Figure 4.16b

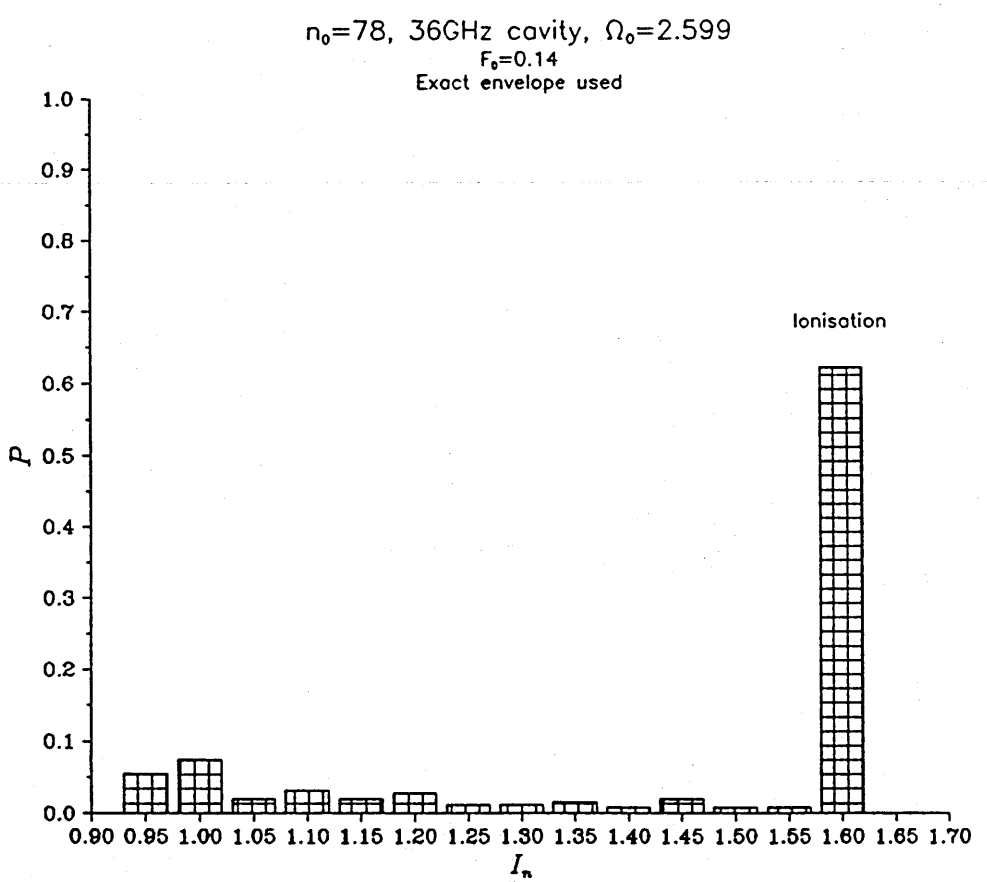
n_0=78, 36GHz cavity, Ω_0=2.599
F_0=0.14
Exact envelope used
Ionisation
P_i
1.0
0.9
0.8
0.7
0.6
0.5
0.4
0.3
0.2
0.1
0.0
0.90 0.95 1.00 1.05 1.10 1.15 1.20 1.25 1.30 1.35 1.40 1.45 1.50 1.55 1.60 1.65 1.70
I_n

Figure 4.16c

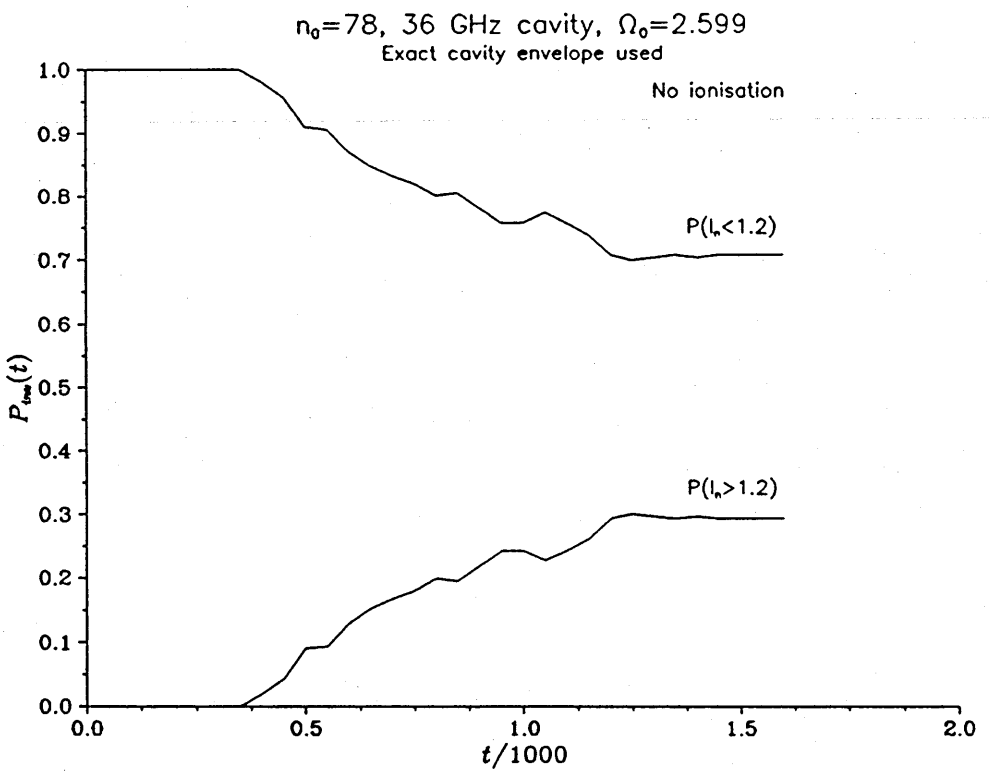
n_0=78, 36 GHz cavity, Ω_0=2.599
Exact cavity envelope used
No ionisation
P(l$_n$<1.2)
P(l$_n$>1.2)
$P_{trans}(t)$
1.0
0.9
0.8
0.7
0.6
0.5
0.4
0.3
0.2
0.1
0.0
0.0
0.5
1.0
1.5
2.0
t/1000

Figure 4.16d

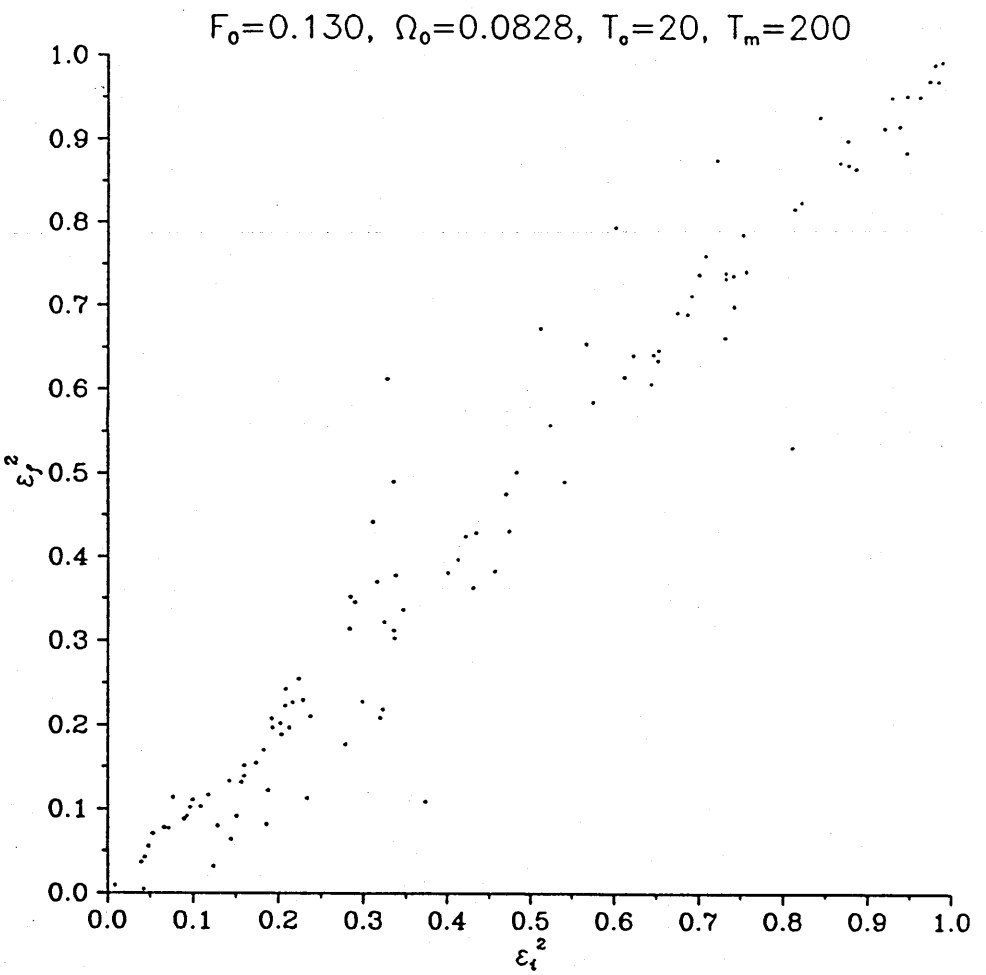
F0=0.130, Ω0=0.0828, T0=20, Tm=200
1.0
0.9
0.8
0.7
0.6
0.5
0.4
0.3
0.2
0.1
0.0
εf2
0.0
0.1
0.2
0.3
0.4
0.5
0.6
0.7
0.8
0.9
1.0
εi2

Figure 4.17

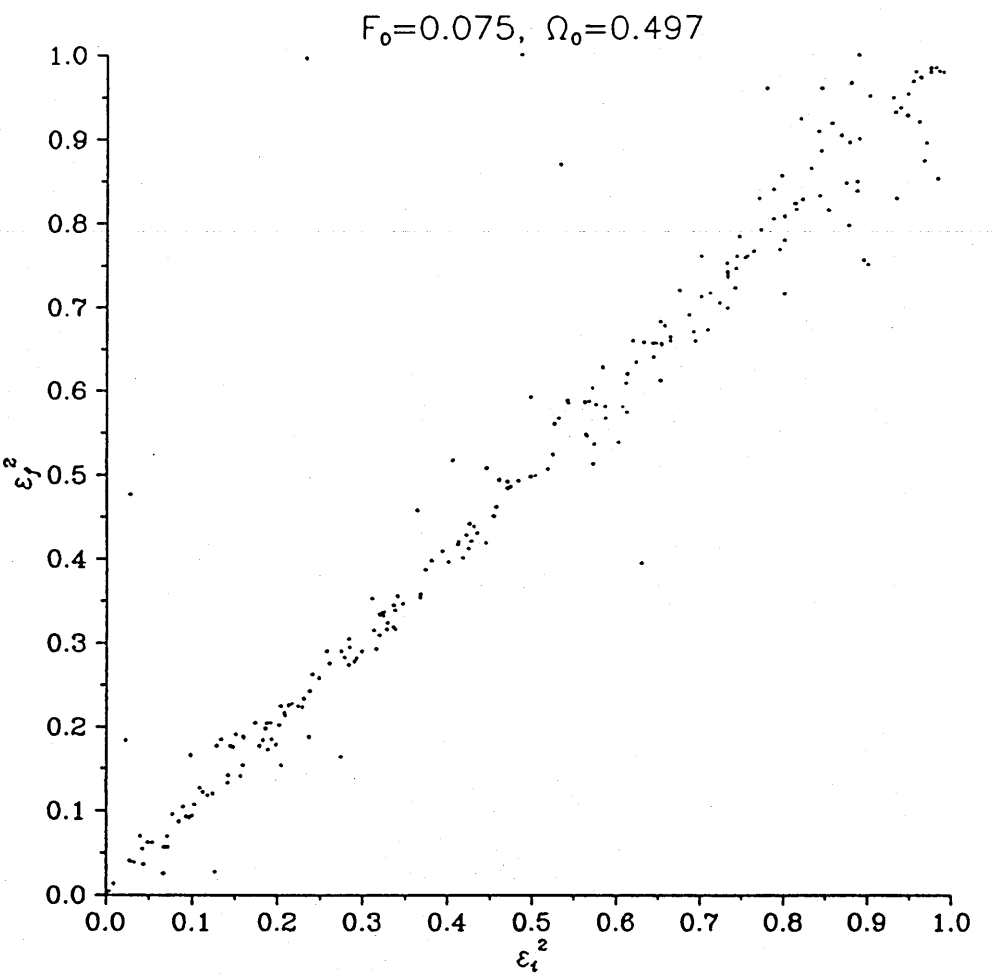
F0=0.075, Ω0=0.497
1.0
0.9
0.8
0.7
0.6
0.5
0.4
0.3
0.2
0.1
0.0
ε_f^2
0.0
0.1
0.2
0.3
0.4
0.5
0.6
0.7
0.8
0.9
1.0
ε_i^2

Figure 4.18a

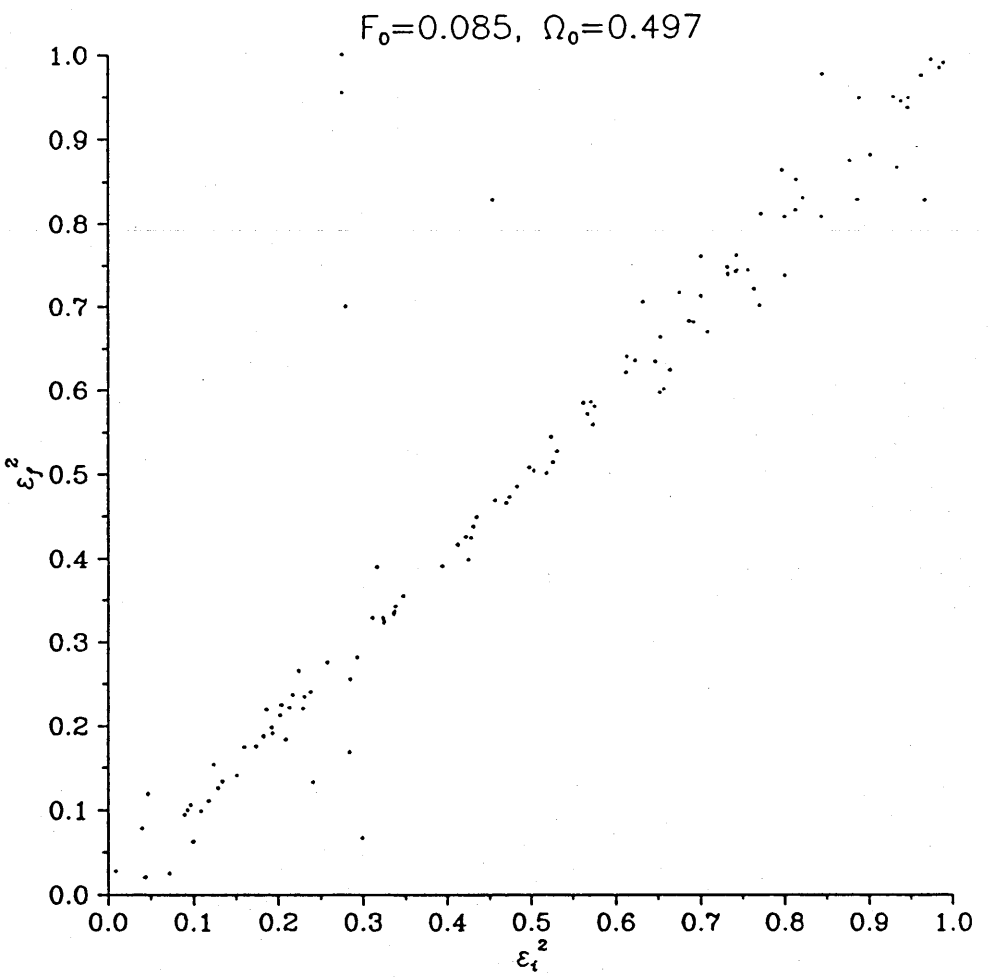
F₀=0.085, Ω₀=0.497
1.0
0.9
0.8
0.7
0.6
0.5
0.4
0.3
0.2
0.1
0.0
ε_f²
0.0
0.1
0.2
0.3
0.4
0.5
0.6
0.7
0.8
0.9
1.0
ε_i²

Figure 4.18b

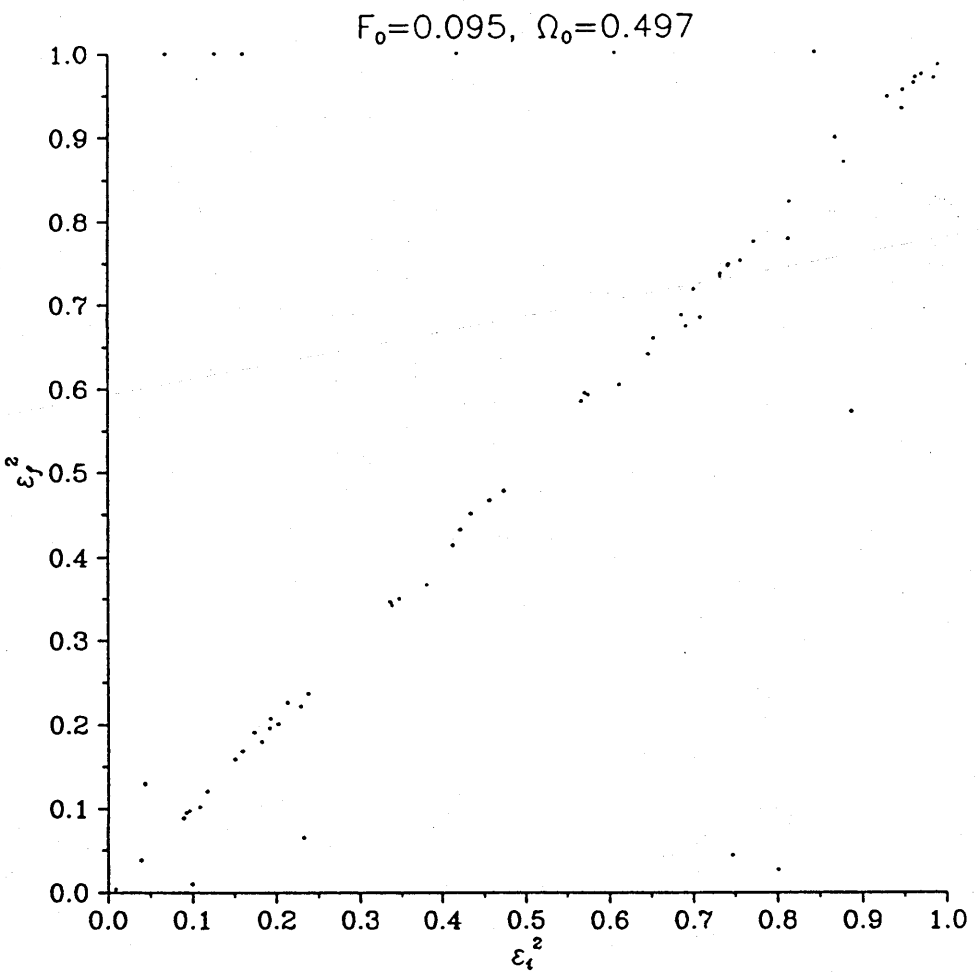
F₀=0.095, Ω₀=0.497
1.0
0.9
0.8
0.7
0.6
0.5
0.4
0.3
0.2
0.1
0.0
ε_f²
0.0
0.1
0.2
0.3
0.4
0.5
0.6
0.7
0.8
0.9
1.0
ε_i²

Figure 4.18c

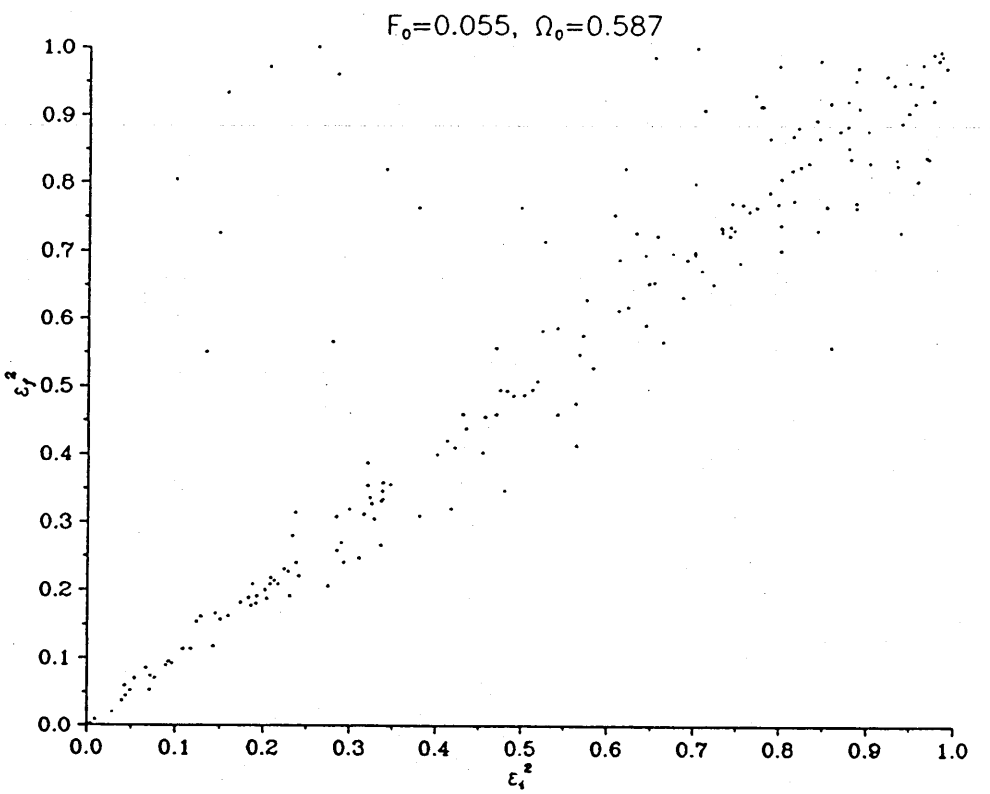
F₀=0.055, Ω₀=0.587
1.0
0.9
0.8
0.7
0.6
0.5
0.4
0.3
0.2
0.1
0.0
0.0
0.1
0.2
0.3
0.4
0.5
0.6
0.7
0.8
0.9
1.0
ε_f²
ε_i²

Figure 4.19a

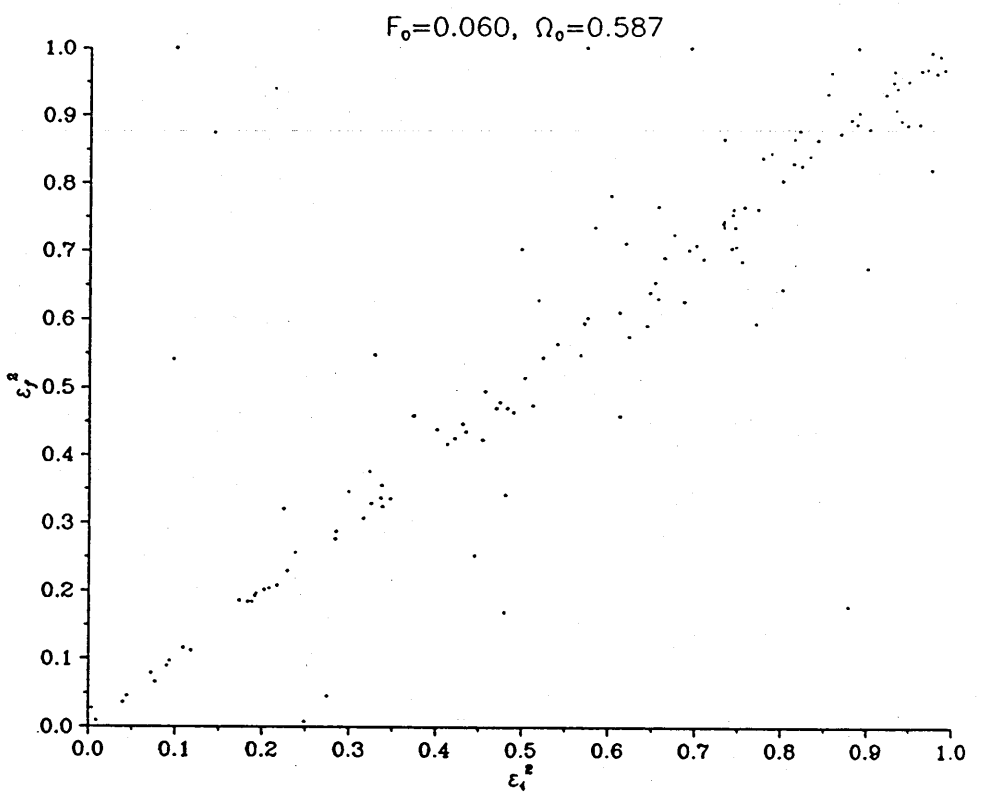
F_0=0.060, Ω_0=0.587
1.0
0.9
0.8
0.7
0.6
0.5
0.4
0.3
0.2
0.1
0.0
0.0
0.1
0.2
0.3
0.4
0.5
0.6
0.7
0.8
0.9
1.0
ε_1^2
ε_4^2

Figure 4.19b

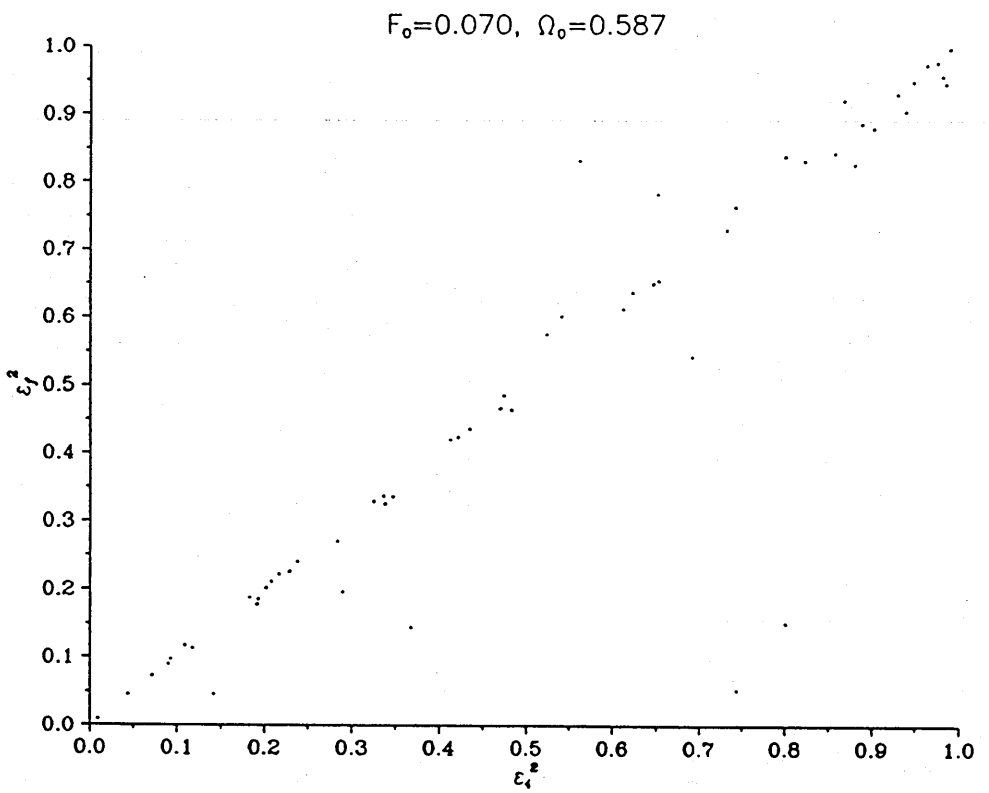
F₀=0.070, Ω₀=0.587
1.0
0.9
0.8
0.7
0.6
0.5
0.4
0.3
0.2
0.1
0.0
0.0
0.1
0.2
0.3
0.4
0.5
0.6
0.7
0.8
0.9
1.0

Figure 4.19c

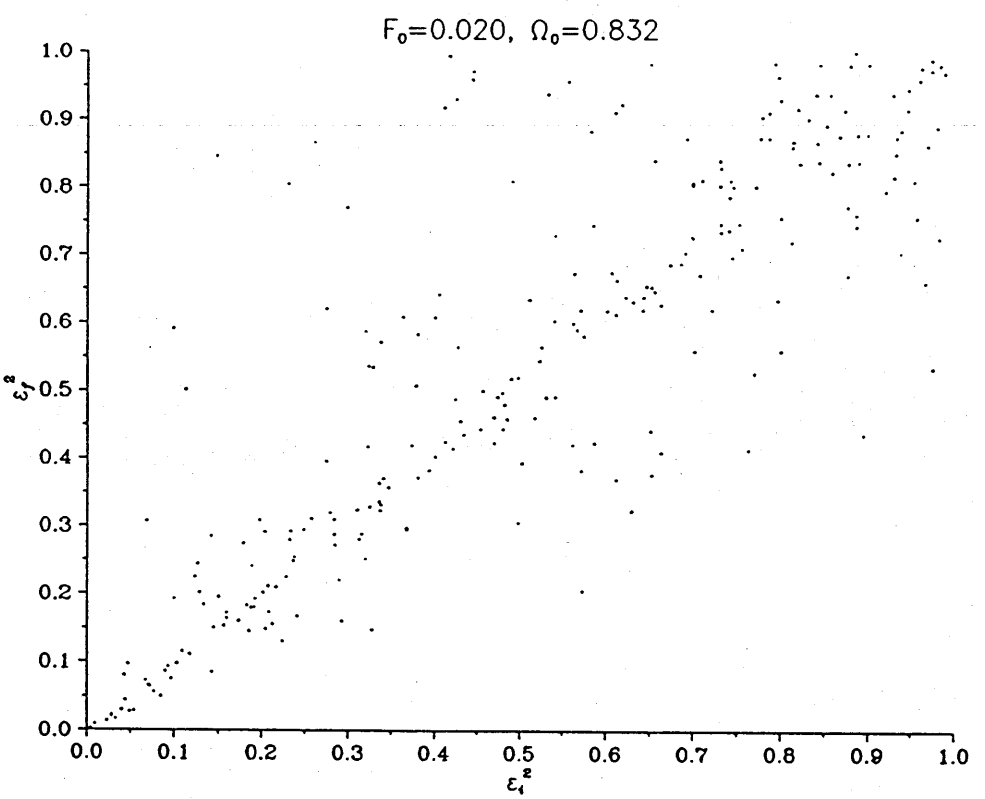
F₀=0.020, Ω₀=0.832
1.0
0.9
0.8
0.7
0.6
0.5
0.4
0.3
0.2
0.1
0.0
0.0
0.1
0.2
0.3
0.4
0.5
0.6
0.7
0.8
0.9
1.0
ε₁²
ε₁²

Figure 4.20a

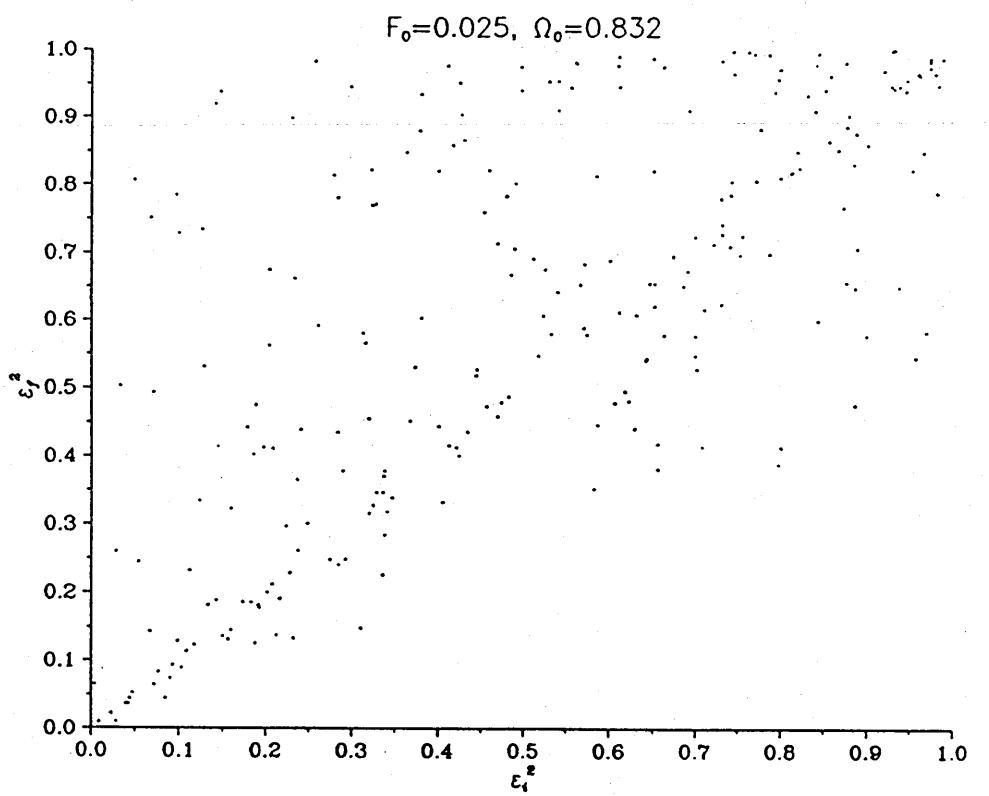
F₀=0.025, Ω₀=0.832
1.0
0.9
0.8
0.7
0.6
0.5
0.4
0.3
0.2
0.1
0.0
0.0
0.1
0.2
0.3
0.4
0.5
0.6
0.7
0.8
0.9
1.0
ε_f²
ε_i²

Figure 4.20b

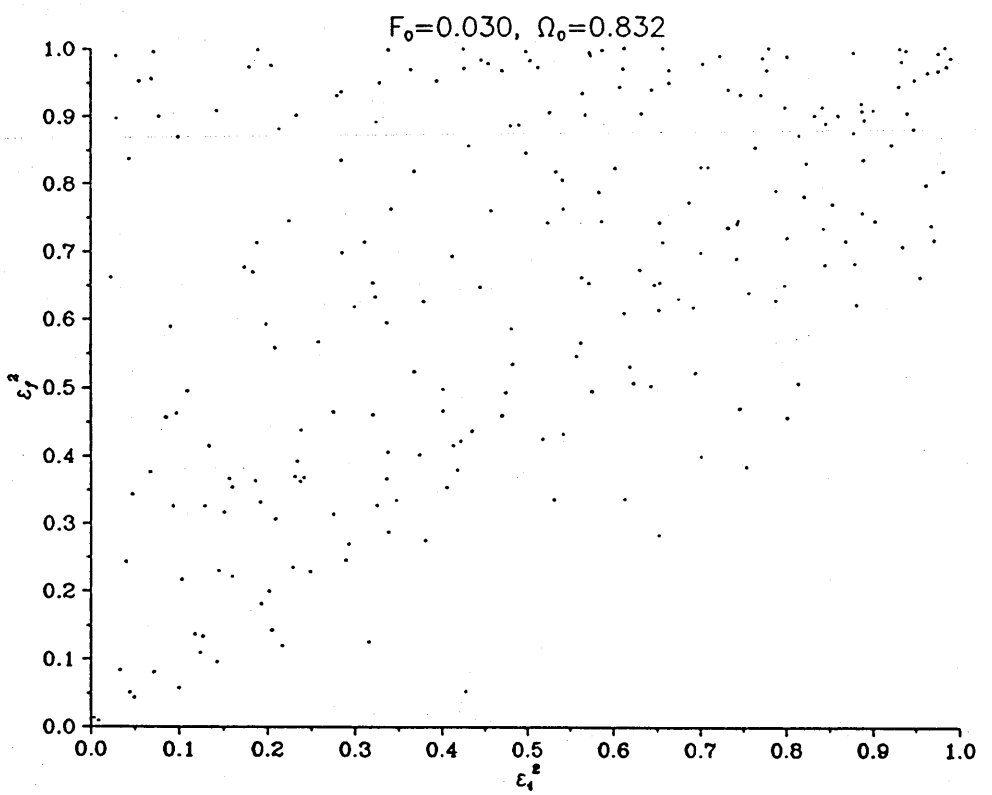
F₀=0.030, Ω₀=0.832
1.0
0.9
0.8
0.7
0.6
0.5
0.4
0.3
0.2
0.1
0.0
0.0
0.1
0.2
0.3
0.4
0.5
0.6
0.7
0.8
0.9
1.0
ε_f²
ε_i²

Figure 4.20c

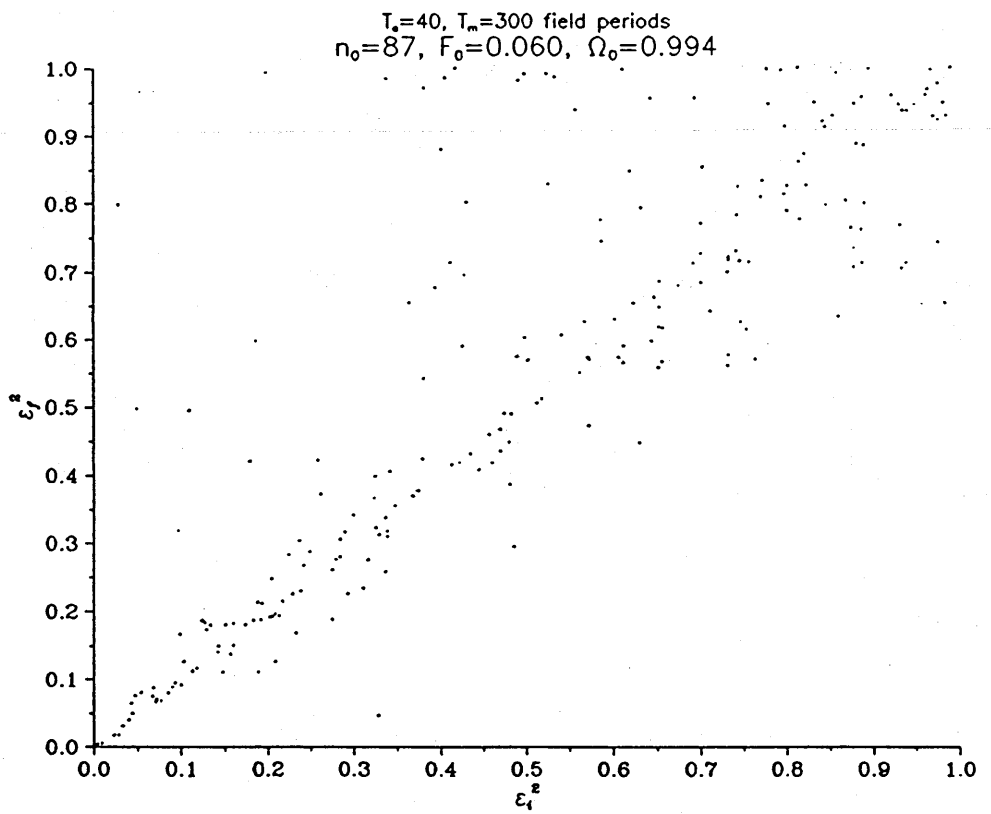
T_e=40, T_m=300 field periods
n_0=87, F_0=0.060, Ω_0=0.994
1.0
0.9
0.8
0.7
0.6
0.5
0.4
0.3
0.2
0.1
0.0
ε_f^2
0.0
0.1
0.2
0.3
0.4
0.5
0.6
0.7
0.8
0.9
1.0
ε_i^2

Figure 4.21a

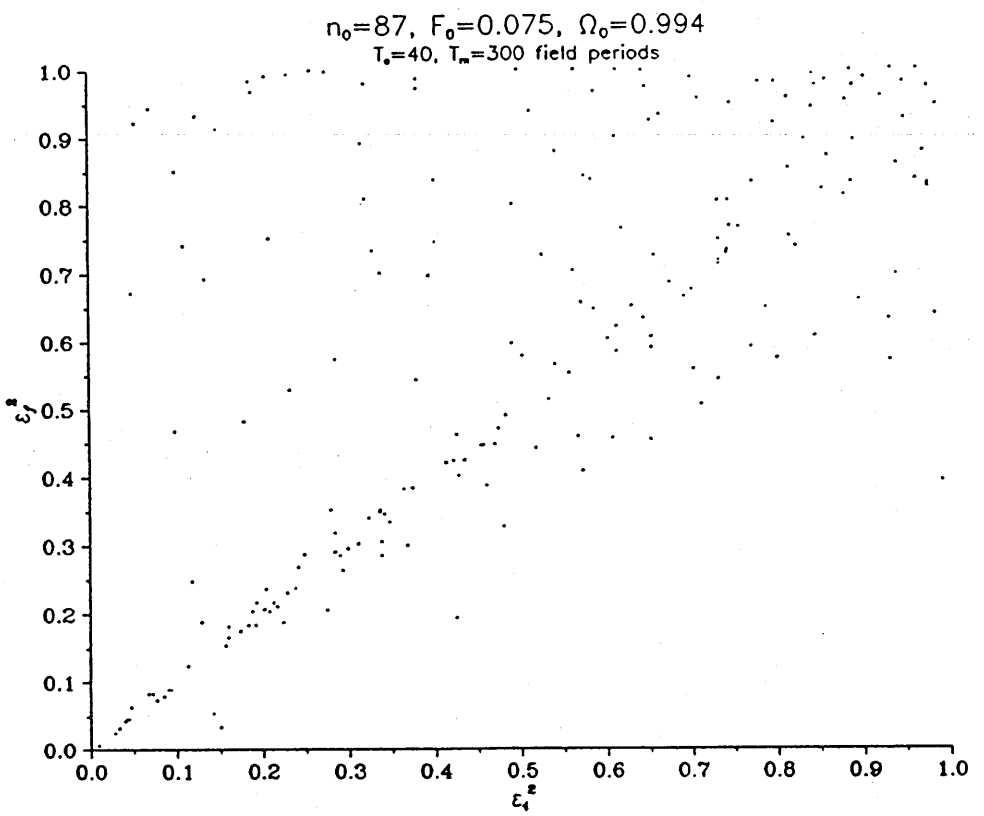
n_0=87, F_0=0.075, Ω_0=0.994
T_e=40, T_m=300 field periods
1.0
0.9
0.8
0.7
0.6
0.5
0.4
0.3
0.2
0.1
0.0
0.0
0.1
0.2
0.3
0.4
0.5
0.6
0.7
0.8
0.9
1.0
ε_1^2
ε_1^2

Figure 4.21b

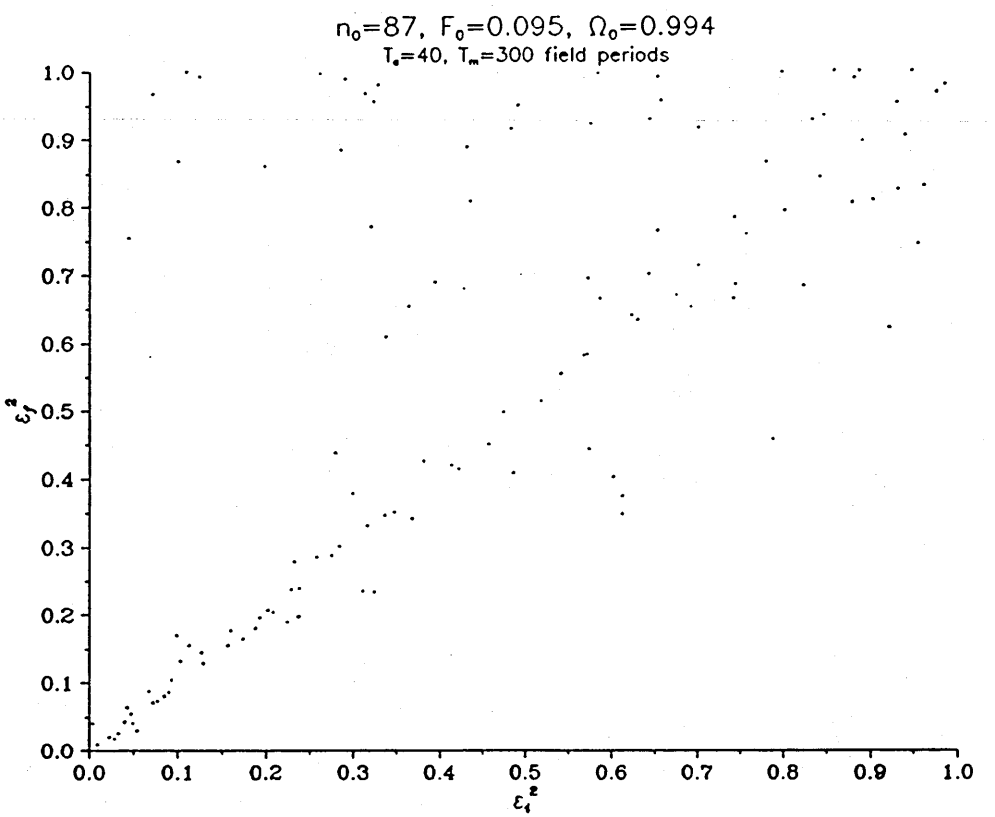
n_0=87, F_0=0.095, Ω_0=0.994
T_e=40, T_m=300 field periods
1.0
0.9
0.8
0.7
0.6
0.5
0.4
0.3
0.2
0.1
0.0
ε_y^2
0.0
0.1
0.2
0.3
0.4
0.5
0.6
0.7
0.8
0.9
1.0
ε_i^2

Figure 4.21c

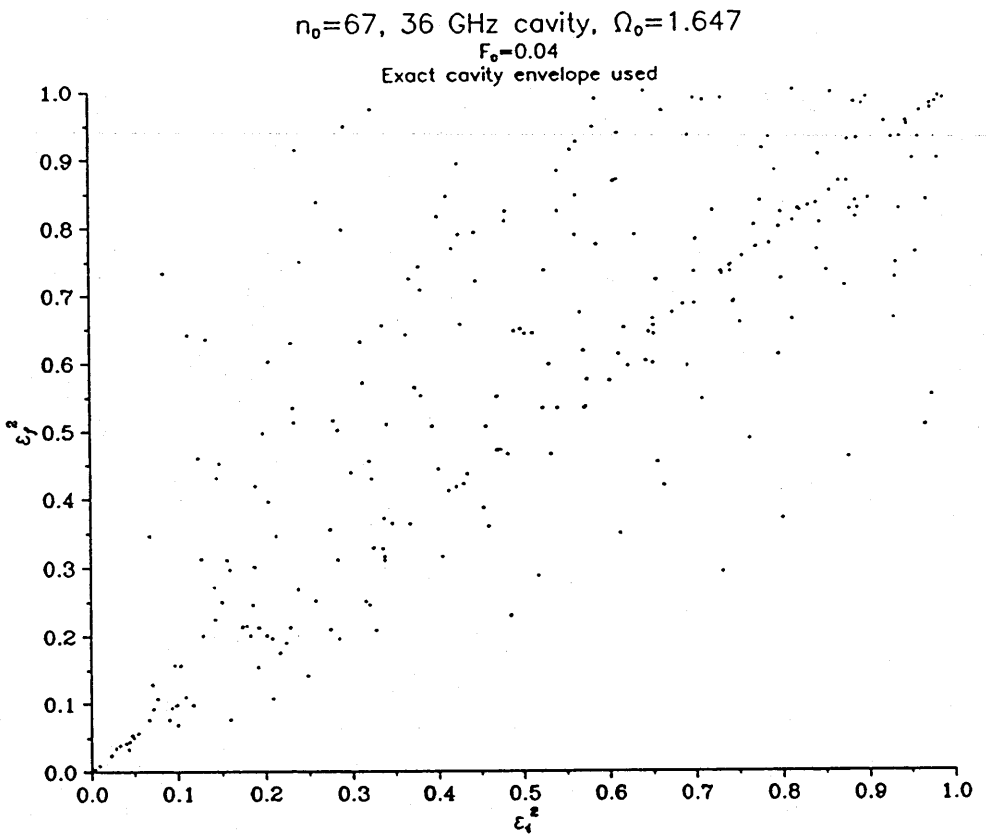
n₀=67, 36 GHz cavity, Ω₀=1.647
F₀=0.04
Exact cavity envelope used
1.0
0.9
0.8
0.7
0.6
0.5
0.4
0.3
0.2
0.1
0.0
ε_f²
0.0
0.1
0.2
0.3
0.4
0.5
0.6
0.7
0.8
0.9
1.0
ε_i²

Figure 4.22a

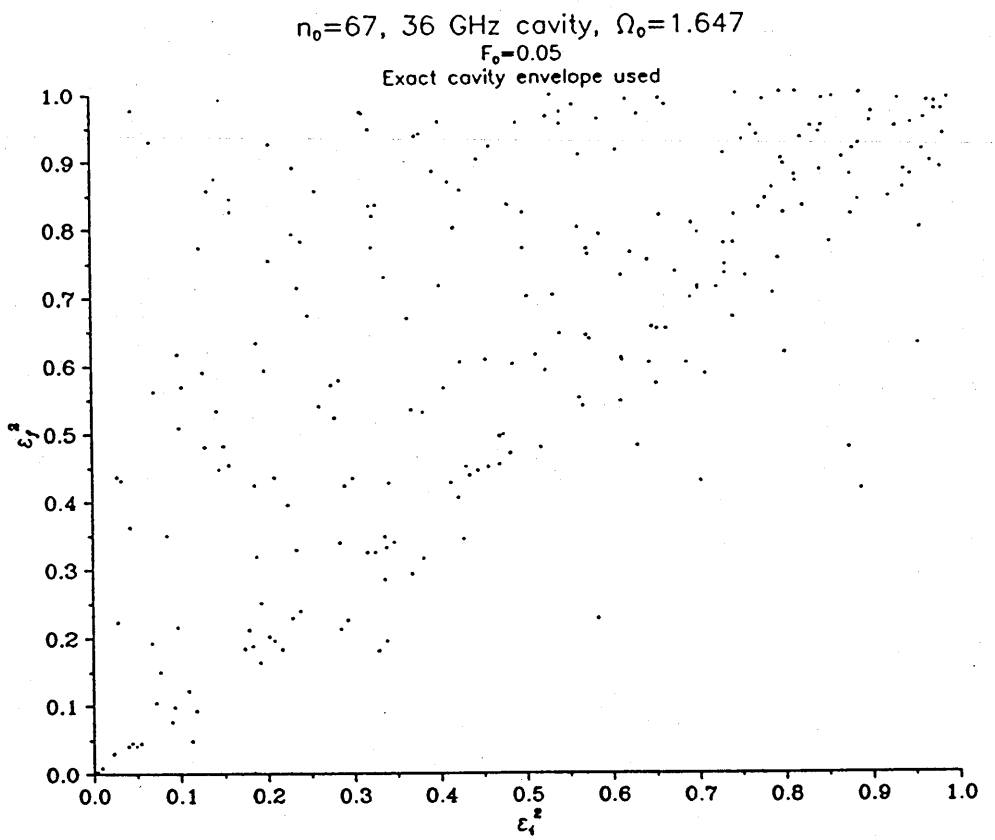
n_0=67, 36 GHz cavity, Ω_0=1.647
F_0=0.05
Exact cavity envelope used
1.0
0.9
0.8
0.7
0.6
0.5
0.4
0.3
0.2
0.1
0.0
ε_f^2
0.0
0.1
0.2
0.3
0.4
0.5
0.6
0.7
0.8
0.9
1.0
ε_i^2

Figure 4.22b

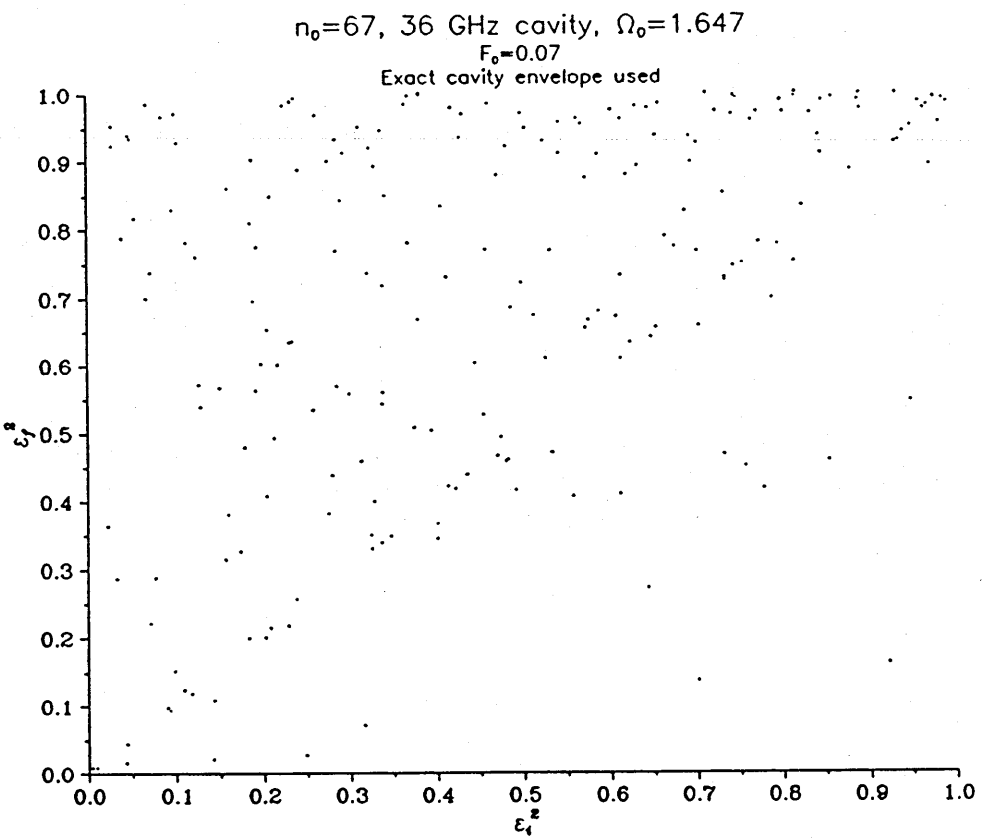
n_0=67, 36 GHz cavity, Ω_0=1.647
F_0=0.07
Exact cavity envelope used
1.0
0.9
0.8
0.7
0.6
0.5
0.4
0.3
0.2
0.1
0.0
ε_2^2
0.0
0.1
0.2
0.3
0.4
0.5
0.6
0.7
0.8
0.9
1.0
ε_1^2

Figure 4.22c

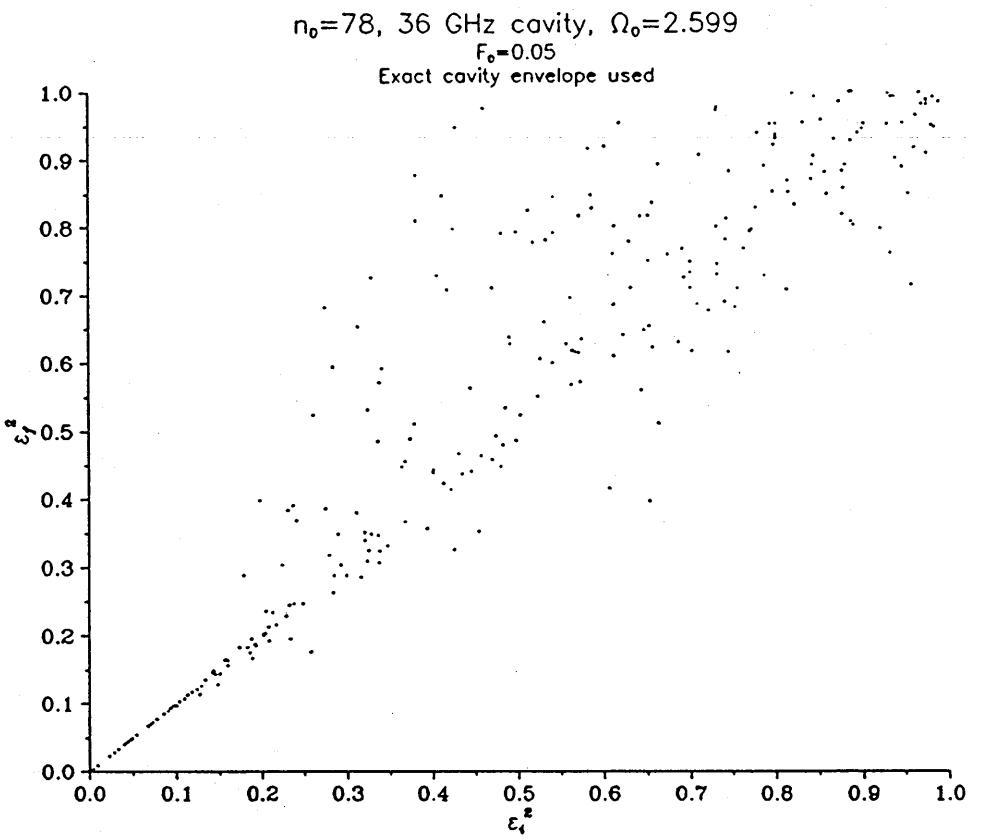
n_0=78, 36 GHz cavity, Ω_0=2.599
F_0=0.05
Exact cavity envelope used
1.0
0.9
0.8
0.7
0.6
0.5
0.4
0.3
0.2
0.1
0.0
ε_f^2
0.0
0.1
0.2
0.3
0.4
0.5
0.6
0.7
0.8
0.9
1.0
ε_i^2

Figure 4.23a

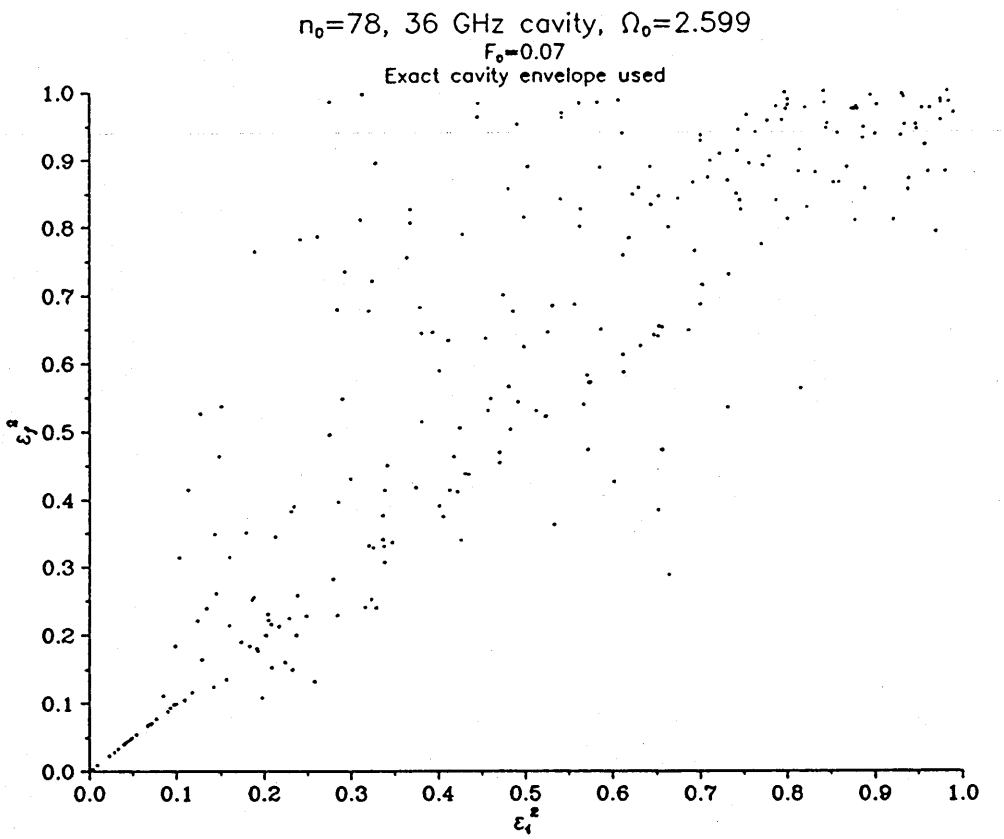
n₀=78, 36 GHz cavity, Ω₀=2.599
F₀=0.07
Exact cavity envelope used
1.0
0.9
0.8
0.7
0.6
0.5
0.4
0.3
0.2
0.1
0.0
0.0
0.1
0.2
0.3
0.4
0.5
0.6
0.7
0.8
0.9
1.0
ε₁²
ε₁²

Figure 4.23b

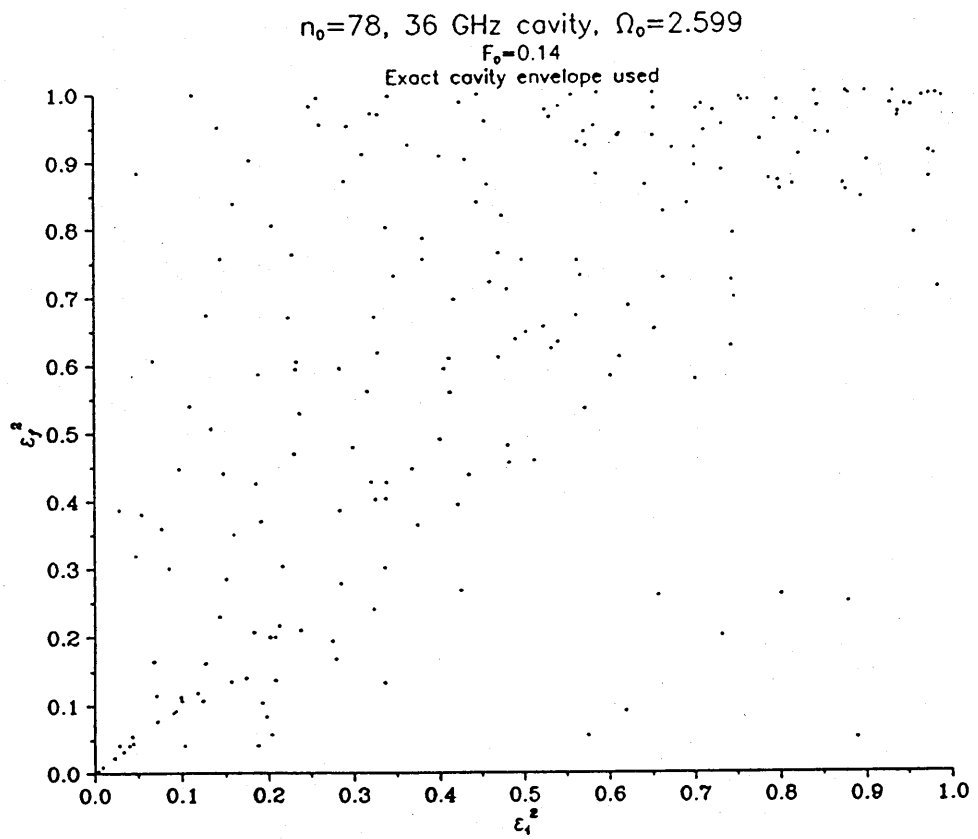
n_0=78, 36 GHz cavity, Ω_0=2.599
F_0=0.14
Exact cavity envelope used
1.0
0.9
0.8
0.7
0.6
0.5
0.4
0.3
0.2
0.1
0.0
ε_f^2
0.0
0.1
0.2
0.3
0.4
0.5
0.6
0.7
0.8
0.9
1.0
ε_i^2

Figure 4.23c

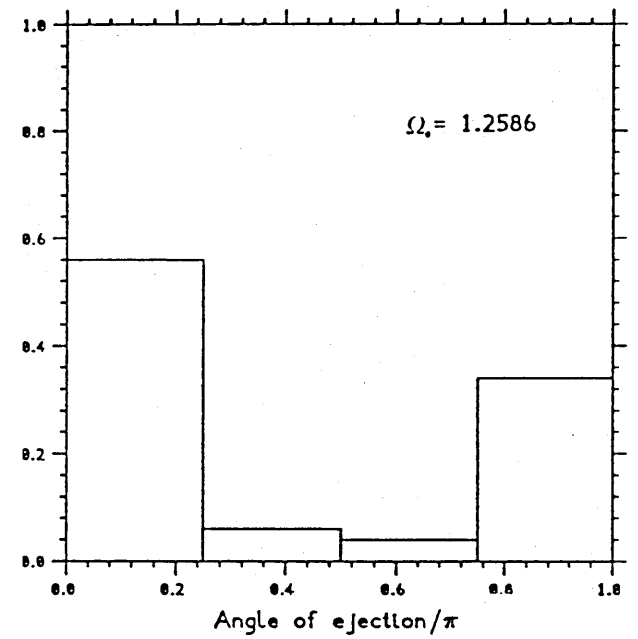
Ω_e= 1.2586
Angle of ejection/π

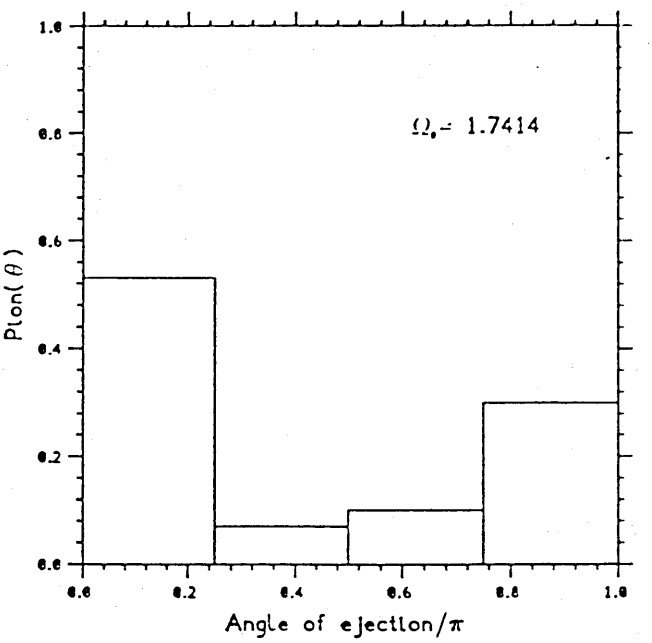
Ω_e= 1.7414
Pion(θ)
Angle of ejection/π

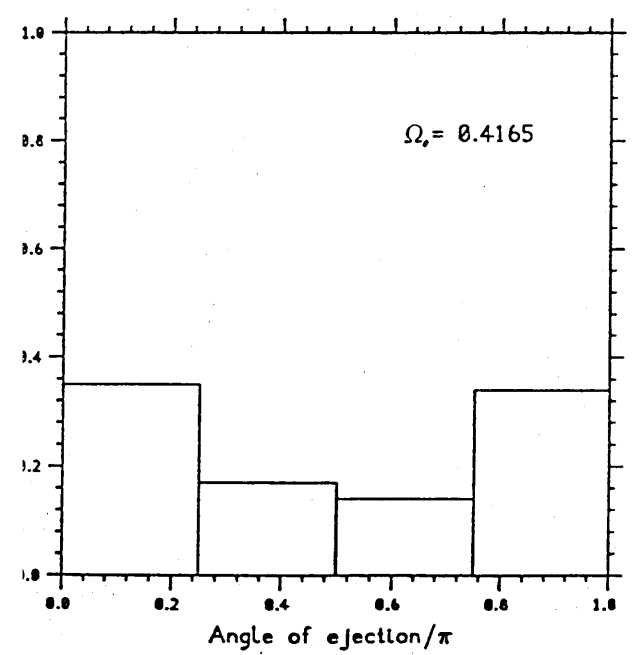
Ω_e= 0.4165
Angle of ejection/π

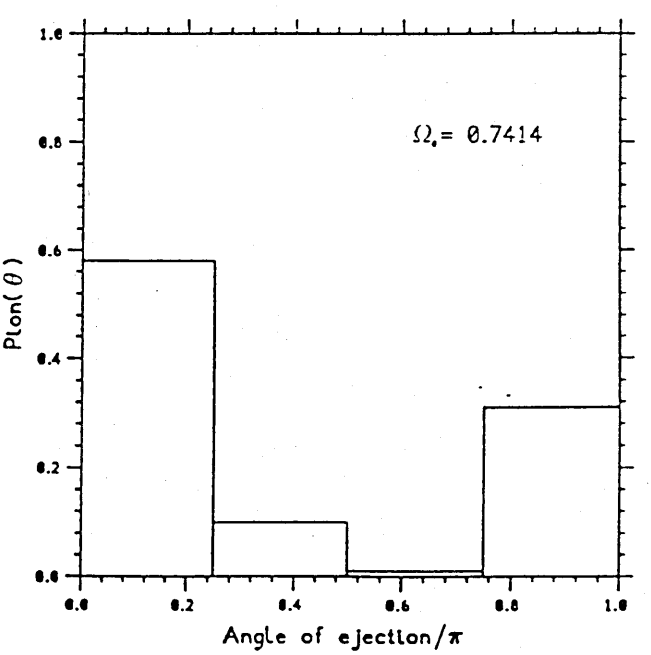
Ω_e= 0.7414
Pion(θ)
Angle of ejection/π

Figure 4.24a

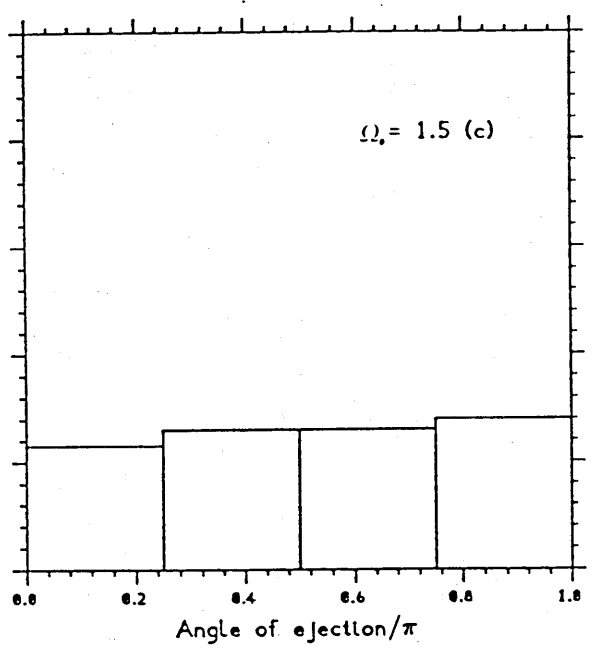
Ω_0= 1.5 (c)
0.0
0.2
0.4
0.6
0.8
1.0
Angle of ejection/π

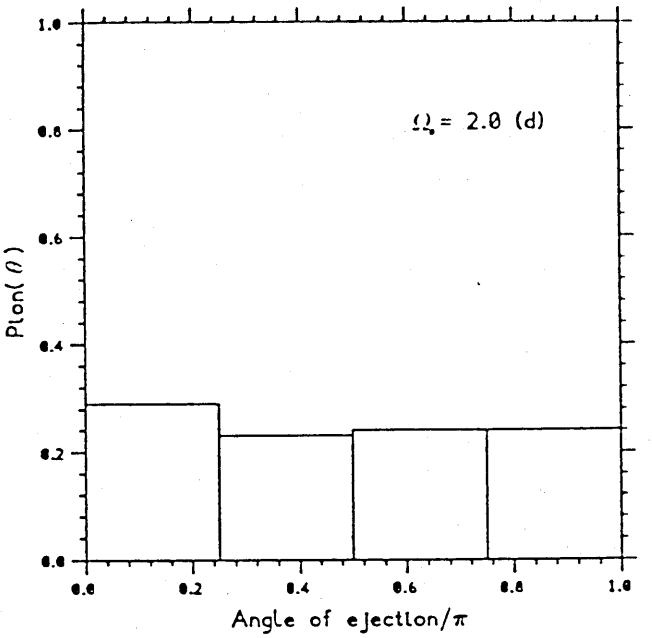
Ω_0= 2.0 (d)
Pion(θ)
0.0
0.2
0.4
0.6
0.8
1.0
Angle of ejection/π

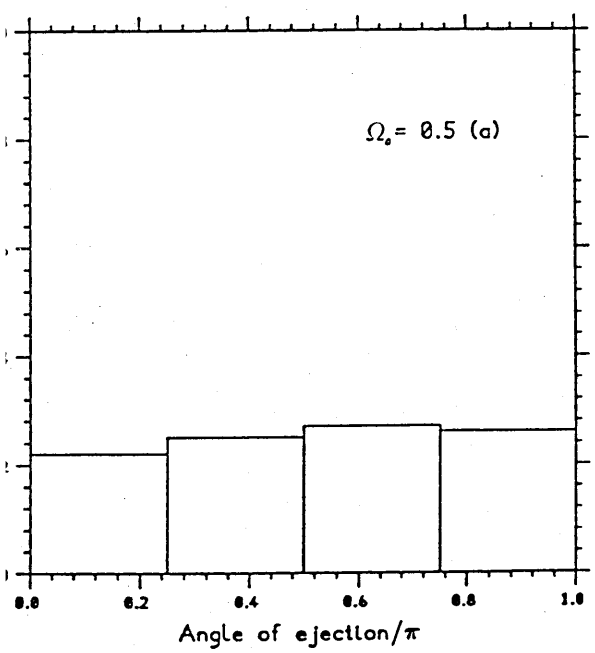
Ω_0= 0.5 (a)
0.0
0.2
0.4
0.6
0.8
1.0
Angle of ejection/π

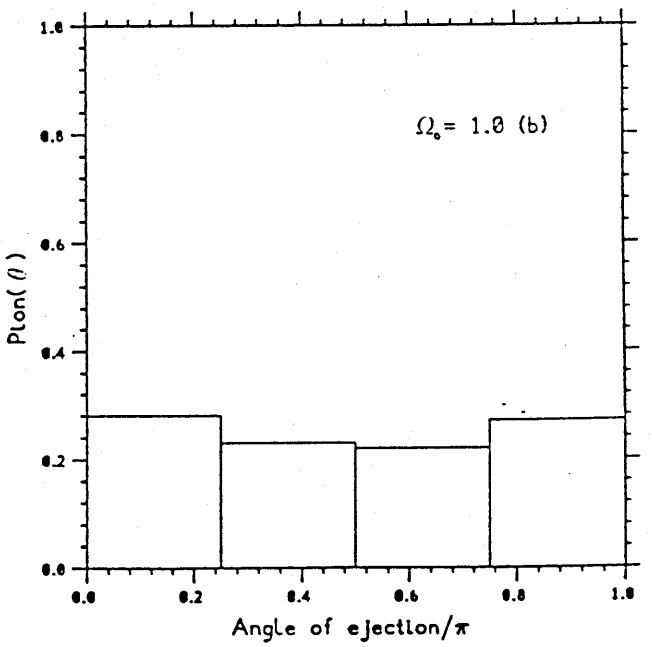
Ω_0= 1.0 (b)
Pion(θ)
0.0
0.2
0.4
0.6
0.8
1.0
Angle of ejection/π

Figure 4.24b

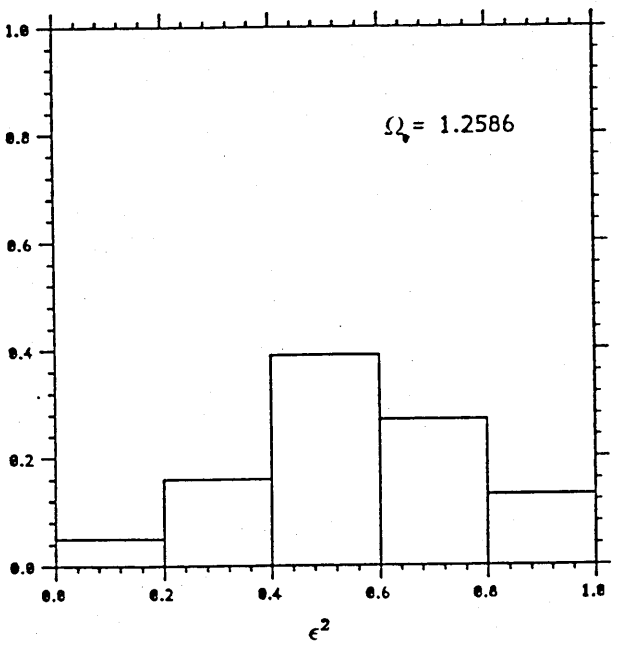
Ω_0= 1.2586
ϵ^2

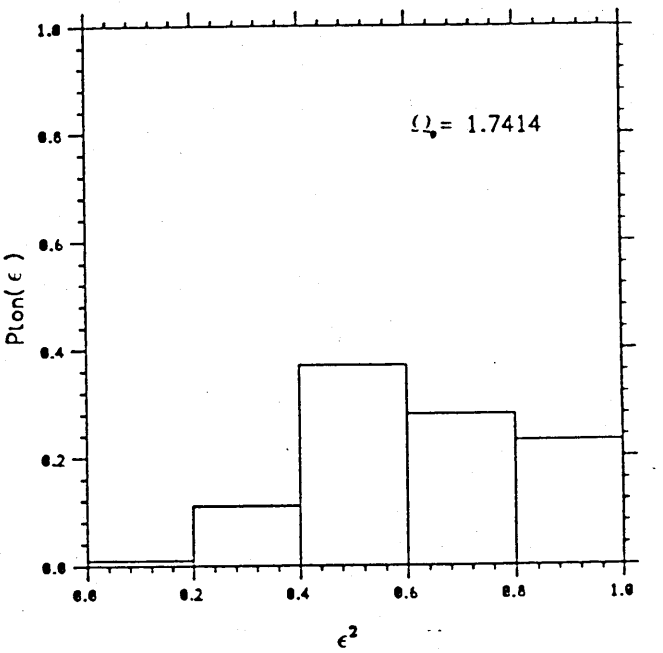
Ω_0= 1.7414
Plon(ϵ)
ϵ^2

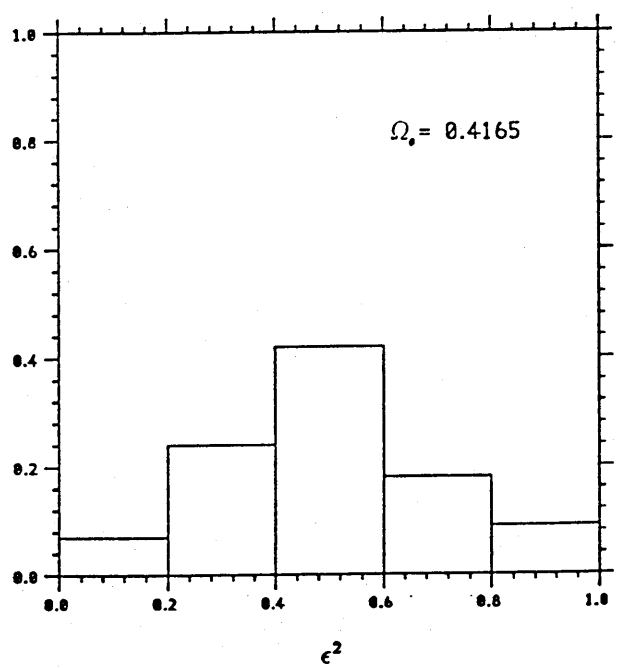
Ω_0= 0.4165
ϵ^2

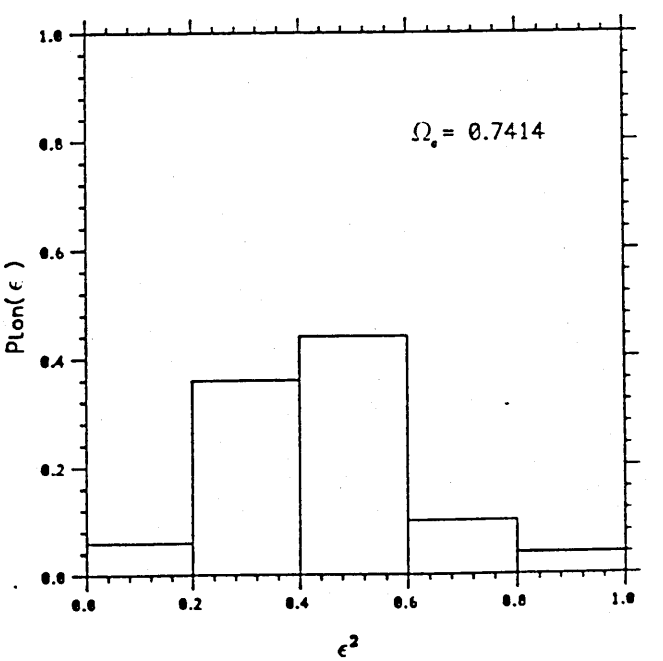
Ω_0= 0.7414
Plon(ϵ)
ϵ^2

Figure 4.25a

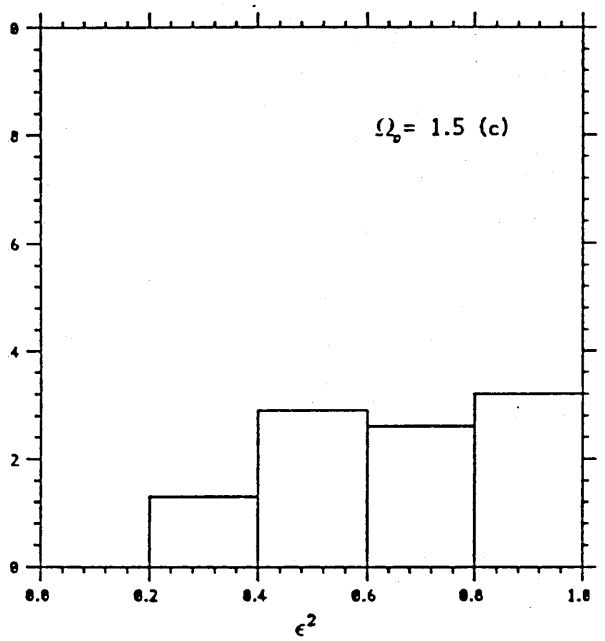
Ω_0= 1.5 (c)
ϵ^2

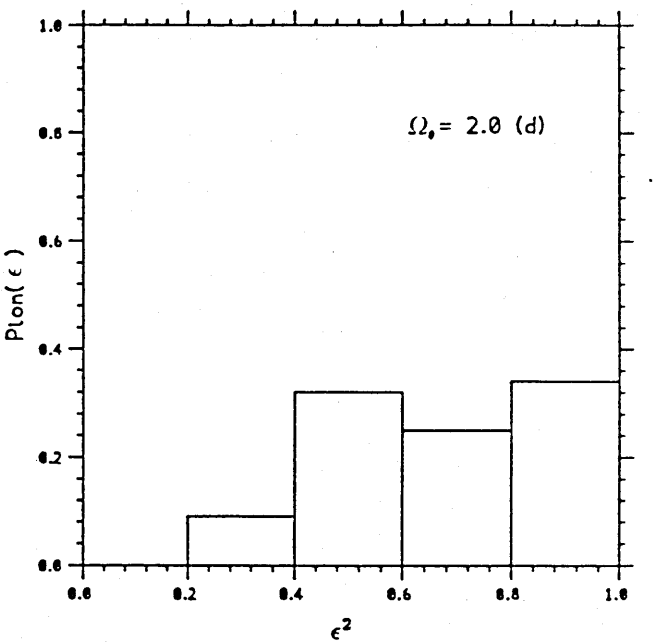
Ω_0= 2.0 (d)
Plon(ϵ)
ϵ^2

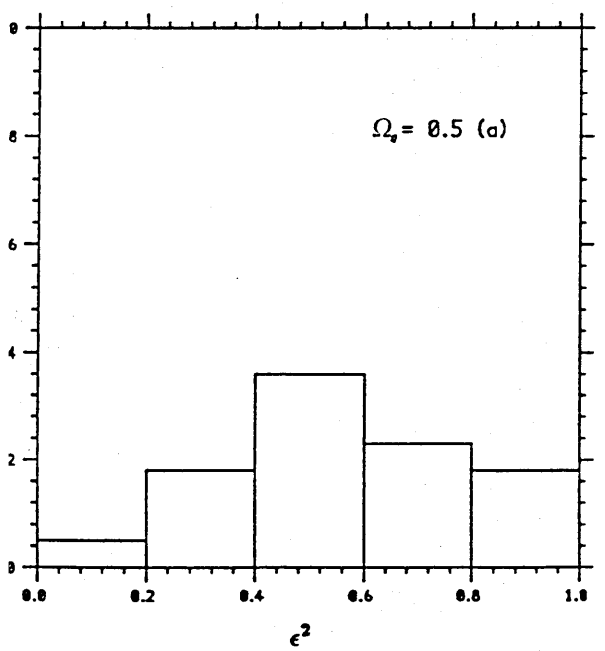
Ω_0= 0.5 (a)
ϵ^2

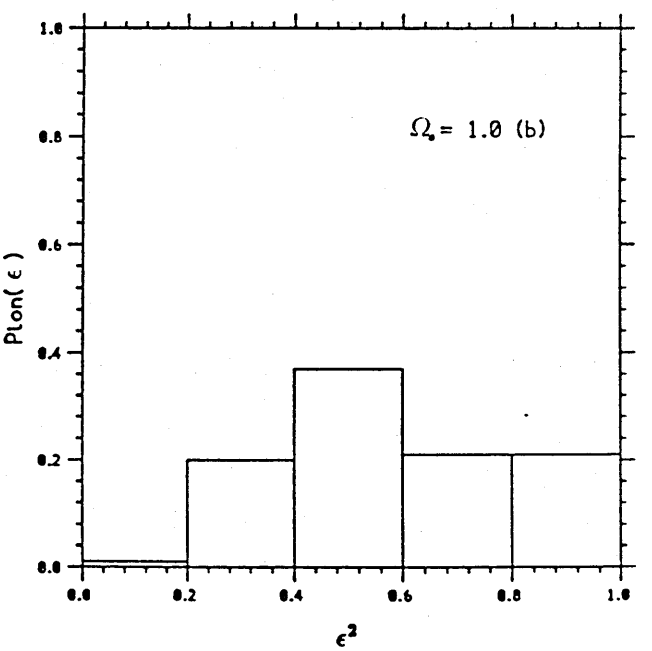
Ω_0= 1.0 (b)
Plon(ϵ)
ϵ^2

Figure 4.25b

$\Omega_0 = 0.7414$

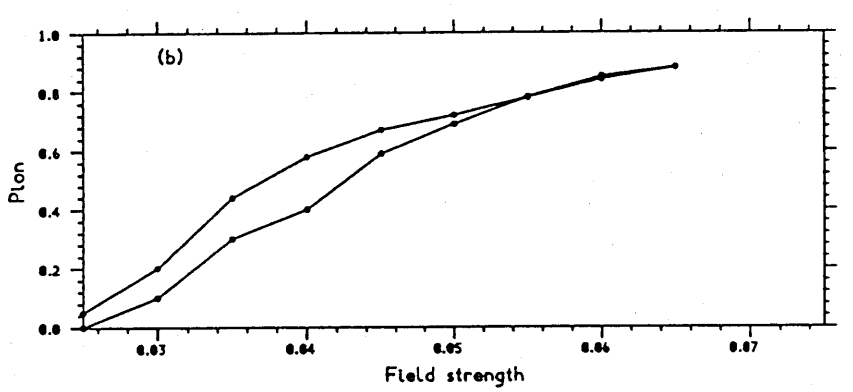

$\Omega_0 = 0.5$

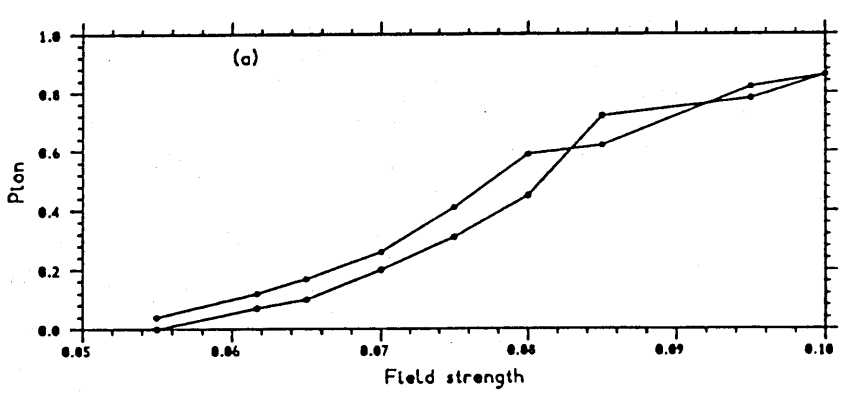

Figure 4.26

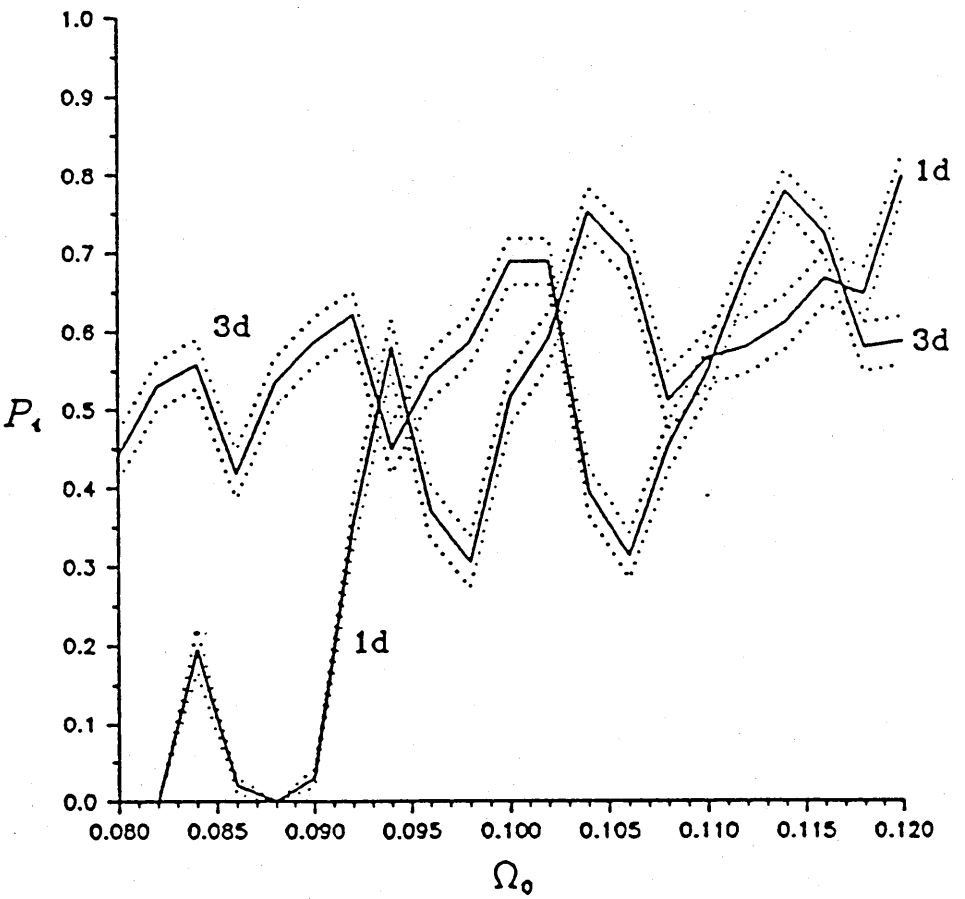
1.0
0.9
0.8
0.7
0.6
0.5
0.4
0.3
0.2
0.1
0.0
P_1
0.080
0.085
0.090
0.095
0.100
0.105
0.110
0.115
0.120
Ω_0
1d
3d
3d
1d

Figure 4.27

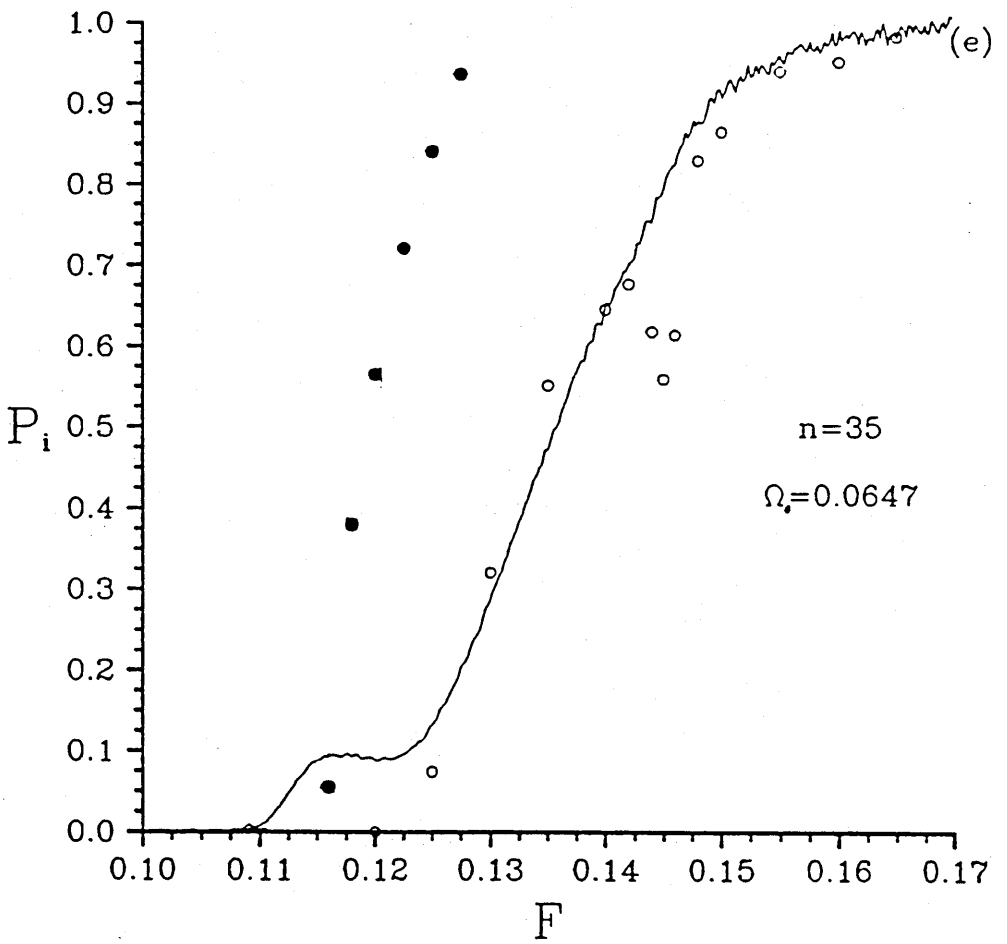
1.0
0.9
0.8
0.7
0.6
0.5
0.4
0.3
0.2
0.1
0.0
P_i
0.10
0.11
0.12
0.13
0.14
0.15
0.16
0.17
F
(e)
n=35
Ω_s=0.0647

Figure 4.28

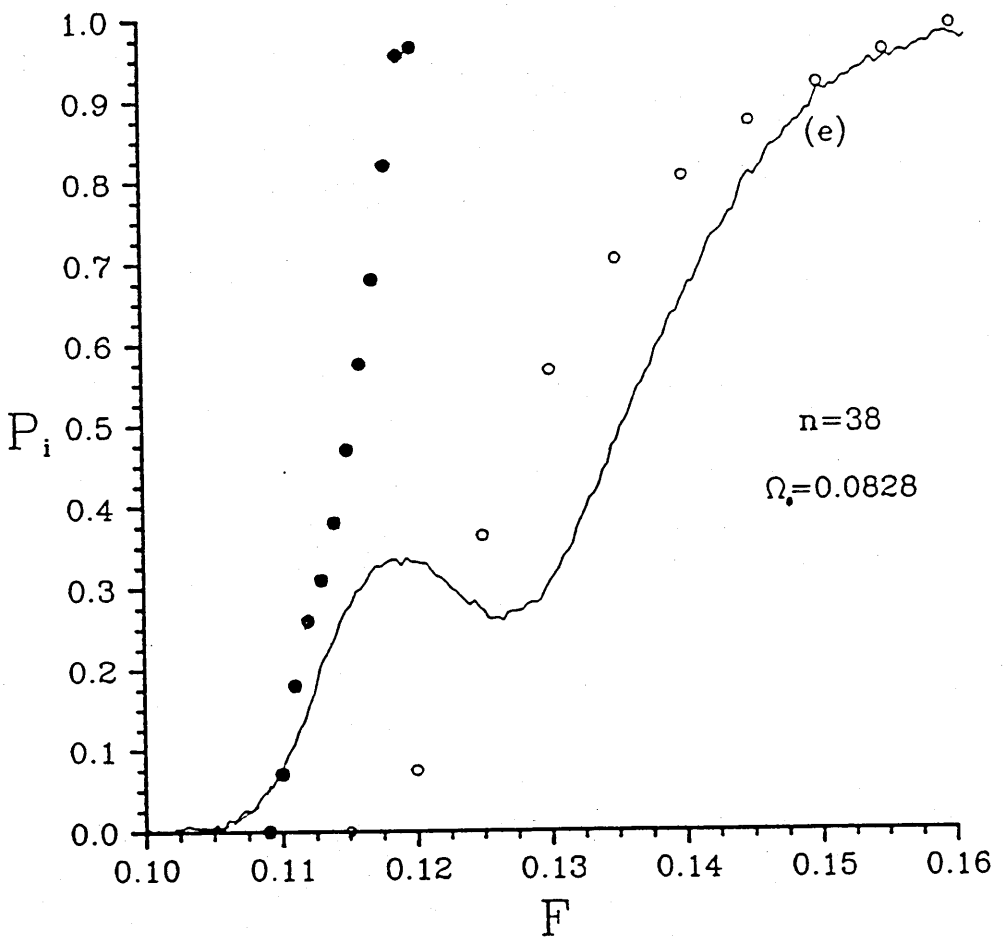
1.0
0.9
0.8
0.7
0.6
0.5
0.4
0.3
0.2
0.1
0.0
P_i
0.10
0.11
0.12
0.13
0.14
0.15
0.16
F
(e)
n=38
Ω_s=0.0828

Figure 4.29

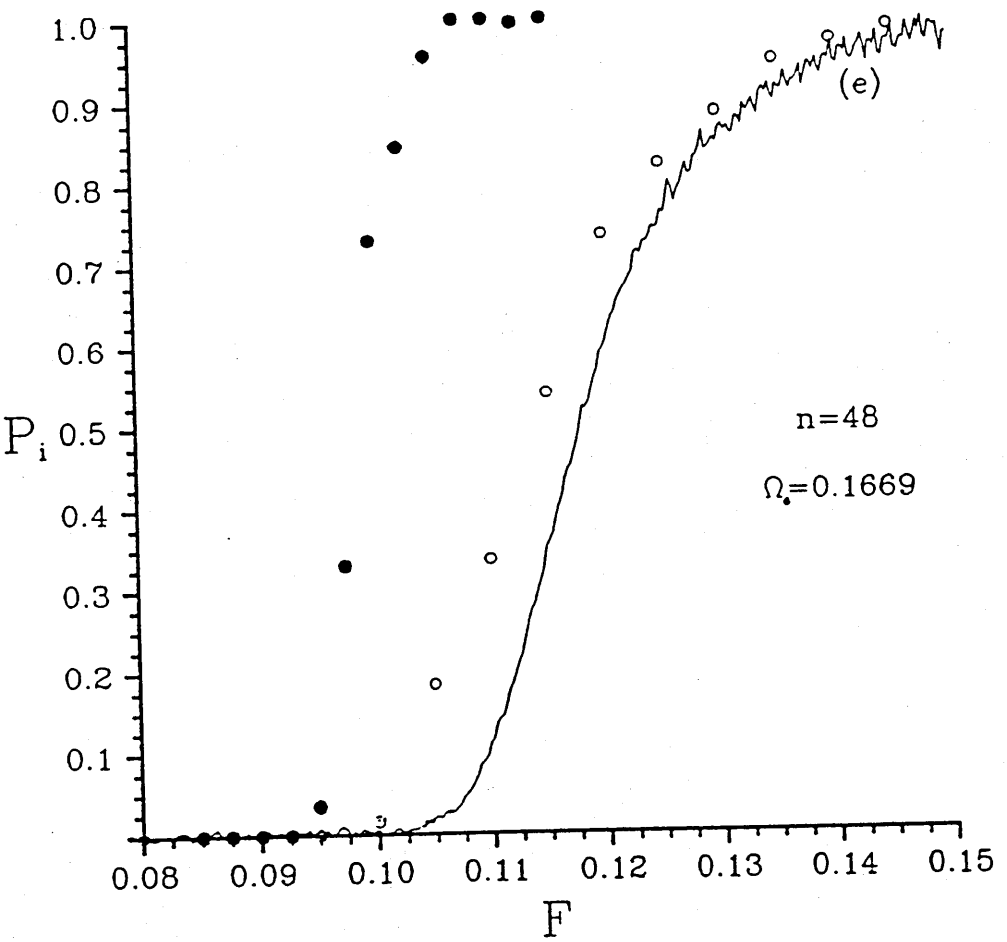
1.0
0.9
0.8
0.7
0.6
0.5
0.4
0.3
0.2
0.1
P_i
0.08
0.09
0.10
0.11
0.12
0.13
0.14
0.15
F
(e)
n=48
Ω_0=0.1669

Figure 4.30

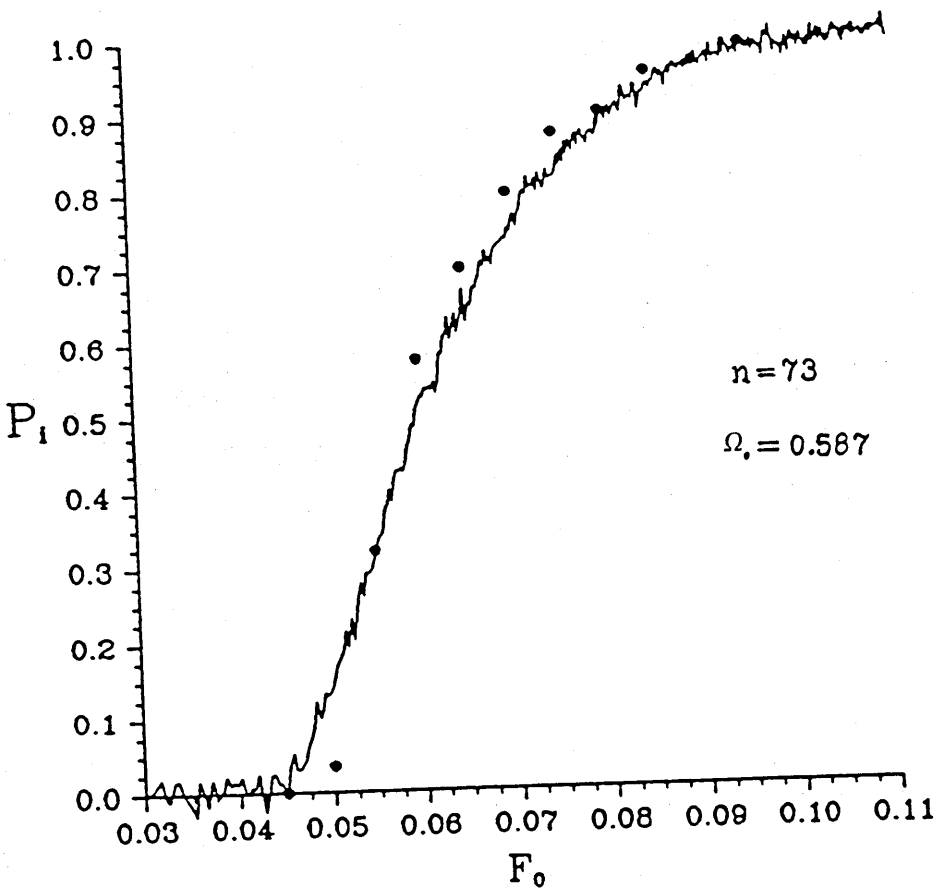
1.0
0.9
0.8
0.7
0.6
0.5
0.4
0.3
0.2
0.1
0.0
P_1
0.03
0.04
0.05
0.06
0.07
0.08
0.09
0.10
0.11
F_0
n=73
$\Omega_* = 0.587$

Figure 4.31

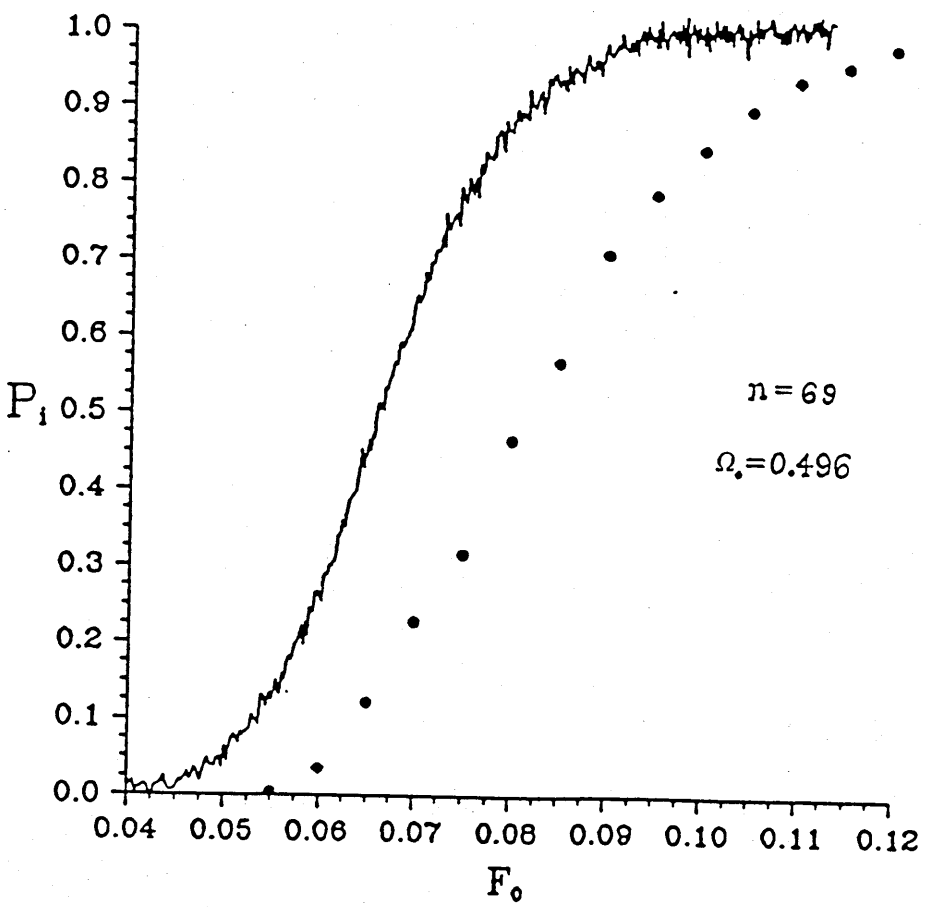
1.0
0.9
0.8
0.7
0.6
0.5
0.4
0.3
0.2
0.1
0.0
P_i
0.04
0.05
0.06
0.07
0.08
0.09
0.10
0.11
0.12
F_0
n = 69
$\Omega_* = 0.496$

Figure 4.32

$F_1 + F_2 = .07$

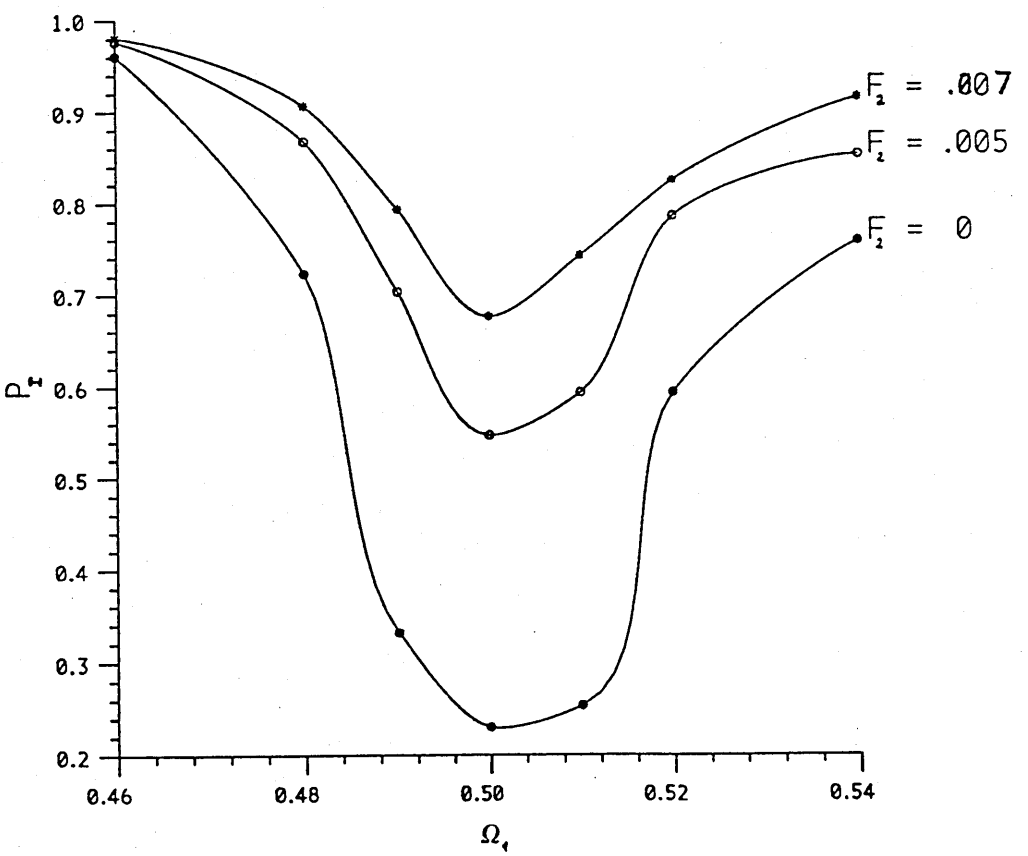

Figure 4.33

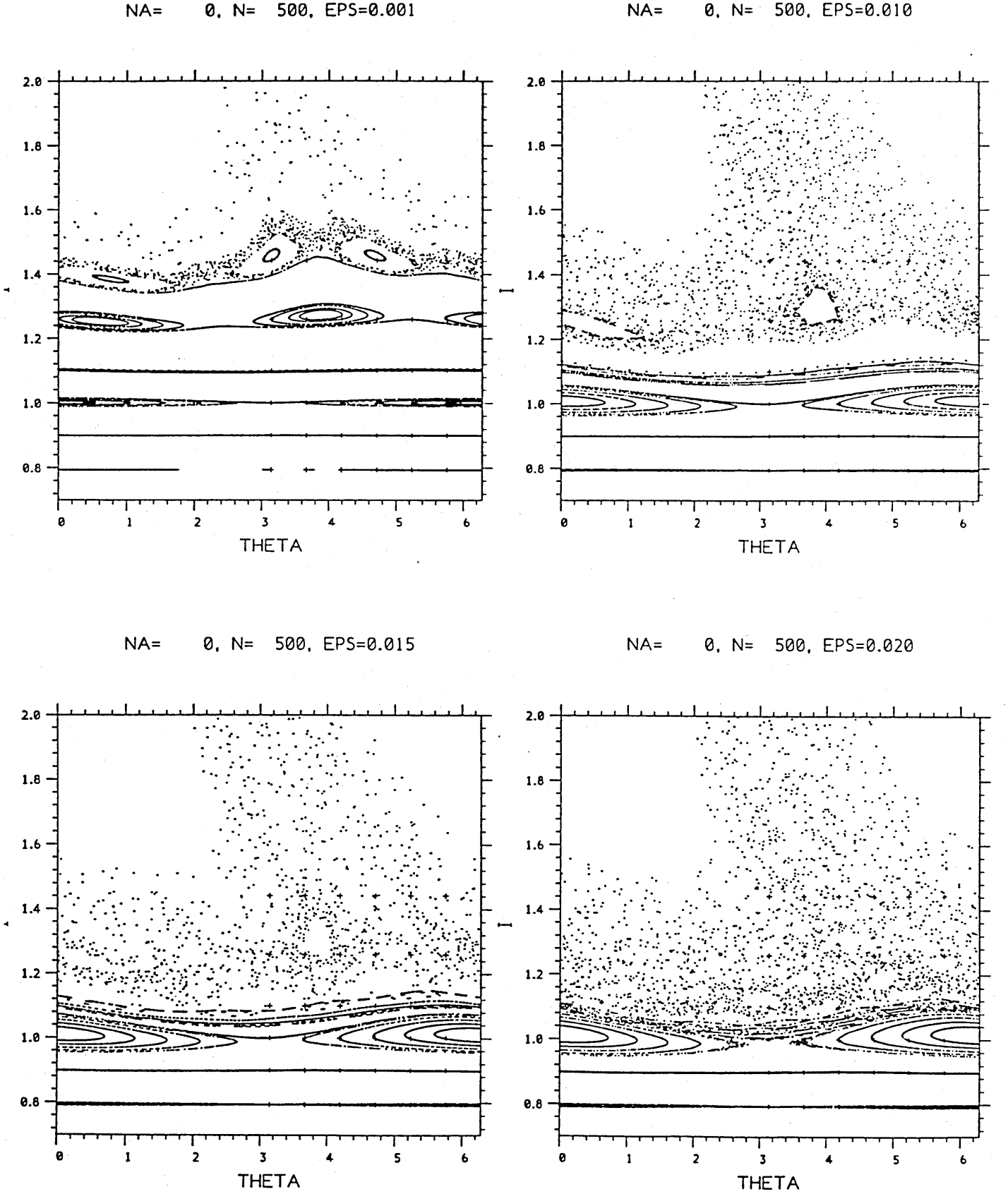
NA= 0, N= 500, EPS=0.001
NA= 0, N= 500, EPS=0.010
NA= 0, N= 500, EPS=0.015
NA= 0, N= 500, EPS=0.020
I
THETA
2.0
1.8
1.6
1.4
1.2
1.0
0.8
0
1
2
3
4
5
6

Figure 5.1

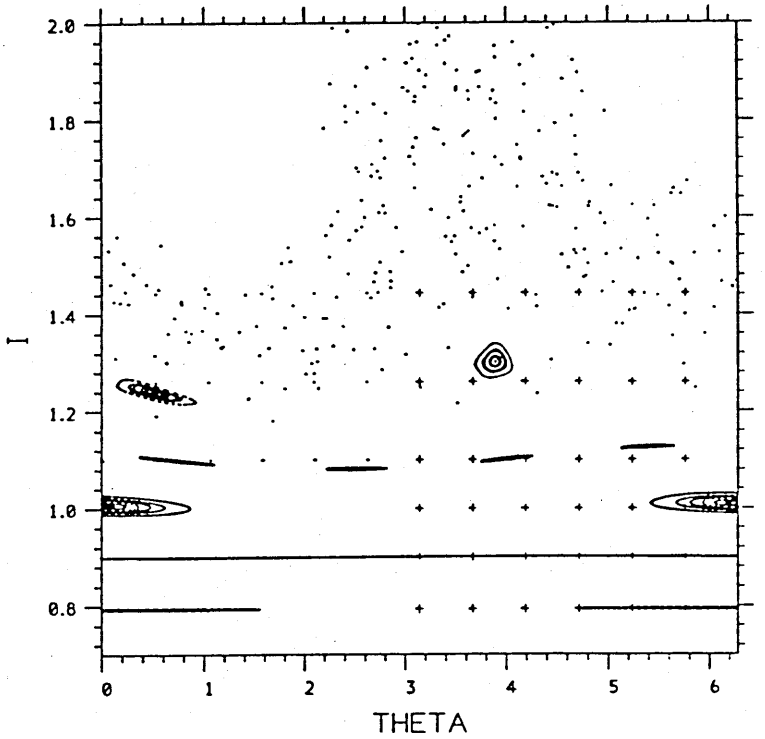
NA= 1000, N= 1500, EPS=0.010
2.0
1.8
1.6
1.4
1.2
1.0
0.8
I
0
1
2
3
4
5
6
THETA

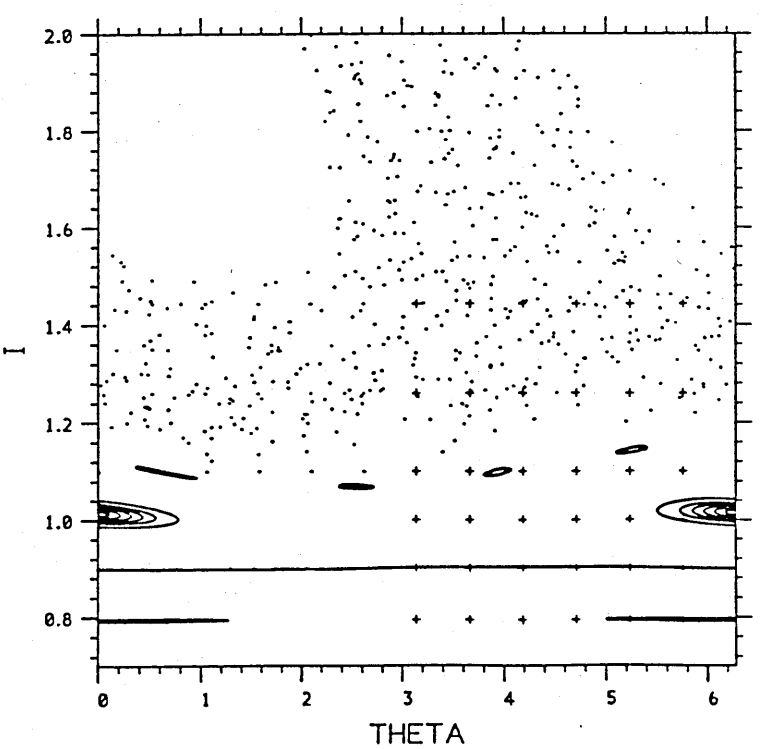
NA= 1000, N= 1500, EPS=0.020
2.0
1.8
1.6
1.4
1.2
1.0
0.8
I
0
1
2
3
4
5
6
THETA

Figure 5.2

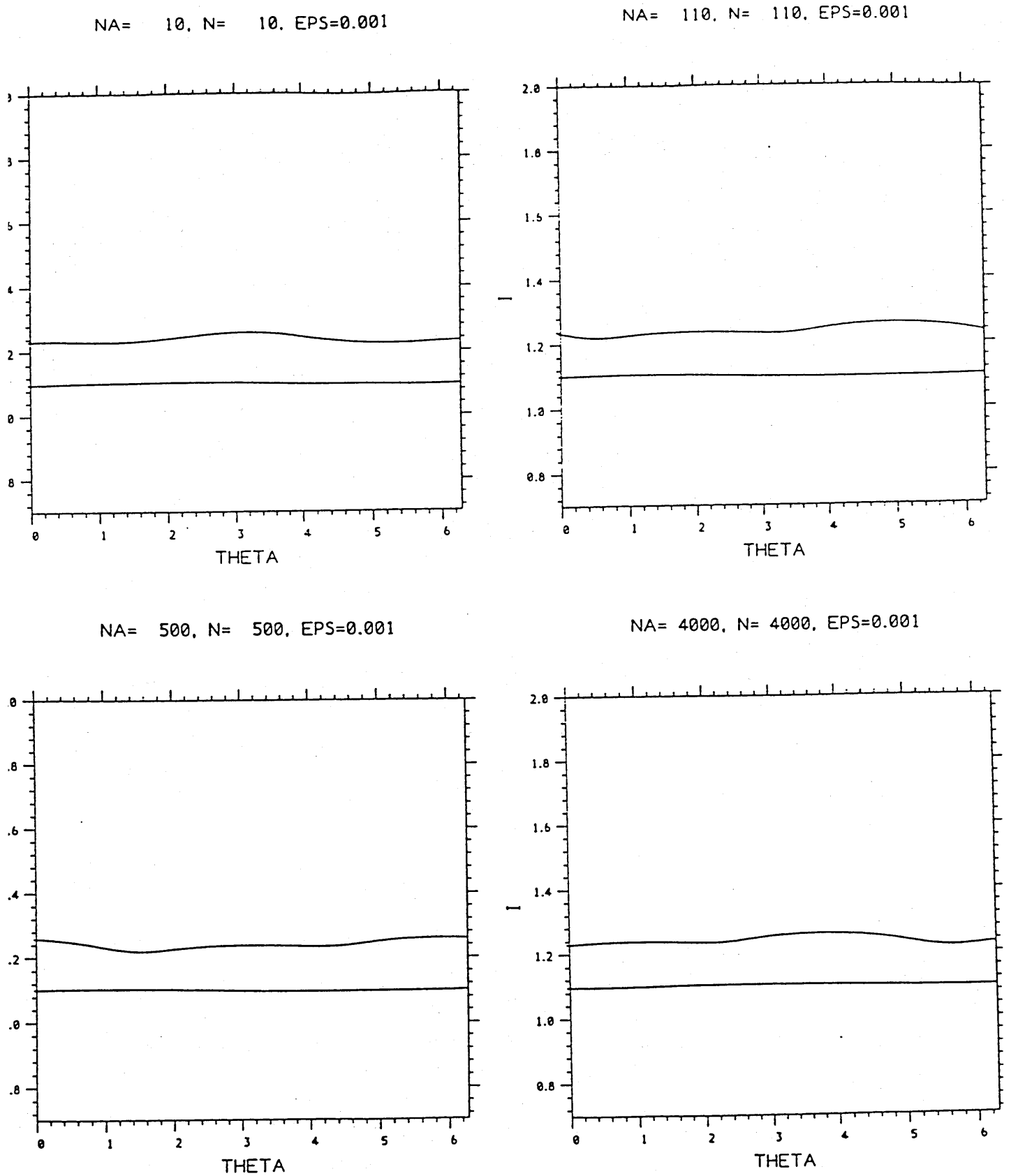
NA= 10, N= 10, EPS=0.001
NA= 110, N= 110, EPS=0.001
NA= 500, N= 500, EPS=0.001
NA= 4000, N= 4000, EPS=0.001
I
THETA

Figure 5.3a

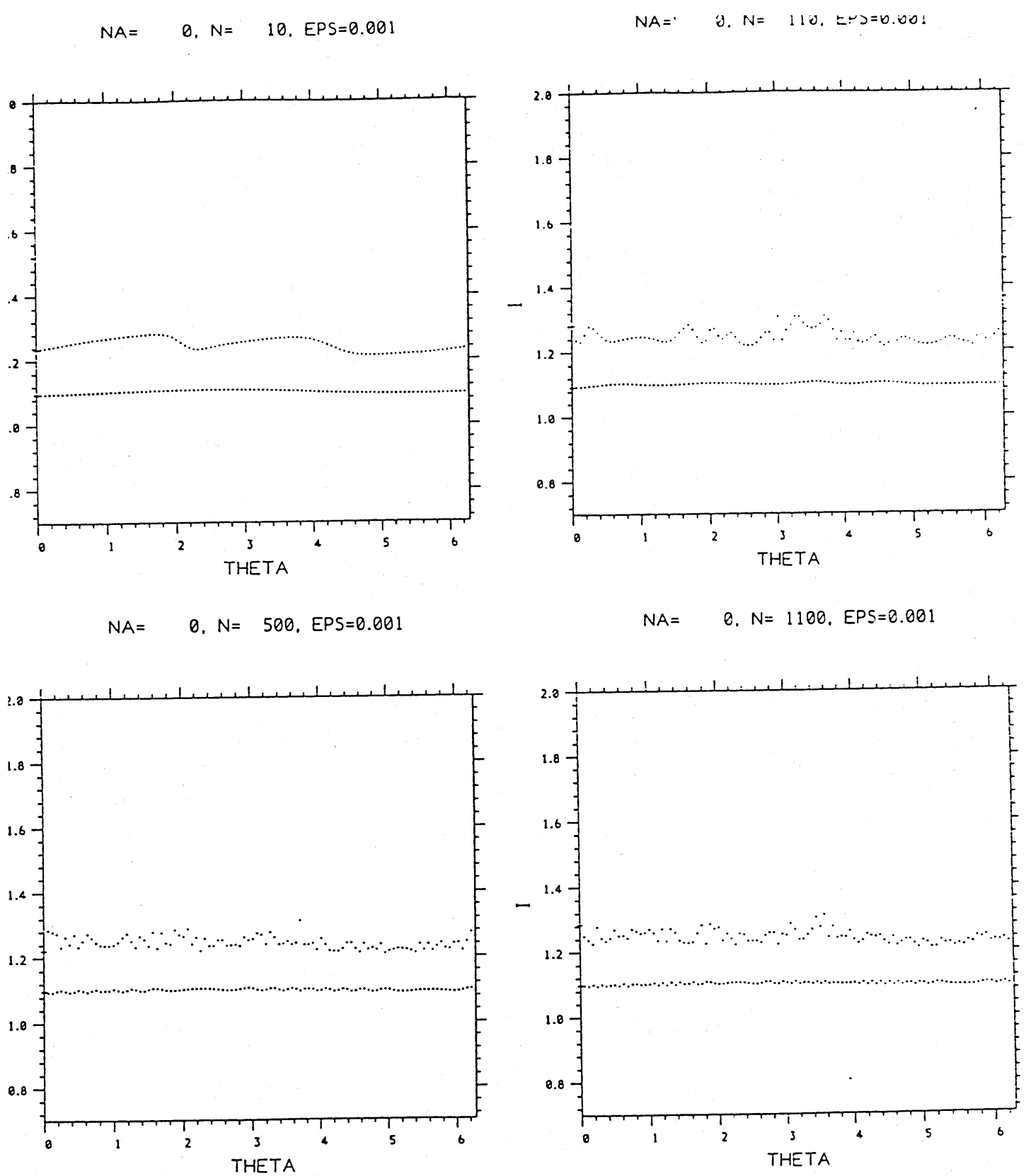
NA= 0, N= 10, EPS=0.001
NA= 0, N= 110, EPS=0.001
NA= 0, N= 500, EPS=0.001
NA= 0, N= 1100, EPS=0.001
I
THETA

Figure 5.3b

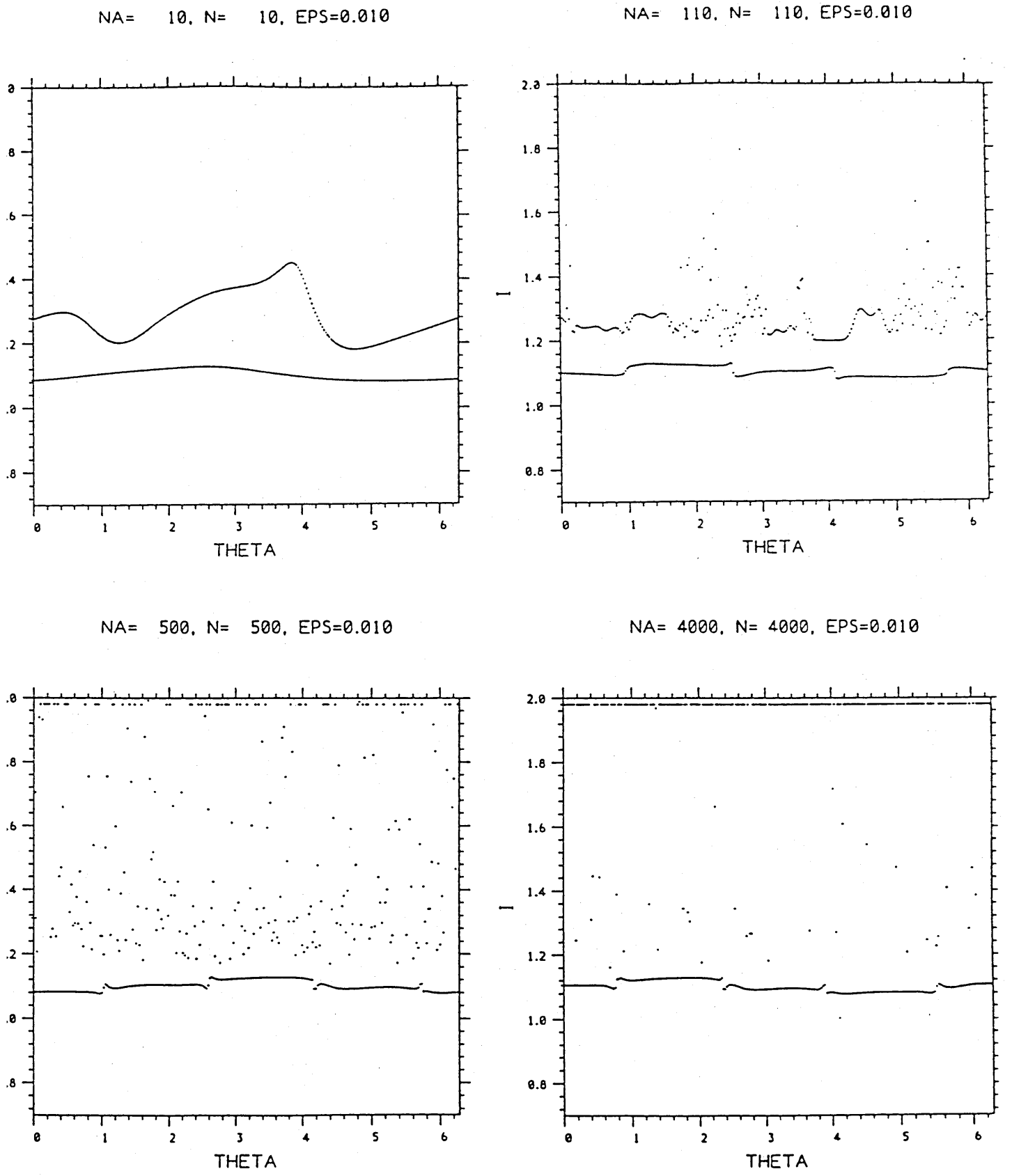
NA= 10, N= 10, EPS=0.010
NA= 110, N= 110, EPS=0.010
NA= 500, N= 500, EPS=0.010
NA= 4000, N= 4000, EPS=0.010
I
THETA

Figure 5.4a

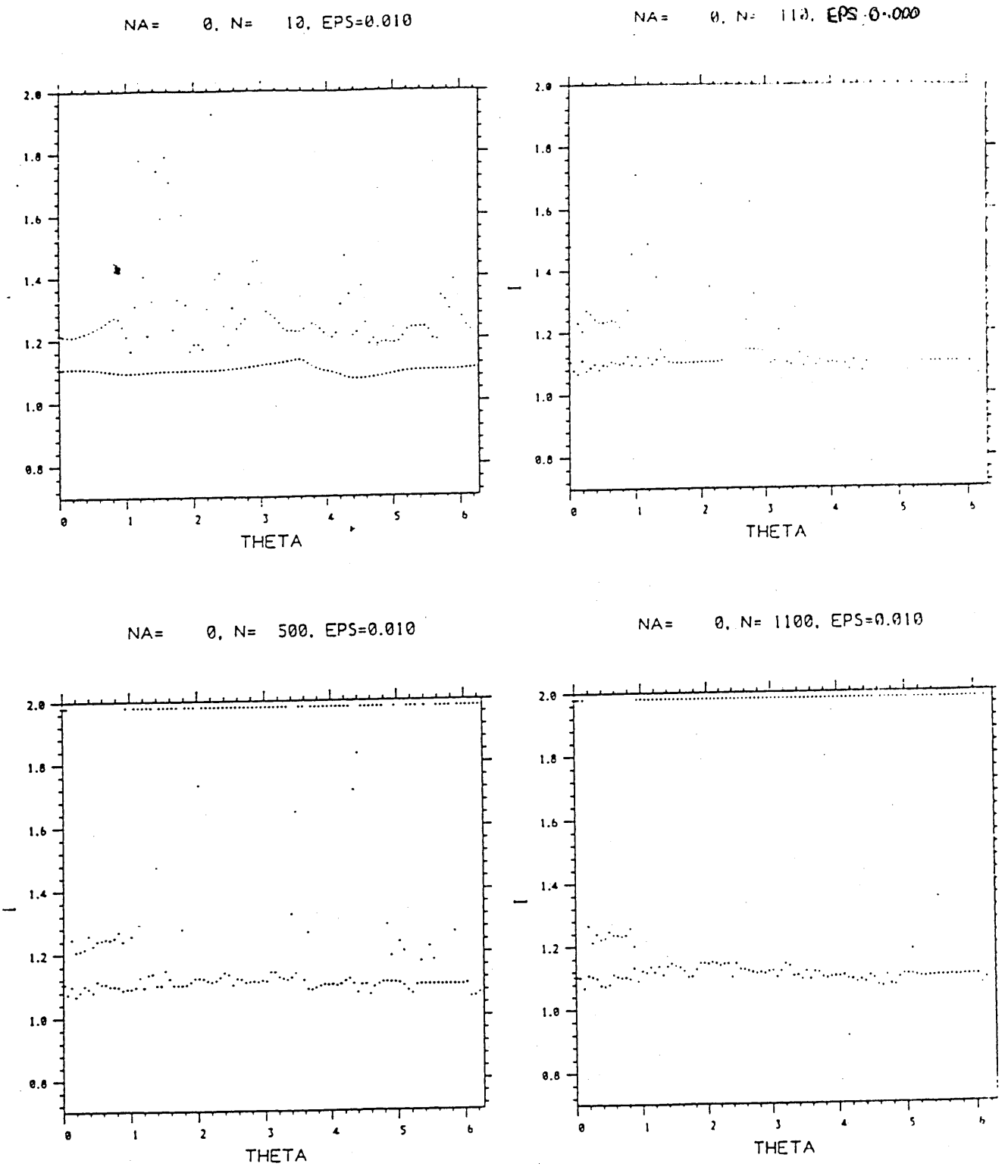
NA= 0, N= 10, EPS=0.010
NA= 0, N= 110, EPS=0.000
NA= 0, N= 500, EPS=0.010
NA= 0, N= 1100, EPS=0.010
I
THETA

Figure 5.4b

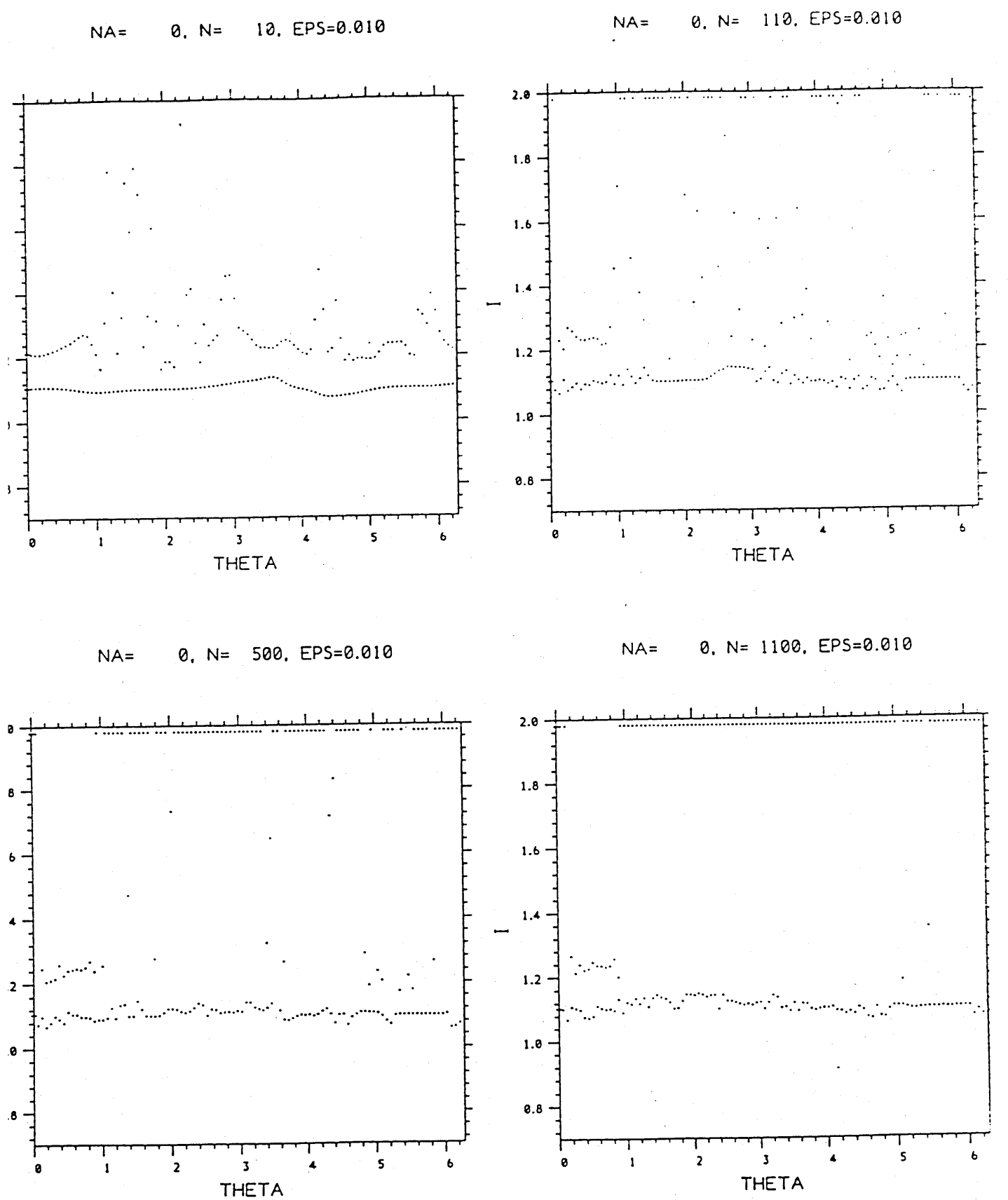
NA= 0. N= 10. EPS=0.010
NA= 0. N= 110. EPS=0.010
NA= 0. N= 500. EPS=0.010
NA= 0. N= 1100. EPS=0.010
THETA
THETA
THETA
THETA

Figure 5.4b

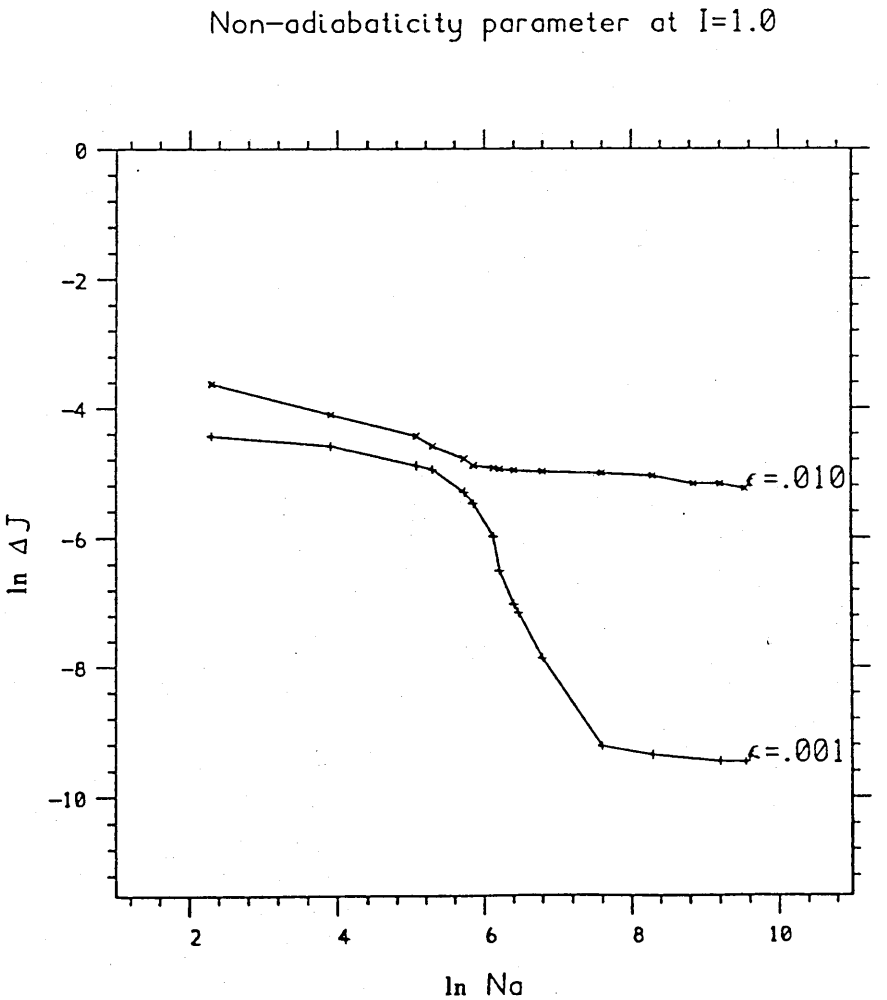
Non-adiabaticity parameter at I=1.0
0
-2
-4
-6
-8
-10
ln ΔJ
2
4
6
8
10
ln Na
ε=.010
ε=.001

Figure 5.5a

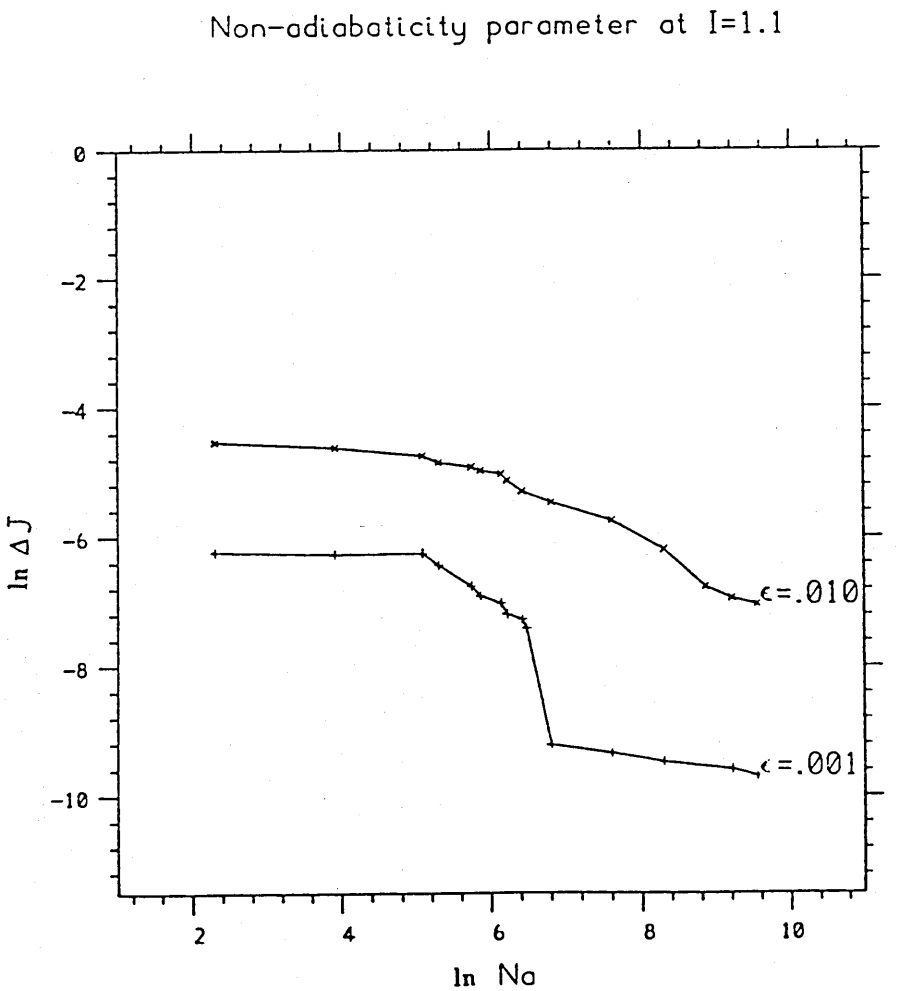
Non-adiabaticity parameter at I=1.1
0
-2
-4
-6
-8
-10
ln ΔJ
2
4
6
8
10
ln Na
ε=.010
ε=.001

Figure 5.5b

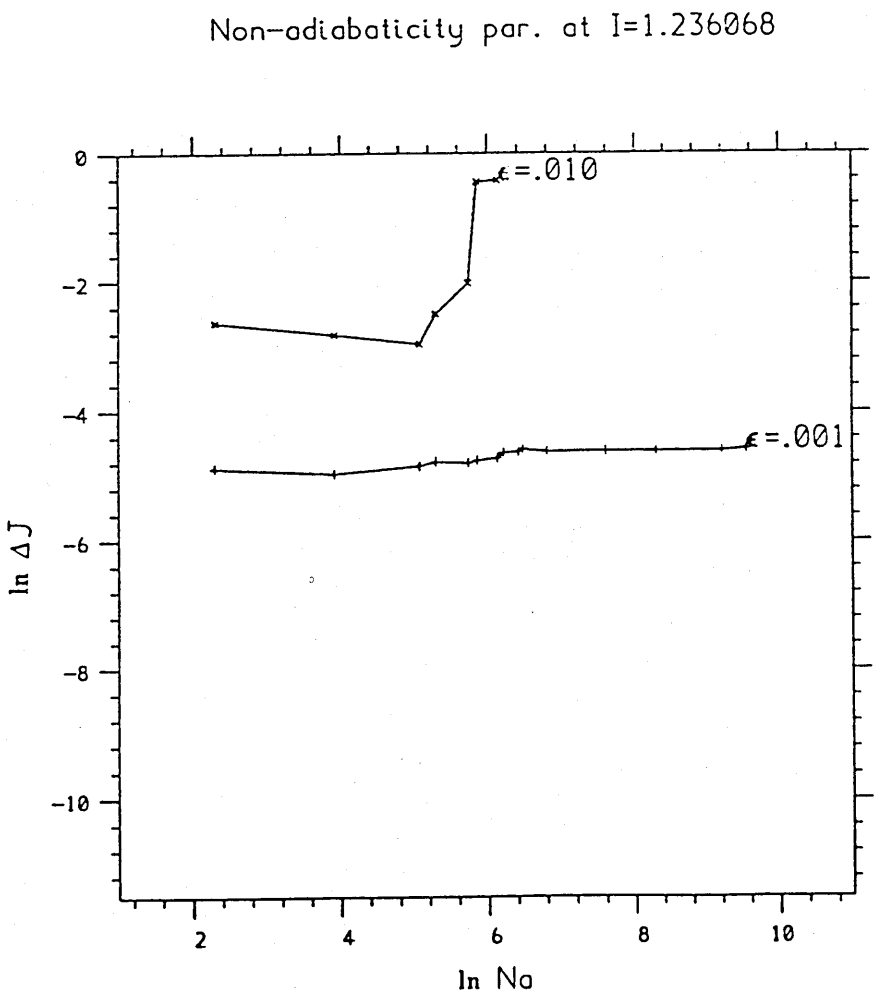
Non-adiabaticity par. at I=1.236068
0
-2
-4
-6
-8
-10
ln ΔJ
ε=.010
ε=.001
2
4
6
8
10
ln Na

Figure 5.5c

I = 1.0

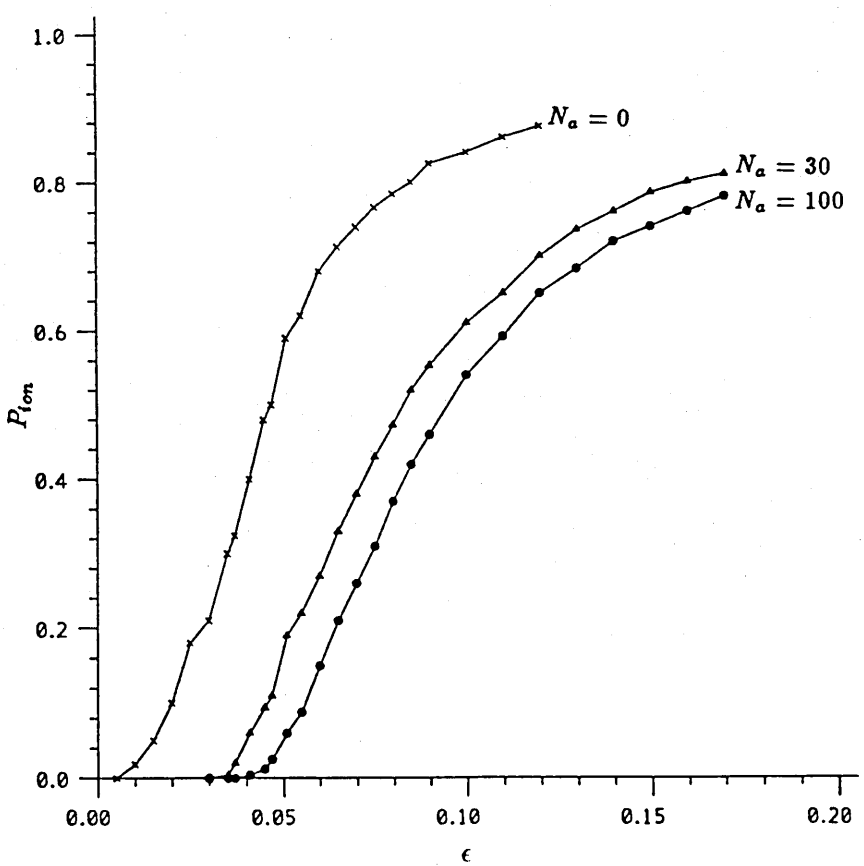

Figure 5.6a

I = 1.236068

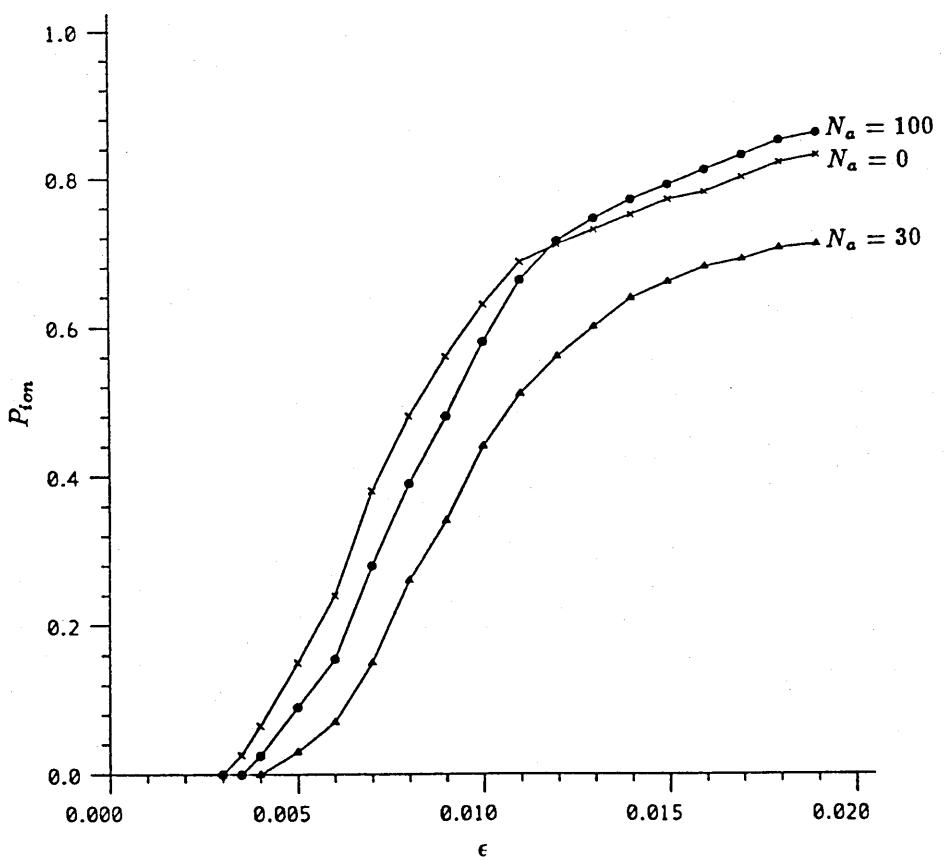

Figure 5.6b